FORECASTING PRODUCTION IN LIQUID RICH SHALE PLAYS

A Dissertation

by

HANIEH NIKFARMAN

Submitted to the Office of Graduate and Professional Studies of
Texas A&M University
in partial fulfillment of the requirements for the degree of

DOCTOR OF PHILOSOPHY

Chair of Committee,	W. John Lee
Co-Chair of Committee,	Maria A. Barrufet
Committee Members,	Peter Valko
	Duane A. McVay
Head of Department,	A. Daniel Hill

May 2016

Major Subject: Petroleum Engineering

ABSTRACT

Production from Liquid Rich Shale (LRS) reservoirs is taking center stage in the exploration and production of unconventional reservoirs. Production from the low and ultra-low permeability LRS plays is possible only through multi-fractured horizontal wells (MFHW's). There is no existing workflow that is applicable to forecasting multi-phase production from MFHW's in LRS plays. This project presents a practical and rigorous workflow for forecasting multiphase production from MFHW's in LRS reservoirs.

There has been much effort in developing workflows and methodology for forecasting in tight/shale plays in recent years. The existing workflows, however, are applicable only to single phase flow, and are primarily used in shale gas plays. These methodologies do not apply to the multi-phase flow that is inevitable in LRS plays. To account for complexities of multiphase flow in MFHW's the only available technique is dynamic modeling in compositional numerical simulators. These are time consuming and not practical when it comes to forecasting production and estimating reserves for a large number of producers.

A workflow was developed, and validated by compositional numerical simulation. The workflow honors physics of flow, and is sufficiently accurate while practical so that an analyst can readily apply it to forecast production and estimate reserves in a large number of producers in a short period of time. To simplify the complex multiphase flow in MFHW, the workflow divides production periods into an initial period where large production and pressure declines are expected, and the subsequent period where production decline may converge into a common trend for a number of producers across an area of interest in the field.

Initial period assumes the production is dominated by single-phase flow of oil and uses the tri-linear flow model of Erdal Ozkan to estimate the production history. Commercial software readily available can simulate flow and forecast production in this period.

In the subsequent Period, dimensionless rate and dimensionless time functions are introduced that help identify transition from initial period into subsequent period. The production trends in terms of the dimensionless parameters converge for a range of rock permeability and stimulation intensity. This helps forecast production beyond transition to the end of life of well. This workflow is applicable to single fluid system.

DEDICATION

This dissertation is gratefully dedicated to my loving parents, Frahanaz and Reza. You taught me determination, and without your encouragement and support I would have never been able to accomplish this.

ACKNOWLEDGEMENTS

I would like to thank my committee co-chairs, Dr. John Lee, and Dr. Maria Barrufet for their guidance and support throughout the course of this research. I also would like to thank my committee members, Dr. Peter Valko, and Dr. Duane McVay, for their valuable feedback.

Particular thanks also go to my friends and colleagues and the department faculty and staff for making my time at Texas A&M University an exceptional experience.

Finally, I would like to extend especial thanks to my family including my husband, Ali, for his patience; my brothers, Mohammad, Mehdi, and Amin, for their continued encouragement; and my parents, Farahnaz and Reza, for keeping me motivated.

NOMENCLATURE

A	Flow area (ft^2)
A_f	Total fracture face flow area (ft^2)
b_L	Intercept of $\frac{\Delta p}{q}$ vs. $\sqrt{t}$ plot for linear flow
b_B	Intercept of $\frac{\Delta p}{q}$ vs. $\sqrt[4]{t}$ plot for bilinear flow
B	Formation volume factor (res bbl/stb)
B_{oi}	Formation volume factor of oil at initial reservoir condition (res bbl/stb)
c_{oi}	Compressibility of oil at initial reservoir condition (1/psi)
c_{fi}	Formation compressibility at initial reservoir condition (1/psi)
c_t	Total compressibility (1/psi)
d_i	Distance of investigation (ft)
d	Distance between adjacent hydraulic fracture stages (ft)
D	Completed lateral length of well (ft)
h_f	Fracture height (ft)
h	Formation thickness (ft)
k	Permeability (md)
k_f	Fracture permeability (md)
k_I	Inner reservoir permeability in trilinear flow model (md)
k_O	Outter reservoir permeability in trilinear flow model (md)
k_{srv}	Permeability of stimulated rock (md)
k_{mat}	Permeability of matrix (md)
k_x	Permeability of matrix in x-direction (md)

k_y	Permeability of matrix in y-direction (md)
k_z	Permeability of matrix in z-direction (md)
L_e	Horizontal lateral length (ft)
m_L	Slope of $\frac{\Delta p}{q}$ vs. $\sqrt{t}$ plot for linear flow
m_B	Slope of $\frac{\Delta p}{q}$ vs. $\sqrt[4]{t}$ plot for bilinear flow
n_F	Number of hydraulic fractures along the horizontal wellbore
n_f	Number of hysraulic stimulation stages
N_P	Total production
p	Pressure (psi)
p_{bp}	Bubble point pressure of oil (psi)
p_{ch}	Characteristic pressure (psi)
p_D	Dimensionless pressure
p_i	Initial pressure (psi)\
p_{wf}	Well flowing bottom-hole pressure (psi)
q	Flow rate (stb/day)
q_D	Dimensionless rate
q_{ext}	Specific flux (stb/day)
q_f	Flow rate for each hydraulic fracture (stb/day)
R_{soi}	Solution gas-oil ratio (scf/stb)
r_w	Well-bore radius (ft)
s_f	Skin factor
S_{wi}	Saturation of water at initial reservoir condition
S_{oi}	Saturation of oil at initial reservoir condition
t	Time (days or hours)

t_D	Dimensionless time
T_R	Reservoir temperature (°F)
w_f	Fracture width/aperture (ft)
x_D	Dimensionless distance
x_e	Distance from wellbore to drainage boundary (ft)
x_f	Fracture half length (ft)
$x_{f,eff}$	Effective fracture half length (ft)
y_e	Half distance between adjacent hydraulic fracture stages (ft)
$y_{e,eff}$	Effective half distance between adjacent hydraulic fracture stages (ft)
φ	Porosity
γ_o	Specific gravity of oil (°API)
μ	Viscosity (cP)
μ_{oi}	Viscosity of oil at initial reservoir condition (cP)
ρ_{oi}	Density of oil at initial reservoir condition (lb/ft^3)

TABLE OF CONTENTS

Page

Page

Page

LIST OF FIGURES

Page

Page

Page

Page

Page

Page

LIST OF TABLES

Page

Page

CHAPTER I

INTRODUCTION

Background

Pervasive accumulation of hydrocarbons over large areas, either as source rock or very tight reservoirs previously thought impossible to produce, form a part of what is referred to as unconventional resources. Unconventional resources include many other types of plays and hydrocarbons such as tight gas, heavy oil, coal bed methane, and basin centered gas. Production is possible from the unconventional resources through specialized technology such as hydraulic stimulation of the rock to improve permeability.

Unconventional production, in the context of this project, refers to production of liquid rich shale (LRS) plays where production from very low permeability rock in the range of 100's of nD to 10's of μD becomes possible through hydraulic fracture stimulation of horizontal wells, referred to as multi-fractured horizontal well(s) (MFHW).

MFHW's are inherently complex and non-unique. The horizontal length varies. For the same completion design the effectiveness of the stimulation can vary from well to well, and sometimes stimulation may only be partially successful. Sharp pressure and rate declines during early production period are common. There is a limited amount of control that operators have on rates and pressure declines. Performance of these wells has to be compared on the basis of their productivity indices, in other words, both rates and bottom-hole pressures have to be taken into account. Flow in MFHW's in LRS plays are further complicated with the impact of the second phase that becomes significant when the pressure drops below the bubble point.

Forecasting of single phase gas production in such reservoirs is relatively simpler and in recent years much effort has been devoted to developing practical workflows that can be used in MFHW's with single phase gas flow. These workflows unfortunately do not apply to the more complicated multiphase flow in LRS's.

Forecasting production of individual wells in liquid rich shale (LRS) plays has become a very difficult task in the industry. Some rely on conventional decline curve analysis (DCA); others use modified DCA, they divide the production into multiple periods, and use several DCA's to forecast production. In all these cases, the underlying assumption is that all wells have the same productivity index and behave similarly over their lives. This methodology completely ignores bottom-hole pressure responses that could vary significantly, especially during the early production period of a MFHW.

Compositional numerical simulators which account for pressure response and multi-phase flow, although robust, are not practical when it comes to forecasting hundreds of wells in an asset. This is because modelling MFHW's, history matching production, and forecasting with dynamic numerical software is tedious and time consuming. This exercise could take days or weeks for an individual well, provided enough expertise is available. Therefore, this is not a practical solution.

Other production data analysis workflows developed for single flow of gas into MFHW's are not applicable to LRS, as they do not account for multiphase flow.

Importance of Research

There are many theoretical and empirical forecasting methods that are commonly used in conventional reservoirs; there are also workflows for single phase gas flow in tight gas unconventional reservoirs. These approaches do not work in LRS plays. There have been attempts to use multi-phase approximations with single-phase workflows; so far the forecasts have not been validated. Operators require production forecasts to make investment decisions. Production forecasts are necessary for booking reserves consistent

with U.S. Securities and Exchange Commission (SEC) requirements. Ideally, forecasting should be as accurate as possible but with the shortest possible turnaround time. As an example, Arps' decline model for conventional wells (where applicable) takes only minutes and has proved to be reasonably accurate. Forecasting is not as simple in unconventional LRS plays, in which relatively reliable forecasting with complex numerical simulators can take days or weeks. There is a need for an alternative that maintains the reasonable accuracy of forecasting but with a quicker turnaround time. Economic evaluations for many exploration and development decisions require accurate production forecasts for a minimum of 5 years. The forecast has to be reasonable within 2-6 months after production begins. We need to confirm that existing workflows do not apply to LRS plays, and therefore should not be used as forecasting techniques; and to introduce a workflow that is practical yet accurate enough to enable us to make good investment and operating decisions.

Objective

The objective of this research is to present a practical and reasonably accurate workflow to forecast production and estimate reserves in multi-phase production of multi-fractured horizontal wells (MFHW) in liquid rich shale (LRS) reservoirs.

To achieve this, it is necessary to investigate whether there are any methodologies capable of sufficiently accurate forecasting of production in LRS with MFHW's in nD-microD permeability rock.

In the absence of any existing workflow that is appropriate, we need to develop a workflow that honors physical principles of flow, accounts for multiphase flow, and is soundly based in theory yet practical enough for an analyst to apply readily to forecast production and estimate reserves in a large number of producers.

Our approach is to simplify and break down the complex multi-phase flow in MFHW's in LRS while maintaining realistic forecasts. To validate the workflow, we will compare

our results to those from compositional numerical simulator with similar inputs and assumptions.

The workflow should be applicable to a section of a development area that includes production from a relatively uniform fluid system; e.g., the in-situ fluid is consistently volatile oil, black oil, or retrograde condensate. Also, in the development area, the stimulation design should be similar, although some variations in well architecture are expected and should be accounted for. Such a generic model would encompass hundreds to thousands of wells in some well-known LRS plays, such as Eagle Ford or Duvernay. The generic model for one development area would not necessarily be applicable to all LRS's. The generic model would likely take two or three weeks to develop.

Assumptions and Baseline

Compositional numerical simulation was selected as a benchmark to validate the workflow. The workflow is validated if a production forecast is within about 10% of the forecast a compositional numerical simulator produces. Similar inputs and assumptions would be used in both cases. Although we desire to achieve a good comparison between the workflow and numerical simulation in all products at all times, more weight is given to early production due to much higher net present value. Also, oil is a higher-value product than gas, and thus should be given a greater weight in comparison.

Structure of Dissertation

This dissertation is structured into 9 chapters. In CHAPTER I, a brief background on unconventional LRS plays and production through MFHW's is presented, the importance of research is reiterated and objectives of the project are laid out. In CHAPTER II, principles of flow and the diffusivity equation as it applies to fractured horizontal wells is reviewed. In CHAPTER III, some common methodology for forecasting are visited. The methodology reviewed includes decline curve analysis (DCA), type curves, more recent modifications of DCA such as Duong's, power-law,

and stretched exponential decline models. In CHAPTER IV, the hypothesis of developing a workflow for MFHW's in LRS is presented, and here it is suggested to simplify the complex workflow into a single phase initial and multiphase subsequent flow periods. For this hypothesis to hold, it has to be shown that after a transient period where flow is mostly dominated by single phase flow of oil, the production history follows a characteristic pattern. CHAPTER V is dedicated to testing the hypothesis that, after an initial period, the flow from an area with common reservoir and fluid properties and stimulation design behaves such that the decline parameters converge to a single set. Decline parameters for various scenarios in a common area of interest where reservoir permeability and initial pressure vary within a given range, and a given fluid system are developed in CHAPTER VII. In CHAPTER VI, the focus shifts to analysis of the early part of production history in MFHW's in LRS's. CHAPTER VIII verifies that the workflow produces reliable forecasts by comparing the production history of a number of wells using the workflow and a compositional numerical simulator. CHAPTER IX presents the conclusions of the study.

CHAPTER II

FLUID FLOW THEORY AND STIMULATION GEOMETRY

As mentioned in the previous chapter the objective of this project is to present a workflow for forecasting production and estimating reserves in unconventional liquid rich shale (LRS) plays. It was also mentioned that production from the tight rocks is only possible through hydraulic stimulation of horizontal wells. Finally, production of multi-fractured horizontal wells (MFHW's) from over-pressured LRS plays often starts with a single phase flow of oil that goes through a steep initial decline in pressure and production rate. In order to develop a simplified workflow to estimate production from these plays, this chapter is dedicated to review of the physics of flow and flow regimes in MFHW's.

Diffusivity Equation

The theory for fluid flow in petroleum reservoirs is based on conservation of mass combined with Darcy's law of fluid flow through porous media (usually) and an equation of state for the specific fluid in the reservoir. This, along with the appropriate boundary conditions, results in mathematical equations that are solvable with numerous techniques.

Conservation of mass specifies:

Mass In-Mass Out + Mass Consumed - Mass Produced = Mass Accumulated (1)

Darcy's law of fluid flow through porous media relates the velocity of fluid flow to the permeability of the medium, viscosity of fluid, and pressure drop across a certain

distance. This along with conservation of mass equation, and equation of state that defines fluid properties at any given temperature and pressure is the underlying principle of flow. With known reservoir properties such as permeability and porosity, and a fluid system defined with an equation of state, fluid flow could be modeled with compositional numerical simulation. To solve the diffusivity equation analytically simplifying assumptions are required. In case of multiphase flow in MFHW's in LRS plays, it is necessary to breakdown the flow regimes and make assumptions about dominant flow regimes and fluid phases wherever possible.

In production from a reservoir there are no chemical reactions, and therefore the conservation of mass combined with Darcy's law for single-phase Newtonian fluid at isothermal conditions leads to the diffusivity equation

$$\nabla^2 p = \frac{\varphi \mu c_t}{k} \frac{\partial p}{\partial t} \tag{2}$$

In LRS's due to very low permeability, linear flow and often a combination of several linear flow regimes are believed to dominate. Therefore, the diffusivity equation for linear flow is further explored. Note that the derivation of solutions for linear flow presented in equations (3) to (83) are directly from Blasingame (1995) PETE 620 course notes. Although these derivations are available in references, they are presented here to highlight the assumptions and boundary conditions in deriving the solutions and also for comparisons with the tri-linear solution that will be discussed later in this chapter.

For linear flow,

$$\nabla^2 a = \frac{\partial^2 a}{\partial x^2} + \frac{\partial^2 a}{\partial y^2} + \frac{\partial^2 a}{\partial z^2} \tag{3}$$

Therefore equation (2) in linear coordinates becomes

$$\frac{\partial^2 p}{\partial x^2} + \frac{\partial^2 p}{\partial y^2} + \frac{\partial^2 p}{\partial z^2} = \frac{\varphi \mu c_t}{k} \frac{\partial p}{\partial t} \tag{4}$$

Assuming that flow in x-direction dominates and that pressure gradient in z and y-directions are negligible,

$$\frac{\partial^2 p}{\partial y^2}=0 \tag{5}$$

$$\frac{\partial^2 p}{\partial z^2}=0 \tag{6}$$

Equation (4) reduces to

$$\frac{\partial^2 p}{\partial x^2}=\frac{\varphi \mu c_t}{k}\frac{\partial p}{\partial t} \tag{7}$$

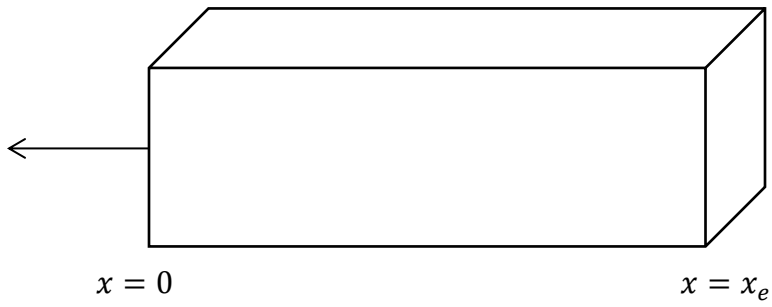

Figure 1—Physical behavior in linear flow system (Blasingame 1995)

Boundary conditions are:

1- Initial condition- uniform initial pressure distribution

$$p=(x,t=0)=p_i \tag{8}$$

2- Inner boundary condition- constant production rate

$$q=\frac{kA}{B\mu}\left[\frac{\partial p}{\partial x}\right]_{x=0} \tag{9}$$

3- Outer boundary conditions:

a. $p(x \to \infty, t)= p_i$ Infinite acting reservoir (10)

b. $p(x \to x_e, t)= p_i$ Constant pressure (11)

c. $q_{ext}=\frac{kA}{B\mu}\left[\frac{\partial p}{\partial x}\right]_{x=x_e}$ Specified flux (12)

In order to find a solution to the diffusivity equation, equation (7) is expressed in dimensionless form using the following definitions of dimensionless parameters.

Dimensionless distance, x_D, is based on the length of the reservoir and defined as:

$$x_D=\frac{x}{x_e} \tag{13}$$

Dimensionless pressure, p_D, that satisfies the following for boundary conditions

a. $p_D(x_D,t_D=0)=0$ (initial boundary condition) (14)

b. $\left[\frac{\partial p_D}{\partial x_D}\right]_{x_{D=0}}=-1$ (the constant rate inner boundary condition) (15)

Dimensionless time, t_D, which takes care of the remaining terms

Plugging back (13) into (7)

$$\frac{\partial^2 p}{\partial (x_D x_e)^2}=\frac{\varphi\mu c_t}{k}\frac{\partial p}{\partial t} \tag{16}$$

But x_e is a constant, and therefore (16) becomes

$$\frac{\partial^2 p}{\partial x_D{}^2}=\frac{\varphi\mu c_t x_e{}^2}{k}\frac{\partial p}{\partial t} \tag{17}$$

P_D should be defined such that $p_D(x_D,t_D=0)=0$, with use of a characteristic pressure, p_{ch}

$$p_D=\frac{1}{p_{ch}}(p_i-p) \qquad \text{OR} \qquad p=p_i- p_{ch}p_D \tag{18}$$

Plugging this into equation (17)

$$\frac{\partial^2(p_i - p_{ch}p_D)}{\partial x_D{}^2} = \frac{\varphi\mu c_t x_e{}^2}{k}\frac{\partial(p_i - p_{ch}p_D)}{\partial t} \tag{19}$$

But since p_i is constant, equation (19) reduces to

$$-p_{ch}\frac{\partial}{\partial x_D}\left(\frac{\partial p_D}{\partial x_D}\right) = \frac{\varphi\mu c_t x_e{}^2}{k}(-p_{ch})\frac{\partial p_D}{\partial t} \tag{20}$$

$$\frac{\partial^2 p_D}{\partial x_D{}^2} = \frac{\varphi\mu c_t x_e{}^2}{k}\frac{\partial p_D}{\partial t} \tag{21}$$

Plugging (18) and (13) into equation (9)

$$\frac{qB\mu}{kA} = \left[\frac{\partial(p_i - p_{ch}p_D)}{\partial(x_D x_e)}\right]_{x_D x_e = 0} \tag{22}$$

With x_e, p_i, and p_{ch} all being constant, (22) becomes

$$\left[\frac{\partial p_D}{\partial x_D}\right]_{x_D=0} = -\frac{qB\mu}{kA}\frac{x_e}{p_{ch}} \tag{23}$$

To define p_{ch}, the dimensionless inner boundary (15) is compared with (23)

$$\frac{qB\mu}{kA}\frac{x_e}{p_{ch}} = 1 \tag{24}$$

$$p_{ch} = \frac{qB\mu x_e}{kA} \tag{25}$$

Therefore (18) becomes

$$p_D = \frac{kA}{qB\mu x_e}(p_i - p) \tag{26}$$

Turning focus on defining t_D, in equation (21) replacing the remaining parameters with

$$t_D = \frac{k}{\varphi\mu c_t x_e{}^2}t \tag{27}$$

reduces equation (21) to

$$\frac{\partial^2 p_D}{\partial x_D{}^2} = \frac{\partial p_D}{\partial t_D} \tag{28}$$

where dimensionless parameters are as defined before:

$$x_D = \frac{x}{x_e} \tag{29}$$

$$p_D = p_{DC} \frac{kA}{qB\mu x_e}(p_i - p) \qquad \text{(where k,B,μ are constant)} \tag{30}$$

$$t_D = t_{DC} \frac{k}{\varphi \mu c_t x_e{}^2} t \qquad \text{(where k, φ,μ,c}_t\text{are constant)} \tag{31}$$

Where p_{DC} and t_{DC} are coefficients, in field units, 1.127 $x10^{-3}$ and $2.637x10^{-3}$ respectively. t is in hours.

Boundary conditions in terms of dimensionless parameters are given by:

1- Initial condition- uniform initial pressure distribution

$$p_D(x_D, t_D=0)=0 \tag{32}$$

2- Inner boundary condition- constant production rate

$$\left[\frac{\partial p_D}{\partial x_D}\right]_{x_{D=0}} = -1 \tag{33}$$

3- Outer boundary conditions-

a. $$p_D(x_D \to \infty, t_D)= 0 \qquad \text{Infinite acting reservoir} \tag{34}$$

b. $$p_D(x_D=1, t_D)= \frac{kA}{qB\mu x_e}(p_i - p_i)=0$$
$$p_D(x_D=1, t_D)=0 \qquad \text{constant pressure} \tag{35}$$

c. $$q_{ext} = \frac{kA}{B\mu}\left[\frac{\partial p}{\partial x}\right]_{x=x_e} \tag{12}$$

Substituting (13) and (16) here

$$\left[\frac{\partial p_D}{\partial x_D}\right]_{x_D=1} = -q_{D\,ext}(t_D) \qquad q_{D\,ext}(t_D) \text{ is a function of } t_D \tag{36}$$

In an effort to develop solutions to the diffusivity equation, we restate the diffusivity equation and boundary conditions in the Laplace domain.

$$l\left\{\frac{\partial f(t)}{\partial x_D}\right\} = \frac{d\bar{f}(u)}{dx_D} \tag{37}$$

$$l\{p_D(x_D, t_D)\} = \bar{p}_D \tag{38}$$

Using Laplace transforms defined in (37) and (38), the diffusivity equation (28) becomes

$$\frac{d^2 p_D}{dx_D^2} = u\,\bar{p}_D - p_D(t_D=0) \quad \text{(from initial condition)}$$

which reduces to

$$\frac{d^2 \bar{p}_D}{dx_D^2} = u\,\bar{p}_D \tag{39}$$

Taking the Laplace transform of the remaining boundary conditions, we have

1- Inner boundary condition- constant production rate

$$\left[\frac{d\bar{p}_D}{dx_D}\right]_{x_{D=0}} = \frac{-1}{u} \tag{40}$$

2- Outer boundary conditions-

a. $\bar{p}_D(x_D \to \infty, u) = 0$ infinite acting reservoir (41)

b. $\bar{p}_D(x_D=1, u)=0$ constant pressure (42)

c. $\left[\frac{d\bar{p}_D}{dx_D}\right]_{x_D=1} = -\bar{q}_{ext}(u)$ specified flux (43)

For $\bar{p}_D = \exp(mx_D)$, the left hand side of equation (39) becomes

$$\frac{d^2\bar{p}_D}{dx_D{}^2}=\frac{d}{dx_D}\left[\frac{de^{mx_D}}{dx_D}\right]=\frac{d}{dx_D}\left[m\ e^{mx_D}\right]=m^2\ e^{mx_D} \tag{44}$$

Substituting this into (39),

$$m^2\ e^{mx_D}=u\ e^{mx_D}$$

Therefore

$$m^2=u$$

$$m=\pm\sqrt{u} \tag{45}$$

where equation (45) leads to the following general solution

$$\bar{p}_D(u, x_D)= c_1e^{\sqrt{u}x_D}+c_2e^{-\sqrt{u}x_D} \tag{46}$$

The derivative of the general solution with respect to x_D is

$$\frac{d}{dx_D}\bar{p}_D(u, x_D)= c_1\sqrt{u}e^{\sqrt{u}x_D}-c_2\sqrt{u}\ e^{-\sqrt{u}x_D} \tag{47}$$

The Laplace transform approach for obtaining the particular solution for an infinite acting reservoir is outlined in the following derivation.

Derivative of the general solution with respect to $x_{D,}$ in equation (47) combined with the inner boundary condition (40) gives,

$$\left[c_1\sqrt{u}e^{\sqrt{u}x_D}-c_2\sqrt{u}\ e^{-\sqrt{u}x_D}\right]_{x_D=0}=-\frac{1}{u} \tag{48}$$

The general solution (46) combined with the outer boundary condition (41) gives

$$\lim_{x_D\to\infty}\left[c_1e^{\sqrt{u}x_D}+c_2e^{-\sqrt{u}x_D}\right]=0 \tag{49}$$

For finite values, equation (49) requires that $c_1=0$; we therefore must use equation (48) to determine c_2.

Solving equation (48) for c_2

$$c_2=\left[\frac{1}{u^{3/2}}\ e^{\sqrt{u}x_D}\right]_{x_D=0}=\frac{1}{u^{3/2}} \tag{50}$$

Recalling that $c_1=0$, and substituting and (50) into the general solution (46) gives

$$\bar{p}_D(u, x_D)=\frac{1}{u^{3/2}}e^{-\sqrt{u}x_D} \tag{51}$$

Using the Laplace transform to obtain particular solution for the specific flux outer boundary condition is outlined here,

From (48) the general inner boundary condition is

$$c_1\sqrt{u}-c_2\sqrt{u}=-\frac{1}{u} \tag{52}$$

Combining the derivative of the general solution (47) with the outer boundary condition (43) gives

$$\left[c_1\sqrt{u}e^{\sqrt{u}x_D}-c_2\sqrt{u}\ e^{-\sqrt{u}x_D}\right]_{x_D=1}-\bar{q}_{ext}(u) \tag{53}$$

Therefore

$$c_1\sqrt{u}e^{\sqrt{u}}-c_2\sqrt{u}\ e^{-\sqrt{u}}=-\bar{q}_{ext}(u) \tag{54}$$

Manipulating (53) and (54) results in

$$c_1-c_2=-\frac{1}{u\sqrt{u}} \tag{55}$$

$$c_1-c_2e^{-2\sqrt{u}}=\frac{-e^{-\sqrt{u}}}{\sqrt{u}}\bar{q}_{ext}(u) \tag{56}$$

$$c_1=c_2-\frac{1}{u\sqrt{u}} \tag{57}$$

Substituting into (57) into (56), rearranging and solving for c_2,

$$c_2=\frac{1}{u\sqrt{u}(1-e^{-2\sqrt{u}})}-\frac{e^{-\sqrt{u}}}{\sqrt{u}(1-e^{-2\sqrt{u}})}\bar{q}_{ext}(u) \tag{58}$$

And solving for c_2 in (55)

$$c_2 = c_1 + \frac{1}{u\sqrt{u}} \tag{59}$$

Substituting (59) into (58) and solving for c_1,

$$c_1 = \frac{1}{u\sqrt{u}}\left[\frac{1}{(1-e^{-2\sqrt{u}})} - 1\right] - \frac{e^{-\sqrt{u}}}{\sqrt{u}(1-e^{-2\sqrt{u}})}\bar{q}_{ext}(u) \tag{60}$$

Substituting (59) and (60) into the general solution (46) gives the particular solution,

$$\begin{aligned}\bar{p}_D(u, x_D) = \frac{1}{u\sqrt{u}}\left[\left[\frac{1}{(1-e^{-2\sqrt{u}})} - 1\right] e^{\sqrt{u}x_D} + \frac{1}{(1-e^{-2\sqrt{u}})} e^{-\sqrt{u}x_D}\right] \\ -\bar{q}_{ext}(u)\frac{1}{\sqrt{u}}\ \frac{e^{-\sqrt{u}}}{(1-e^{-2\sqrt{u}})}\left[e^{\sqrt{u}x_D} + e^{-\sqrt{u}x_D}\right]\end{aligned} \tag{61}$$

To reduce this equation and express in using hyperbolic sine and cosine functions, note the following algebra:

$$\frac{1}{(1-e^{-2\sqrt{u}})} = \frac{e^{\sqrt{u}}}{e^{\sqrt{u}} - e^{-\sqrt{u}}} \tag{62}$$

$$\frac{1}{(1-e^{-2\sqrt{u}})} - 1 = \frac{e^{-\sqrt{u}}}{e^{\sqrt{u}} - e^{-\sqrt{u}}} \tag{63}$$

$$\frac{e^{-\sqrt{u}}}{(1-e^{-2\sqrt{u}})} = \frac{1}{e^{\sqrt{u}} - e^{-\sqrt{u}}} \tag{64}$$

Also

$$2\sinh(x) = e^x - e^{-x} \tag{65}$$

$$2\cosh(x) = e^x + e^{-x} \tag{66}$$

Substituting the above simplifications and using the above identities into (61)

$$\bar{p}_D(u, x_D) = \frac{1}{u\sqrt{u}}\ \frac{\cosh\left[\sqrt{u}(1-x_D)\right]}{\sinh\left[\sqrt{u}\right]} - \bar{q}_{Dext}(u)\frac{1}{\sqrt{u}}\ \frac{\cosh\left[\sqrt{u}x_D\right]}{\sinh\left[\sqrt{u}\right]} \tag{67}$$

Using the Laplace transform to obtain particular solution for the constant pressure outer boundary condition is outlined here.

From equation (48)

$$c_1\sqrt{u}-c_2\sqrt{u}=-\frac{1}{u} \tag{68}$$

The constant pressure outer boundary condition in the Laplace domain is given by (42) and the general solution by (46). The general solution at $x_D=1$ gives

$$\bar{p}_D(u, x_D)=c_1e^{\sqrt{u}}+c_2e^{-\sqrt{u}}=0 \tag{69}$$

Dividing equation (52) by $\sqrt{u}$ and equation (67) by $e^{\sqrt{u}}$

$$c_1-c_2=-\frac{1}{u\sqrt{u}} \tag{70}$$

$$c_1+c_2e^{-2\sqrt{u}}=0 \tag{71}$$

Subtracting (68) from (69) and solving for c_2,

$$c_2=\frac{1}{u\sqrt{u}}\frac{1}{1+e^{-2\sqrt{u}}} \tag{72}$$

Substituting into (69) and solving for c_1,

$$c_1=\frac{-1}{u\sqrt{u}}\quad\frac{e^{-2\sqrt{u}}}{(1+e^{-2\sqrt{u}})} \tag{73}$$

Substituting (70) and (71) into general solution (46),

$$\bar{p}_D(u, x_D)=\frac{1}{u\sqrt{u}}\quad\left[\frac{-e^{-2\sqrt{u}}}{(1+e^{-2\sqrt{u}})}e^{\sqrt{u}x_D}+\frac{1}{1+e^{-2\sqrt{u}}}\ e^{-\sqrt{u}x_D}\right] \tag{74}$$

The exponential terms in the above equation can be expressed as

$$\frac{-e^{-2\sqrt{u}}}{(1+e^{-2\sqrt{u}})}=\frac{e^{2\sqrt{u}}}{e^{\sqrt{u}}+e^{-\sqrt{u}}} \tag{75}$$

$$\frac{1}{1+e^{-2\sqrt{u}}}=\frac{e^{\sqrt{u}}}{e^{\sqrt{u}}+e^{-\sqrt{u}}} \tag{76}$$

Substituting (73) and (74) in to (72), collecting and rearranging,

$$\bar{p}_D(u, x_D) = \frac{1}{u\sqrt{u}} \left[\frac{e^{\sqrt{u}(1-x_D)} - e^{-\sqrt{u}(1-x_D)}}{e^{\sqrt{u}} + e^{-\sqrt{u}}} \right] \tag{77}$$

Substituting the definitions of sinh(x) and cosh(x), (65) and (66) where appropriate gives the final form of this particular solution

$$\bar{p}_D(u, x_D) = \frac{1}{u\sqrt{u}} \frac{\sinh\left[\sqrt{u}(1-x_D)\right]}{\cosh\left[\sqrt{u}\right]} \tag{78}$$

Solutions to the linear diffusivity equation in Laplace domain for the following cases are summarized in Table 1.

Case	$\bar{p}_D(u, x_D)$
Infinite Acting Reservoir	$\frac{1}{u^{3/2}} e^{-\sqrt{u}x_D}$
Specified Flux Outer Boundary Condition	$\frac{1}{u\sqrt{u}} \frac{\cosh\left[\sqrt{u}(1-x_D)\right]}{\sinh\left[\sqrt{u}\right]}$ $-\bar{q}_{Dext}(u) \frac{1}{\sqrt{u}} \frac{\cosh\left[\sqrt{u}x_D\right]}{\sinh\left[\sqrt{u}\right]}$
Constant Pressure outer Boundary Condition	$\frac{1}{u\sqrt{u}} \frac{\sinh\left[\sqrt{u}(1-x_D)\right]}{\cosh\left[\sqrt{u}\right]}$

Table 1—Diffusivity equation solutions for linear flow in Laplace domain.

To obtain solutions for the above cases in the real domain, inverse Laplace transform look ups are used. For the infinite-acting reservoir case, the functions in Table 2 are used.

$\bar{f}(s)$	f(t)	Reference
$\frac{1}{\sqrt{s}}e^{-a\sqrt{s}}$	$\frac{1}{\sqrt{\pi t}}e^{-\frac{a^2}{4t}}$	Roberts and Kaufman (1966)
$\frac{1}{s}\frac{1}{\sqrt{s}}e^{-a\sqrt{s}}$	$\frac{2\sqrt{t}}{\sqrt{\pi}}e^{-\frac{a^2}{4t}}-a\,\mathrm{erfc}\left[\frac{a}{2\sqrt{t}}\right]$	Roberts and Kaufman (1966)

Table 2—Inverse Laplace transform-1.

Inverting equation (51) gives

$$p_D(t_D, x_D)=\frac{2\sqrt{t_D}}{\sqrt{\pi}}e^{-\frac{x_D^2}{4t_D}}-x_D\,\mathrm{erfc}\left[\frac{x_D}{2\sqrt{t_D}}\right] \tag{79}$$

For the specified-flux outer boundary condition, in equation (67), $\bar{q}_{Dext}(u)$ must be known, here we assumed that there is no flow, therefore $q_{Dext}(t_D)=0$, and use the inverse functions in Table 3.

$\bar{f}(s)$	f(t)	Reference
$\frac{1}{\sqrt{s}}\ \frac{\cosh\left[v\sqrt{s}\right]}{\sinh\left[a\sqrt{s}\right]}$	$a^{-1}\theta_4\left[\frac{v}{2a},\frac{t}{a^2}\right]$	Roberts and Kaufman (1966)

where $\theta_4[z,x]=\frac{1}{\sqrt{\pi x}}\sum_{n=-\infty}^{\infty}e^{-\frac{1}{x}\left(x+\frac{1}{2}+n\right)^2}$

Table 3— Inverse Laplace transform-2.

Using fundamentals of Laplace transform and more complex mathematics, the solution for two cases of $x_D=0$ and $x_D=1$ are given as

$$p_D(t_D, x_D=0)=\sum_{n=-1}^{\infty}\left[\frac{2\sqrt{t_D}}{\sqrt{\pi}}e^{-\left[\frac{a_n}{2\sqrt{t_D}}\right]^2}-a_n\left[1-\text{erf}\left[\frac{a_n}{2\sqrt{t_D}}\right]\right]\right]+\sum_{n=-\infty}^{-2}\left[\frac{2\sqrt{t_D}}{\sqrt{\pi}}e^{-\left[\frac{a_n}{2\sqrt{t_D}}\right]^2}+a_n\left[1+\text{erf}\left[\frac{a_n}{2\sqrt{t_D}}\right]\right]\right] \quad (80)$$

$$p_D(t_D, x_D=1)=\sum_{n=0}^{\infty}\left[\frac{2\sqrt{t_D}}{\sqrt{\pi}}e^{-\left[\frac{a_n}{2\sqrt{t_D}}\right]^2}-a_n\left[1-\text{erf}\left[\frac{a_n}{2\sqrt{t_D}}\right]\right]\right]+\sum_{n=-\infty}^{-1}\left[\frac{2\sqrt{t_D}}{\sqrt{\pi}}e^{-\left[\frac{a_n}{2\sqrt{t_D}}\right]^2}+a_n\left[1+\text{erf}\left[\frac{a_n}{2\sqrt{t_D}}\right]\right]\right] \quad (81)$$

Case 1; $x_D=0$; n=-2, $a_{-2}<0$ and at n=-1, $a_{-1}\geq 0$

Case 2: $x_D=1$; n=-2, $a_{-1}<0$ and at n=0, $a_0\geq 0$

For constant pressure outer boundary conditions, in equation (78), we use the inverse functions in Table 4.

$\bar{f}(s)$	f(t)	Reference
$\frac{1}{\sqrt{s}}\frac{\cosh\left[v\sqrt{s}\right]}{\sinh\left[a\sqrt{s}\right]}$	$-a^{-1}\theta_1\left[\frac{v}{2a},\frac{t}{a^2}\right]$	Roberts and Kaufman (1966)

where $\theta_1[z,x]=\frac{1}{\sqrt{\pi x}}\sum_{n=-\infty}^{\infty}(-1)^n e^{-\frac{1}{x}(z-\frac{1}{2}+n)^2}$

Table 4— Inverse Laplace transform-3

Using fundamentals of Laplace transform and more complex mathematics, the solution for two cases of $x_D=0$ and $x_D=1$ are given as

Case 1; $x_D=0$;n=-1, $a_{-1}<0$ and at n=0, $a_0\geq 0$

Case 2: $x_D=1$;n=0, $a_0<0$ and at n=1, $a_1\geq 0$

$$p_D(t_D, x_D=0)=\sum_{n=0}^{\infty}(-1)^n\left[\frac{2\sqrt{t_D}}{\sqrt{\pi}}e^{-\left[\frac{a_n}{2\sqrt{t_D}}\right]^2}-a_n\left[1-\text{erf}\left[\frac{a_n}{2\sqrt{t_D}}\right]\right]\right]+$$
$$\sum_{n=-\infty}^{-1}(-1)^n\left[\frac{2\sqrt{t_D}}{\sqrt{\pi}}e^{-\left[\frac{a_n}{2\sqrt{t_D}}\right]^2}+a_n\left[1+\text{erf}\left[\frac{a_n}{2\sqrt{t_D}}\right]\right]\right] \quad (82)$$

$$p_D(t_D, x_D=1)=\sum_{n=1}^{\infty}(-1)^n\left[\frac{2\sqrt{t_D}}{\sqrt{\pi}}e^{-\left[\frac{a_n}{2\sqrt{t_D}}\right]^2}-a_n\left[1-\text{erf}\left[\frac{a_n}{2\sqrt{t_D}}\right]\right]\right]+$$
$$\sum_{n=-\infty}^{0}(-1)^n\left[\frac{2\sqrt{t_D}}{\sqrt{\pi}}e^{-\left[\frac{a_n}{2\sqrt{t_D}}\right]^2}+a_n\left[1+\text{erf}\left[\frac{a_n}{2\sqrt{t_D}}\right]\right]\right] \quad (83)$$

Solution for Linear and Bi-Linear Flow in Hydraulic Fractured Wells

The solution for constant rate linear flow at x=0 is given by Anderson and Mattar (2003),

$$p_D(t_D, 0)=\sqrt{\pi t_D} \quad (84)$$

To include the impact of fracture skin, the term s_f, must be added to equation (84),

$$p_D=\sqrt{\pi t_D}+s_f \quad (85)$$

Using dimensionless variables

$$p_D=\frac{kh\Delta p}{141.2\ qB\mu} \quad (86)$$

and

$$t_D=\frac{0.0002637kt}{\varphi\mu c_t x_f^2} \quad (87)$$

where all parameters are in field units, and t is in hours.

Substituting definitions of p_D and t_D into equation (85) the result is

$$\frac{\Delta p}{q}=\frac{4.064}{hx_f}\sqrt{\frac{t}{k\varphi\mu c_t}}+\frac{kh}{141.2qB\mu}s_f \tag{88}$$

If we let area of flow for a single stage hydraulic fracture to be

$$A_f=4x_fh \tag{89}$$

Then the solution for transient linear flow at constant rate for slightly compressible fluid becomes

$$\frac{\Delta p}{q}=\frac{16.26}{A_f}\sqrt{\frac{t}{k\varphi\mu c_t}}+\frac{kh}{141.2qB\mu}s_f \tag{90}$$

For the case of constant bottom-hole pressure (BHP), the solution for transient linear flow in dimensionless form is provided by Poe (2002) in equation (105).

$$q_D=\frac{2}{\pi\sqrt{\pi t_D}} \tag{91}$$

To include the impact of fracture skin, the term S_f, must be added to equation (105)

$$\frac{1}{q_D}=\frac{\pi\sqrt{\pi t_D}}{2}+s_f \tag{92}$$

where dimensionless rate is

$$q_D=\frac{141.2qB\mu}{kh\Delta p} \tag{93}$$

Using the dimensionless variables similar to constant rate, the solution for linear transient flow for constant BHP at x=0, for a hydraulically fractured well with fracture half-length of x_f can be approximated as

$$\frac{\Delta p}{q}=\frac{25.54}{A_f}\sqrt{\frac{t}{k\varphi\mu c_t}}+\frac{kh}{141.2qB\mu}s_f \tag{94}$$

Note that the inverse of this solution for linear transient flow at constant bottom-hole pressure has the general form

$$\frac{\Delta p}{q}=m_L t^{1/2}+b_L s_f \tag{95}$$

And derivative of

$$t\frac{\partial(\frac{\Delta p}{q})}{\partial t}=\frac{1}{2}m_L t^{1/2} \tag{96}$$

Cinco-Ley et al. (1981) proposed the solution for the bilinear flow. Bilinear flow means that there are two simultaneous linear flows, linear flow from within the stimulated rock to the fracture face, and linear flow within the fracture to the wellbore. For bilinear flow to occur, the fracture must have a finite conductivity (C_{fD} < 300). In our work, it is always assumed that the fracture has infinite conductivity, so bilinear flow is of only minor importance in our study (but a component of Ozkan's (2009) tri-linear flow model).

Dimensionless parameters for bilinear flow,

$$(k_f w_f)_D=\frac{k_f w_f}{k x_f} \tag{97}$$

$$p_D=\frac{kh(p_i-p_{wf})}{141.2qB\mu} \tag{98}$$

$$t_D=\frac{0.0002637kt}{\varphi\mu c_t x_f^2} \tag{99}$$

$$n_{fD}=\frac{k_f\varphi c_t}{\varphi_f k c_{ft}} \tag{100}$$

$$CfD_f=\frac{w_f\varphi_f c_t}{\pi\varphi x_f c_t} \tag{101}$$

$$k_f w_f=\pi CfD_f n_{fD} \tag{102}$$

Cinco-Ley (1981) provided the solution to bilinear flow in terms of dimensionless variables for constant rate solution. Including a fracture skin this becomes

$$p_D = \frac{2.45}{\sqrt{(k_f w_f)_D}} t^{1/4}_D + s_f \tag{103}$$

The solution to diffusivity equation in terms of real variables is then

$$\frac{p_i - p_{wf}}{q} = \frac{44.1\ B\mu}{h\sqrt{k_f w_f}\sqrt[4]{\varphi \mu c_t k}} \sqrt[4]{t} + \frac{kh}{141.2 q B\mu} s_f \tag{104}$$

Therefore, solution to bilinear flow has general form and derivative of:

$$\frac{\Delta p}{q} = m_B t^{1/4} + b_B s_f \tag{105}$$

$$t\frac{\partial \frac{\Delta p}{q}}{\partial t} = \frac{1}{4} m_B t^{1/4} \tag{106}$$

For variable rate and BHP, there is no rigorous solution. Analysts commonly use the constant BHP solution for variable rate cases. This is a good approach in most cases. There is a difference in the constant rate and constant BHP solutions, but in both cases $\frac{\Delta p}{q}$ is proportional to $t^{1/2}$ for linear flow, and $t^{1/4}$ for bilinear flow. Therefore, the diagnostic plots have the potential to do a good job in identifying these flow regimes for variable rate production situations. While we identify flow regimes correctly, it may be more difficult to calculate $A_f\sqrt{k}$ correctly since the governing equation is somewhere in between the constant rate and constant BHP cases. However it is probably much closer to the constant BHP case.

At this point, we have summarized derivations of solution to the diffusivity equation for linear and bi-linear flow. In the following sections superposition time and material balance time concepts are briefly presented.

Superposition Time

Many solutions consider the simple operating conditions of either constant rate or constant pressure (see Figure 2).

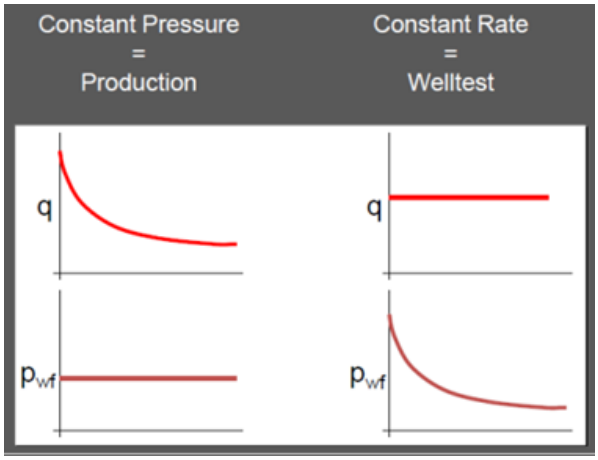

Figure 2—Simplified operating conditions (Fekete 2013)

Actual production includes variable rate and variable pressure data. The principle of superposition in time allows us to overcome the limitation of either constant pressure or constant rate, Figure 3.

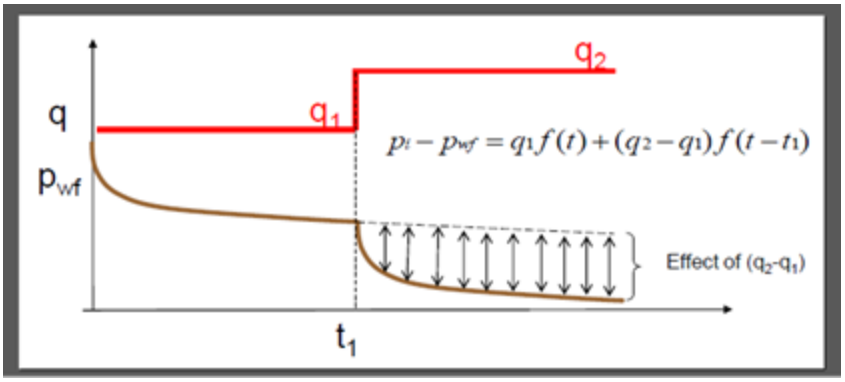

Figure 3—Principle of superposition, example of two rate history (Fekete 2013)

Superposition Time converts multiple rate history into an equivalent single rate history by re-plotting data points at their "superposed" times .

$$\frac{p_i - p_{wf}}{q_N} = \sum_{j=1}^{N} \frac{\left(q_j - q_j - 1\right)}{q_N} f(t - t_j - 1) \qquad (107)$$

As noted before, actual production is at variable rates and variable flowing pressures. Material Balance Time (MBT) is a superposition time function that converts general production conditions into an equivalent constant rate solution (Figure 4). Blasingame et al. (1991) showed that MBT is rigorous for boundary dominated flow, i.e. volumetric depletion. Poe (2002) showed that MBT is also effective for transient flow regimes when constant pressure solutions are used rather than constant rates solutions. To identify flow regimes, superposition time, and material balance time are sometimes used instead of time.

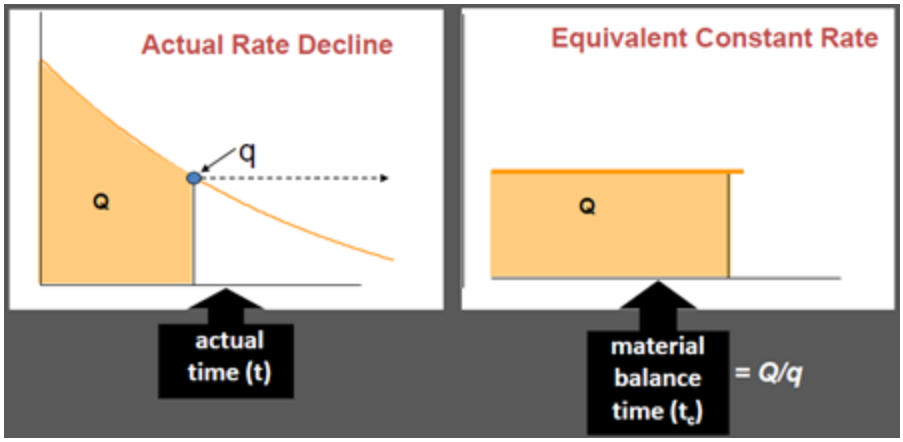

Figure 4—Definition of material balance time (Fekete 2013)

Anderson and Mattar (2003) provided theoretical proof of the validity of MBT for converting boundary dominated production of single phase oil production at constant pressure with smoothly varying rates into an equivalent constant rate.

Anderson and Mattar (2003) developed corrections to convert constant pressure solution to an equivalent constant rate. With dimensionless time corresponding to the constant pressure solution defined as t_{DP}, and for the constant solution as t_{Dr}, they showed that the correction required to convert the constant pressure solution to an equivalent constant rate is to multiply the measured time by 2.46 which only applies during pure linear flow. For converting constant pressure solution to an equivalent constant rate, the material balance time should be multiplied by 1.23.

In Figure 5, they showed the solution for vertical

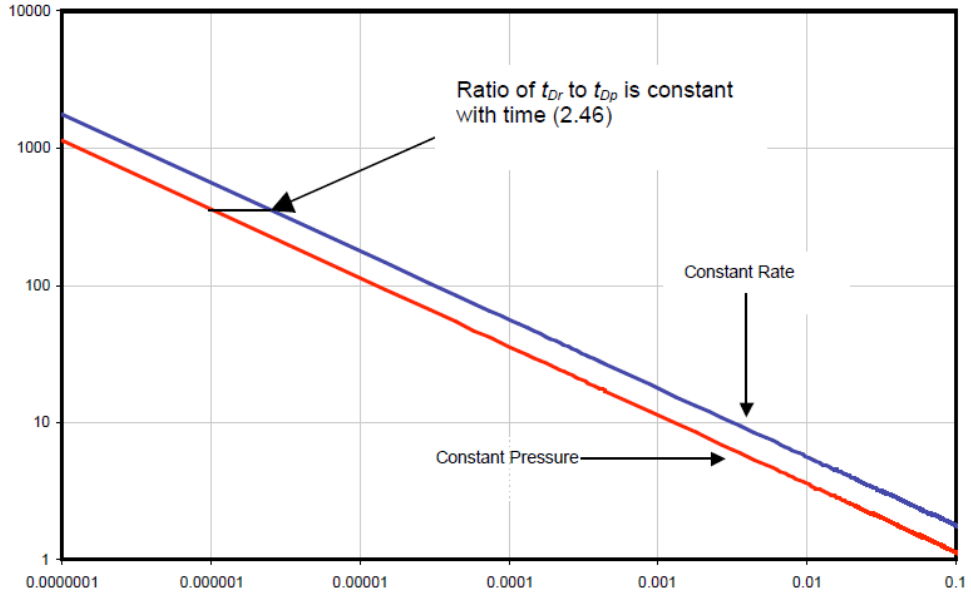

t_D

(a)

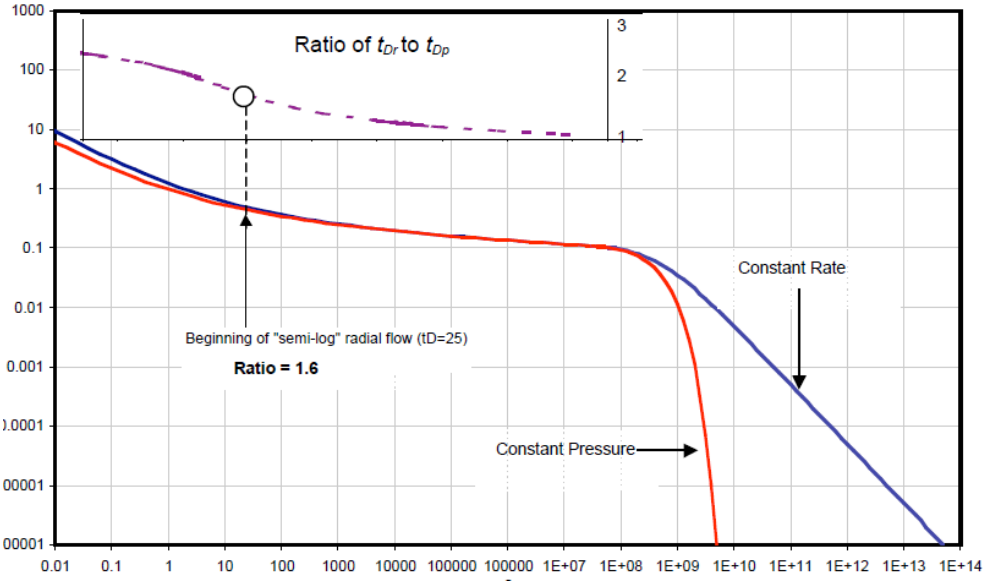

t_D

(b)

Figure 5—Comparison of constant pressure and constant rate solutions (a) for fracture linear flow part (b) for complete solution for cylindrical reservoir with vertical well in center (Anderson and Mattar, 2003)

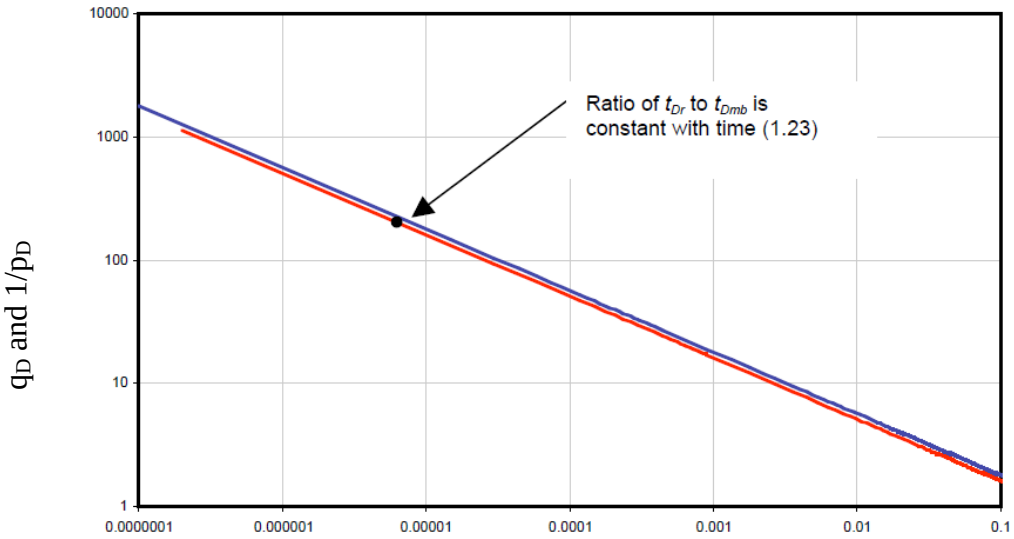

(a)

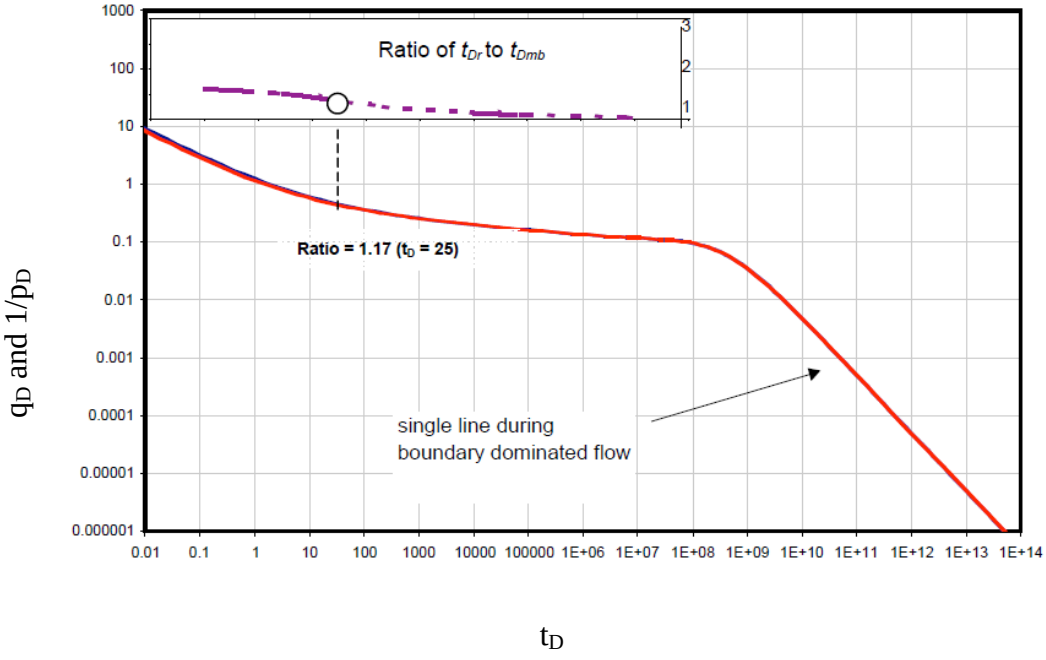

(b)

Figure 6—Comparison of constant pressure (material balance time corrected) and constant rate solutions (a) for fracture linear flow (b) cylindrical reservoir with vertical well in center (Anderson and Mattar, 2003)

As presented in Figures 5 and 6, Anderson and Mattar (2003) showed that during infinite acting flow, MBT is not a rigorous solution. Instead a time superposition function, which follows the observed flow regime, i.e. radial, linear, bilinear, etc., provides a more rigorous conversion to the equivalent constant rate solution. It is common practice to assume a time superposition function that follows the "dominant" flow regime. These include: square root for linear, 4^{th} root for bilinear, MBT for volumetric.

Stimulation Geometry in Hydraulically Fractured Horizontal Wells

Hydraulic fracture stimulation of shale probably results in non-uniform geometry that is difficult to predict. Nevertheless, defining a specific geometry of fracture stimulation is a necessary starting point for developing any type of prediction. This is equally important in analytical and in numerical modeling. Therefore assumptions have to be made about geometry, and often assuming a uniform geometry of some sort is required for a reasonably efficient prediction methodology. Although much effort has gone into refining our understanding of what the stimulation geometry may be, there is still no consensus on this topic. Microseismic studies seem to suggest certain shapes of stimulated region; however, there have been studies where microseimic predictions do not agree with production logs, and most of this information is not publicly available yet. The literature on expected flow geometry in MFHW's is reviewed in CHAPTER III. In the course of this study, stimulation geometry is always assumed to be uniform around the wellbore with identical fracture stages as shown in Figure 7. Identical stage geometries allow us to take advantage of symmetry in modelling, as it can be assumed that an identical unit of the reservoir is repeated over and over. In analysis of MFHW's in LRS, it is assumed that there are three simultaneous linear fluid flow regimes: from the unstimulated matrix into the stimulated rock, from within the stimulated rock volume to the fracture, and from the fracture to the wellbore as shown in Figure 8.

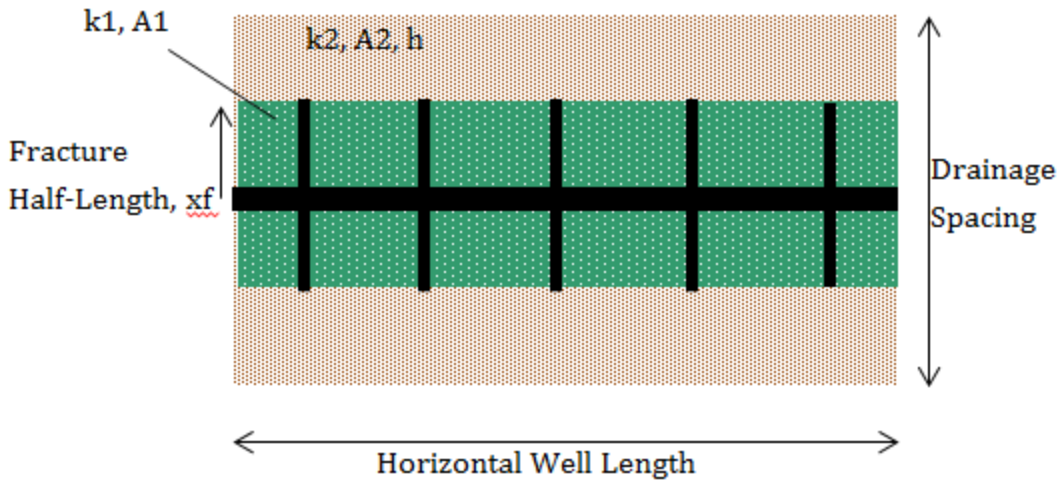

Figure 7—Stimulation geometry for a multi-fractured horizontal well

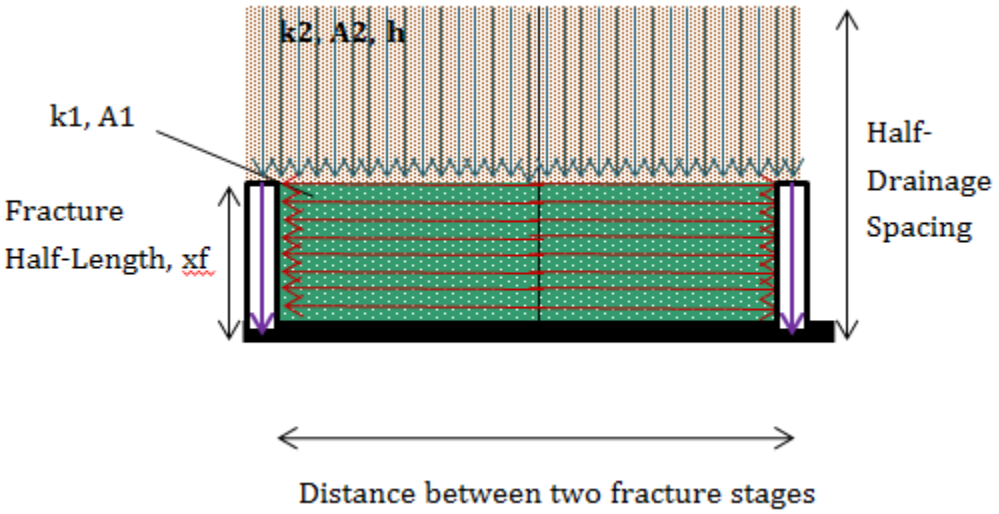

Figure 8—Linear flow regimes between two fracture stages in a multi-fractured horizontal well

In MFHW's where long, highly conductive vertical fractures exist, the common flow In MFHW's where long, highly conductive vertical fractures exist, the common initial flow regime is linear flow. In fact, in MFHW's, due to the contrast that is often observed

between the permeability of the matrix, the permeability of the simulated zone, and the conductivity of the fracture, multiple linear flows may exist simultaneously.

For a case of single phase oil production in a MFHW, flow is expected to go through an initial linear flow period, a second linear, or possibly bilinear flow when simultaneous flow into the fracture and within the fracture occurs. Linear flow from outside the SRV into the SRV may also be occurring at the same time. As presented earlier, after the fracture skin term becomes negligible, the linear flow regime can be identified with ½ slope on log-log plot of pressure-normalized rate versus time. Given a sufficiently long time, which may not occur during the economic life of a well, the flow is expected to become boundary-dominated; the signature of this is a unit slope on the log-log plot of pressure normalized rate versus material-balance time (Figure 9).

In practice, in production of shale oil where multiphase flow exists, it is rare to see the clear distinction between flow regimes and therefore we have to make assumptions about stimulation geometry, and therefore types of flow regimes.

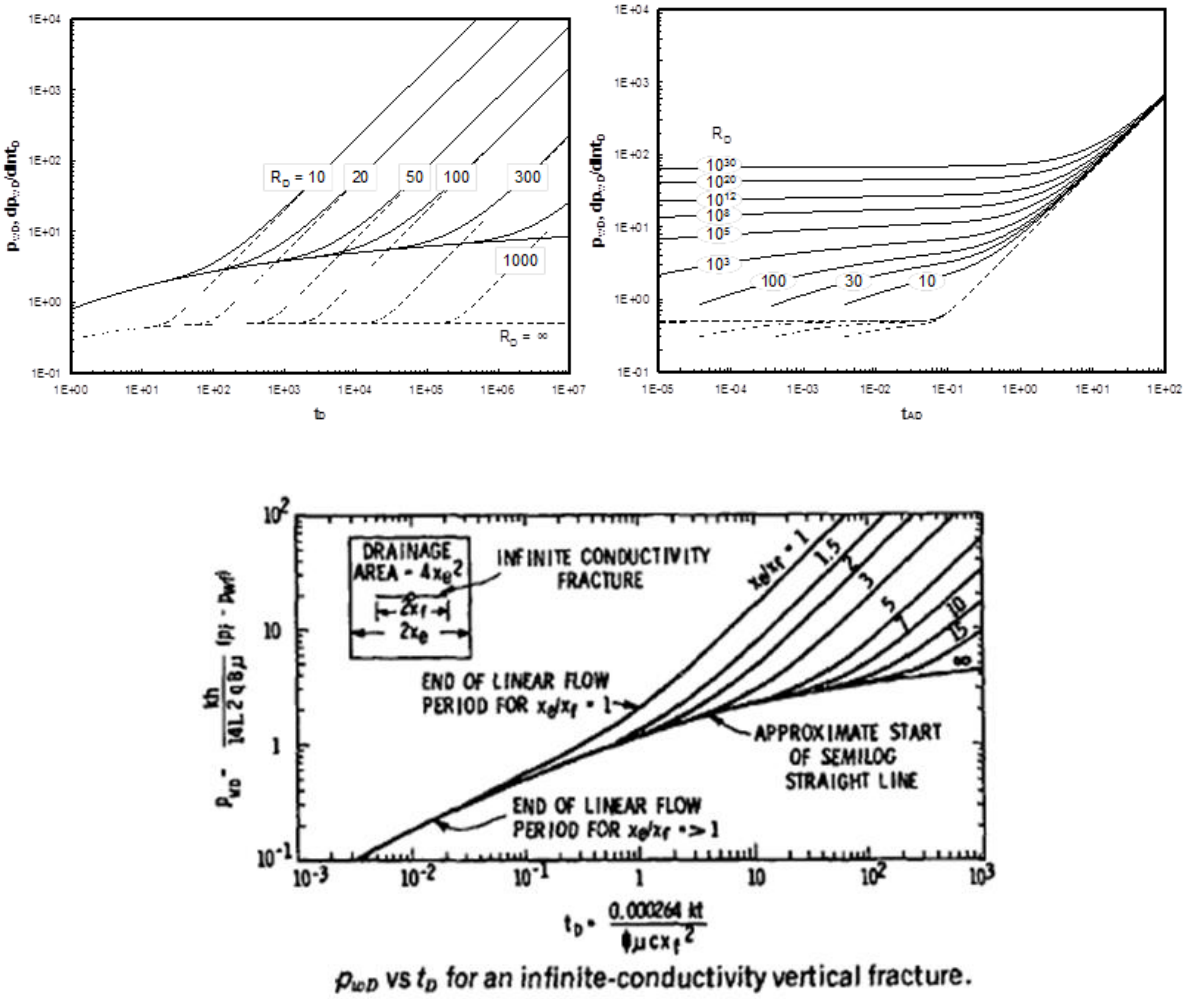

Figure 9—Examples of linear flow regime and transition into boundary-dominated flow (Gringarten et al. 1975)

Theory of Trilinear-Flow Model for Fractured Horizontal Wells

Overview and Assumptions

Miller, Jenkins et al. (2010) suggest that, in production of MFHW's in shale reservoirs, an internal linear transient flow regime occurs initially within the stimulated rock volume, followed by boundary dominated flow when the pressures between fractures

interfere, followed by an external transient linear flow from the drainage volume outside of the stimulated rock, and finally a boundary dominated flow if and when the pressure drawdown reaches the well's drainage boundary. In the very low permeability (nano- to micro-Darcy) LRS plays, the latter boundary dominated flow may not happen during the economic life of a well.

Flow in hydraulically fractured horizontal wells with finite conductivity fractures is further complicated with a possible third linear flow regime. With the assumption of single phase flow, either gas or oil, the solution to the tri-linear flow is the basis for most analytical evaluations to history match production and forecast flow in MFHW's. The important point to note is this analytical solution, like the others mentioned in this chapter, cannot model multiphase flow properly. The solution for tri-linear flow for liquids in terms of dimensionless variables is shown below. This solution (Ozkan 2009) is the basis for all analytical evaluations in this study.

Ozkan et al. (2009)'s trilinear solution is based on the fact that permeability in unconventional tight rock is much lower than that in conventional systems. Therefore, unlike conventional systems, in tight rock the flow beyond the fracture tips is usually negligible and when present never develops to full radial flow. At best, in tight rock, the flow convergence beyond the fracture tips is linear and perpendicular to the stimulated rock volume. Therefore, Ozkan et al. represented a multi-fractured horizontal well with a system whose long-term performance is analogous to that of a single effective fracture with length equal to that of the spacing between the two outermost fractures and referred to the work of Raghavan et al. (1997). Ozkan et al. (2009) presented a study of performance characteristics of fractured-horizontal wells and presented the solution to the trilinear-flow model.

In this solution, Ozkan et al. refer to fracture conductivity; the schematic of a single hydraulic fracture in Figure 10 is used to describe the definition of fracture conductivity.

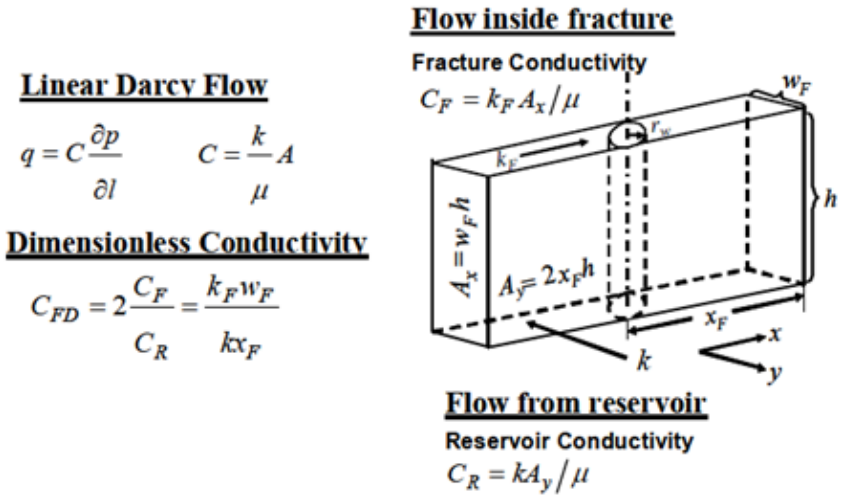

Figure 10—Single hydraulic fracture and definition of conductivity (Ozkan 2009)

As mentioned before, in their work, Ozkan et al. (2009) assumed that the long-term performance of a MFHW can be represented by that of a single hydraulic fracture with dimensions as shown in Figure 11.

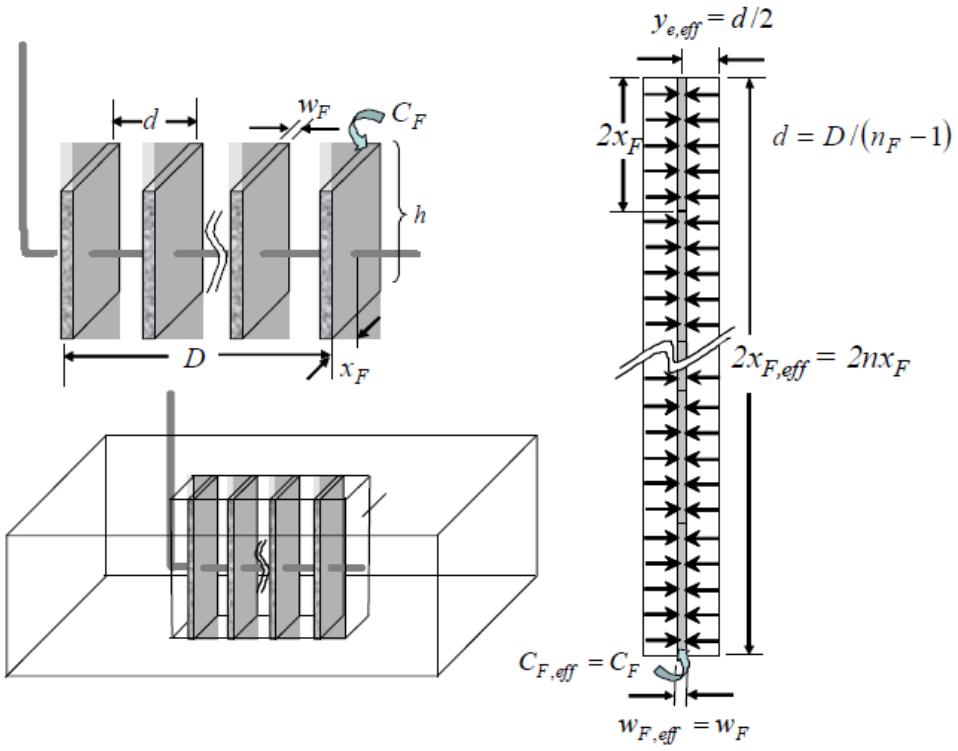

Figure 11—Effective fracture concept for a multi-fractured-horizontal-well (Ozkan 2009)

This assumption is problematic: for finite-conductivity fractures, the flux into each individual fracture is far from uniform, being greater near the tip of the fracture than near the wellbore. Representing all fractures as a single fracture is thus quite unrealistic. In our study, we avoided this problem by assuming infinite fracture conductivity. Ozkan et al. (2009) then use the single effective hydraulic fracture properties to describe the performance of the MFHW in terms of effective fracture conductivity, and effective fracture half length, as illustrated in Figures 11 and 12.

$$C_{f,eff} = \frac{k_f w_f h_f}{\mu} \tag{108}$$

$$x_{f,eff} = n_f x_f \tag{109}$$

$$y_{e,eff}=\frac{D}{2(n_f-1)} \tag{110}$$

Ozkan et al. (2009) further assumed that, for the productive life a MFHW, three linear flow regimes dominate performance of the well. These include the outer reservoir, the inner reservoir between the fractures, and within the hydraulic fracture. The total production in a well is the sum of flow in each hydraulic fracture stage. See Figure 12.

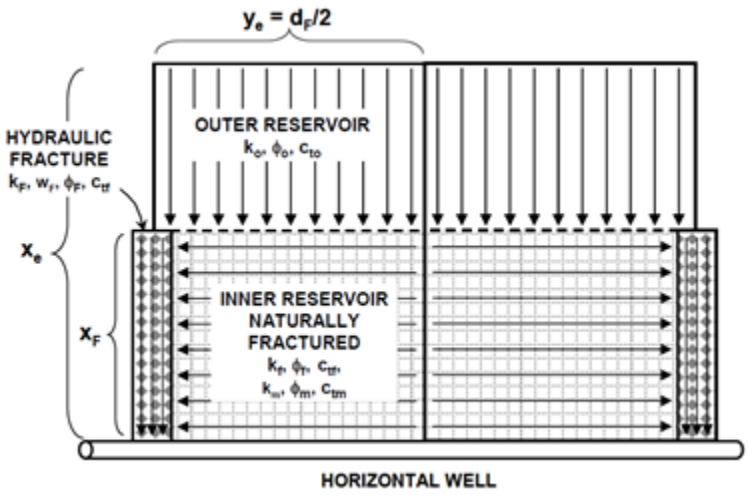

Figure 12—Schematic of the trilinear-flow model used for the analytical solution of the MFHW performance (Ozkan 2009)

In Ozkan et al.'s (2009) derivation of trilinear-flow model, and in this work, it is assumed that identical hydraulic fracture stages are uniformly distributed along the wellbore and therefore average fracture properties are used.

In case of MFHW's in LRS where production is impossible without stimulation of matrix, the inner reservoir consists of a stimulated rock volume. In Ozkan et al.'s (2009) work, and also in this work, the properties in the stimulated rock volume are assumed to

be uniform and the same as matrix or outer reservoir with the exception of permeability, k_{SRV} .

Solution to Tri-Linear Flow Model

Brown et al. 2009 derived the solution for the outer reservoir, the inner reservoir, and within the hydraulic fracture, and then the solutions were coupled using flux and pressure continuity conditions at the interferences between the regions. Solution to the trilinear flow model in Ozkan et al.'s (2009) work is presented in terms of dimension variables listed in equations (111) through (165). Some of the major steps in deriving the trilinear solution for the homogenous inner reservoir with slightly compressible fluid from Brown et al.'s work are highlighted as well.

Dimensionless flowing bottom-hole pressure, p_{wD} for liquid flow:

$$p_{wD}=\frac{k_I h}{141.2 q_f B\mu}\left(p_i-p_{wf}\right) \tag{111}$$

where q_f is the flow rate for each hydraulic fracture (stb/d).

In this work, the inner reservoir permeability between hydraulic fracture stages is described with matrix properties and an enhanced permeability, k_{SRV}. h defined as the height growth of fractures; in this work, it is assumed to be the same as the thickness of the formation.

$$k_I h=k_{SRV} h \tag{112}$$

Dimensionless time:

$$t_D=\frac{2.637\times 10^{-4} k_I t}{[(\varphi c_t)_I]_i \mu_i x_f^2} \tag{113}$$

t in hours, and $(\varphi c_t)_I=(\varphi c_t)_{SRV}$ for stimulated rock volume inner zone. $(\varphi c_t)_{SRV}$ is the porosity-compressibility product of the stimulated rock volume and is assumed to be the same as that of the matrix.

Dimensionless variable definitions for the reservoir and fracture geometry and conductivities are listed below (see Figure 12):

$$x_{eD}=\frac{x_e}{x_f} \tag{114}$$

$$y_{eD}=\frac{y_e}{x_f} \tag{115}$$

$$w_{FD}=\frac{w_f}{x_f} \tag{116}$$

$$c_{FD}=\frac{k_f w_f}{\tilde{k}_I x_f} \tag{117}$$

$$c_{RD}=\frac{\tilde{k}_I x_f}{k_o y_e} \tag{118}$$

Diffusivity ratios are also defined:

$$\eta_{fD}=\frac{\eta_f}{\eta_I} \tag{119}$$

$$\eta_{OD}=\frac{\eta_O}{\eta_I} \tag{120}$$

where η_I is diffusivity of the inner reservoir and η_F and η_O are diffusivities of the hydraulic fracture and the outer reservoir, respectively. They are defined as

$$\eta_f=2.637\times 10^{-4}\frac{k_{Ff}}{(\varphi C_t)_f \mu} \tag{121}$$

$$\eta_O=2.637\times 10^{-4}\frac{k_O}{(\varphi C_t)_O \mu} \tag{122}$$

Solution for the outer reservoir (Brown et al. 2009):

Assuming 1D flow in the x-direction, the diffusivity equation and the boundary conditions for the outer reservoir are given by

$$\frac{\partial^2 \bar{p}_{OD}}{\partial x_D^2}-\frac{x}{\eta_{OD}}\bar{p}_{OD}=0 \tag{123}$$

$$\left(\frac{\partial \bar{p}_{OD}}{\partial x_D}\right)_{x_D=x_{eD}} = 0 \tag{124}$$

$$\bar{p}_{OD}|_{x_D=1} = \bar{p}_{ID}|_{x_D=1} \tag{125}$$

The bars indicate dimensionless pressures in the Laplace domain, and s is the Laplace transform parameter with respect to dimensionless time, t_D. The outer reservoir solution in the Laplace domain is

$$\bar{p}_{OD} = \bar{p}_{ID}|_{x_D=1} = \frac{\cosh\left[\sqrt{s/\eta_{OD}}\,(x_{eD}-x_D)\right]}{\cosh\left[\sqrt{s/\eta_{OD}}\,(x_{eD}-1)\right]} \tag{126}$$

Solution for the inner reservoir (Brown et al. 2009):

Assuming 1D flow in the y-direction, the diffusivity equation and the boundary conditions for the inner reservoir are

$$\frac{\partial^2 \bar{p}_{ID}}{\partial y_D^2} + \left(\frac{1}{y_{eD} C_{RD}}\right) \frac{\partial \bar{p}_{OD}}{\partial x_D}|_{x_D=1} - u\bar{p}_{ID} = 0 \tag{127}$$

where

$$u = sf(s) \tag{128}$$

and for a homogeneous inner reservoir

$$f(s) = 1 \tag{129}$$

Substituting from (126),

$$\frac{\partial \bar{p}_{OD}}{\partial x_D}|_{x_D=1} = -\beta_O \bar{p}_{ID}|_{x_D=1} \tag{130}$$

where

$$\beta_O = \sqrt{s/\eta_{OD}}\tanh\left[\sqrt{s/\eta_{OD}}(x_{eD}-1)\right] \tag{131}$$

and assuming $p_{ID} \neq f(x_D)$ equation (127) becomes

$$\frac{\partial^2 \bar{p}_{ID}}{\partial y_D^2} - \alpha_O \bar{p}_{ID} = 0 \tag{132}$$

where

$$\alpha_O = \frac{\beta_O}{y_{eD} C_{RD}} + u \tag{133}$$

The boundary condition for the reservoir is given by

$$\left(\frac{\partial \bar{p}_{ID}}{\partial y_D} \right)_{y_D = y_{eD}} = 0 \tag{134}$$

and

$$\bar{p}_{ID}|_{y_D = w_D/2} = \bar{p}_{FD}|_{y_D = w_D/2} \tag{135}$$

The solution to inner reservoir with these boundary conditions is

$$\bar{p}_{ID} = \left(\bar{p}_{FD}|_{y_D = w_D/2} \right) \frac{\cosh\left[\sqrt{\alpha_O} (y_{eD} - y_D) \right]}{\cosh\left[\sqrt{\alpha_O} (y_{eD} - w_D/2) \right]} \tag{136}$$

which relies on the hydraulic fracture solution $\bar{p}_{FD}|_{y_D = w_D/2}$.

Solution for the hydraulic fracture (Brown et al. 2009):

$$\frac{\partial^2 \bar{p}_{FD}}{\partial x_D^2} + \frac{2}{C_{FD}} \frac{\partial \bar{p}_{ID}}{\partial y_D}|_{y_D = w_D/2} - \frac{s}{\eta_{FD}} \bar{p}_{FD} = 0 \tag{137}$$

From equation (136),

$$\frac{\partial \bar{p}_{ID}}{\partial y_D}|_{y_D = w_D/2} = -\beta_F \bar{p}_{FD}|_{y_D = w_D/2} \tag{138}$$

Then equation (137)

$$\frac{\partial^2 \bar{p}_{FD}}{\partial x_D^2} + \frac{2}{C_{FD}} \frac{\partial \bar{p}_{ID}}{\partial y_D}|_{y_D = w_D/2} - \frac{s}{\eta_{FD}} \bar{p}_{FD} = 0 \tag{137}$$

becomes

$$\frac{\partial^2 \bar{p}_{FD}}{\partial x_D^2} - \alpha_F \bar{p}_{FD} = 0 \tag{139}$$

In equations (138) and (139),

$$\beta_F = \sqrt{\alpha_O} \tanh\left[\sqrt{\alpha_O}\left(y_{eD} - \frac{w_D}{2}\right)\right] \tag{140}$$

$$\alpha_F = \frac{2\beta_F}{C_{FD}} + \frac{s}{\eta_{FD}} \tag{141}$$

with boundary conditions

$$\frac{\partial \bar{p}_{FD}}{\partial x_D}\Big|_{x_D=1} = 0 \tag{142}$$

and

$$\frac{\partial \bar{p}_{FD}}{\partial x_D}\Big|_{x_D=0} = \frac{\pi}{C_{FD} s} \tag{143}$$

The dimensionless pressure solution for the hydraulic fracture is

$$\bar{p}_{FD} = \frac{\pi}{C_{FD} s \sqrt{\alpha_F}} \frac{\cosh[\sqrt{\alpha_F}(1-x_D)]}{\sinh(\sqrt{\alpha_F})} \tag{144}$$

The wellbore pressure solution at $x_D=0$ in (144) is

$$\bar{p}_{wD} = \bar{p}_{FD}(x_D=0) = \frac{\pi}{C_{FD} s \sqrt{\alpha_F} \tanh(\sqrt{\alpha_F})} \tag{145}$$

So far, it was assumed that the flow is linear within the hydraulic fracture. To account for the radial convergence of flow toward the wellbore within the hydraulic fracture and adding the choking skin (146) to equation (145),

$$s_c = \frac{k_I h_I}{k_F w_F}\left[\ln\left(\frac{h}{2r_w}\right) - \frac{\pi}{2}\right] \tag{146}$$

the solution to the trilinear flow for a MFHW in Laplace domain is

$$\bar{p}_{wD}=\frac{\pi}{C_{FD}s\sqrt{\alpha}\tanh\left(\sqrt{\alpha}\right)}+\frac{s_c}{s} \tag{147}$$

Wellbore storage to take into account early times is defined as

$$\bar{p}_{wD,\ storage}=\frac{\bar{p}_{wD}}{1+C_D s^2\bar{p}_{wD}} \tag{148}$$

where C_D is given by

$$C_D=\frac{5.615C}{2\pi(\varphi ch_t)_I x_F^2} \tag{149}$$

To simplify the complex multiphase flow in MFHW's in LRS plays, in addition to identifying dominant flow regimes, it is important to also determine the dominant fluid phase. For example, can the initial linear flow regime be dominated by single-phase flow of oil, in which case analytical solutions readily available can be used to describe the flow and forecast production? The following section provides an overview of the reservoir fluids.

Reservoir Fluids

Unconventional tight reservoirs, with ultra-low permeabilities, include all categories of reservoir fluids, i.e., black oil, volatile oil, retrograde condensate, wet gas, and dry gas. The industry has much better experience in dealing with forecasting production in gas reservoirs simply because the reservoir remains mostly in a single phase. It is when the flowing bottom-hole pressures drop below saturation pressures that the problem becomes challenging. For liquid-rich shale reservoirs where the in-situ fluid is volatile oil or black oil, and due to steep pressure declines, the reservoir fluid inevitably drops below saturation pressure and 2-phase flow begins early in the production life of the well (see Figure 13).

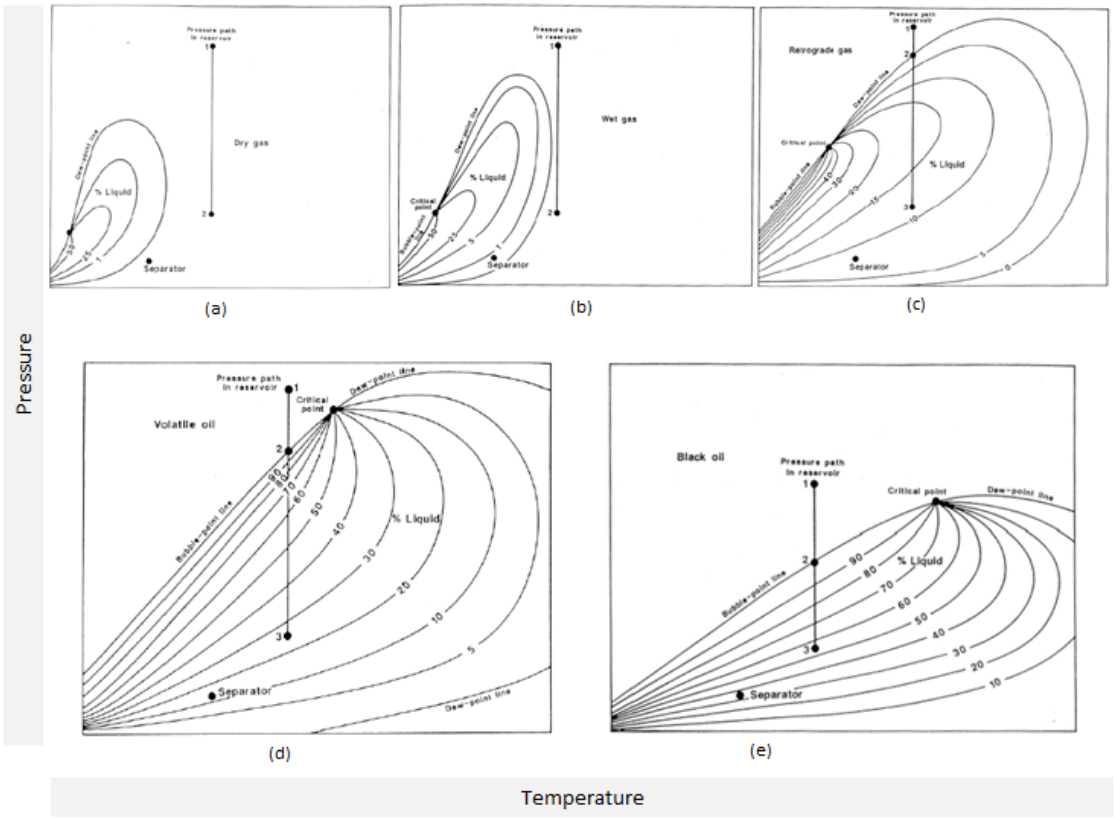

Figure 13—Phase envelopes for the five reservoir fluids. (a) dry gas, (b) wet gas, (c) retrograde condensate, (d) volatile oil, (e) black oil (McCain 1990).

It is worth noting that sampling and characterization of fluids in liquid rich shale plays remain a challenge. This is because, due to the very tight rock, sampling prior to stimulation is not possible. After stimulation and significant disturbance to pressure and addition of fracturing fluid, the well has to be allowed to clean up. Due to very large permeability contrasts near the well bore and further away from the wellbore, significant pressure drops are expected. This leaves a small window for collecting a representative reservoir fluid before the bottom-hole pressure drops below saturation pressure.

Once the fluid samples are collected, laboratory analysis such as compositional analysis, constant composition expansion, differential liberation, separator test, and viscosity

measurements are carried out to characterize the fluid. An equation of state, for example, Peng and Robinson, may be used to define the fluid. The laboratory measurements are then used to tune the equation of state (McCain 1990).

Depth of Investigation

Lee (1982) used the impulse function for the instantaneous line source (Carslaw and Jaeger, 1959), to derive the depth of investigation for radial flow. Note that the impulse function for the instantaneous plane source does not depend on the inner boundary condition (constant rate or constant BHP). Therefore, the depth of investigation is also independent of the inner boundary condition. The derivation for the depth of investigation for transient linear flow using a similar approach as Lee (1982) is outlined below.

The impulse function for an instantaneous plane source in an infinite medium presented by Carslaw and Jaeger (1959) provides the solution to the diffusivity equation for linear flow,

$$p_{wf}-p_i=\frac{c_1}{\sqrt{t}}e^{-x^2/4\eta t} \tag{150}$$

where c_1 is a constant, related to the strength of the instantaneous source, and hydraulic diffusivity, η, is

$$\eta=\frac{0.0002637k}{\phi\mu c_t}=\frac{k}{3{,}792\phi\mu c_t} \tag{151}$$

The time at which the pressure disturbance is at a maximum at d_i is found by differentiating and setting the result equal to zero,

$$\frac{dp}{dt}=\frac{-c_1}{2t^{3}/_{2}}\ e^{-x^2/4\eta t}+\frac{c_1 x^2}{4\eta t^{5}/_{2}}\ e^{-x^2/4\eta t}=0 \tag{152}$$

Solving for the time t at which the pressure disturbance is a maximum at a distance x = d_i,

$$t=\frac{d_i^{\,2}}{2\eta} \tag{153}$$

Thus, for both constant rate and constant BHP production, depth of investigation, d_i, is

$$d_i=\sqrt{\frac{kt}{1{,}896\ \phi\mu c_t}} \tag{154}$$

where time, t, is in hours.

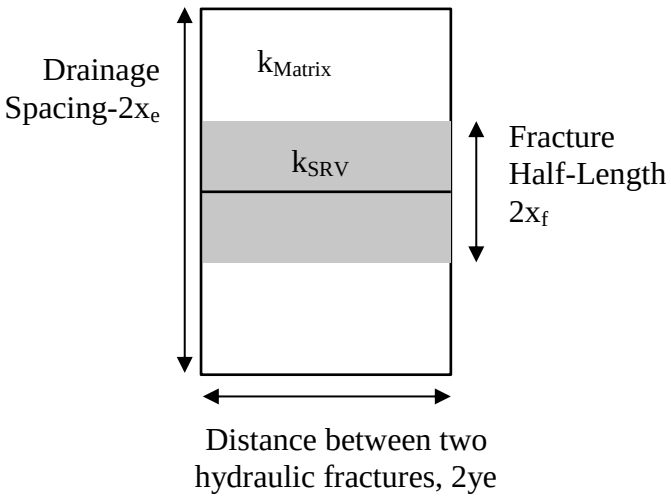

Figure 14—Schematic of a single hydraulic stimulation stage

For a single hydraulic stimulation stage as shown in Figure 14 , with hydraulic fractures at 200m spacing, with a range of permeability values in the SRV of 0.001 to 3.2 mD,

fractures may interfere at times from less than a day to 195 days. Therefore, depending on the SRV permeability, the ½ slope signature of linear flow on log-log plots may or may not be clearly identifiable.

Let us consider a few values of permeability both inside the stimulated rock volume (SRV) and outside, in the matrix, Table 5.

Permeability (mD)	x_e (ft)	x_f (ft)	Distance (ft)	Time (days)	Comments
1.0 e-3	-	-	200	195	Frac interference within 6 mon
3.2 e 1	-	-	200	<1	Frac interference immediate
1.0 e-5	660	150	360	63,500	BDF will not be observed
8.0 e-3	660	150	360	79	BDF should be observed
1.0 e-5	660	30	600	4,230,400	BDF will not be observed
8.0 e-3	660	30	600	220	BDF should be observed

Table 5—Depth of investigation for selected values of permeability

Using depth of investigation, we can also estimate the time at which boundary dominated flow begins. Provided that the matrix permeability is large enough, for fixed drainage spacing, increasing x_f shortens time to boundary-dominated flow. In most LRS plays, the matrix permeability is not expected to allow the pressure transients to reach the drainage boundaries of a well during its economic life. It is, however, important to consider the possibility of boundary-dominated flow and include it in predictions.

Fetkovich (1980) presented the constant pressure analytical solution for slightly compressible, single-phase radial flow in terms of dimensionless rate and dimensionless time as stated in equations (155) and (156). In equation (156), real time is in days.

$$q_D = \frac{141.2\ q(t)\mu B}{kh(p_i - p_{wf})} \tag{155}$$

$$t_D = \frac{0.00633kt}{\varphi\mu c_t r_w^2} \tag{156}$$

Using a similar approach, we defined dimensionless rate and dimensionless time for linear flow in MFHW's as shown below. These definitions provide the basis for converging the production histories and identifying the trend beyond a transition time, as we will discuss in more detail in following chapters.

$$q_{oil\ D} = \frac{q_{oil}(t)\mu_{oil}}{k_{mat}h(p_i - p_{wf})} \tag{157}$$

$$t_D = \frac{k_{mat}t}{\varphi c_t \mu_{oil}(2x_e - 2x_f)^2} \tag{158}$$

CHAPTER III

PRODUCTION DATA ANALYSIS

The objective of this work is to develop a technique that can be applied to production of multi-fracture horizontal wells (MFHW's) in liquid rich shale (LRS) to forecast production of oil and gas. Techniques for analyzing production data and forecasting flow are not new; robust techniques date back to the early 1900's. Applicability of these forecasting techniques to the MFHW's in LRS's with limited amounts of production data is the major issue addressed in this chapter.

Much work has been done to provide analysis and interpretation methods of production data in conventional resources. With much interest in exploitation of unconventional resources, production analysis techniques are being extended to include low and ultra-low permeability reservoirs including tight oil and gas, and shale oil and shale gas. El-Banbi and Wattenberger (1998) provided methods for analyzing production during linear flow. Clarkson et al. (2013) provide systematic methods for analyzing production data in Coalbed Methane and tight gas. Medeiros et al. (2008) developed a semi-analytical solution to model the production performance of fractured horizontal wells. Cheng el at. (2008) presented procedures for decline curve analysis in multilayer tight gas reservoirs. Lewis and Hughes (2008) developed a method to analyze production data from shale-gas wells with a modified material balance time function. Ilk et al. (2008a) presented an empirical power-law exponential rate decline model for decline curve analysis. Valko and Lee (2010) presented a different form of power-law exponential decline model to analyze production data for Barnett Shale producers.

Production analysis can be divided into conventional and modern techniques. Empirical decline curve analysis (DCA) and type curves (TC) are covered under conventional

techniques. Diagnostic methods and rate transient analysis (RTA) are covered under modern techniques. It is important to note that, although none of these techniques are fully applicable to MFHW's in LRS, they help in breaking down this complex problem into manageable parts where some of the conventional methodology might be applicable. RTA as it applies to MFHW's in LRS's based on trilinear flow model is covered in CHAPTER VI.

Conventional Production Analysis Techniques

Conventional production analysis started in the 1920's and in 1945 Arps published empirical exponential, hyperbolic, and harmonic rate decline models (Arps, 1945) for constant BHP production. In the 1960's Fetkovich developed new decline type curves, still with the underlying assumption of constant flowing pressure, where he combined two families of type curves for transient and boundary dominated flow periods. Numerous other type-curves were developed later for gas wells, layered and fractured reservoirs, etc. Blasingame et al. (2009) introduced a variable rate/variable pressure type-curve as a log-log plot of productivity index versus material balance time. Additional solutions accounted for various well and reservoir configuration and have recently been implemented in commercial software.

Conventionally, analysts fit historical trends of production data empirically, either graphically or with decline models. The historical trends were then extrapolated to forecast production. Since empirical curve fitting of historical production is based on analogy, it assumes that the operating conditions remain constant, therefore all estimates rely on the assumption that no variability of flow regimes and boundary conditions occur for the life of the well. Conventional methods are advantageous in the sense that they are easy and convenient to use, but they are limited as they implicitly assume operating conditions remain constant, which is not the case with MFHW's in LRS's. Also, empirical production analysis provides very limited information, if any, about the

reservoir. Following is a brief review of some common decline curve analysis, type curves, and some recent advanced decline curve analysis techniques.

Arps Decline Curve Analysis

The work by Arps (1945) has been used in analysis of production data for many years. The theoretical basis for Arps' decline equation is that production was at constant BHP and the well/reservoir flow in the boundary dominated flow regime. In other words, for the life of the well, there is no transient flow; productivity index, and radius of drainage all were assumed to be constant. These conditions are required to support the single most important assumption in using Arps' hyperbolic decline model, i.e., constant decline parameter b (Arps, 1945). Furthermore, it is assumed that the skin factor remain constant over time. Although the assumptions in Arps decline model are sufficient evidence that this technique does not apply to the highly transient MFHW's in LRS plays, a brief overview of the technique and definition of decline parameters is presented below. Arps model parameters are important because complex evaluations for a certain area of interest could be converted to Arps model parameters that can be readily applied to individual wells. Arps model parameters are useful in describing specific scenarios where the assumptions might partially hold. For example, once the initial transient flow of the MFHW ends, the remaining flow might behave similarly such that a set of general decline parameters might be sufficient to predict a part of future production. There will be a more in depth discussion about this possibility in subsequent chapters.

Arps decline model parameters are described in the following equations.

Arps' defined decline rate, D (1/time):

$$D=-\frac{\frac{dq}{dt}}{q} \tag{159}$$

and loss ratio, b, as change in 1/D with time:

$$b=\frac{d(\frac{1}{D})}{dt} \tag{160}$$

He observed that, for most wells he studied, b was constant.

Integration assuming constant b leads to Arps' hyperbolic decline model:

$$q(t)=\frac{q_i}{(1+bD_it)^{\frac{1}{b}}} \tag{161}$$

When b=0, the decline is referred to as exponential. For 0<b<1, decline is referred to as hyperbolic, for b=1, decline is referred to as harmonic.

The general approach for defining the decline parameters consists of determining the three parameters, q_i, b, and D, directly by non-linear regression of historical production. Once decline parameters have been obtained, it is possible to estimate ultimate recovery to a specified economic limit rate. Decline rates may be expressed as nominal (or instantaneous) or effective decline rates.

Some Typical decline exponent, b, values are tabulated in Table 6:

Drive Mechanism	Typical b
Typical volumetric gas reservoir, Boundary Dominated flow, Constant Flowing Bottom Hole Pressure	0.4
Typical volumetric solution-gas drive reservoir, Boundary Dominated flow, Constant Flowing Bottom Hole Pressure	0.3
Layered Volumetric Oil or Gas Reservoir, Constant Flowing Bottom Hole Pressure	0.6-0.8
Low Permeability Oil or Gas Reservoir, Transient Formation Linear flow, Constant Flowing Bottom Hole Pressure	2

Table 6—Typical values of decline exponent for some drive mechanisms

One of the major issues with using decline curve analysis is that under certain circumstances, particularly transient or unstabilized flow, the best-fit b can be greater than 1. However, as shown in the following equations, b greater than 1 leads to infinite ultimate recovery. For example, transient linear flow leads to a b of 2. This is often observed in initial flow of MFHW in LRS plays.

b=0:
$$\lim_{t\to\infty} N_p(t) = \lim_{q(t)\to 0} \frac{q_i - q(t)}{D_i} = \frac{q_i}{D_i} \tag{162}$$

b<1:
$$\lim_{t\to\infty} N_p(t) = \lim_{q\to 0} \frac{q_i^b}{D_i(1-b)} (q_i^{1-b} - q^{1-b}) = \frac{q_i}{D_{i(1-b)}} \tag{163}$$

b=1:
$$\lim_{t\to\infty} N_p(t) = \lim_{q\to 0} \frac{q_i}{D_i} \ln\left(\frac{q_i}{q}\right) = \infty \tag{164}$$

b>1:
$$\lim_{t\to\infty} N_p(t) = \lim_{q\to 0} \frac{q_i^b}{D_i(1-b)} (q_i^{1-b} - q^{1-b}) = \infty \tag{165}$$

For a robust prediction, there must always be a final flow regime where b is less than 1; this avoids estimates of infinite ultimate recovery. In analysis of MFHW's, it is often observed that, due to perceived lack of better alternatives, analysts tend to use multi-segment Arps decline models where b greater than 1 is required to fit early transient data, and to avoid overestimating production, a subsequent decline segment with b value of less than 1 (often 0) for decline to the final rates is used. The main issue with this is that additional decline segments introduce more uncertain decline parameters, which can lead to greater uncertainty in forecasting. In summary, Arps' decline model is not valid for unconventional reservoirs where transient flow dominates much of the life of the well. The errors in predicting reserves using a single b factor increase with less production history and higher initial b factor. Still, Arps decline models, based on physical principles and defined appropriately, can help simplify complex problems by identifying parts of the forecast where the assumptions of the Arps model hold.

Type Curves

Type curves are mathematical/graphical models of reservoir and well systems, usually presented using dimensionless variables. They usually assume constant operating conditions. They are often log-log plots of solutions for various idealized reservoir models. They are basically solutions to flow equations presented graphically for a particular reservoir model and operating conditions. When the reservoir is as assumed in developing the type curves, actual field data compared with the solutions provides a description of the reservoir and flow parameters. When the assumptions of constant operating conditions are valid, type curves can be valuable tools for interpretation of production and pressure data. For production of MFHW's in LRS plays with significant variations in production rate and bottom-hole pressure, at least during early production, type curves are rarely used. Below is a condensed summary of some of the existing type curves for various applications; there are many that are based on radial flow, and none are applicable to the linear flow in MFHW's. There are currently no type curves available for analysis of multiphase flow from MFHW's in LRS plays.

To overcome the limitation of the boundary-dominated flow requirement for applicability of Arps' decline models, Fetkovich (1980) and Fetkovich et al. (1987) developed type curves to forecast production and characterize reservoir parameters. The transient solutions on the Fetkovich type curve are for transient radial flow, and not transient linear flow as expected in MFHW's. Therefore, they are not applicable to MFHW's. These type curves allowed identification of flow regimes including infinite acting reservoir flow and boundary dominated flow. Curve fitting leads to characterization of the reservoir by estimating permeability, drainage area, and skin factor. By presenting both periods, the type curve helps us avoid incorrectly matching transient data on decline curves. The Fetkovich type-curve was developed assuming slightly compressible liquid flow and constant flowing pressure; extensions can be made to gas. The challenge with type curves, including Fetkovich's, is that we cannot forecast with confidence until boundary dominated flow is observed. As mentioned earlier, MFHW's could be in transient flow for the life of the well.

Araya and Ozkan (2002) presented important points about use of type curves for vertical, fractured, and horizontal wells. Fuentes-Cruz et al. (2004) extended use of type curves to naturally fractured reservoirs. Blasingame et al. (2007) presented type curves for a system with hydraulic fractures in the center of an elliptical reservoir. To overcome the limitation in Fetkovich's type curve of constant flowing pressure, Blasingame and McCray used a pressure normalized flow rate. They developed a method to transform the variable pressure/variable rate solution into an equivalent constant pressure or constant rate solution by introducing a specific time function.

Recent Advanced Decline Curve Analysis Techniques

There has been much effort in the recent years to modify Arps' simple and practical DCA technique for unconventional reservoir production forecasting. Ilk and Blasingame (2009) developed the power law decline model, and Valko and Lee (2010) developed the stretched exponential decline model. Both models are useful for forecasting single phase gas flow in unconventional resources where a long transient flow period is expected and an Arps decline parameter b greater than 1 is required to history match early production. As mentioned earlier, Arps' model in this case can lead to unrealistically large EUR's; the power law and stretched exponential models address this issue and forecast realistic EUR's. Unfortunately, experience has shown that, given only limited production history, these models can lead to unreliable forecasts. Furthermore, they have been validated only for single phase flow and therefore have not been proved to be applicable to MFHW's in LRS.

Duong (2010) developed a new decline model based on the assumption of transient near-linear flow for the life of the well with no limiting BDF; this method, without modification, has proved to be optimistic and therefore is not valid for our purpose.

Modern Production Data Analysis

Modern production analysis involving analysis of long production histories including both rate and pressure data is often referred to as rate transient analysis (RTA). Modern production analysis is simplified with readily available commercial software. In brief, once production data is input, analytical or numerical models are selected, parameters are set and production data is compared with model response. A typical workflow for modern production data analysis involves these steps:

1- Diagnostics to validate accuracy of data and extract reservoir signals
2- Interpretation and analysis to identify dominant flow regimes and estimate reservoir properties and system parameters and quantify uncertainties. For MFHW's, log-log plots of pressure-normalized rate versus time, or dimensionless time functions may allow identification of linear flow regimes. It is worth mentioning that the linear flow signatures are not always distinguishable as mentioned in the previous chapter.
3- Using analytical or numerical models, history matching to validate interpretation and optimize solution by including complexities
4- Forecasting

Diagnostic Methods

Diagnostic methods are qualitative investigations of data before modeling and analysis. They are intended to be quick and simple, and are a vital component of production data analysis. There are several diagnostic methods: Mattar and Anderson (2003) and Anderson and Mattar (2004) provide guidelines and examples for production data diagnosis using type curves. Kabir and Izgec (2006) provide guidance on using of pressure-rate data to characterize reservoir production mechanisms. Nobakht et al. (2009) provide guidance to recognize operational problems such as liquid loading and distinguish them from reservoir responses to avoid misinterpretation of the production

data. They presented a series of diagnostic plots to determine consistency of data and advised us to look at all available diagnostic plots and investigate anomalies. Ilk et al. (2008b) presented a workflow that includes diagnostic plots for reserves assessment in tight gas sands; much of this applies to diagnostics in oil wells. As Ilk et al. (2010) described, typical production data analysis includes the following steps:

1- Review and quality check of data including rate and pressure history, physical wellbore and completion data, reservoir and fluid parameters.
2- Ensure that data correlate; for example, pressures decrease when rates increase.
3- Develop a preliminary diagnosis of data, with special emphasis on identifying flow regimes and establishing the reservoir model.

Diagnostics are essential steps in any workflow, regardless of the whether the analysis uses a reservoir simulator or a type curve. Figure 15 (after Ilk et al. 2010) illustrates common reservoir models where transient flow and boundary-dominated flow are present, and (a) shows the schematic diagnostic plot for production data analysis in "well-test" equivalent behavior format, increasing pressure functions with time, and (b) presents a decline-type-curve format with rate functions decreasing with time.

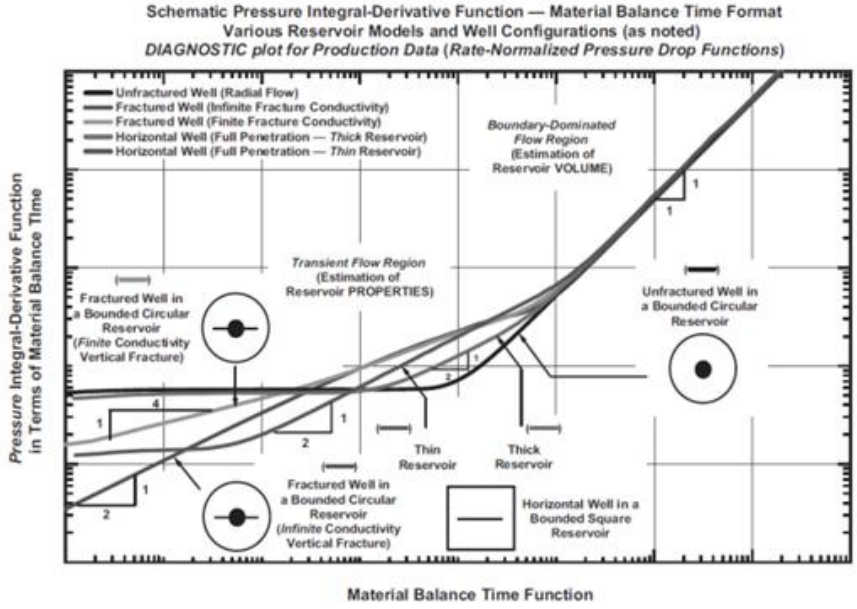

(a)

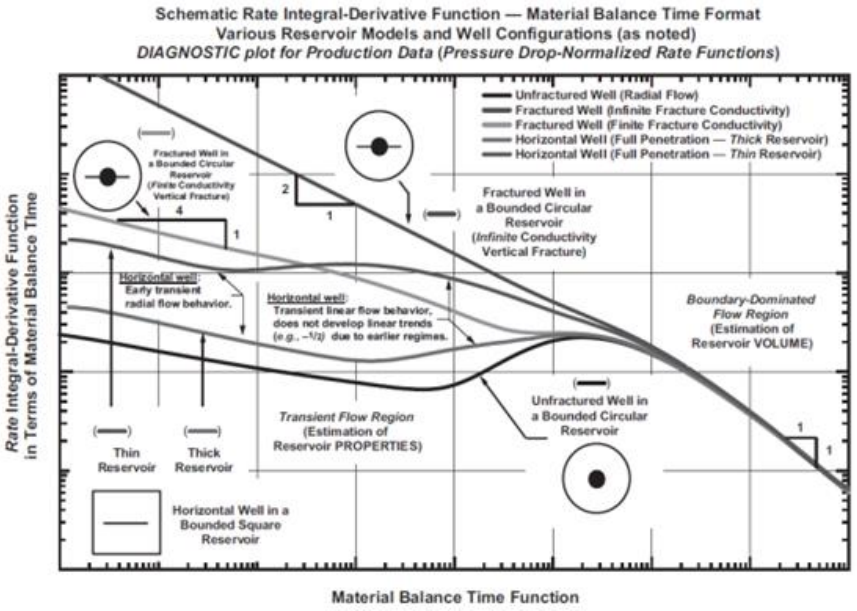

(b)

Figure 15—Schematic diagnostic plot for production data analysis (a) in "well-test" equivalent behavior format, increasing pressure functions with time, and (b) in decline-type-curve format with decreasing rate functions with time (Ilk et al. 2010).

Given an accurate and complete set of data, production analysis should help identify the reservoir and well model, estimate the reservoir and completion properties including matrix and stimulated rock volume permeability and geometry, and estimate ultimate recovery of the well if the drainage area volume is determined. Ilk et al. (2010) summarized some of the more commonly encountered problems with production analysis. It is important to understand and recognize these problems even if they cannot be addressed. Ilk et al. also provided a graphical guidebook for generic diagnosis of production data. In MFHW's, it is often difficult to distinguish between the different flow regimes, and boundary dominated flow may not be reached during the available production history.

Conventional Rate Transient Analysis

For a single phase flow, given flow rate and pressure data, Rate Transient Analysis (RTA) can be used to characterize reservoir and completion properties, including permeability, skin, and drainage area, and also to forecast production. RTA is similar to pressure transient analysis (PTA) in the sense that they are both based on the same governing equations and hence solutions. They are different in that data for pressure transient analysis is collected under a controlled environment as part of an experiment. For example, during a pressure build up test, when the well is shut it, there is a constant rate of zero. Data for production analysis is collected during actual production of a well with much variance and very little control. Data for pressure transient analysis are collected at higher frequency and accurately over a relatively shorter period of time, usually extending from hours to days. Production data, however, is often of lower quality in terms of frequency and accuracy of data points, but can be collected during the full history of production, and hence over long times. RTA can be considered to be analysis of an extended drawdown test. The challenge with RTA is that flow rate is not constant. An advantage of RTA is that there is no production loss during testing. In low permeability reservoirs, such as in MFHW's, where it is not practical and often not possible to conduct a buildup test, RTA is the only available tool. Analytical methods can be applied to both single phase oil and gas production data. They are often quite

efficient and practical for individual well analysis, history matching and forecasting. Analytical tools are limited to single phase, therefore they may be partially useful in MFHW's where flow starts with single phase fluid, but pressures decline below saturation point fairly rapidly, often in the first 12 to 18 months of production.

Rate Transient Analysis in Tight Gas Reservoirs

Nobakht et al. (2010) presented a "simple, yet rigorous" method to forecast production in tight/shale gas. Since there are no rigorous analytical methods to forecast liquid rich production in shale oil reservoirs, we explored this method further to determine whether it might be extended to LRS reservoirs, either fully or partially. Nobakht et al.'s method relies on the observation that flow of gas in tight/shale reservoir exhibits extended periods of transient linear flow. It uses the inverse rate versus square root time plot and combines linear flow during transient period with Arps' hyperbolic decline model during boundary dominated flow. The method was validated with numerical simulation models. They found excellent correlation between rates forecasted with their method and numerically simulated rates. They assumed that the drainage area extends only to the tip of the fracture and flow from beyond the fracture tip is insignificant, similar to others (e.g., Carlson and Mercer, 1991: Mayerhofer et al. 2007; and Bello and Watternbarger, 2008). Figure 16 depicts the mental model of the stimulation geometry for this work. Contrary to Nobakht et al., in developing our workflow to forecast production in LRS MFHW's, we allowed flow from beyond the stimulated rock, i.e. beyond the fracture tips, and included it in our workflow (Figure 14).

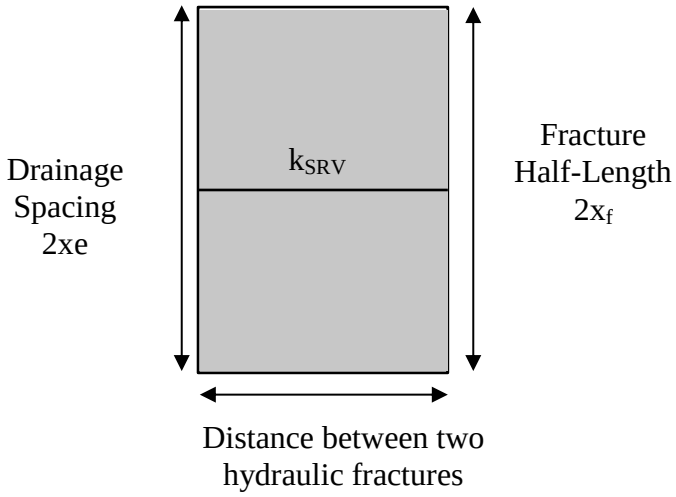

Figure 16—Schematic of a single hydraulic stimulation stage in Nobakht et al.'s (2010) work

In this model, linear flow continues until, the reservoir boundary, Ye, is reached at which point the flow becomes boundary dominated. Therefore the development of the underlying equations reflected the linear flow behavior, the duration of linear flow, and the boundary dominated flow.

Therefore Nobakht et al. showed that the forecast is divided into two parts. During transient linear flow, analytical methods were applied, and beyond that Arps traditional hyperbolic was used. This is important because in developing a workflow for MFHW's in LRS, we are seeking a simplified methodology where the complex flow behavior could be divided into segments where a transition point could be defined before which analytical models are applied, and after which some predetermined simple model is applied.

Since the work of Nobakhat et al. (2010) and with increased activity in LRS plays, there have been some recent attempts by Behmanesh et al. (2013), Eker et al. (2014), Behmanesh et al. (2015), Clarkson and Qanbari (2015) to use multi-phase

approximations with single-phase workflows. The validity of these approximations has not been confirmed and a need remains for a verified workflow.

Numerical simulation

When the diffusivity equation is non-linear (as in multiphase flow), the durations and characteristics of flow regimes expected in single-phase flow will be distorted and analytical solutions are no longer valid. In volatile oil reservoirs, numerical simulations are required for oil flow below bubble point to account for multiphase flow. This will require relative permeability relationships and equations of state as inputs to the model. MFHW's in over-pressured LRS's should produce single-phase oil initially, but, when pressures drop below the bubble point, simple analytical solutions are no longer sufficient to describe the full multiphase flow and forecast production.

CHAPTER IV

FORECASTING PRODUCTION OF MULTI-FRACTURED HORIZONTAL WELLS IN LIQUID RICH SHALE PLAYS-WORKFLOW

In previous chapters we presented a review of existing workflow for production analysis. We showed that, although there have been many advances in production analysis workflow for various types of resources including production of single-phase fluid in unconventional tight reservoirs, none of these are applicable to multiphase flow in multi-fractured horizontal wells (MFHW's) in liquid-rich shale (LRS) plays. In this chapter a hypothesis about a practical workflow for forecasting production and estimating reserves in MFHW's in LRS will be presented. In remaining chapters the hypothesis is validated and the workflow results are compared to numerical simulations.

Overview

There are currently no accurate workflows to forecast production in liquid rich shale plays. The closest workflow available is the "simple-yet-rigorous" workflow developed by Nobakht et al. (2010) summarized Chapter III. The Nobakht et al. workflow is based on the principles of single-phase flow of slightly compressible fluids, and was extended to the flow of gas in shales. Their workflow, however, is not applicable to multiphase flow that occurs in production of liquid-rich plays. The unique feature of production from multi-fractured horizontal wells in liquid rich play is that, in addition to complexities that come with hydraulic fracture stimulation of extremely low permeability rock, multiphase flow exists, predominately near the wellbore. In the absence of any trustworthy workflow, the only option to obtain forecasts that consider

the complexities of multi-fractured horizontal well and the multiphase flow in liquid-rich shale plays is to use compositional numerical simulators. This is very time consuming and impractical when applied to numerous wells in a field. In the workflow proposed in this project, the compositional numerical simulator is used as the benchmark to verify the workflow. Our simple workflow takes advantage of existing production analysis techniques for single-phase fluid flow and extends it to account for multiphase flow.

Summary of Proposed Workflow for Forecasting Production in Liquid Rich Shales

1- Perform diagnostics to validate accuracy of data and extract reservoir signals, as explained in the previous chapters.
2- Interpret and analyze the production data to identify dominant flow regimes wherever possible, estimate reservoir properties, system parameters, and quantify uncertainties, as explained in the previous chapters.
3- Use an analytical single-phase oil model for MFHW's with appropriate static and dynamic reservoir and completion parameters. History match, validate interpretation, and forecast production to the end of the life of the well (see Chapter VI).
4- Using a predetermined transition point, identify the part of analytical forecast that is valid.
5- Beyond the transition point, forecast oil production using predetermined trends of dimensionless rate versus dimensionless time.
6- Forecast gas production for the life of the well using a predetermined gas-oil ratio trend.

This workflow requires determining a general trend of dimensionless rate versus dimensionless time for a specific area. In this work, this is referred to as an "area of interest." For the area of interest, the transition point and GOR trends are also identified. Details of this are discussed in Chapters V and VII.

Hypothesis

The underlying hypothesis in this workflow is that life cycle production in a MFHW in LRS is divided into two flow periods:

1- Initial period- when flowing bottom-hole pressure (FBHP) is variable, flow is dominated by single-phase flow of oil; therefore, single-phase analytical MFHW rate transient methodology is valid.
2- Subsequent period- FBHP is expected to be relatively constant, multiphase flow is predominant. Dimensionless time and dimensionless rate functions are defined such that their trend beyond transition from initial period is used to forecast production.

In this workflow, the transition point, dimensionless rate versus dimensionless time trend, and also GOR trend are defined for a selected area of interest. The area of interest is defined as an area represented with a single fluid system, for example, a single volatile oil within +/- 3^o API range. In an unconventional play, depending on the size of the area and development plan, one area of interest could cover hundreds or thousands of wells. Once the area of interested is selected, we must then prove that after the initial transient period, all production histories, when expressed in terms of dimensionless rate and time, converge. Furthermore, to forecast production of the secondary phase, i.e. gas, we must show that, for the given area of interest, the existing gas-oil ratio trend can be used to forecast gas production. This hypothesis is validated in the following chapter.

CHAPTER V

PRODUCTION HISTORIES IN AN AREA OF INTEREST

As outlined in the previous chapter, to validate the workflow proposed there, we have to first show that, for an area of interest with a single fluid system and a specific completion design, the production history following an initial transient period converges to the same shape. And, therefore, the subsequent period of production can be predicted with a common decline model, and a common gas-oil ratio trend. The following sections detail how to select an area of interest. Details of the numerical model used to simulate multiphase production histories from a variety of scenarios for MFHW's in LRS's are also presented and used to validate our hypothesis.

Identify Area of Interest

An area of interest in an unconventional liquid rich shale play could include hundreds or thousands of wells. There are three criteria to consider when identifying an area of interest; they include rock properties, fluid system, and completion design. These are described in detail below:

Common Rock Quality

An area of interest encompasses that part of a reservoir in which geology and rock quality are reasonably uniform. Due to the tight rock in shale plays, errors associated with measuring ultra-low permeability values, and variability due to presence of natural fractures, a relatively wide range of rock permeabilities should be allowed in selecting the area of interest. In our examples, permeability was allowed to vary from 1e-5 to 8e-3 md.

Common Fluid System and Single PVT Model

In unconventional plays, for compositional modeling (the most rigorous multiphase modeling method), there are usually large sections of a field that are modeled with one set of PVT properties. This is because obtaining representative fluid samples in shale plays is extremely difficult and hence, there is limited amount of information available regarding the fluid system. As Whitson put it, the general problem for liquid-rich shales is that "what you produce at the surface is not what you have in the reservoir" (Whitson 2012). In ultra-low permeability LRS plays, obtaining reservoir fluid samples at initial reservoir conditions is challenging because the reservoir fluid does not flow prior to stimulation. Therefore, conventional sample collections using tools such as the Modular Dynamic Tester (MDT-Schlumberger) cannot be used to collect bottom-hole reservoir samples. Surface sample collection is possible only after stimulation and sufficient clean-up where ample time is allowed for fracturing fluids to flow back and fracture fluid cut to drop to acceptable levels (e.g., below 15%). This usually leaves a small time window between clean-up and bottom-hole pressure dropping below the bubble-point. Thomas et al. (2009) suggested techniques for sampling and characterizing gas condensate reservoirs that could be extended to sampling in LRS and help improve quality of surface samples and reduce errors associated with conventional sampling techniques. In this workflow, we propose to select an area of interest with a single set of PVT properties, using the same criteria as when assigning a set of PVT properties to an area for performing compositional modeling. In following sections, the impact of using different PVT properties for forecasting is shown.

Common Hydraulic Fracture Design

In addition, the area of interest should have wells with similar hydraulic fracture design. Operators may experiment with several designs to optimize their production, but, after a few trials, an optimal design is usually selected. This is not to say that every hydraulic fracturing treatment results in the same extent of stimulation. Variability in stimulation in terms of permeability enhancement and stimulation geometry (expressed as fracture

half-length) in each well is expected, and our workflow intends to capture this variability. We assume, for a specific stimulation design, the major design parameters are uniform and aim at a specific fracture spacing. The major stimulation design parameters include fluid and proppant type, completion design (i.e., Plug 'N Perf versus open-hole completions), number of completion stages, length of each completion stage, and number of perforation clusters per stage. For example, an operator might elect to complete its LRS wells using Plug 'N Perf with 75ft stages at 5 perforation clusters per stage, and use slick water as the completion fluid with a specific size proppant. The importance of similar completion practices is that any forecasting tool, regardless of degree of complexity, relies heavily on the stimulation geometry. Similar completion practices tend to produce similar fracture geometries and permeability enhancement.

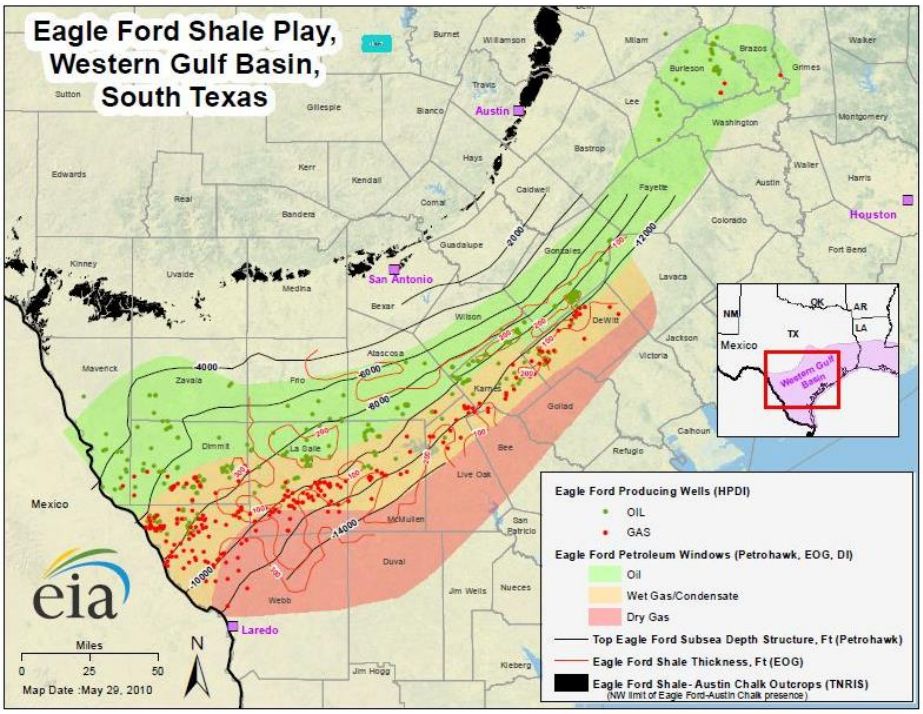

Figure 17—Example of areas of interest in Eagle Ford- Green area, which shows the volatile oil window. The dots represent wells in each petroleum window. (US Energy Information Administration 2010)

Figure 17 shows the Eagle Ford shale divided into 3 petroleum windows of oil, wet gas/condensate, and dry gas. The matrix permeability throughout Eagle Ford is reported to be 180-820 nD (Xu et al. 2012). The oil window is reported to have oil with API gravities from 40-45°, and values of 46-58°API are reported for gas condensate (US Energy Information Administration 2010).

In following sections, for a specific area of interest, we explain how we develop a compositional numerical simulation model to study production histories and gas-oil ratio trends for a volatile oil, and then for a black oil.

Compositional Numerical Model

Multi-fractured horizontal wells, despite the variability in success of stimulation treatments, are often modeled with equal length fractures spaced equally (Figure 18). In this study, we assumed this symmetry and therefore modeled only a single fracture stage.

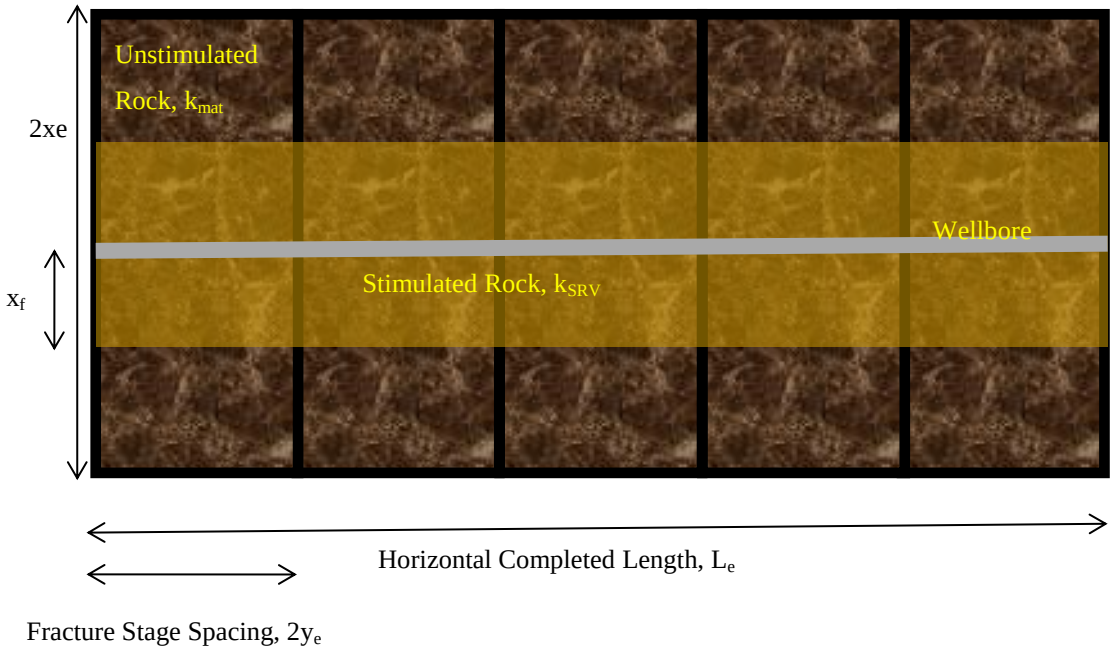

Figure 18—Schematic diagram of simplified stimulation geometry in a typical MFHW

Inputs Into the Simulation Model

Geometry

A three-dimensional Cartesian model is defined in x-, y-, and z-directions:

1- x-direction: The width in the x-direction is determined from the width of a single fracture stage as shown in Figure 18. This parameter is calculated from total horizontal well length and number of fracture stages. The term "effective" refers to the number of successful fracture stages. This number may be different than the attempted number of fracture stages and is often determined by use of tracers, production logs, and microseimic interpretations of the stimulation treatment.

$$\text{Single Fracture Stage}_{\text{width}} = \frac{\text{Total Horizontal Lateral Length}}{\text{Effective Number of Fracture Stages}} \tag{166}$$

For a well with horizontal lateral length of 5000 ft and 25 completion stages, the width of a single fracture stage is 200 ft.

2- y-direction: The length in the y-direction is determined from drainage (area) spacing or well spacing which can be derived from the development plan of a field. In North America, a development section refers to an area of 1 square mile. Therefore, drainage spacing is defined by:

$$\text{Drainage Spacing} = \frac{1 \text{ mile}}{\text{Wells per section}} \tag{167}$$

For 8-wells per section development (Figure 19), drainage spacing is 660 ft:

$$= \frac{5280 \text{ ft}}{8} = 660 \text{ ft} \tag{168}$$

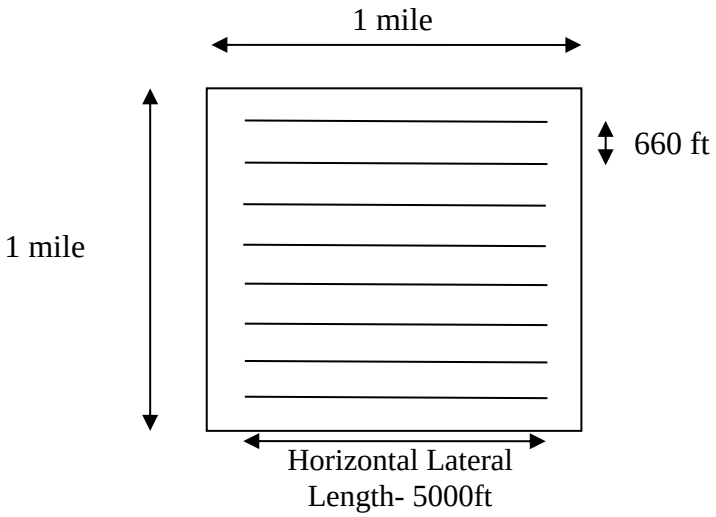

Figure 19—Development spacing 8 wells/section- top view

3- z-direction: The height in the z-direction represents the thickness of the formation. We assume that the fracture does not grow in height beyond the thickness of the formation(s) of interest. In designing stimulation treatments, operators often try to ensure this result. In our study, we assumed a formation thickness of 103 ft and the same fracture height (Figure 20).

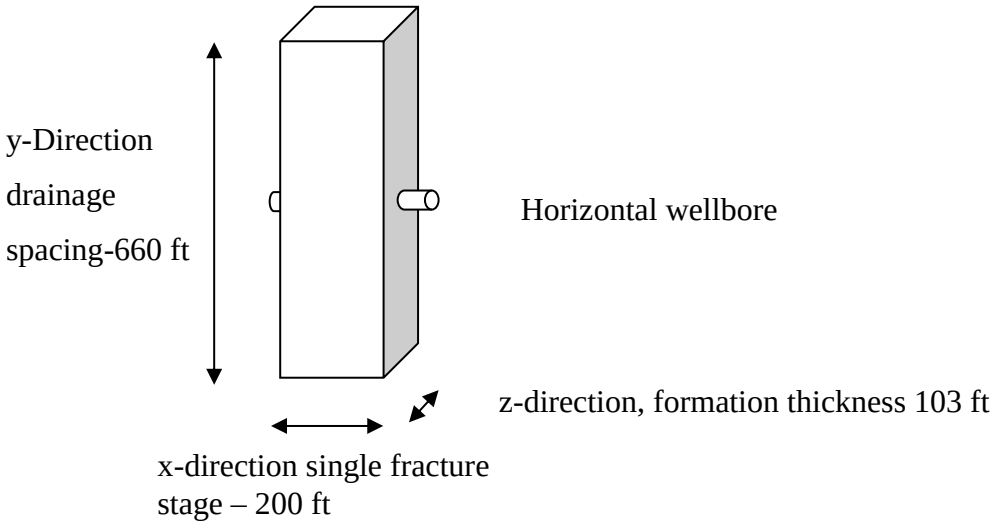

Figure 20—3-D schematic of modeled geometry

Permeability

Two different permeabilities must be defined: matrix permeability and stimulated rock permeability.

In both unstimulated matrix and stimulated zones, we assume that permeability in the x-direction equals that in the y-direction. Permeability in the z-direction is $1/10^{th}$ of permeability in the x-direction. Thus,

$$k_x=k_y \tag{169}$$

$$k_z=0.1\ k_x \tag{170}$$

1- Matrix permeability- A range of permeabilities that covers the area of interest should be selected. In ultra-low permeability rock, it is often found that permeability measurements using different techniques such as core measurements and pressure transient analysis result in values with orders of magnitude variability, and we must ensure the full range is covered. In this study, values of permeability from 0.0001 to 0.08 md were included.

2- Stimulated rock permeability- A range of permeability enhancements should be selected. Based on actual initial history matching of production data, it is possible to determine the stimulation parameters including the permeability of stimulated rock. The degree of stimulation varies and this parameter should allow for the expected range. For example, in our specific area of interest, the stimulated rock permeability varies from 4 times to 4000 times, includes cases for 4, 40, 400, and 4000, the matrix permeability. Once again, this range covers permeability beyond the expected range.

Some typical permeability values from liquid rich plays such as the Eagle Ford are shown in Table 7:

Matrix Permeability	1e-5's to 1e-3's	mD
SRV Permeability	1e-4's to 1's	mD
Ratio SRV to Matrix Permeability	10-1000	
Fracture Half Length	10-100	ft

Table 7—Permeability range for Eagle Ford (Xu et al. 2012)

A porosity permeability cross-plot from the Duvernay LRS is presented in Figure 21.

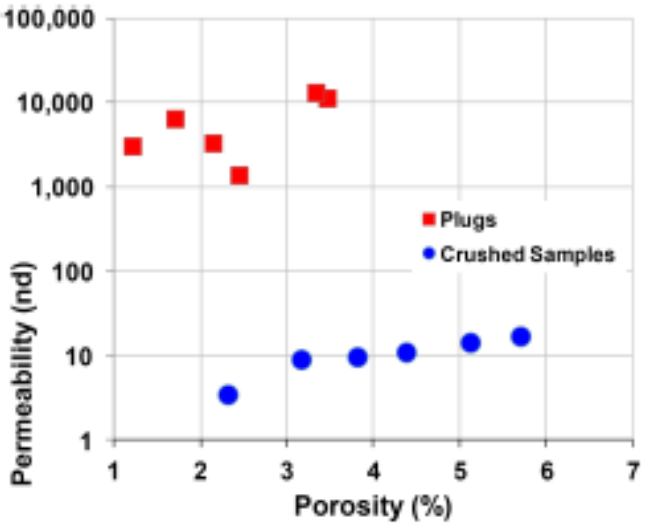

Figure 21—Porosity permeability cross-plot for crushed and core plugs of the Duvernay formation (Wust et al. 2014)

Petrophysical Parameters

A constant porosity of 5% and water saturation of 18.3% was used in our example here.

PVT

A single fluid composition for the entire area is used. Understanding the fluid system in liquid rich shale plays is paramount in modeling the reservoir and the well. As mentioned earlier, collecting fluid samples in nano-Darcy permeability reservoirs is a major challenge. Surface samples collected at FBHP's higher than saturation pressure often provide sufficiently accurate samples that can be recombined at observed surface GOR and analyzed. We highly recommend collection and analysis of fluid samples early in the exploration phase of a project. In the absence of fluid samples, the best alternative is to use analogues. Yang et al. (2014) presented a methodology to estimate in-situ reservoir fluid composition and the corresponding PVT properties based on readily available field data. If representative samples are available, samples are analyzed in the laboratory where typical measurements include differential liberation, constant

composition expansion experiments, viscosity, and composition (McCain 1990). The PVT analysis results are then used in commercial PVT simulators such as WinProp or PVTSim to tune an equation of state (EOS). The Peng-and-Robinson EOS was used in this study. The EOS is used in commercial compositional numerical simulation models such as Eclipse or CMG.

An EOS for volatile oil systems was used in our first example of volatile oil area of interest. The EOS tuned for black oil system was used in the black oil area of interest. The EOS's are not presented in this document.

Initial Reservoir Pressure

A range of initial reservoir pressures, p_i, covering the entire area of interest must be considered. In this specific study, p_i values of 7353 psi +/-10% covered the required range of p_i's.

Flowing Bottom-Hole Pressure History

In general, the flowing bottom-hole pressure history begins at initial reservoir pressure, p_i, and terminates at an abandonment pressure, p_{abd}. In unconventional LRS plays, the typical FBHP history is a steep decline from p_i in the range of 60-90% in the first year of production. Therefore, minimum free flowing bottom-hole pressure is often reached within the first two years of production, and artificial lift is required for the remaining life of the well. In this chapter, where the objective is to study stabilized trends after the initial transient flow regime, a constant FBHP of 450 psi is assumed. In the following chapters, the impact of various FBHP pressure histories will be considered.

Production History and GOR Trends

Volatile Oil Area of Interest

A total of 57 cases (with different matrix permeabilities, stimulated rock permeabilities, and initial reservoir pressures) that include the range of parameters described above were

developed for the volatile oil area of interest (Figure 22). The selection of cases was such that the full ranges of permeabilities and pressures were covered to produce the high and low case scenarios. On average this includes a combination of about 4 permeability, 4 initial reservoir pressures, and 4 stimulation enhancements.

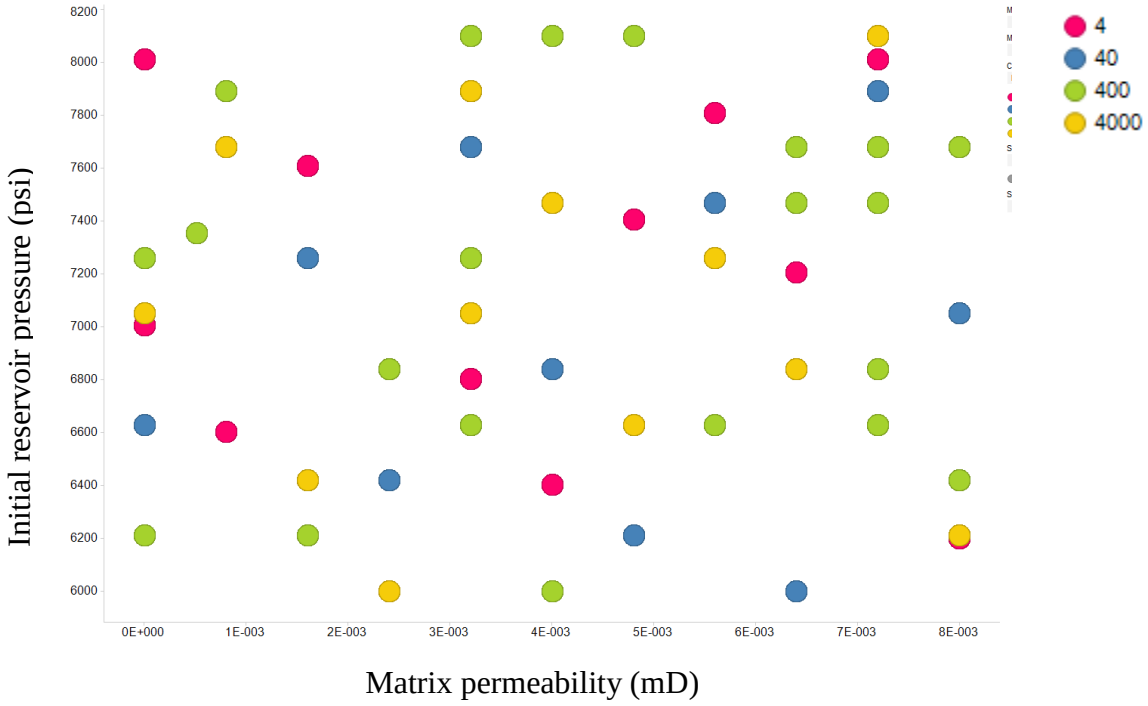

Figure 22—Volatile oil area of interest –57 combinations of k_{mat}, k_{srv}, and p_i

Figures 23 and 24 show the oil and gas production histories. The histories are sorted by stimulation intensity, i.e. permeability enhancement in the stimulated rock volume from the original matrix permeability. The 4 scenarios include stimulated rock permeability, k_{srv}, of 4x, 40x, 400x, and 4000x that of the original matrix permeability, k_{mat}.

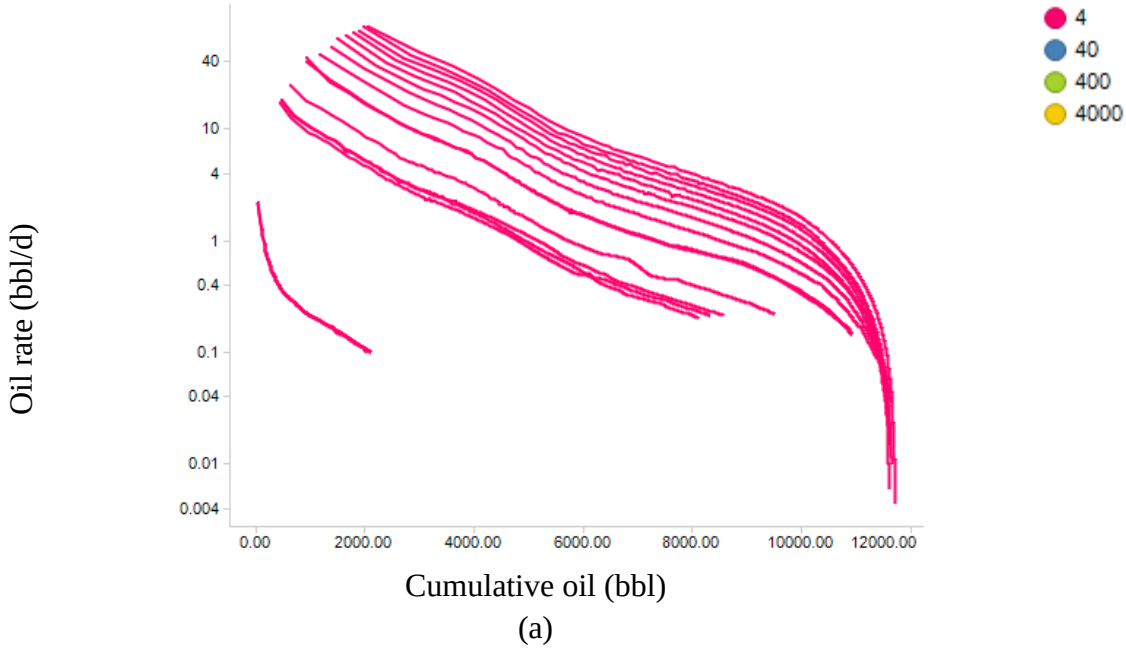

(a)

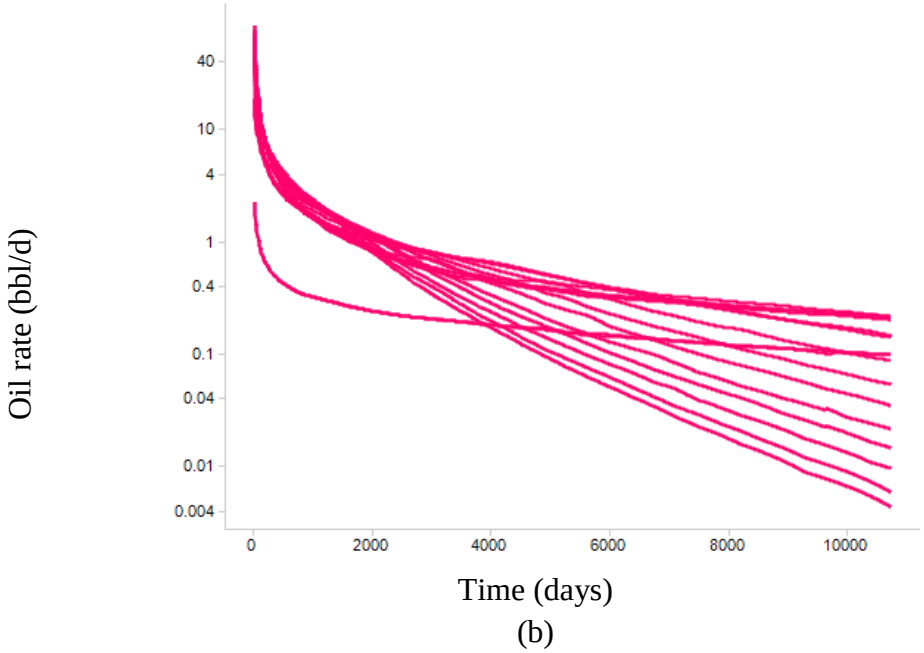

(b)

Figure 23—Oil production history for volatile oil area of interest for a single fracture stage. (a) oil rate vs. cumulative oil production for $k_{srv}=4*k_{mat}$ (b) oil rate vs. production time for $k_{srv}=4*k_{mat}$ (c) oil rate vs. cumulative oil production for $k_{srv}=40*k_{mat}$ (d) oil rate vs. production time for $k_{srv}=40*k_{mat}$(e) oil rate vs. cumulative oil production for $k_{srv}=400*k_{mat}$ (f) oil rate vs. production time for $k_{srv}=400*k_{mat}$ (g) oil rate vs. cumulative oil production for $k_{srv}=4000*k_{mat}$ (h) oil rate vs. production time for $k_{srv}=4000*k_{mat}$

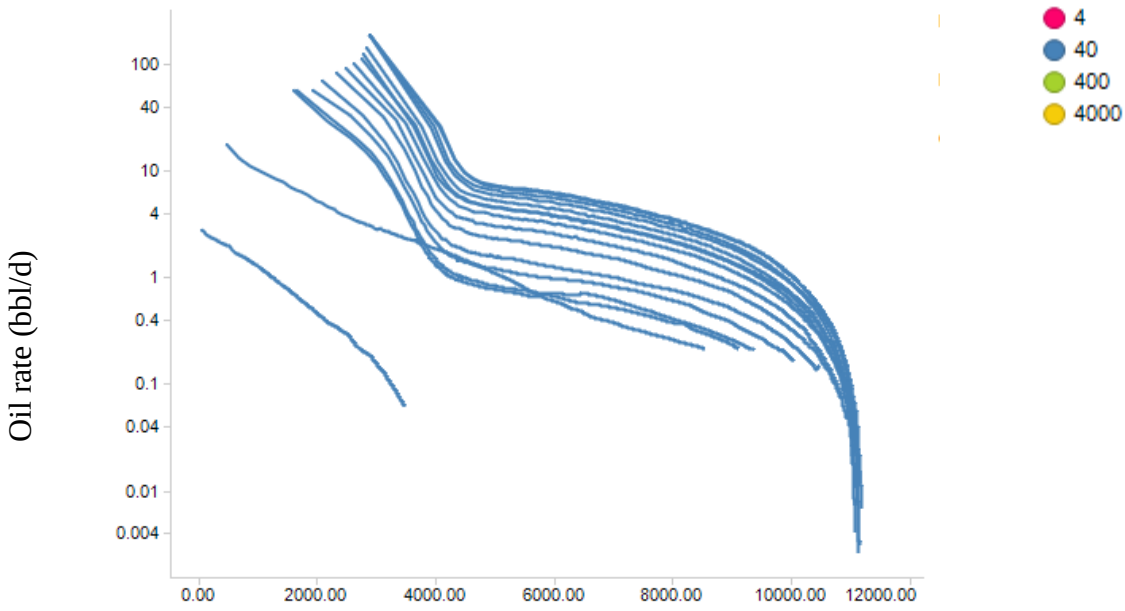

(c)

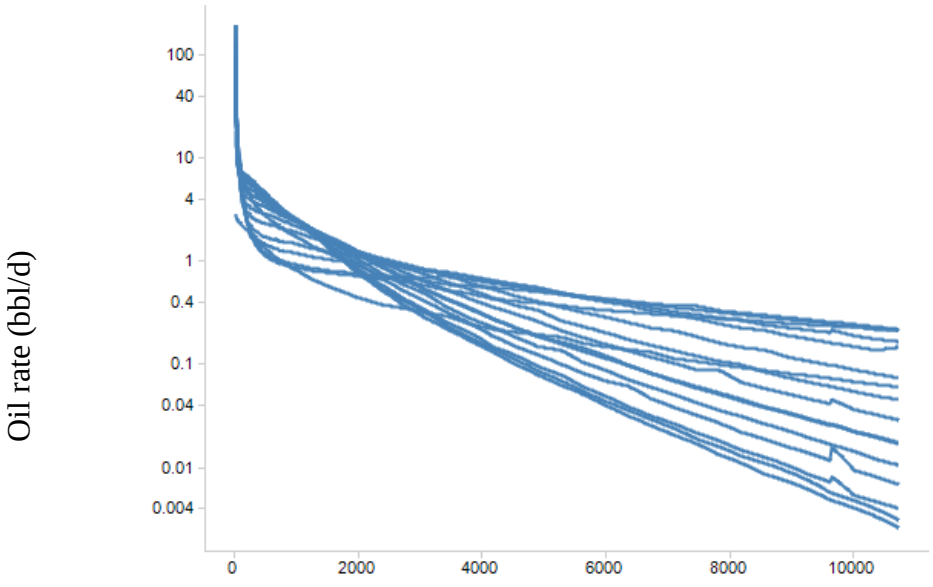

(d)

Figure 23—Continued,

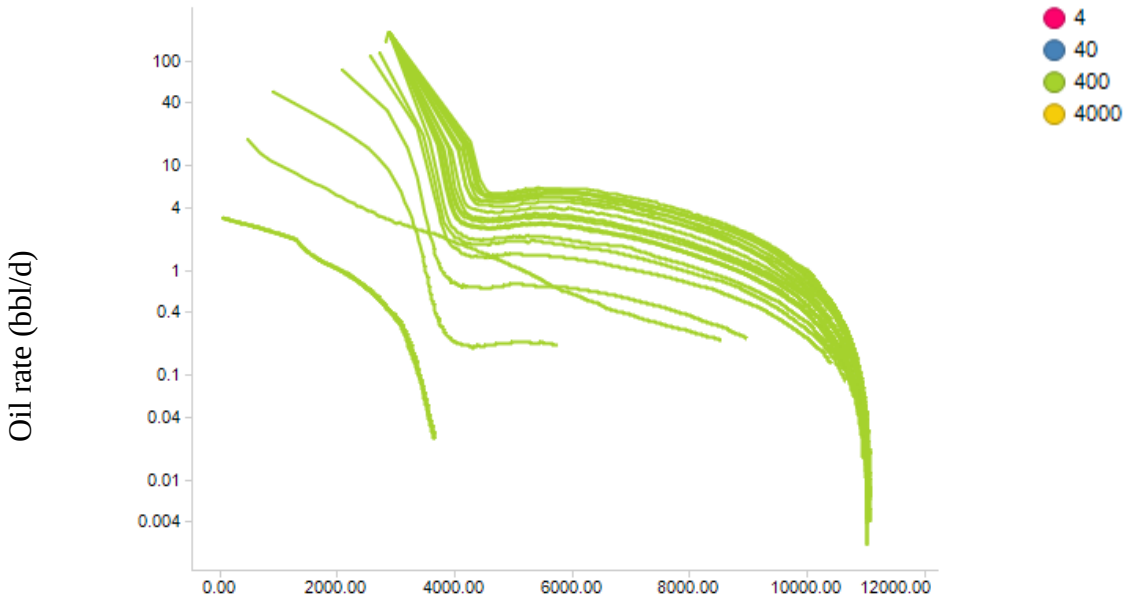

(e)

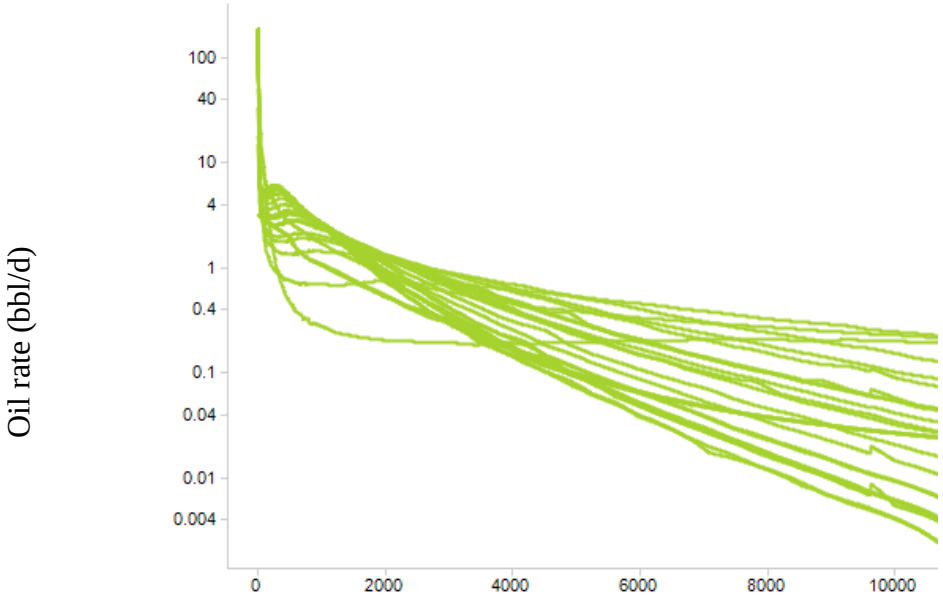

(f)

Figure 23—Continued,

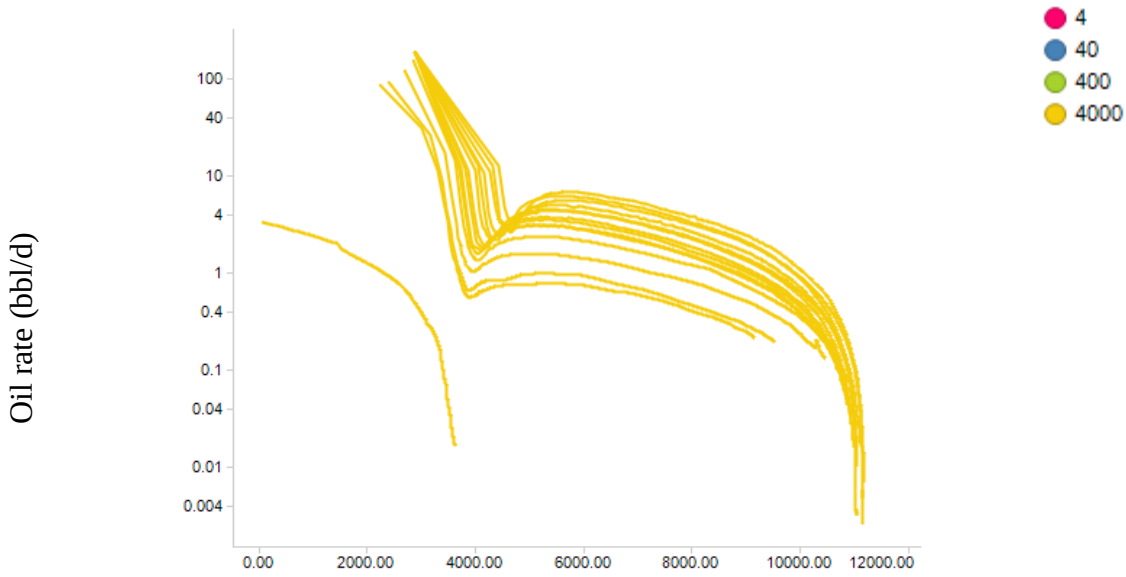

(g)

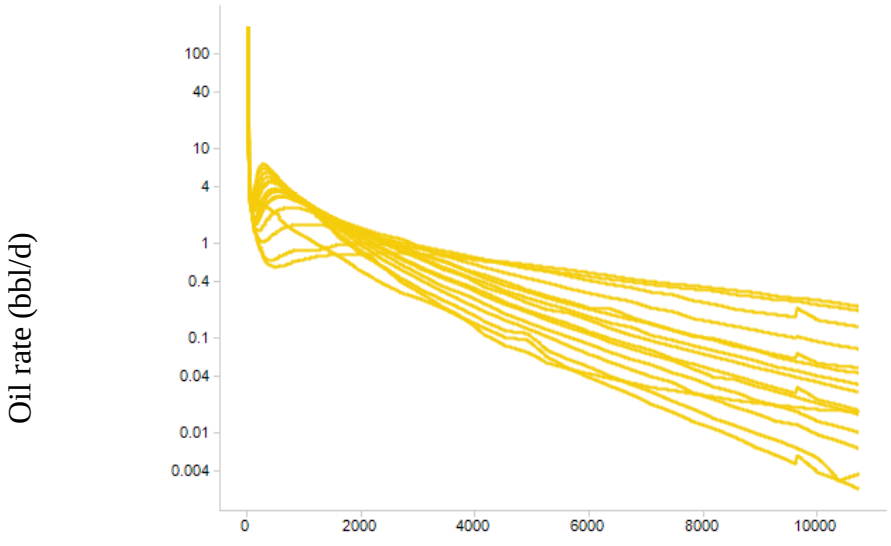

(h)

Figure 23—Continued.

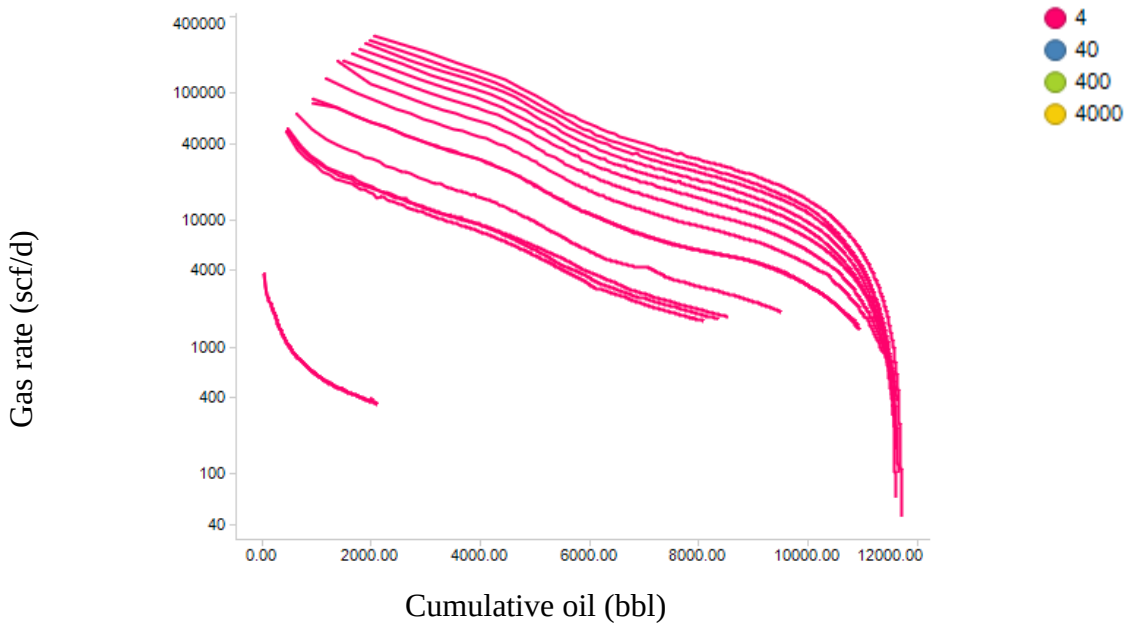

(a)

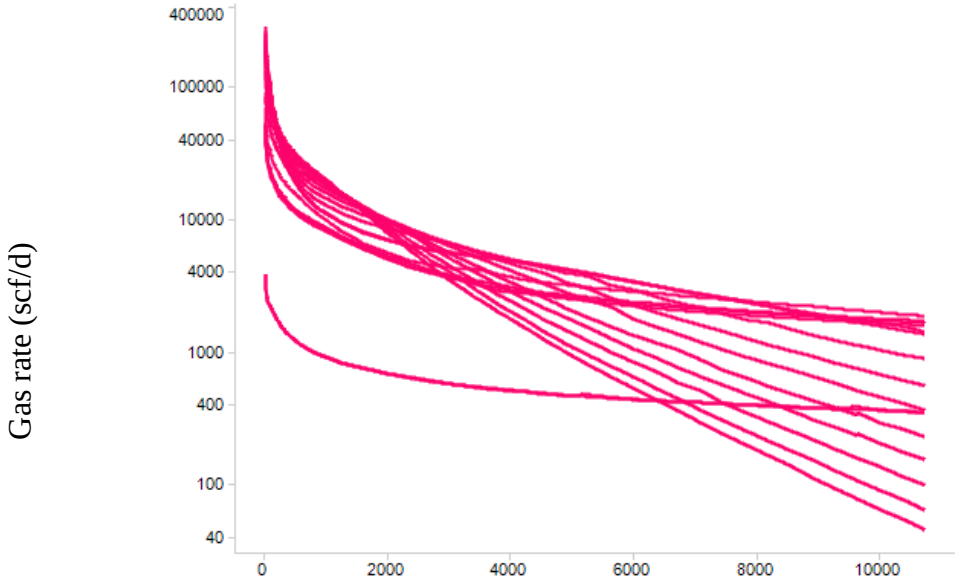

(b)

Figure 24—Gas production history for volatile oil area of interest for a single fracture stage illustrating gas rate versus cumulative oil production and time. (a) gas rate vs. cumulative oil production for $k_{srv}=4*k_{mat}$ (b) gas rate vs. time for $k_{srv}=4*k_{mat}$ (c) gas rate vs. cumulative oil production for $k_{srv}=40*k_{mat}$ (d) gas rate vs. time for $k_{srv}=40*k_{mat}$(e) gas rate vs. cumulative oil production for $k_{srv}=400*k_{mat}$ (f) gas rate vs. time for $k_{srv}=400*k_{mat}$ (g) gas rate vs. cumulative oil production for $k_{srv}=4000*k_{mat}$ (h) gas rate vs. time for $k_{srv}=4000*k_{mat}$

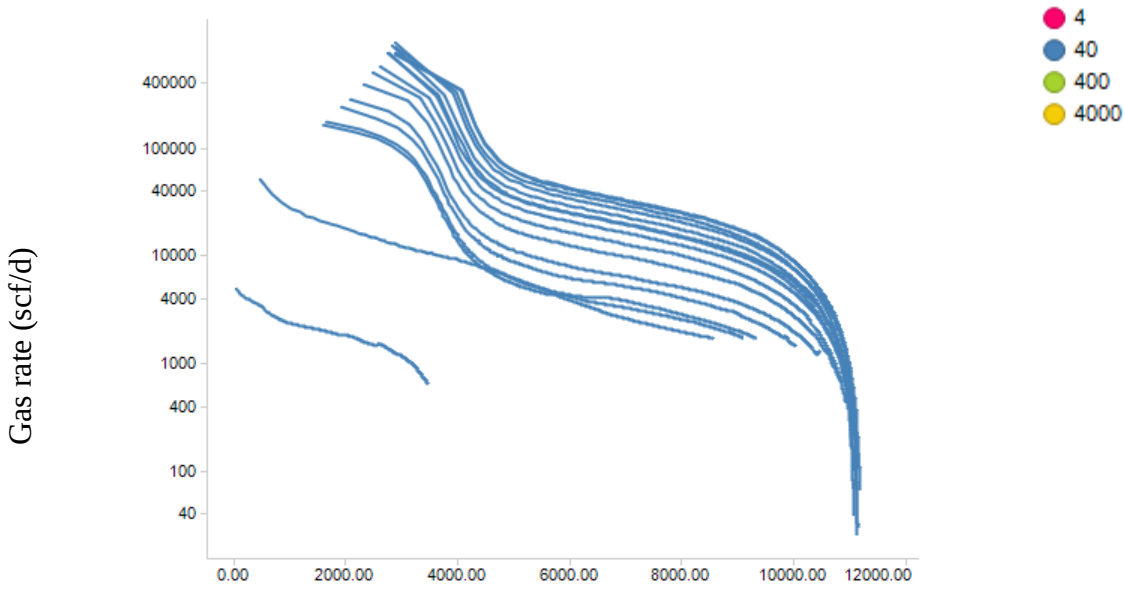

(c)

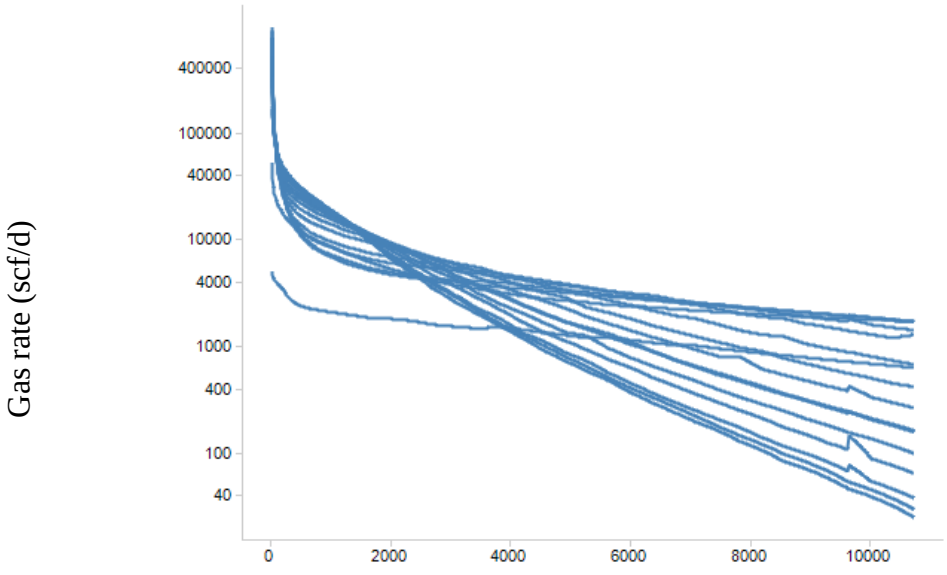

(d)

Figure 24—Continued,

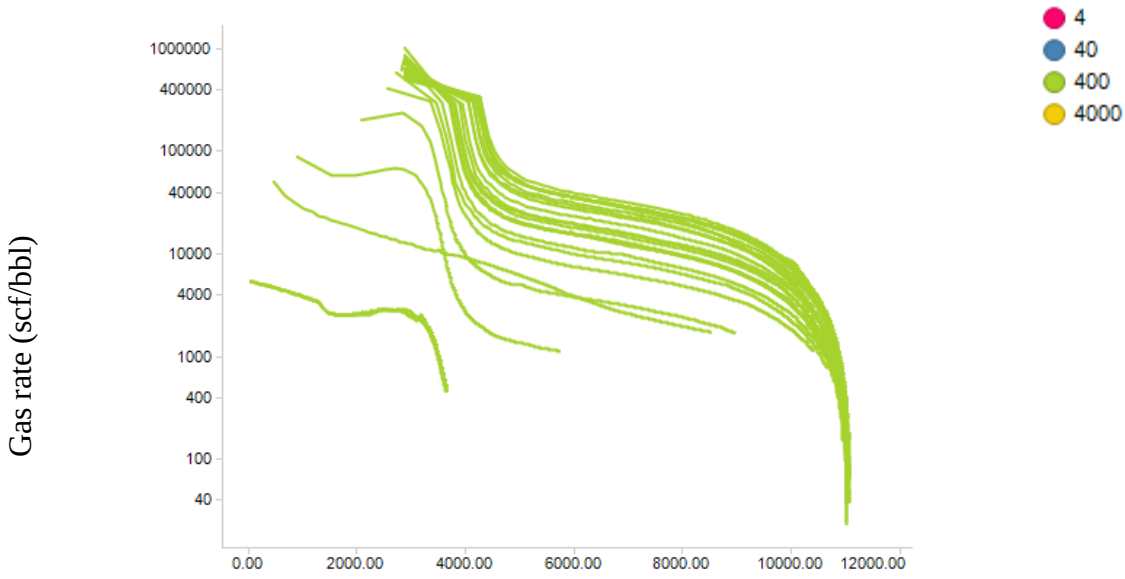

(e)

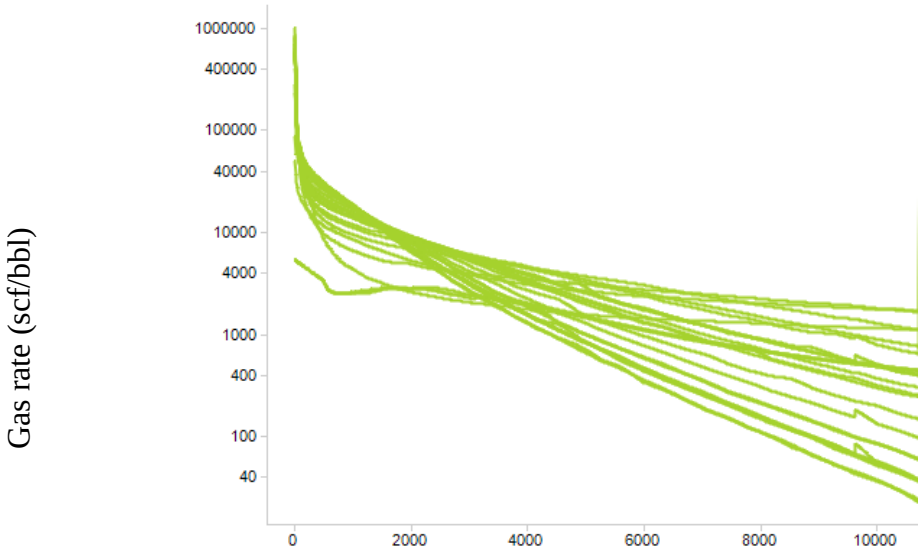

(f)

Figure 24—Continued,

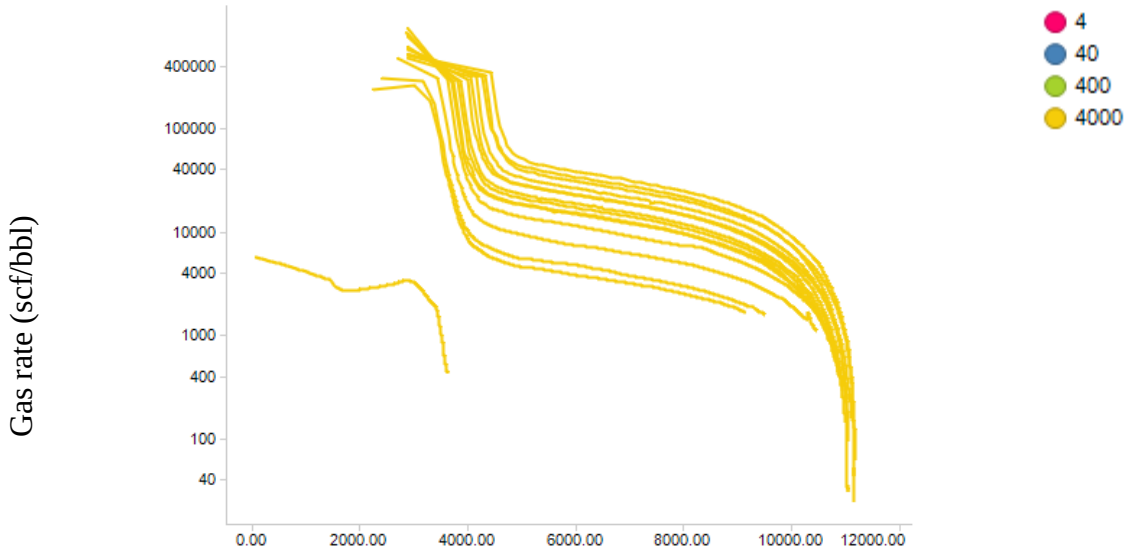

(g)

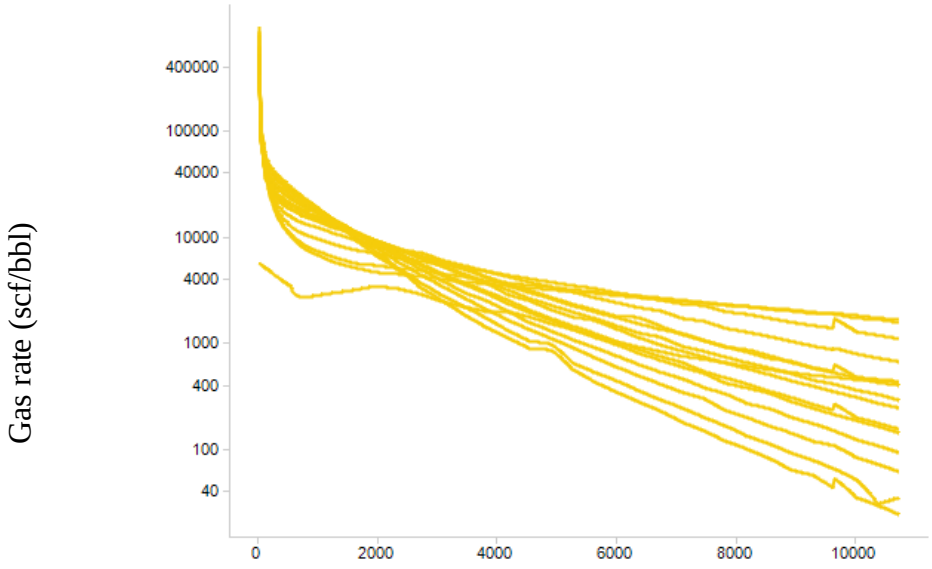

(h)

Figure 24—Continued.

Figures 23 and 24 show that, among each group, after an early transient start, production histories become similar in shape. This is further illustrated with the aid of dimensionless rate and dimensionless time definitions described in Chapter II, (equations (157) and (158)). Plots of dimensionless oil rate and dimensionless gas rate versus Figures 25 and 26.

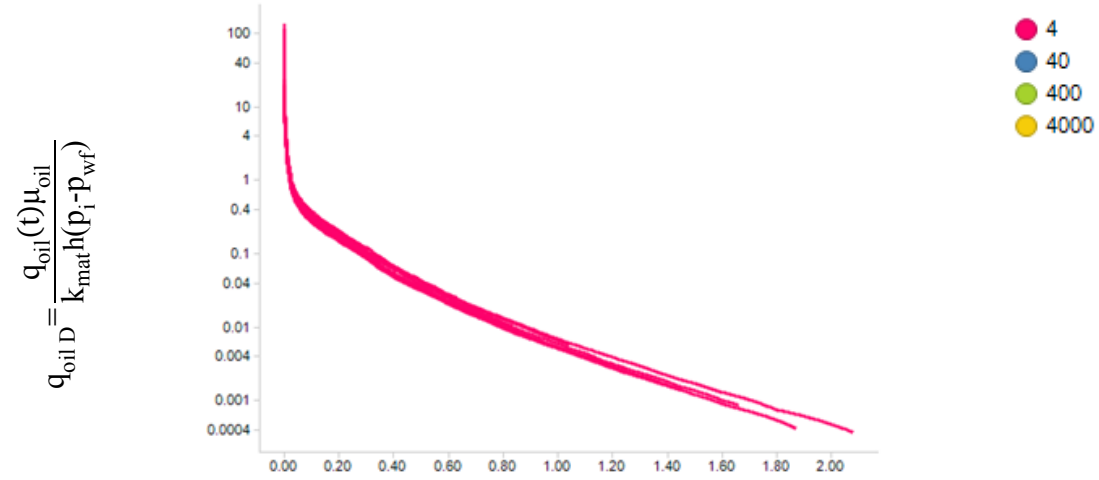

$$q_{oil\,D}=\frac{q_{oil}(t)\mu_{oil}}{k_{mat}h(p_i-p_{wf})}$$

(a)

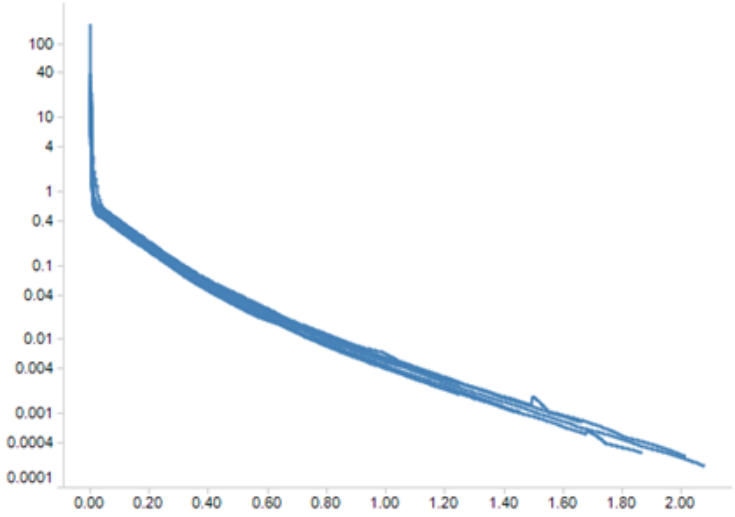

$$q_{oil\,D}=\frac{q_{oil}(t)\mu_{oil}}{k_{mat}h(p_i-p_{wf})}$$

(b)

$$t_D=\frac{k_{mat}t}{\varphi c_t\mu_{oil}(2x_e-2x_f)^2}$$

Figure 25—Dimensionless oil rate versus dimensionless time for volatile oil area of interest. (a) $k_{srv}=4*k_{mat}$ (b) $k_{srv}=40*k_{mat}$ (c) $k_{srv}=400*k_{mat}$ (d) $k_{srv}=4000*k_{mat}$

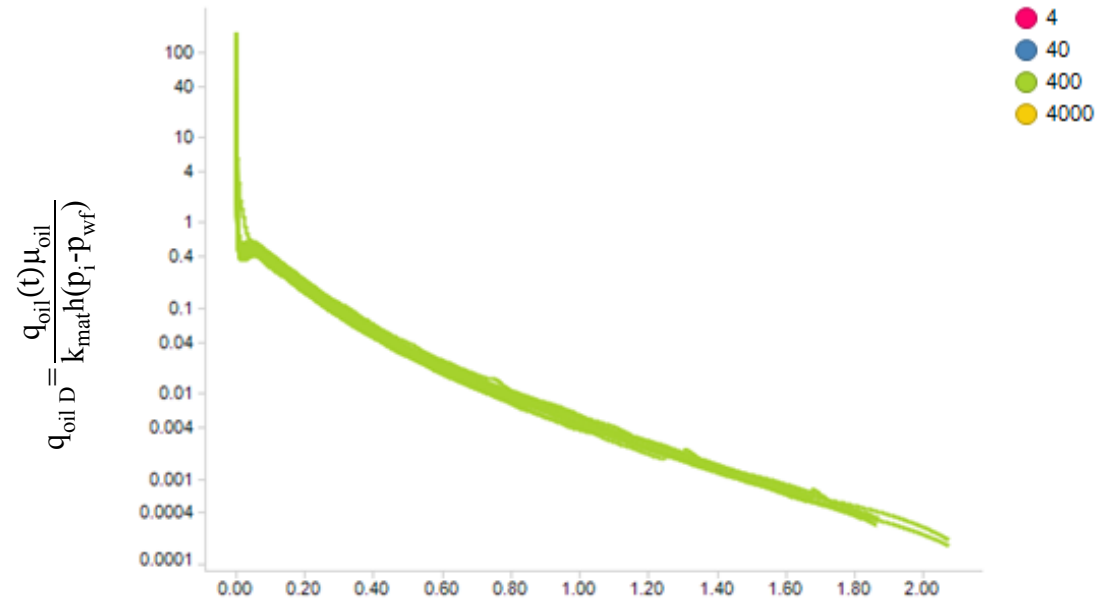

(c)

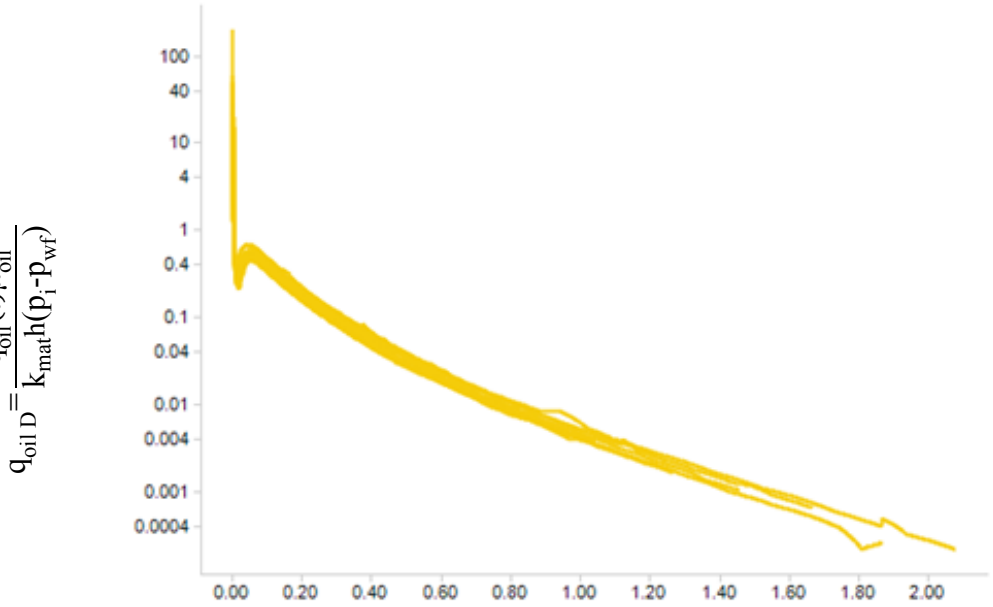

(d)

$$t_D=\frac{k_{mat}t}{\varphi c_t\mu_{oil}(2x_e-2x_f)^2}$$

Figure 25—Continued.

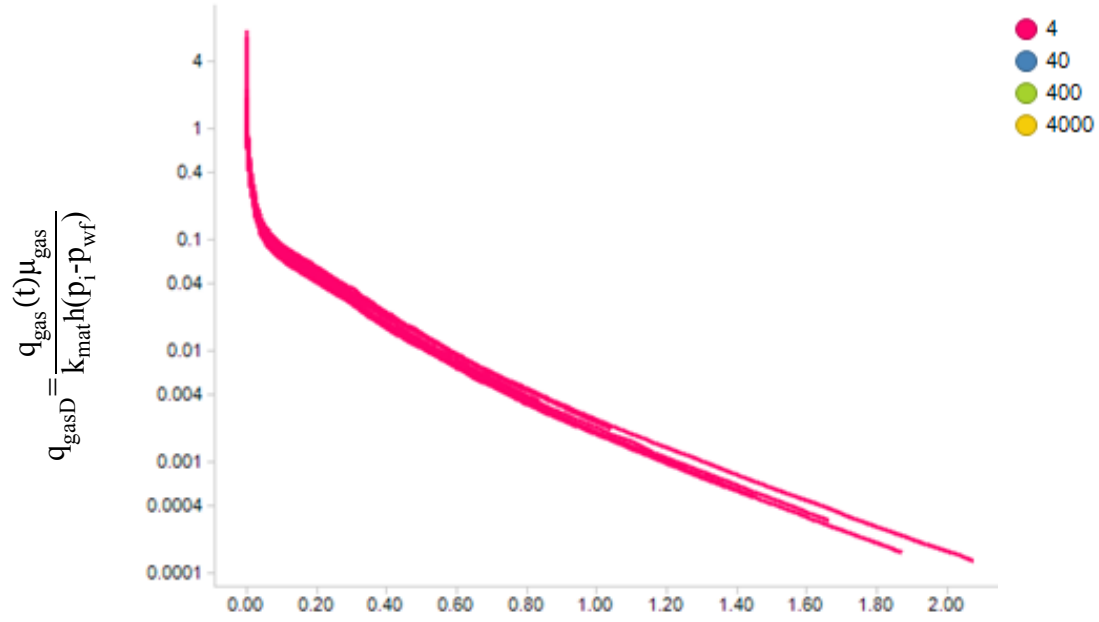

(a)

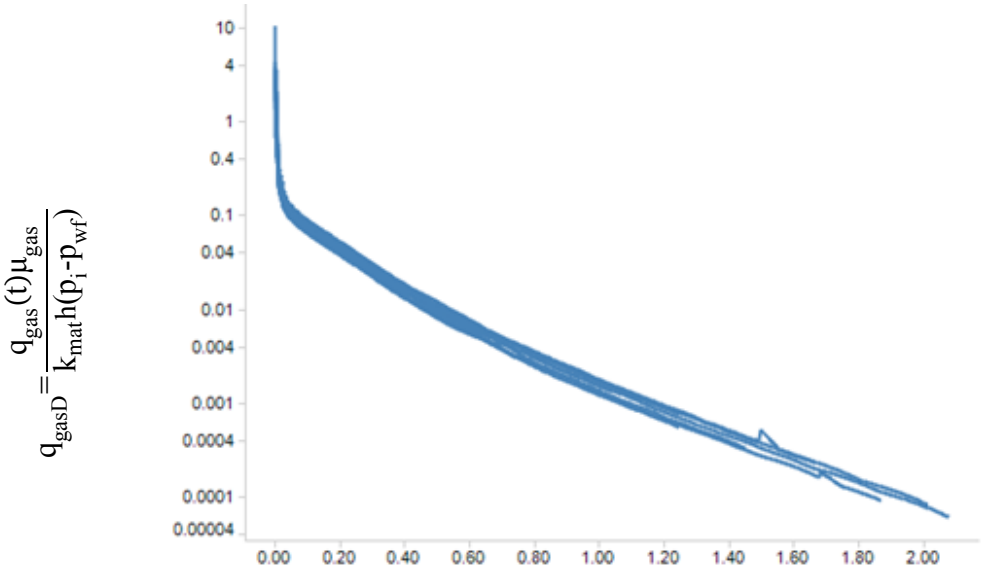

(b)

$$t_D=\frac{k_{mat}t}{\varphi c_t \mu_{oil}(2x_e-2x_f)^2}$$

Figure 26—Dimensionless gas rate versus dimensionless time for volatile oil area of interest. (a) $k_{srv}=4*k_{mat}$ (b) $k_{srv}=40*k_{mat}$ (c) $k_{srv}=400*k_{mat}$ (d) $k_{srv}=4000*k_{mat}$

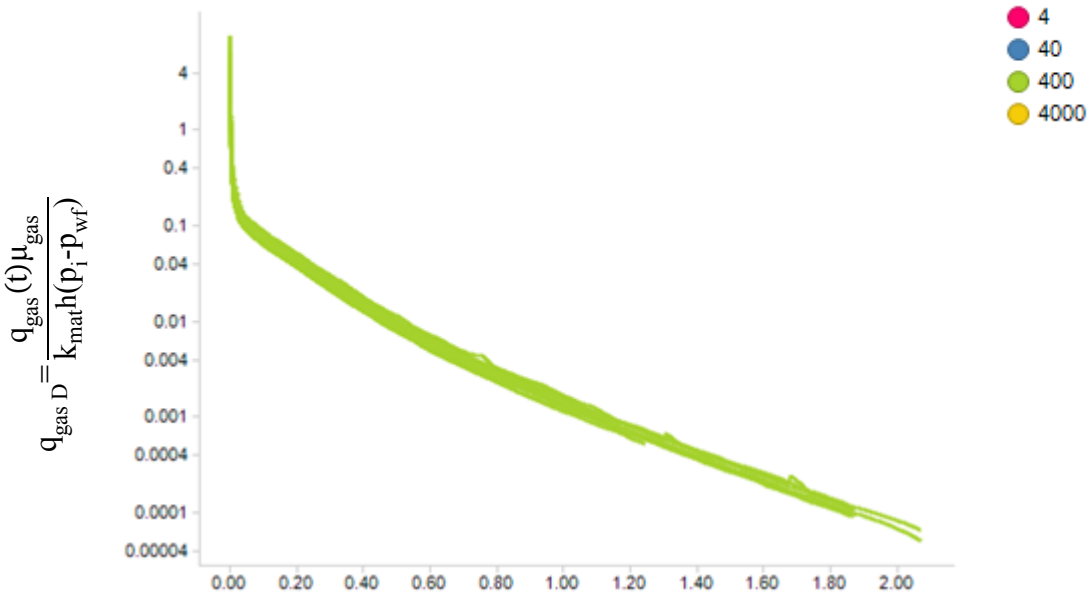

(c)

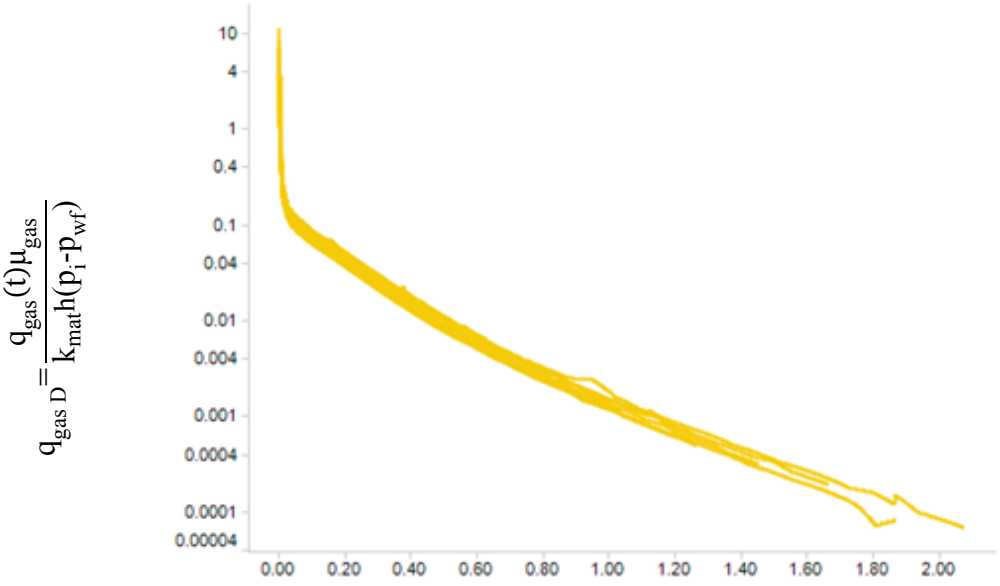

(d)

$$t_D=\frac{k_{mat}t}{\varphi c_t \mu_{oil}(2x_e-2x_f)^2}$$

Figure 26—Continued.

For the range of parameters in all cases simulated here with a single fluid system, dimensionless production histories for all cases are plotted in Figure 27. This figure shows that production histories converge for both oil and gas.

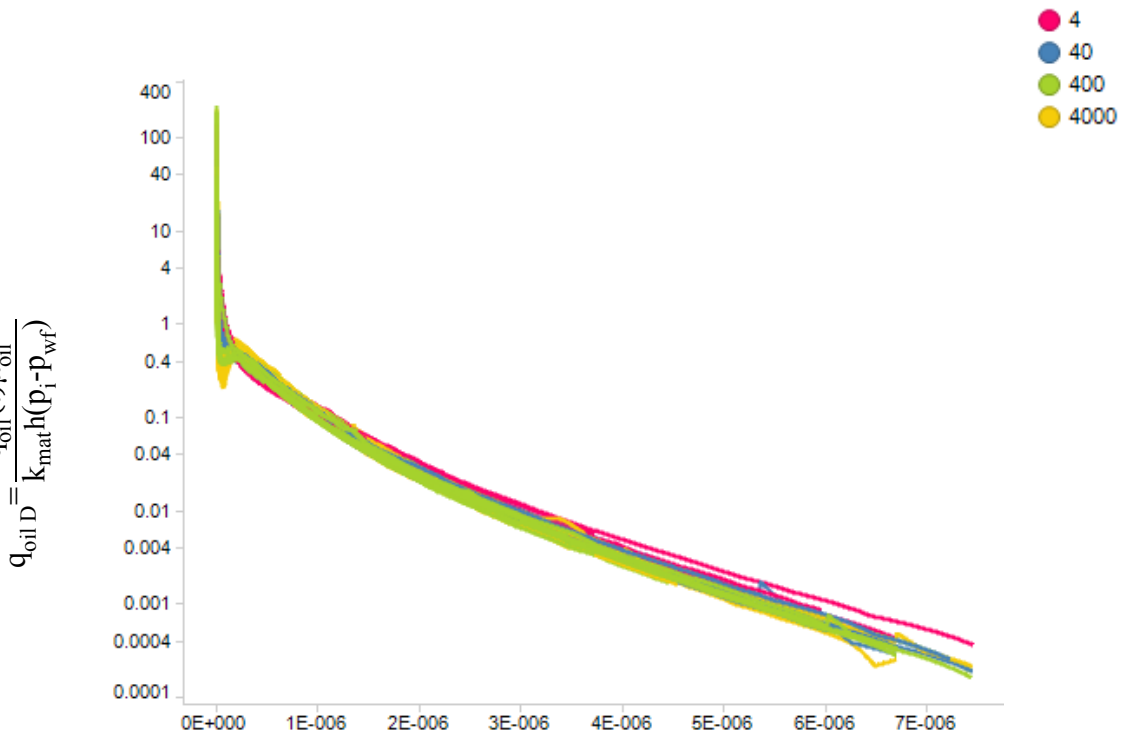

(a)

$$t_D=\frac{k_{mat}t}{\varphi c_t \mu_{oil}(2x_e-2x_f)^2}$$

Figure 27—Dimensionless production histories for volatile oil area of interest. (a) dimensionless oil rate versus dimensionless time for $k_{srv}=4*k_{mat}$, $k_{srv}=40*k_{mat}$, $k_{srv}=400*k_{mat}$, and $k_{srv}=4000*k_{mat}$ (b) dimensionless gas rate versus dimensionless time for $k_{srv}=4*k_{mat}$, $k_{srv}=40*k_{mat}$, $k_{srv}=400*k_{mat}$, and $k_{srv}=4000*k_{mat}$

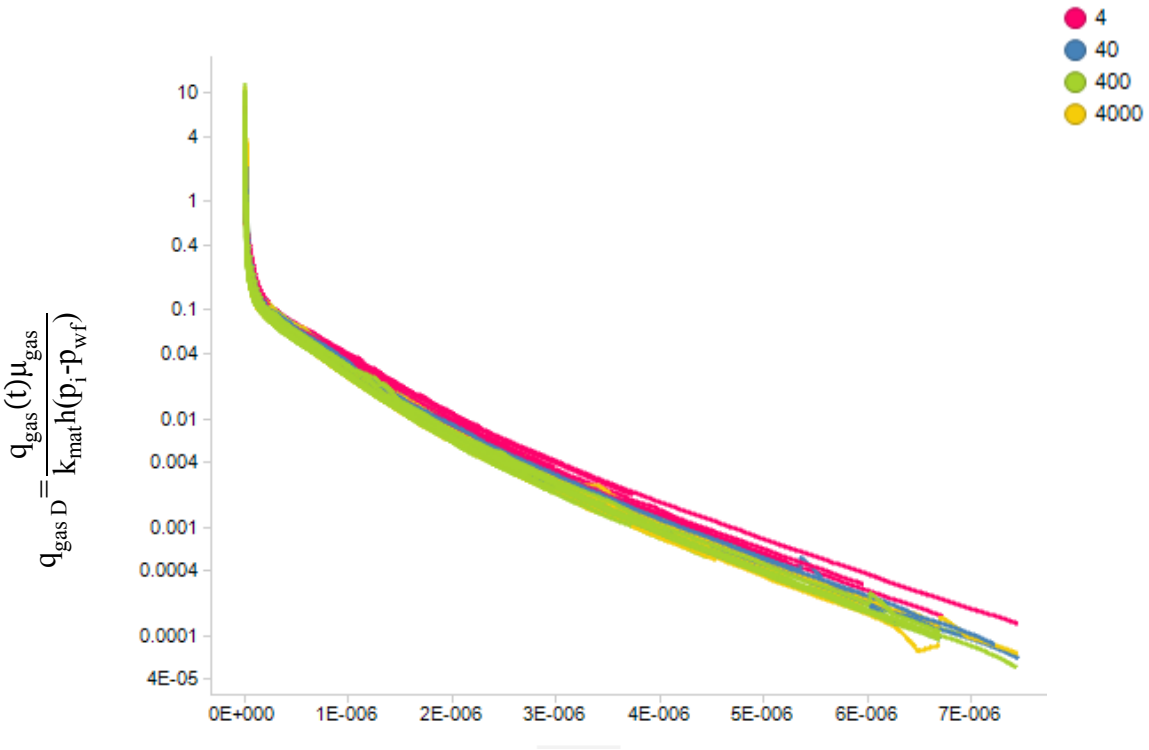

(b)

$$t_D=\frac{k_{mat}t}{\varphi c_t \mu_{oil}(2x_e-2x_f)^2}$$

Figure 27—Continued.

As shown above, the convergence of all cases to a similar trend supports the hypothesis that a single dimensionless rate versus dimensionless time plot may be used beyond the early transient time to forecast both oil and gas production.

Black Oil Area of Interest

Similar analyses of 46 cases with different matrix permeabilities, stimulated rock permeabilities, and initial reservoir pressures that include the range of parameters described above were developed for the black oil area of interest. The permeability and initial pressure properties for these cases are summarized in Figure 28. These combinations cover the range of matrix and stimulated rock permeabilities and initial reservoir pressures that were discussed earlier in the chapter.

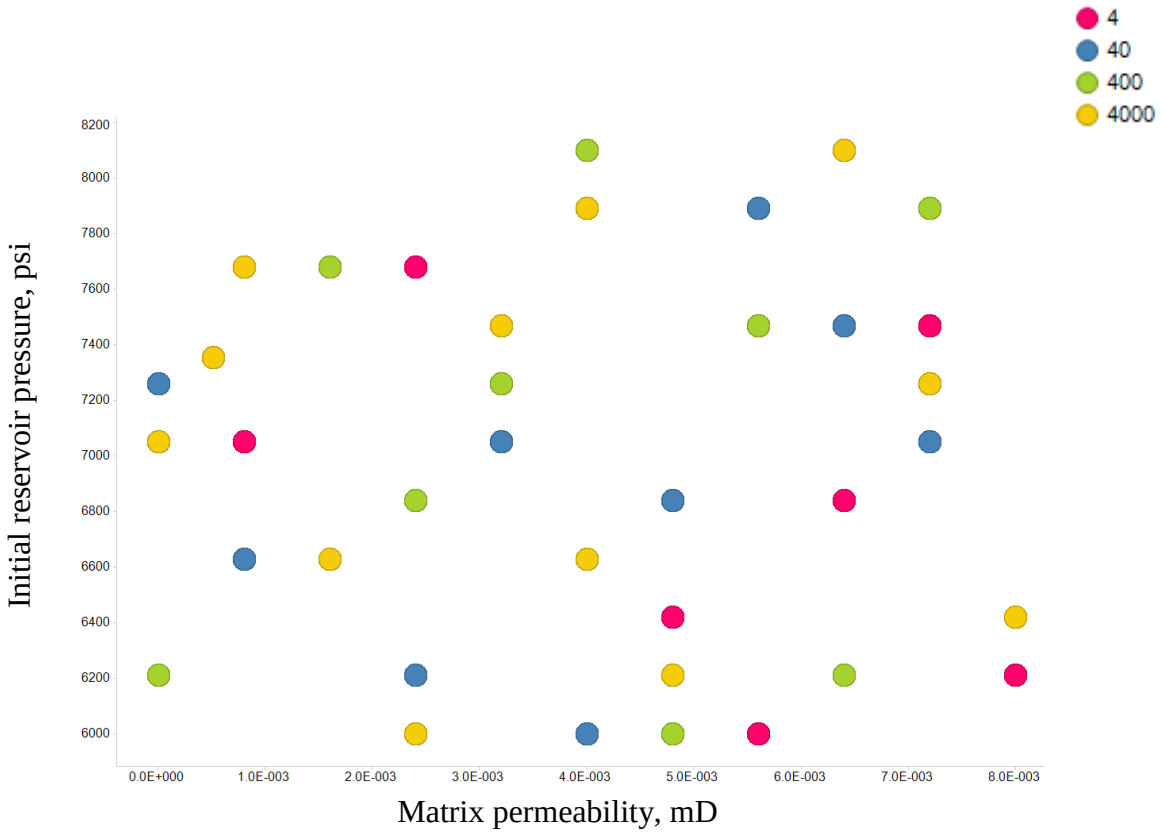

Figure 28—Black oil area of interest. Combination of k_{mat}, k_{srv}, and p_i

The stimulation results for these are shown in Figures 29 and 30 for oil and gas production histories respectively. The histories are broken down into different stimulation intensities. The 4 scenarios include stimulated rock permeability, k_{srv}, of 4x, 40x, 400x, and 4000x that of the original matrix permeability, k_{mat}.

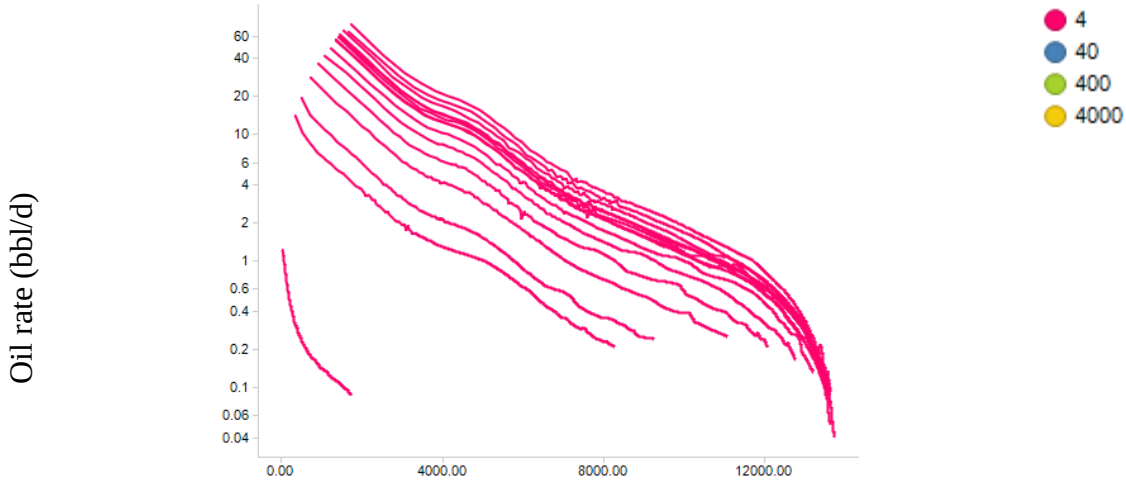

(a)

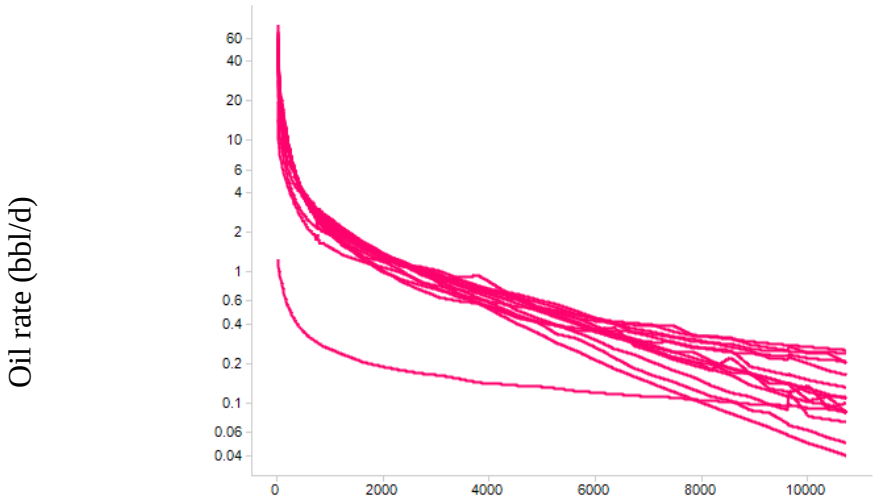

(b)

Figure 29—Oil production history for black oil area of interest for a single fracture stage. (a) oil rate vs. cumulative oil production for $k_{srv}=4*k_{mat}$ (b) oil rate vs. production time for $k_{srv}=4*k_{mat}$ (c) oil rate vs. cumulative oil production for $k_{srv}=40*k_{mat}$ (d) oil rate vs. production time for $k_{srv}=40*k_{mat}$(e) oil rate vs. cumulative oil production for $k_{srv}=400*k_{mat}$ (f) oil rate vs. production time for $k_{srv}=400*k_{mat}$ (g) oil rate vs. cumulative oil production for $k_{srv}=4000*k_{mat}$ (h) oil rate vs. production time for $k_{srv}=4000*k_{mat}$

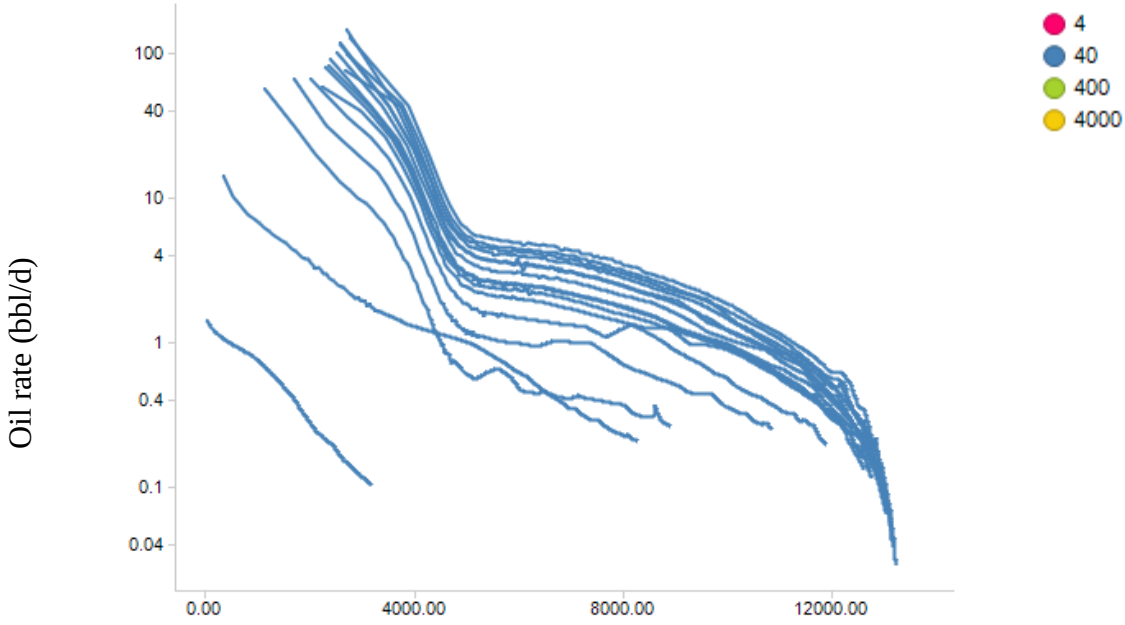

(c)

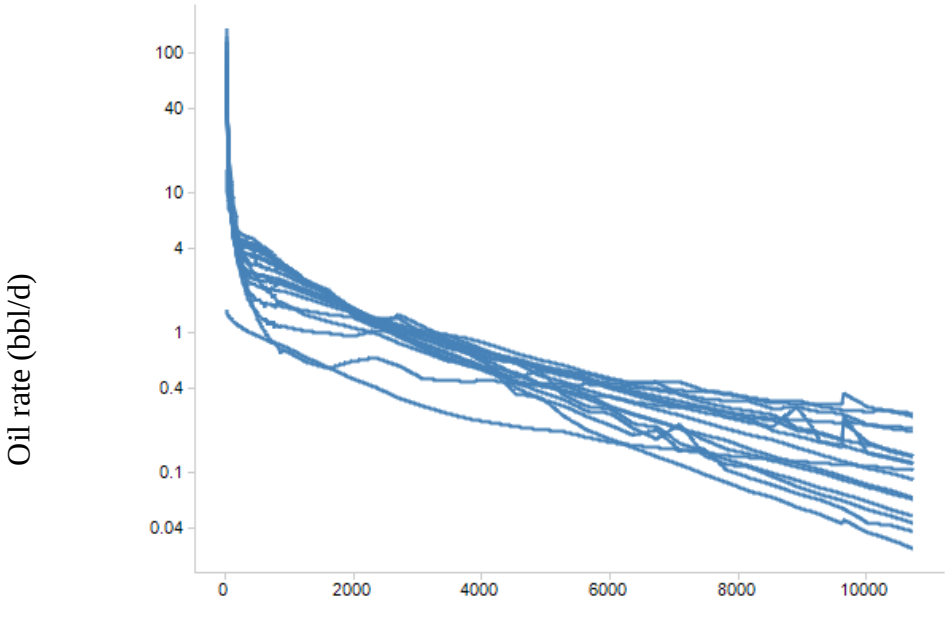

(d)

Figure 29—Continued,

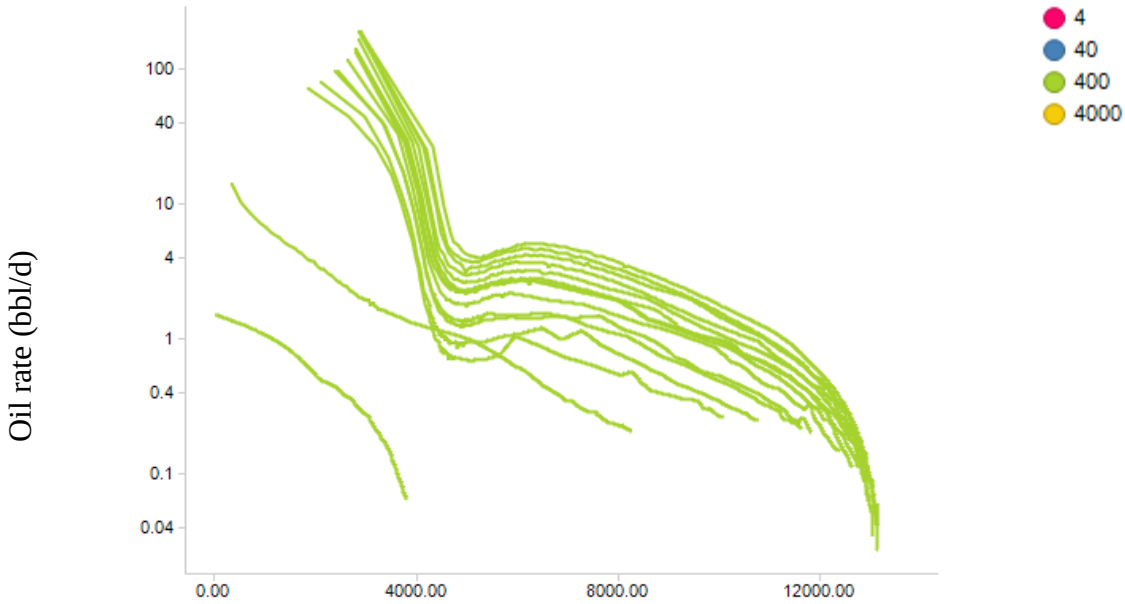

(e)

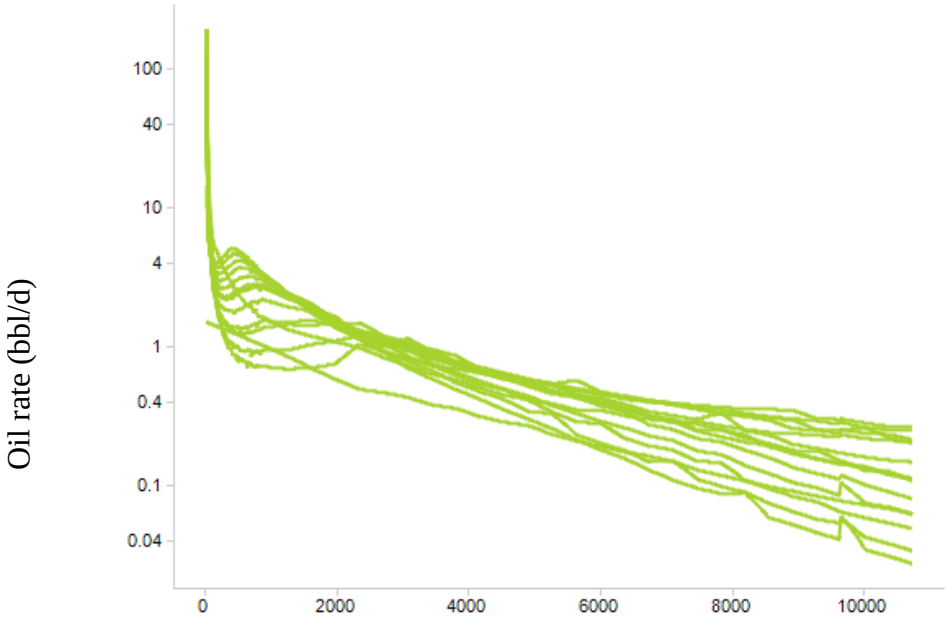

(f)

Figure 29—Continued

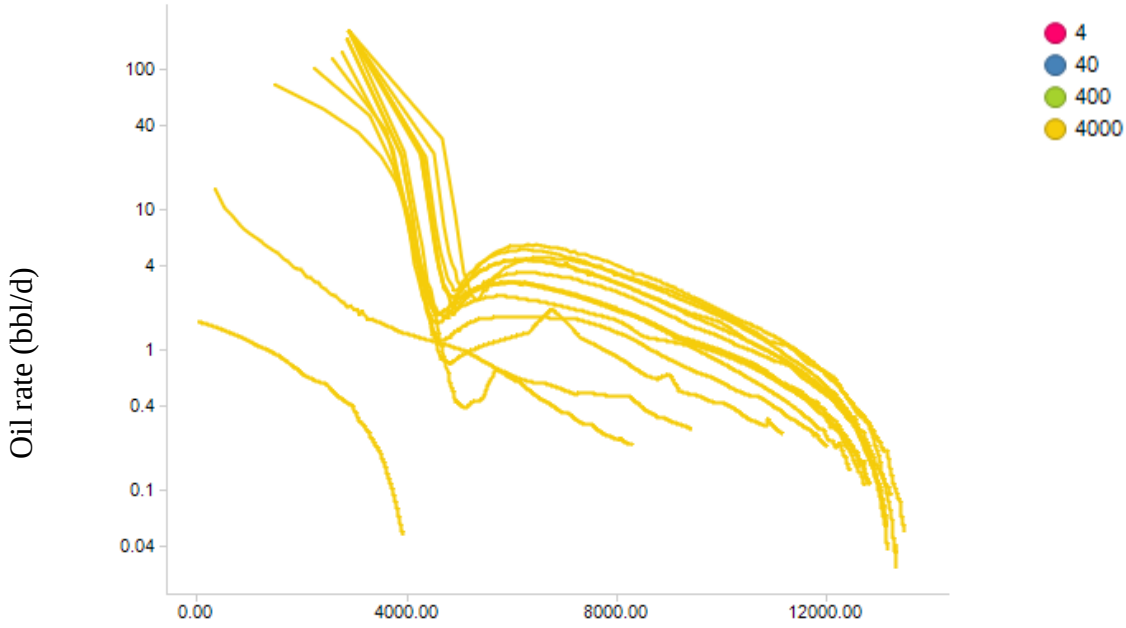

(g)

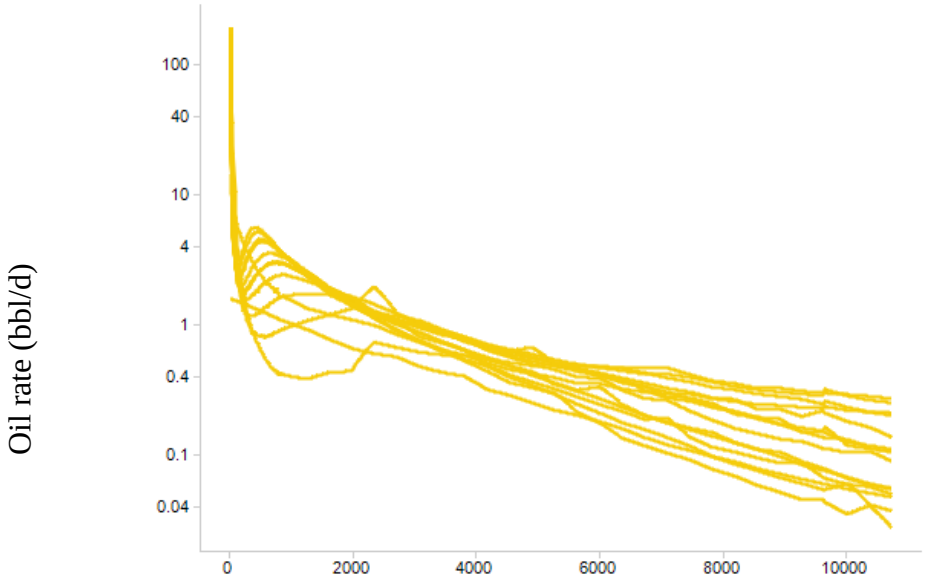

(h)

Figure 29—Continued.

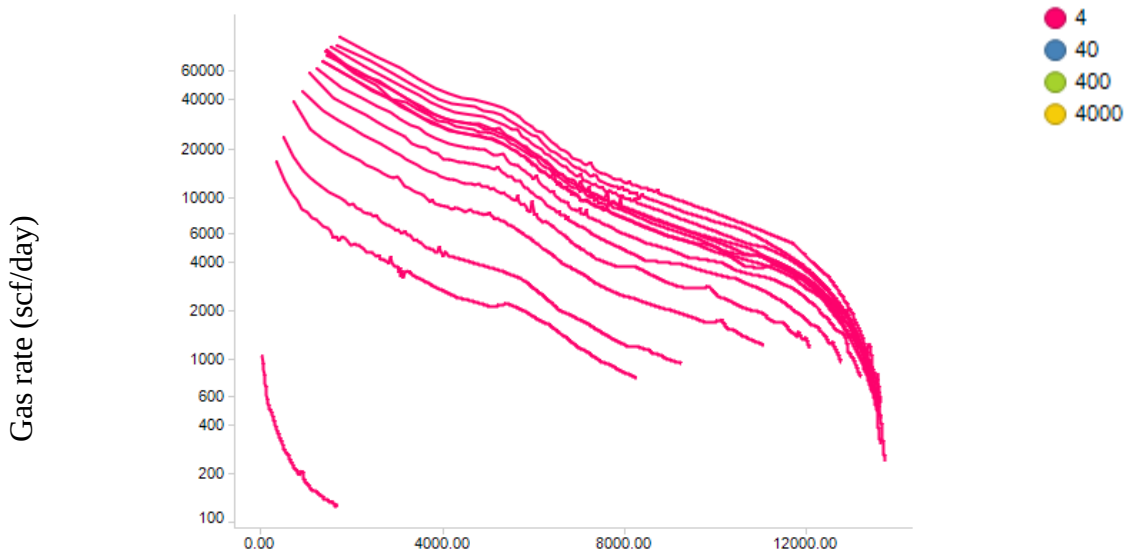

(a)

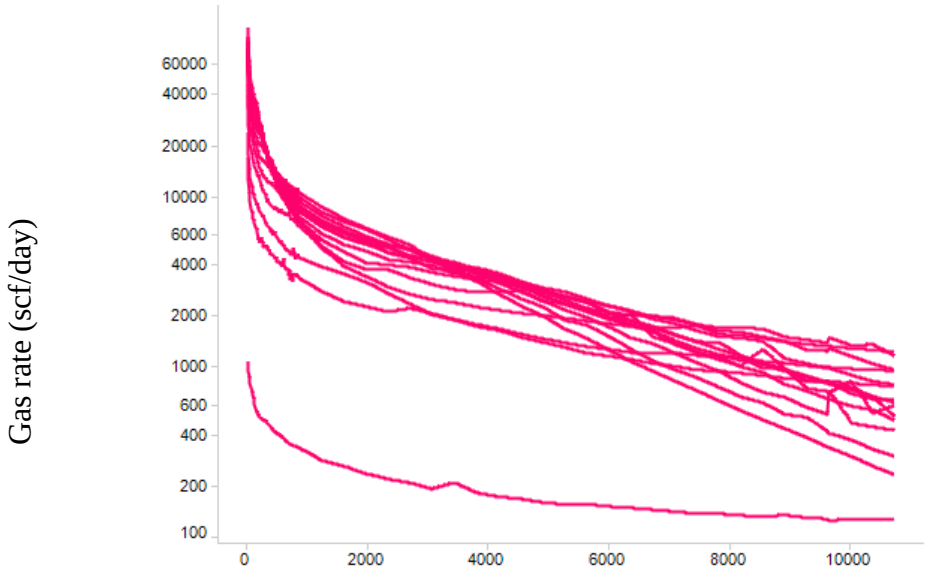

(b)

Figure 30—Gas production history for black oil area of interest for a single fracture stage illustrating gas rate versus cumulative oil production and time. (a) gas rate vs. cumulative oil production for $k_{srv}=4*k_{mat}$ (b) gas rate vs. time for $k_{srv}=4*k_{mat}$ (c) gas rate vs. cumulative oil production for $k_{srv}=40*k_{mat}$ (d) gas rate vs. time for $k_{srv}=40*k_{mat}$(e) gas rate vs. cumulative oil production for $k_{srv}=400*k_{mat}$ (f) gas rate vs. time for $k_{srv}=400*k_{mat}$ (g) gas rate vs. cumulative oil production for $k_{srv}=4000*k_{mat}$ (h) gas rate vs. time for $k_{srv}=4000*k_{mat}$

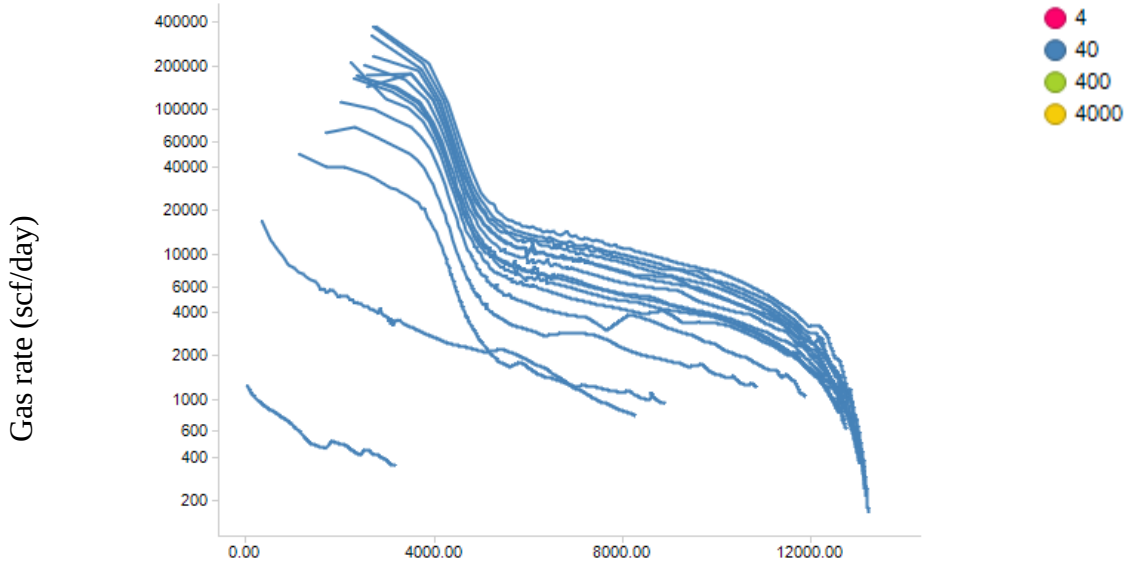

(c)

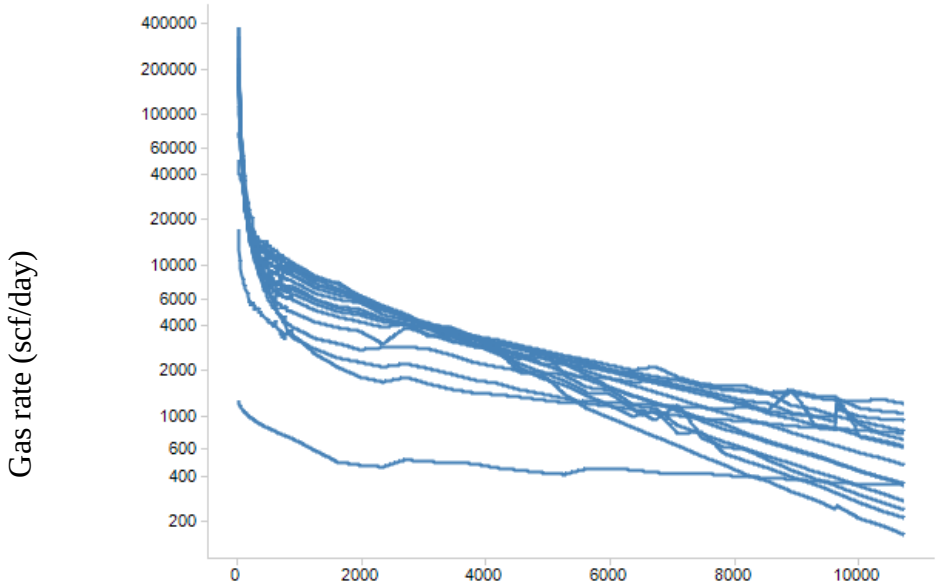

(d)

Figure 30—Continued

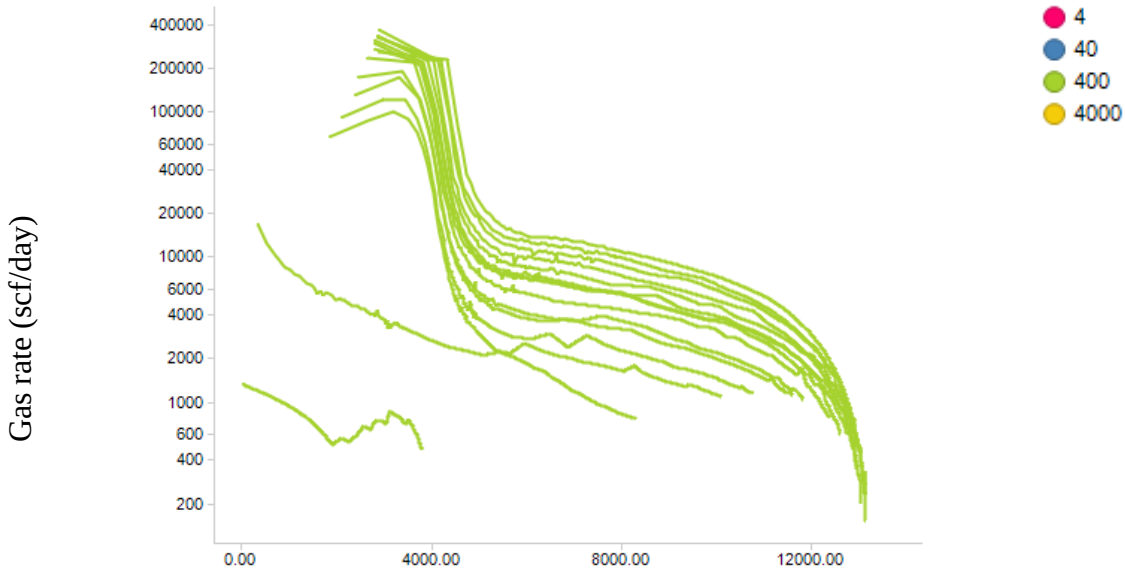

(e)

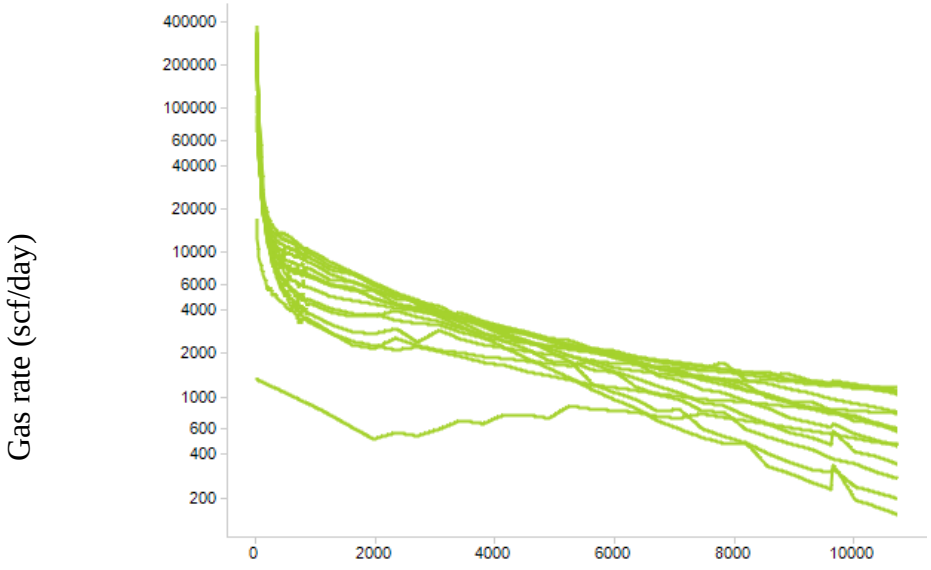

(f)

Figure 30—Continued,

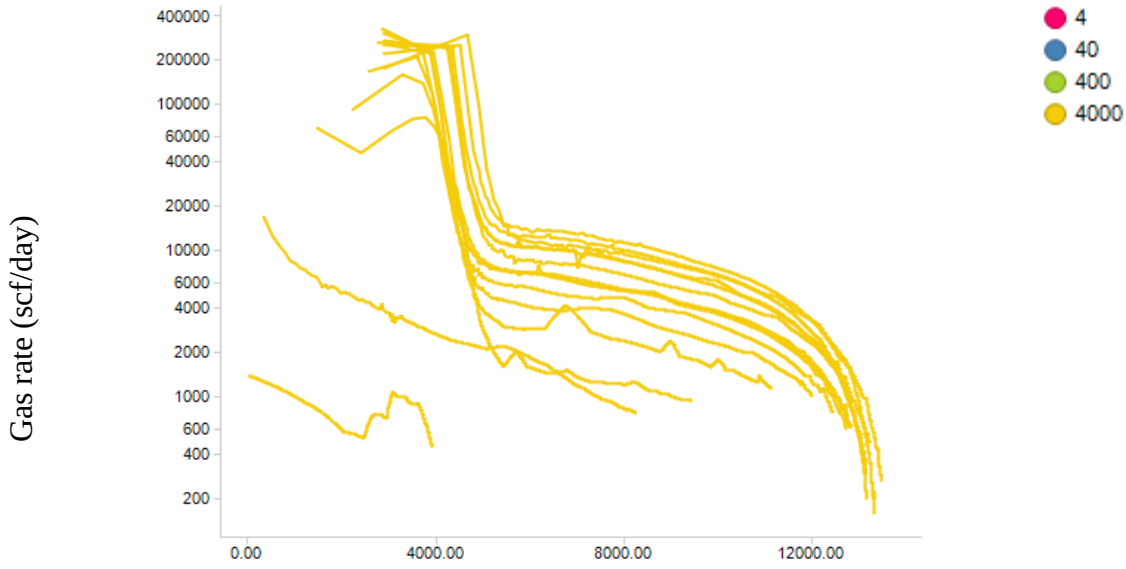

(g)

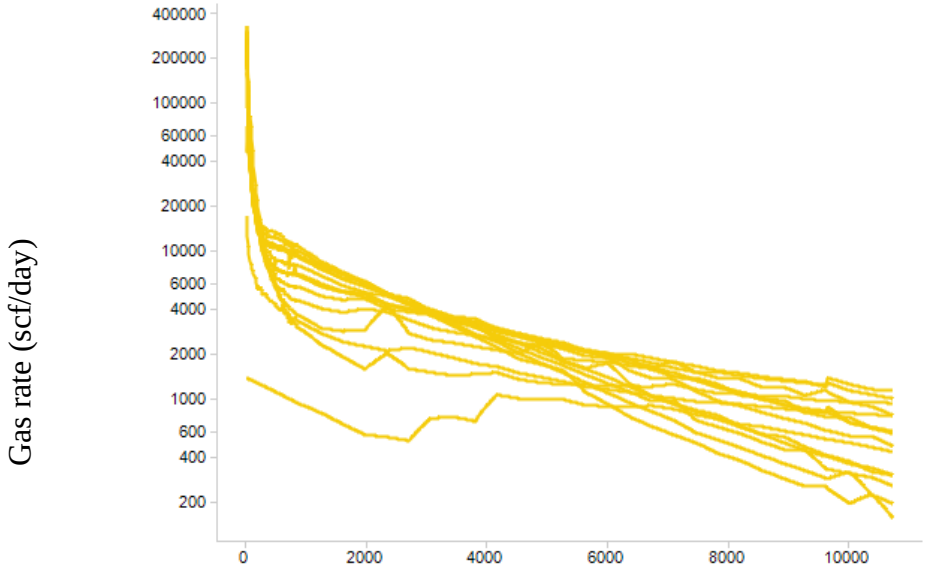

(h)

Figure 30—Continued.

As with the volatile oil area of interest, in this area, the dimensionless rate versus dimensionless time plots in Figures 31 and 32 show that, after an early transient start, production histories converge to a uniform shape.

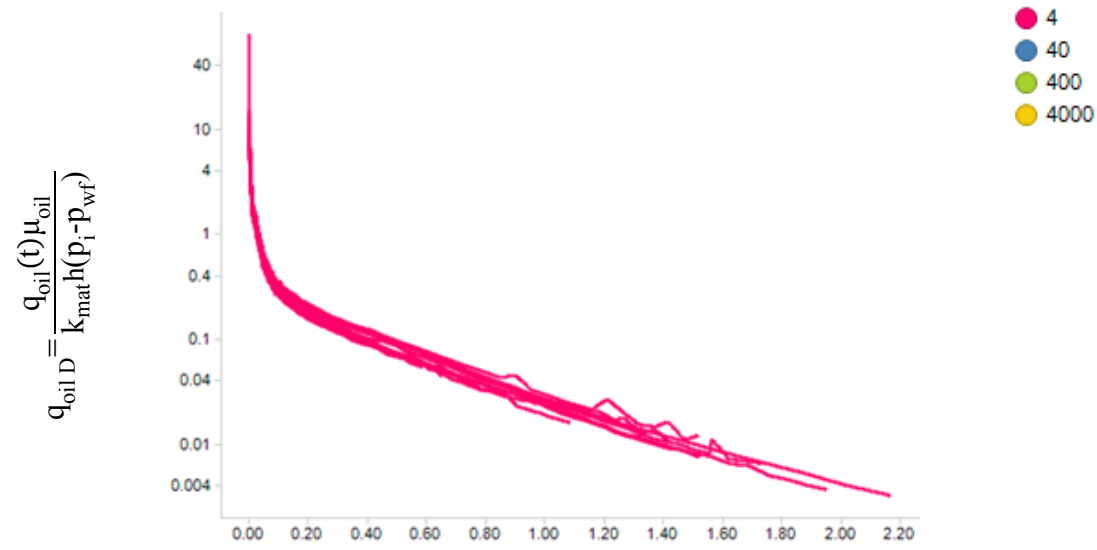

(a)

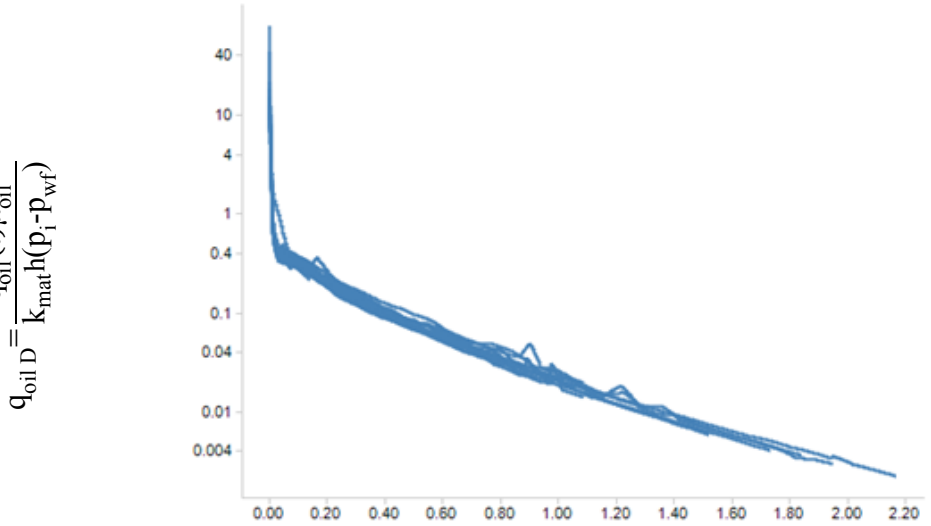

(b)

$$t_D=\frac{k_{mat}t}{\varphi c_t \mu_{oil}(2x_e-2x_f)^2}$$

Figure 31—Dimensionless oil rate versus dimensionless time for black oil area of interest. (a) $k_{srv}=4*k_{mat}$ (b) $k_{srv}=40*k_{mat}$ (c) $k_{srv}=400*k_{mat}$ (d) $k_{srv}=4000*k_{mat}$

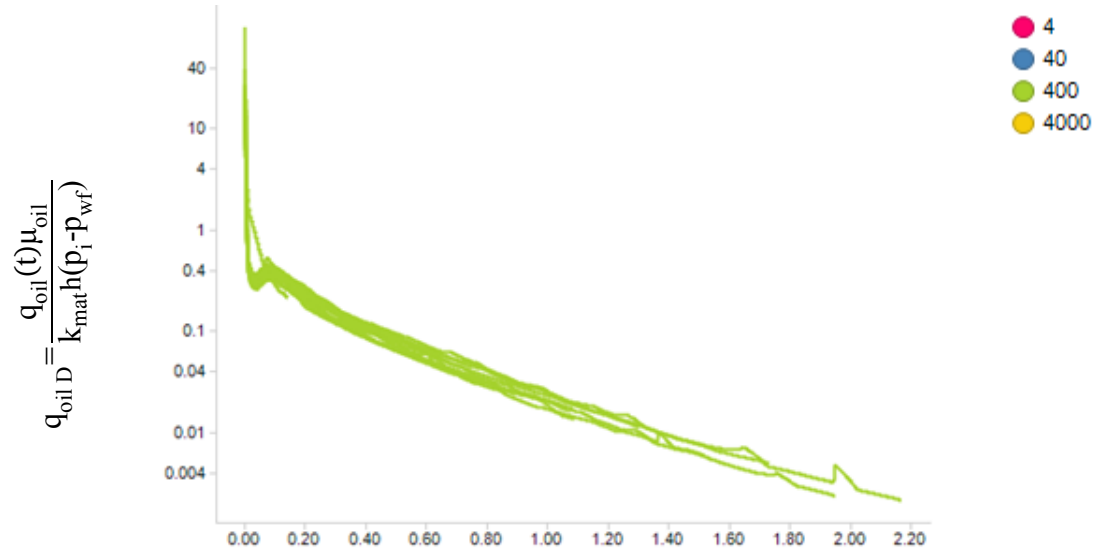

(c)

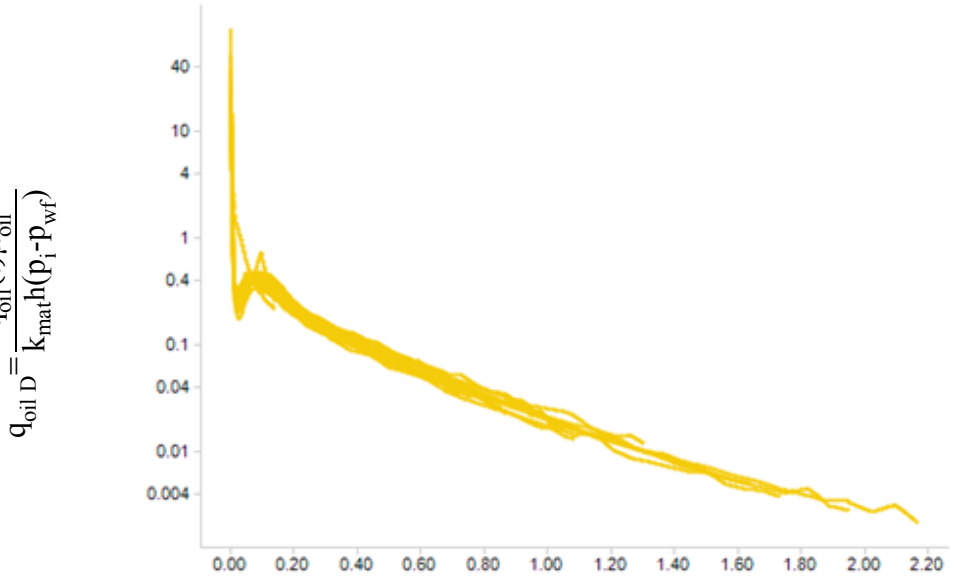

(d)

$$t_D=\frac{k_{mat}t}{\varphi c_t\mu_{oil}(2x_e-2x_f)^2}$$

Figure 31—Continued.

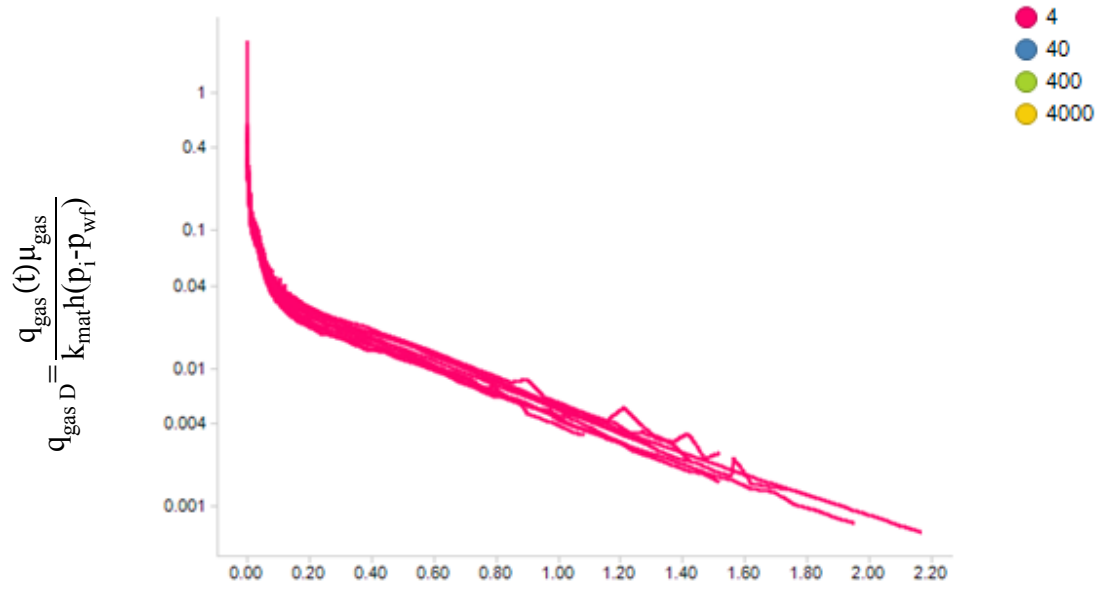

$$q_{gas\,D}=\frac{q_{gas}(t)\mu_{gas}}{k_{mat}h(p_i-p_{wf})}$$

(a)

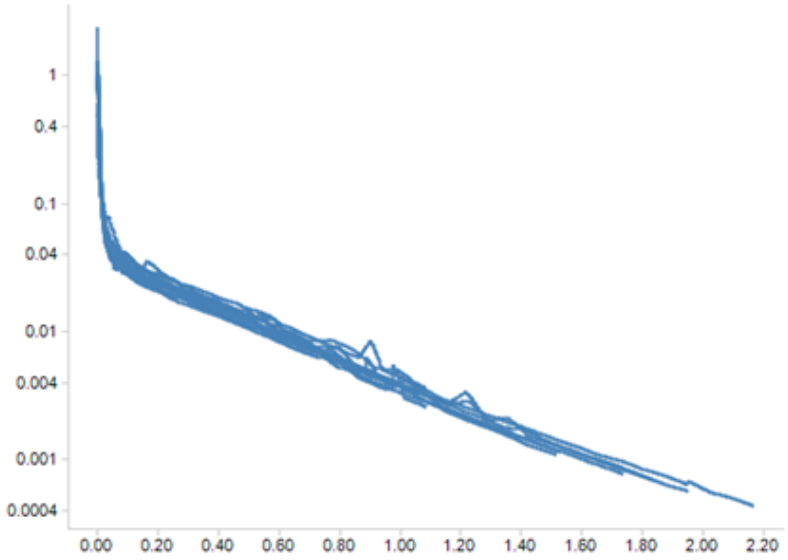

$$q_{gas\,D}=\frac{q_{gas}(t)\mu_{gas}}{k_{mat}h(p_i-p_{wf})}$$

(b)

$$t_D=\frac{k_{mat}t}{\varphi c_t\mu_{oil}(2x_e-2x_f)^2}$$

Figure 32—Dimensionless gas versus dimensionless time for black oil area of interest. (a) $k_{srv}=4*k_{mat}$ (b) $k_{srv}=40*k_{mat}$ (c) $k_{srv}=400*k_{mat}$ (d) $k_{srv}=4000*k_{mat}$

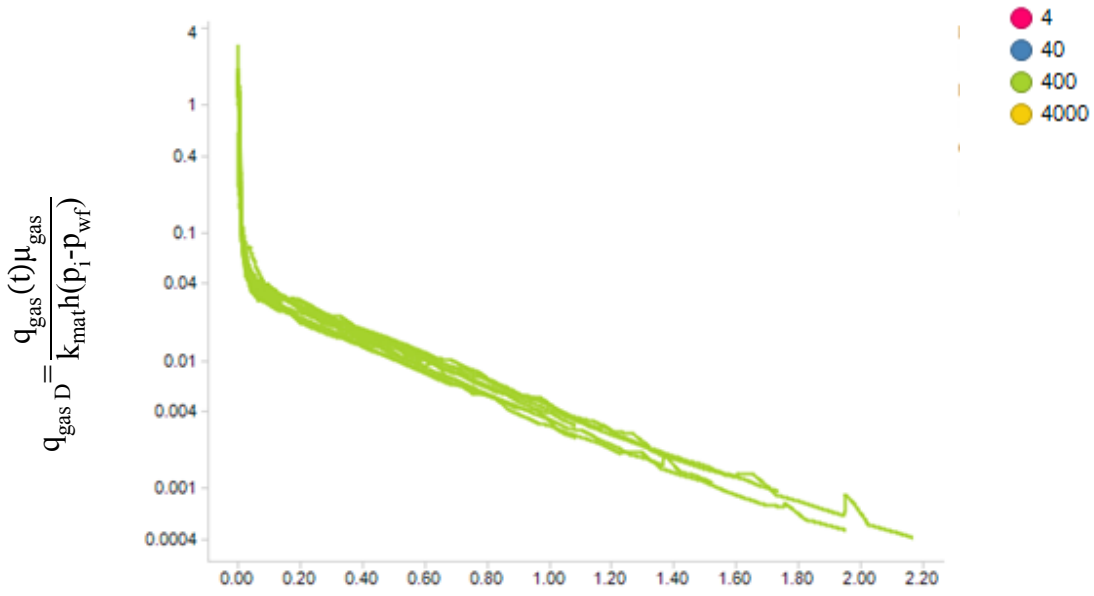

(c)

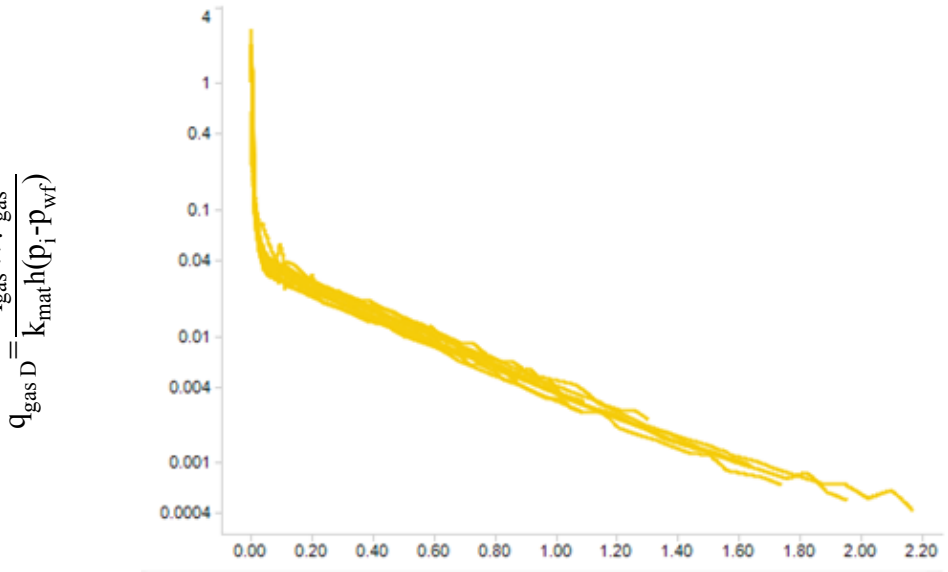

(d)

$$t_D=\frac{k_{mat}t}{\varphi c_t\mu_{oil}(2x_e-2x_f)^2}$$

Figure 32—Continued

Figure 33 illustrates the convergence of dimensionless production histories for all cases in black oil area of interest.

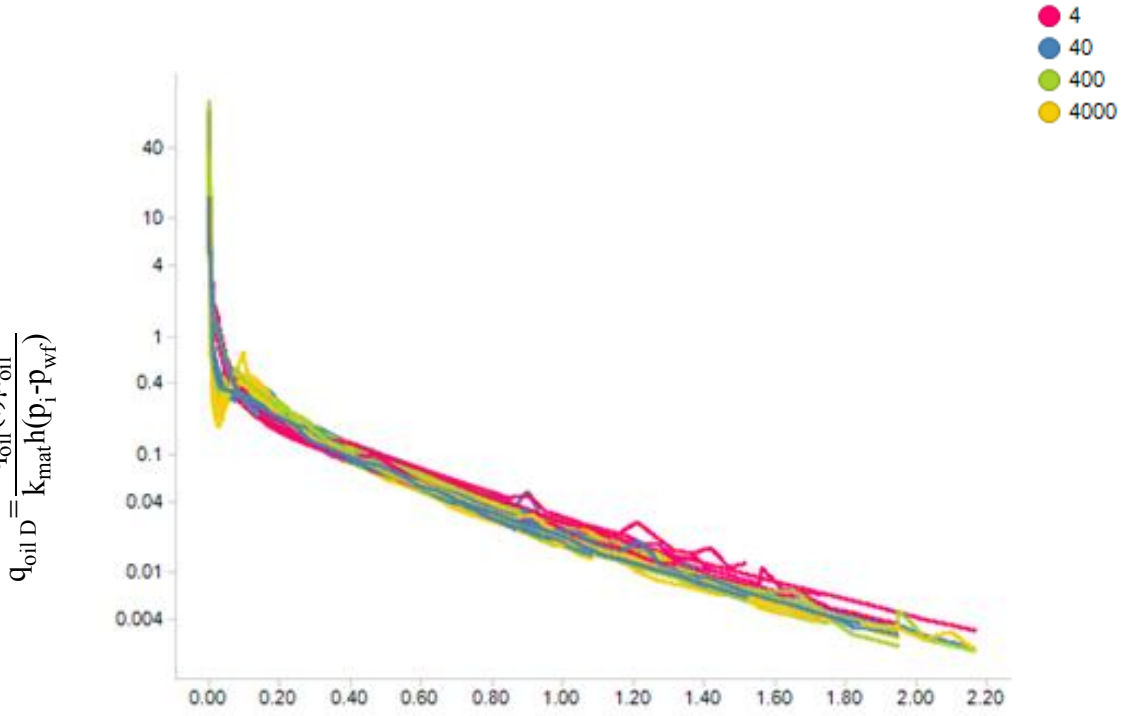

$$t_D=\frac{k_{mat}t}{\varphi c_t\mu_{oil}(2x_e-2x_f)^2}$$

(a)

Figure 33—Dimensionless production histories for black oil area of interest. (a) dimensionless oil rate versus dimensionless time for $k_{srv}=4*k_{mat}$, $k_{srv}=40*_{kmat}$, $k_{srv}=400*k_{mat}$, and $k_{srv}=4000*k_{mat}$ (b) dimensionless gas rate versus dimensionless time for $k_{srv}=4*k_{mat}$, $k_{srv}=40*k_{mat}$, $k_{srv}=400*k_{mat}$, and $k_{srv}=4000*k_{mat}$

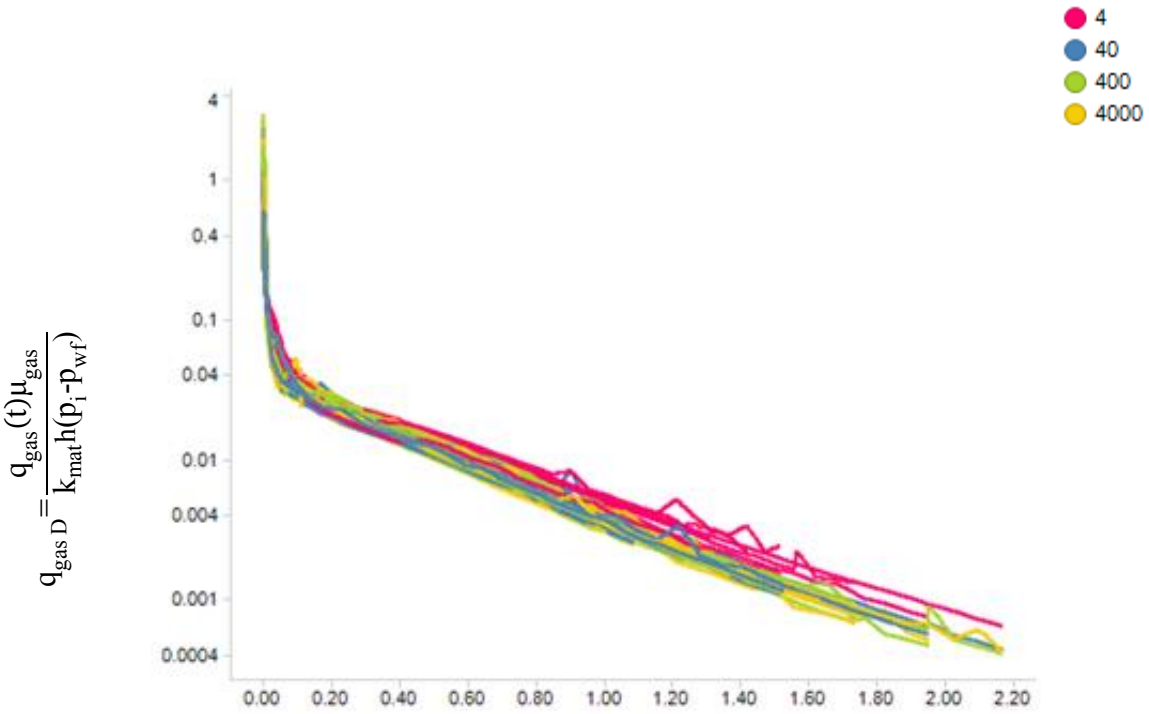

$$t_D=\frac{k_{mat}t}{\varphi c_t \mu_{oil}(2x_e-2x_f)^2}$$

(b)

Figure 33—Continued.

Convergence of all cases in black oil area of interest to a single dimensionless history supports the theory that a single decline model may be used beyond the early transient time to forecast production. This also applies to the secondary gas phase as the gas histories also converge.

Impact of Varying Stimulation Volume

The workflow must allow variability in stimulation geometry. To examine the sensitivity to variability in stimulation geometry a range of stimulation volume, long and short x_f

values were included in the study (Figure 34). Each of the scenarios (a) to (e) represents one simulation run.

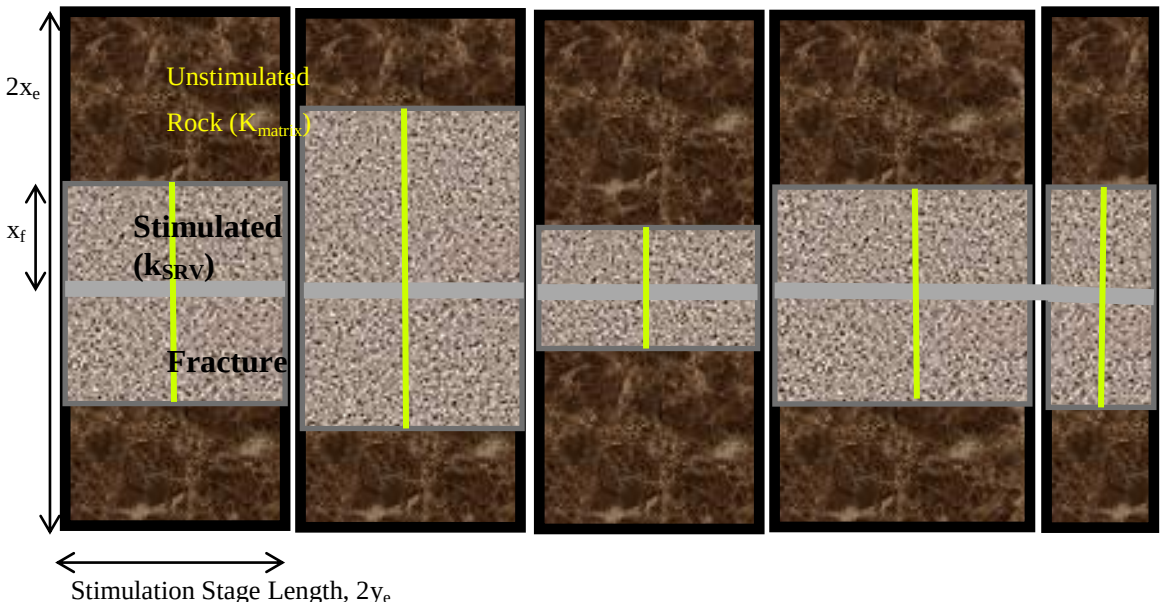

Figure 34—Single stimulation stage, a section of a horizontal well. (a) base case stage and stimulation size, (b) Same as base with longer x_f, large SRV, (c) same as base with shorter x_f, smaller SRV, (d) Same x_f as base but with wider stage length, (e) same x_f as base, but with narrower stage length

The dimensions for these cases are summarized in Table 8 below:

Case	Base (a)	Long (b)	Short (c)	Wide (d)	Narrow (e)
Drainage Boundary, ft	656	656	656	656	656
Stage Width, ft	200	200	200	223	177
x_f, ft	66	150	30	66	66

Table 8—Different stimulation geometries

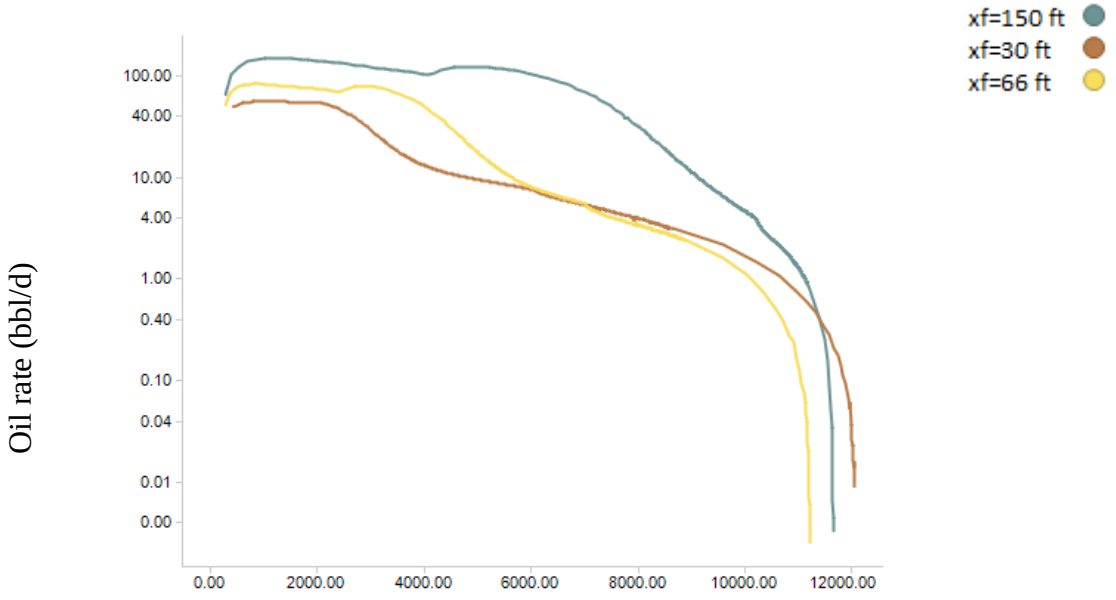

(a)

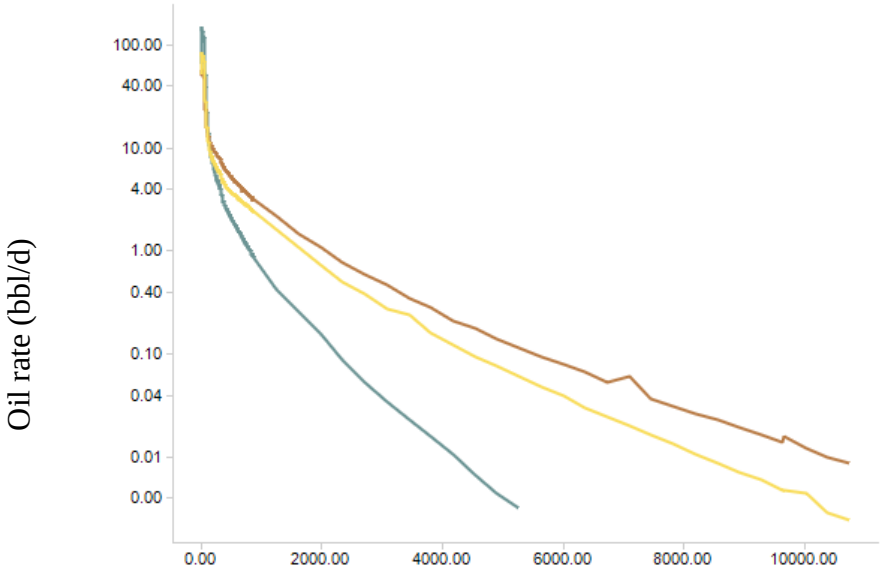

(b)

Figure 35—Production history – impact of stimulation geometry. (a) oil rate versus cumulative oil production, (b) oil rate versus time, (c) gas rate versus cumulative oil production, (d) gas rate versus time

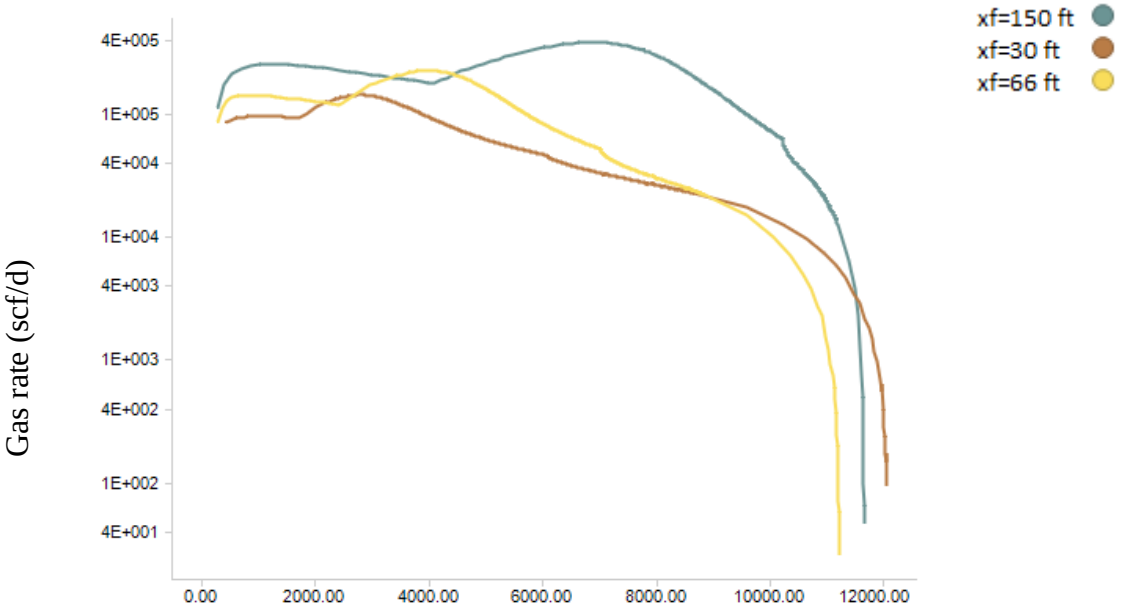

(c)

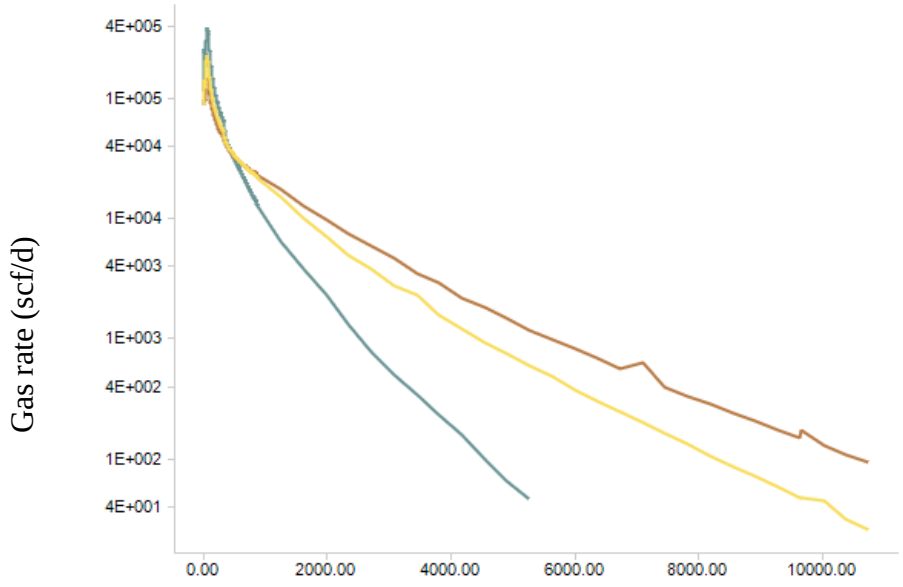

(d)

Figure 35—Continued.

Production histories for the various fracture half-lengths are plotted in Figure 35. The histories diverge more toward the end of the production. The rates for the case with the longest x_f start declining more rapidly than in the other two scenarios. These results indicate that the case with the longest x_f, (150 ft) reaches boundary dominated flow. Although unlikely in general, in the case of a long fracture half-length and large permeability enhancement, it is possible to reach boundary dominated flow; therefore, this needs to be accounted for in our workflow. The dimensionless time definition we propose accounts for this. On the log-log plot of dimensionless time versus dimensionless time, a slope of -1 indicates boundary dominated flow at higher matrix permeabilities (Figure 36).

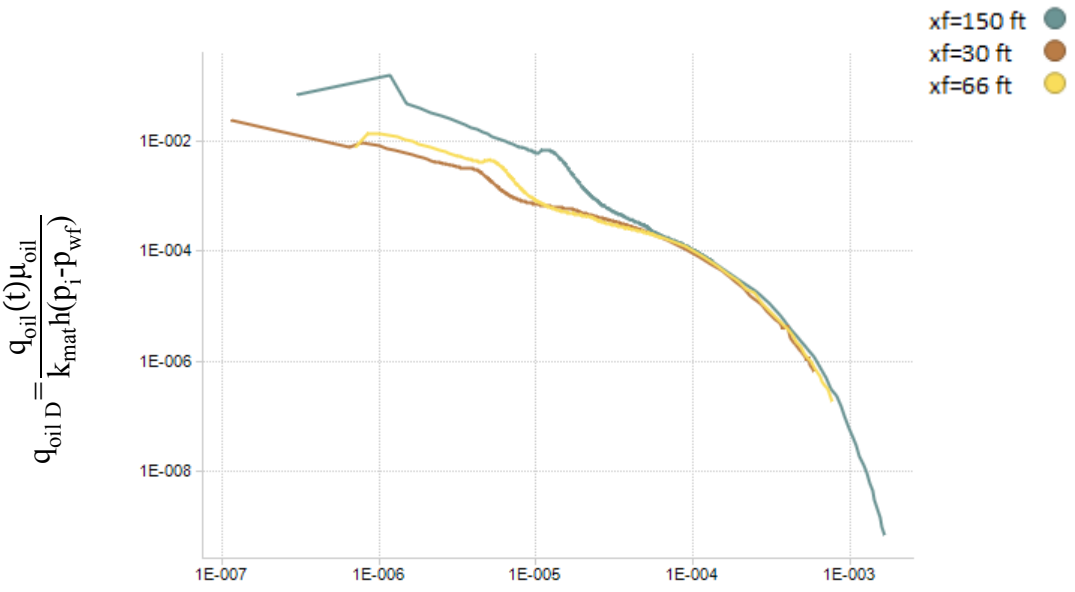

(a)

$$t_D=\frac{k_{mat}t}{\varphi c_t \mu_{oil}(2x_e-2x_f)^2}$$

Figure 36—Dimensionless production histories (log-log). (a) dimensionless oil rate versus dimensionless time for x_f=30ft, x_f=66ft, and x_f=150ft on log-log scale (b) dimensionless gas rate versus dimensionless time for x_f=30ft, x_f=66ft, and x_f=150ft on log-log scale.

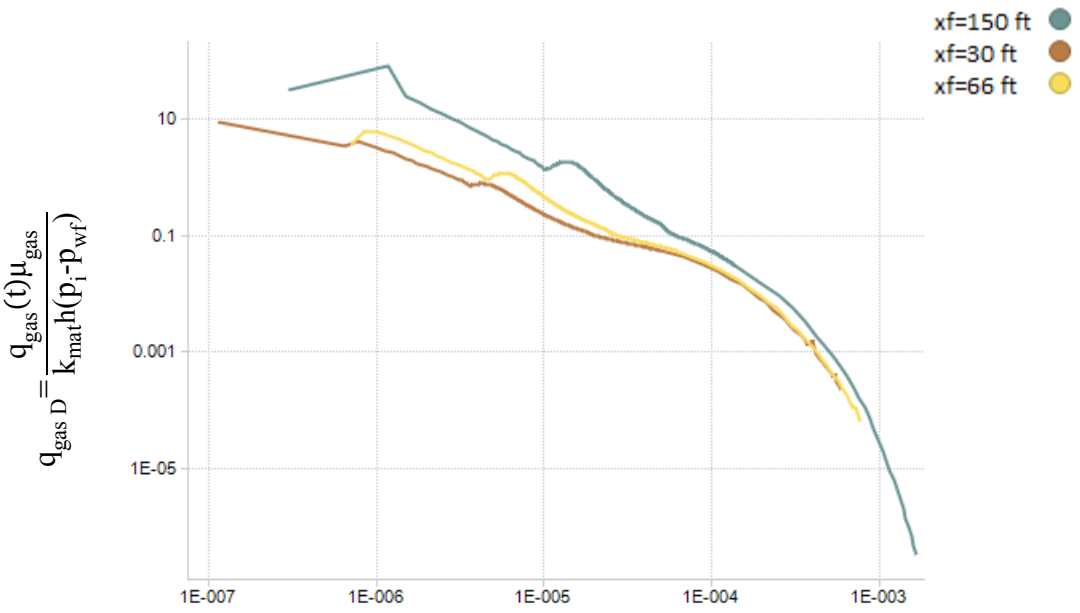

(a)

$$t_D=\frac{k_{mat}t}{\varphi c_t \mu_{oil}(2x_e-2x_f)^2}$$

Figure 36—Continued.

Figure 37 shows the production histories for different fracture half-lengths in a format similar to those presented in black oil and volatile oil areas of interest.

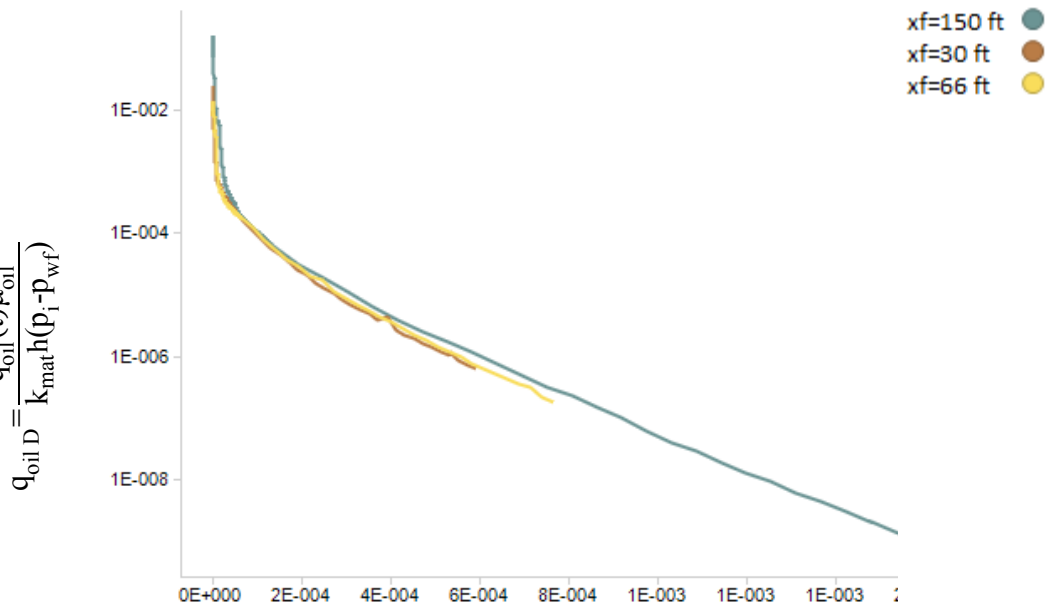

(a)

Figure 37—Dimensionless production histories. (a) dimensionless oil rate versus dimensionless time for x_f=30ft, x_f=66ft, and x_f=150ft (b) dimensionless gas rate versus dimensionless time for x_f=30ft, x_f=66ft, and x_f=150ft

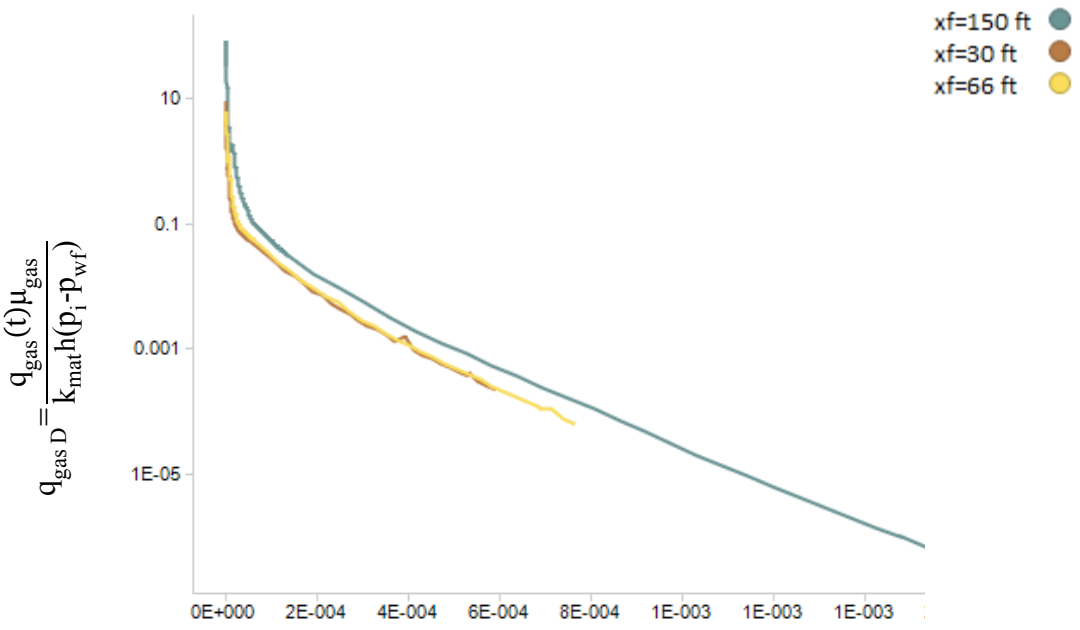

(b)

Figure 37—Continued.

In addition to fracture half-length, variability in fracture spacing was also studied. Figures 38 and 39 show the production histories and the equivalent dimensionless plots for the different stage spacing.

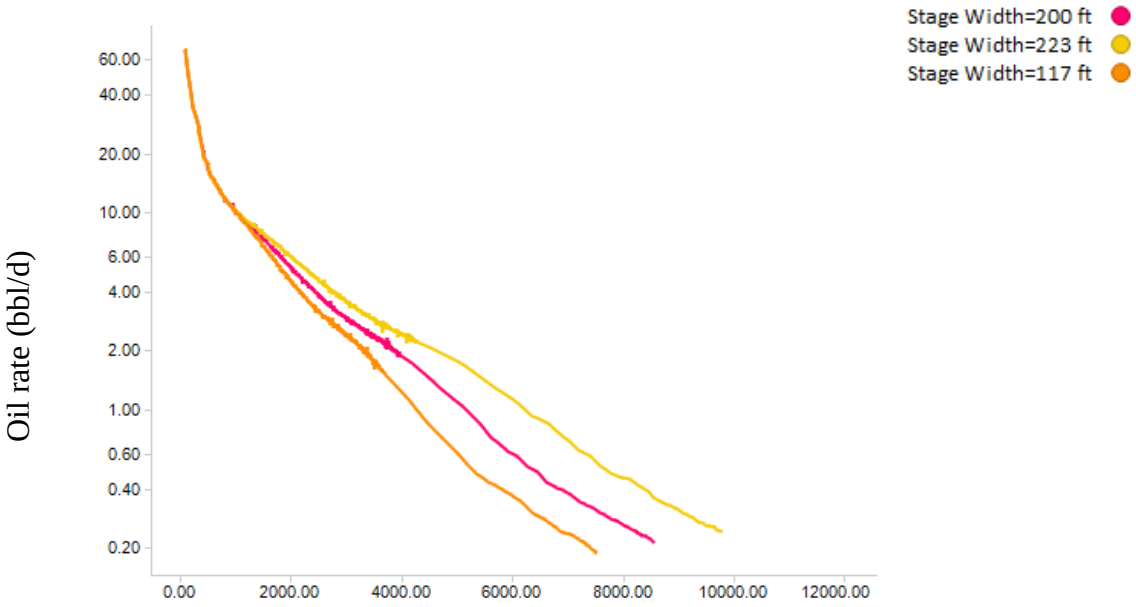

(a)

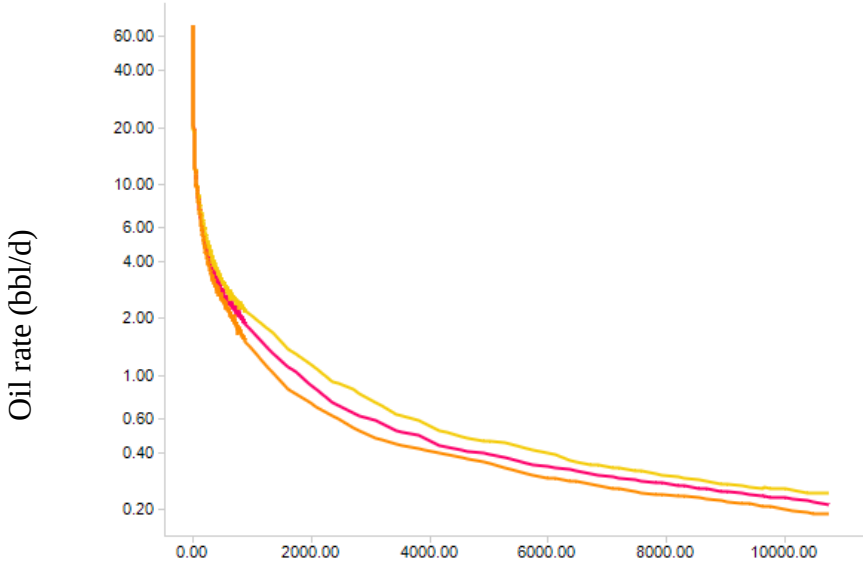

(b)

Figure 38—Production history – effect of stage spacing. (a) oil rate versus cumulative oil production, (b) oil rate versus time, (c) gas rate versus cumulative oil production, (d) gas rate versus time

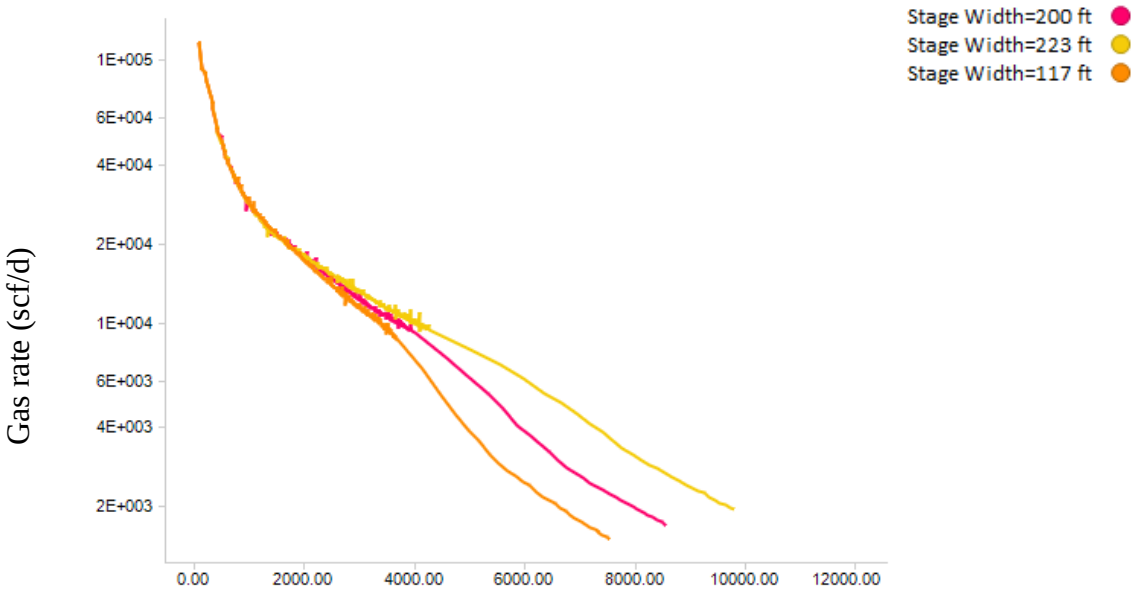

(c)

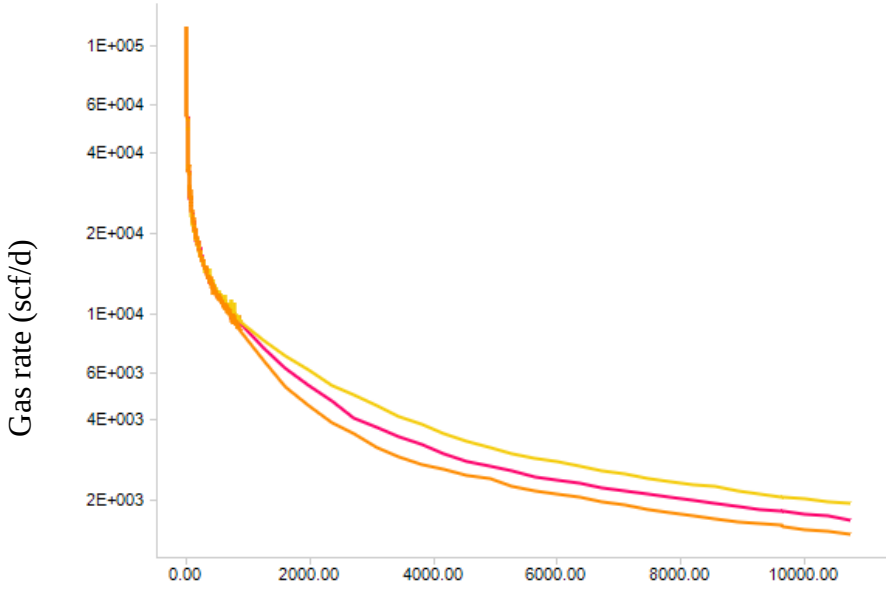

(d)

Figure 38—Continued.

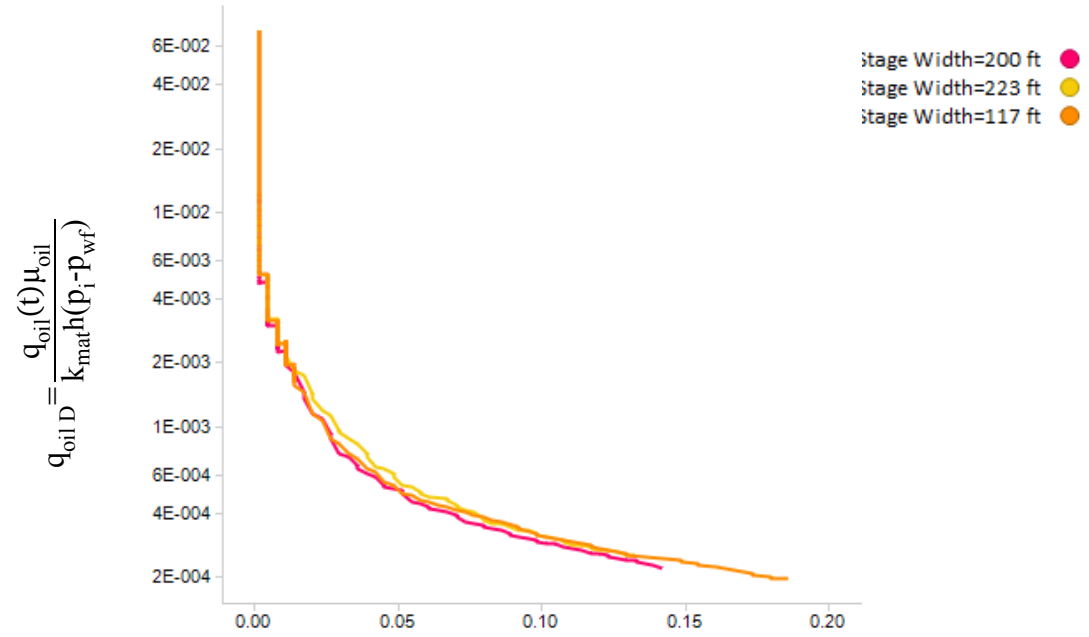

(a)

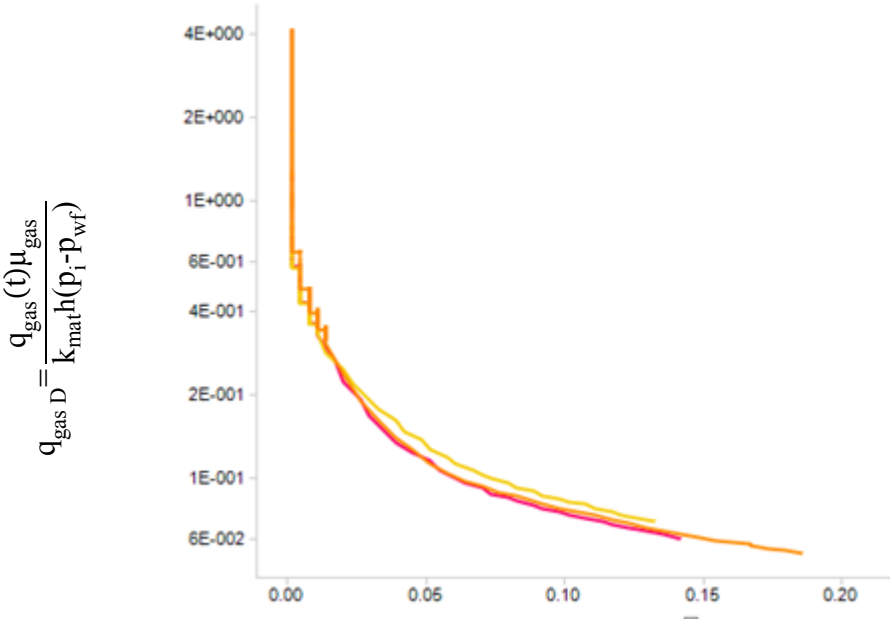

(b)

$$t_D=\frac{k_{mat}t}{\varphi c_t \mu_{oil}(2x_e-2x_f)^2}$$

Figure 39—Dimensionless production history – effect of stage spacing. (a) dimensionless oil rate versus dimensionless time, (b) dimensionless gas rate versus dimensionless time

In all cases in volatile oil and black oil areas of interest, the minimum bottom-hole flowing pressure was assumed to be 450 psi. This was intended to be the pressure at which artificial lift installation was required. This was the constant bottom-hole pressure after an initial decline from p_i to this pressure. In order to study the impact of increasing this minimum bottom-hole flow pressure, two other cases, one at 1200 psi, and the other at 1800 psi, were studied. Figure 40 shows the impact on production rates.

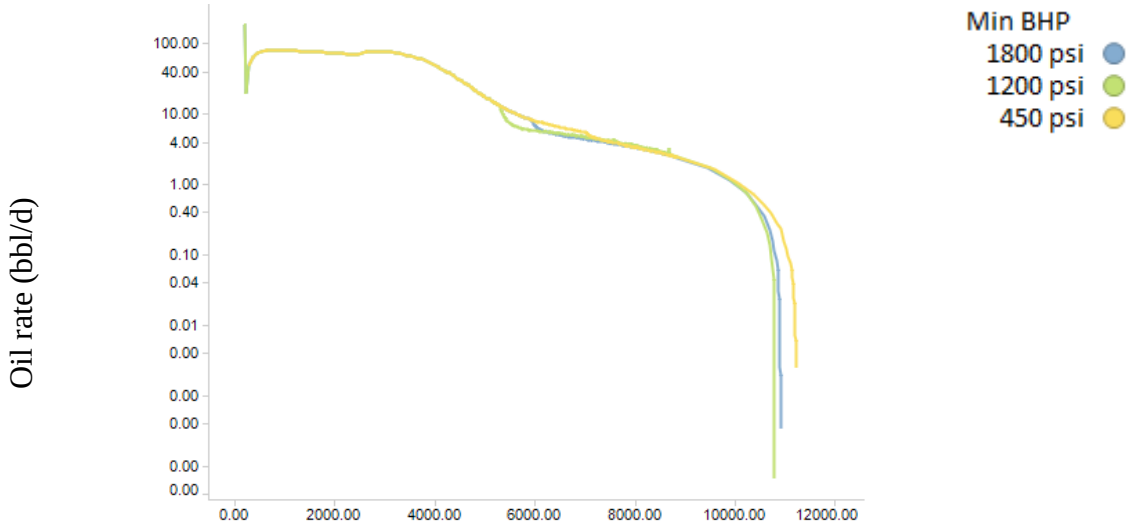

(a) Cumulative oil (bbl)

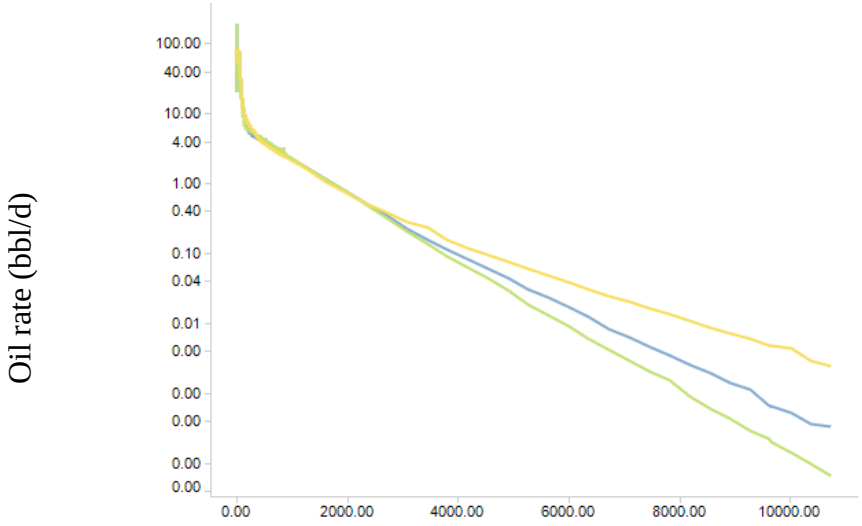

(b) Time (days)

Figure 40—Production history – effect of minimum BHP. (a) oil rate versus cumulative oil production, (b) oil rate versus time, (c) gas rate versus cumulative oil production, (b) gas rate versus time

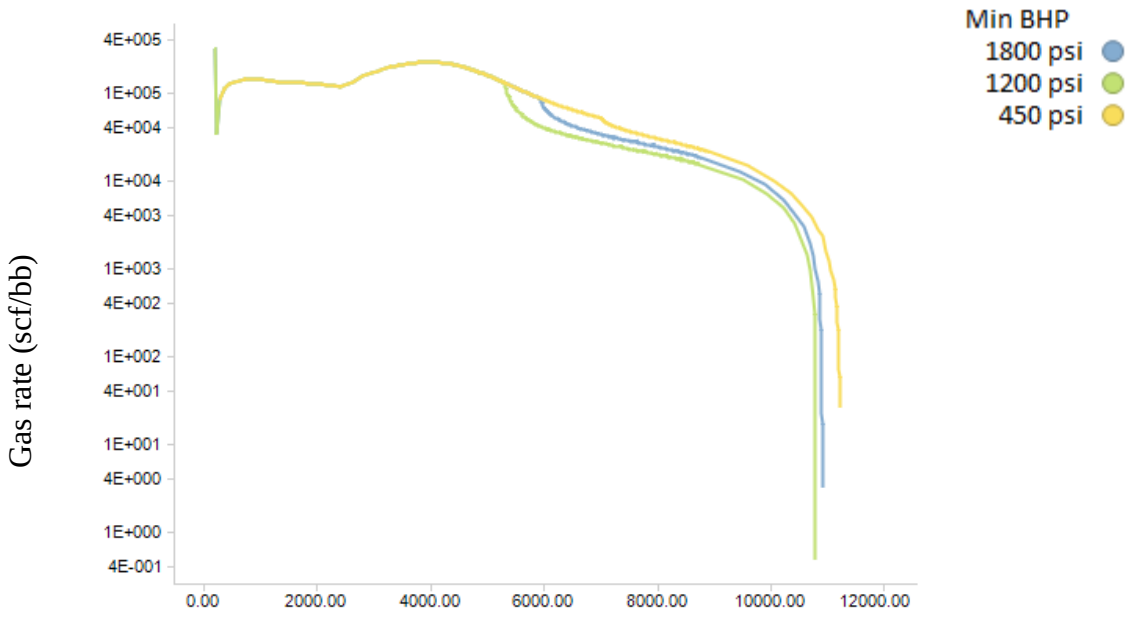

(c)

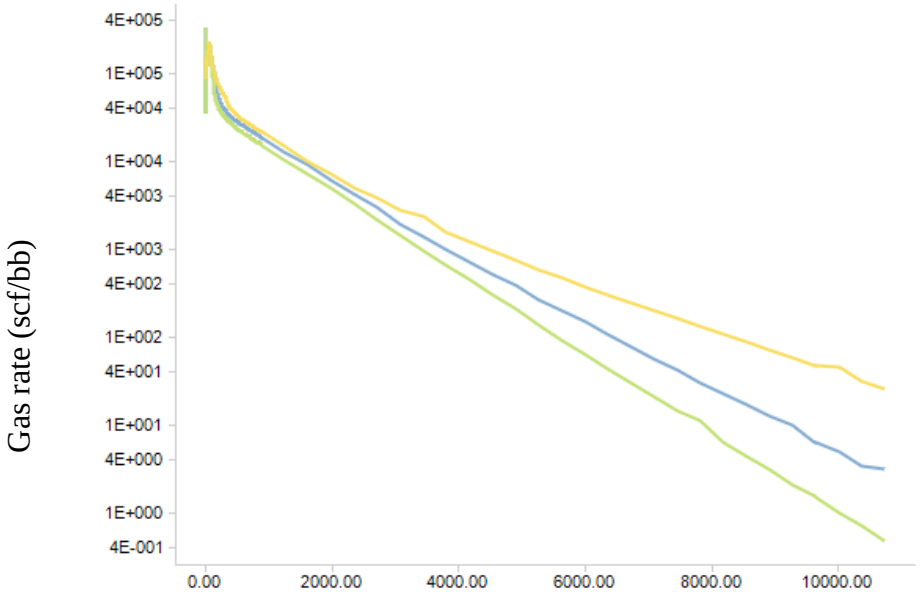

(d)

Figure 40—Continued

As the dimensionless rate includes drawdown pressure, the plot of dimensionless rate versus dimensionless time accounts for this variability and the histories converge as shown in Figure 41.

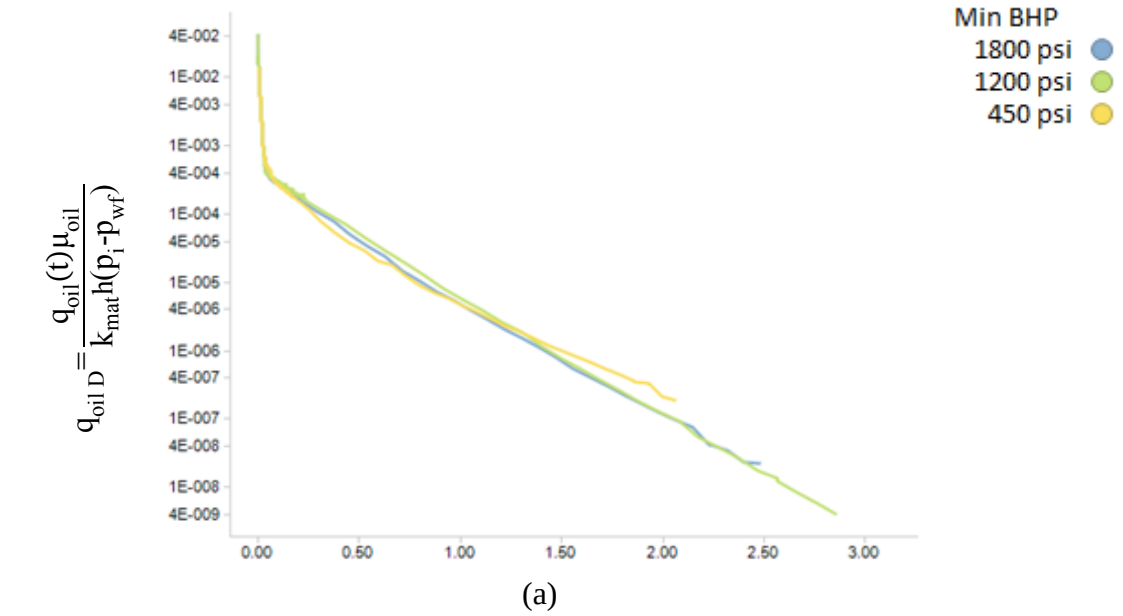

(a)

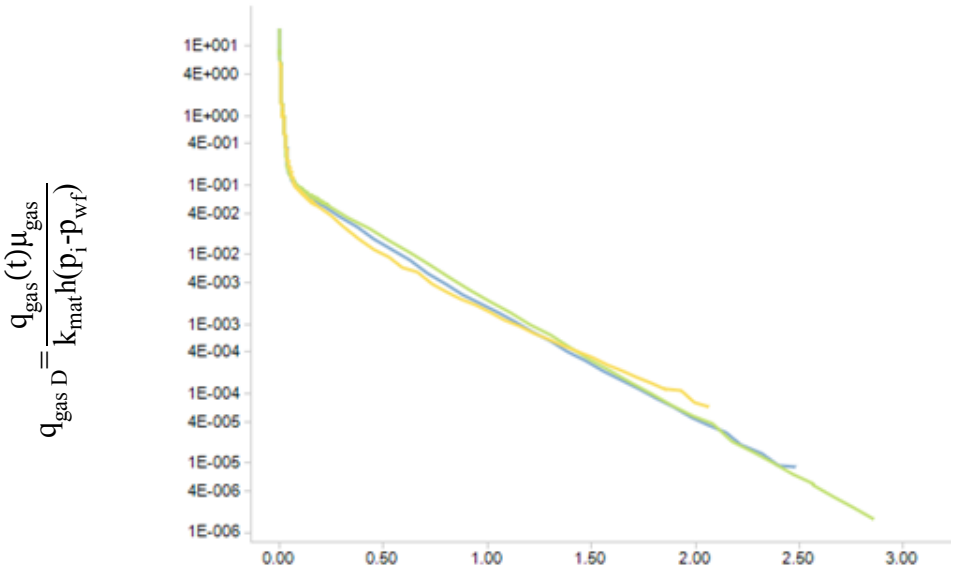

(b)

$$t_D=\frac{k_{mat}t}{\varphi c_t\mu_{oil}(2x_e-2x_f)^2}$$

Figure 41—Dimensionless production history – effect of minimum BHP. (a) dimensionless oil rate versus dimensionless time, (b) dimensionless gas rate versus dimensionless time

Summary and Conclusion

In this chapter, the hypothesis outlined in CHAPTER IV, that, for a given area of interest, following an initial transient period, the production histories of both oil and gas phases converge. This was validated with the aid of dimensionless variables, i.e. dimensionless rate and dimensionless time definitions presented in CHAPTER II. Therefore, a single dimensionless rate versus dimensionless time curve for each fluid system may be used to forecast production. This relationship becomes valid after a certain initial transient period.

In the following chapters, this theory will be applied to two independent areas of interest, volatile oil and black oil, to demonstrate that our workflow produces forecasts within 10% of those from more rigorous and laborious compositional numerical modelling of individual wells.

CHAPTER VI

ANALYTICAL RATE TRANSIENT ANALYSIS EVALUATION OF MULTI-FRACTURED HORIZONTAL WELLS

In CHAPTER II, the theory of tri-linear flow in multi-fracture horizontal well was discussed. Provided that the flow in the reservoir remains single phase, this model can be used to analytically predict production in an efficient and practical manner using commercial software. Another advantage of using the analytical model is that, due to simplicity of the model, it allows the user to history match production and to carry out sensitivity analysis that is much more time consuming in a numerical environment. This chapter will first present an overview of analytical modeling using tri-linear flow theory followed by various examples in different areas of interest, using synthetically generated production data. It will be shown that, with a limited amount of production data, the analytical model can forecast production with the assumption of single phase flow. In the following chapter, the analytical forecast will be truncated at a transition point which will be determined and discussed there. Beyond the transition point, the dimensionless rate versus dimensionless time relationship developed in the previous chapter will be used to forecast for the remaining life of the well.

Analytical Modelling in Typical Commercial Software

The most significant advantage of the workflow presented here is that it allows utilization of readily available commercial software with analytical models for MFHW's based on the tri-linear flow theory. This allows for quick and efficient set up of the models to history match all available production data and to forecast using bottom-hole

pressure or rate constraints. The analytical models also allow for quick sensitivity analysis of the most uncertain inputs.

In using this methodology, if any production data are available, these two steps that must be followed prior to the analytical modelling:

1. Diagnostics to validate accuracy of data and extract reservoir signals, (see Figure 42):

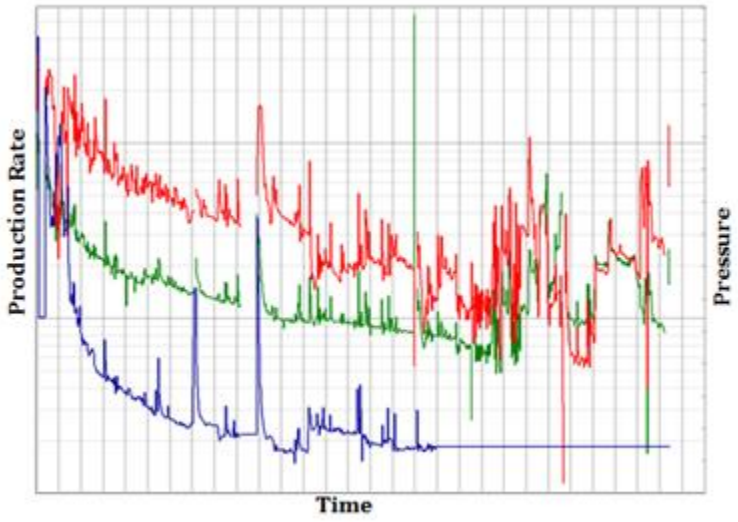

Figure 42—Diagnostic plot- production histories of oil, gas and water with time

This is a simple yet very powerful tool for checking quality and coherency of the data. Anomalies should be identified and investigated.

2. Interpretation and analysis to identify dominant flow regimes and estimate reservoir properties and system parameters and quantify uncertainties. Rate-normalized pressure drawdown versus a superposition time function or material

balance time provides a good indication of flow regimes. Other time functions such as √time plot are also used as a diagnostic tool (Figure 43). The diagnostic plots are often used for an initial estimate of the stimulated rock volume. For example, the slope of line in the figure below is related to the product of stimulated rock permeability and fracture half length.

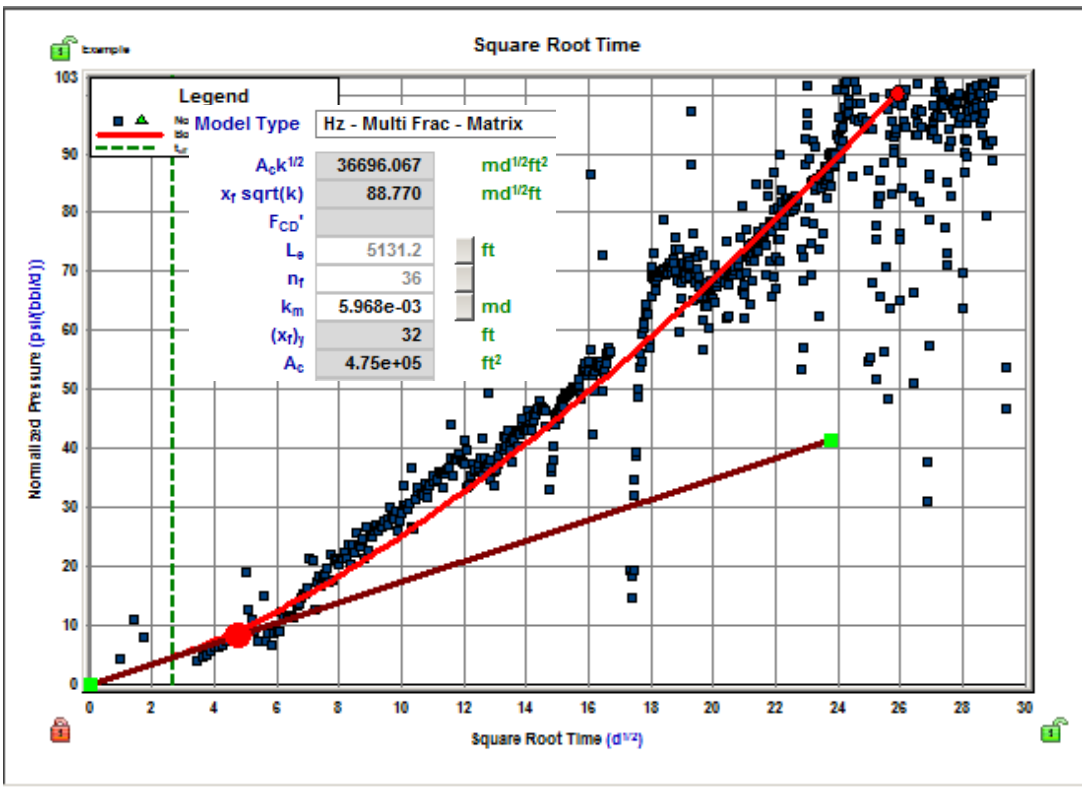

Figure 43—Rate-normalized pressure drawdown versus $\sqrt{t}$ used with a horizontal multifracture model to derive $x_f\sqrt{k}$

Other examples of identifying change in flow regime are demonstrated in Figure 44 with different matrix and SRV permeabilities.

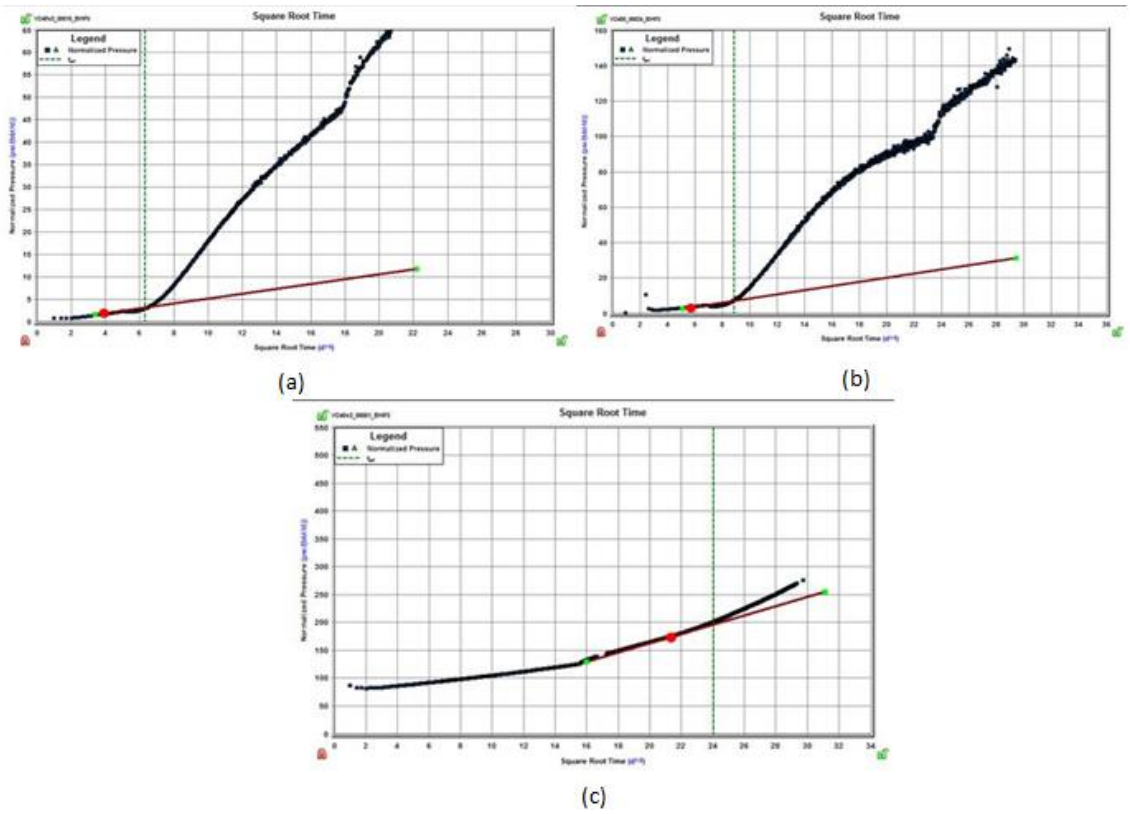

Figure 44—Examples rate-normalized pressure drawdown versus $\sqrt{t}$ used with a horizontal multifracture model to derive $x_f\sqrt{k}$. (a) k_{mat}=4e-3mD, k_{srv}= 0.32 mD (b) k_{mat}= 4e-3mD, k_{srv}=1.6mD (c) k_{mat}=4e-5mD , k_{srv}=4e-4 mD.

Commercial analytical software such as Fekete-Harmony or Ecrin's Topaze offers readily available MFHW models. Therefore, following the initial diagnostics and validation of accuracy with a first estimate of stimulation parameters including stimulated rock permeability and fracture half length, a MFHW model is selected in commercial software. The analytical model is initialized with appropriate static and dynamic reservoir parameters and completion parameters. A history match of available production data is performed to optimize the solution and then the tuned model is used to forecast production. Often, the most uncertain parameters are selected as history matching parameters. Experience shows that the major unknowns include permeability

of matrix and SRV. Fracture half-length is also often not known, and can be selected as a history matching parameter; however, hydraulic fracture stimulation modeling and microseimic data should be used whenever possible to provide first estimates of fracture length. We recommend forecasting production for the life of the well. In our workflow, this forecast will be truncated using a transition point that will be discussed in the following chapter. Forecast beyond the transition point is done using a relationship between the dimensionless rate and dimensionless time, which will also be discussed in the following chapter.

Rate Transient Analysis for History Matching of Individual Wells and Forecasting Earlier Production

As shown above, diagnostic plots such as rate-normalized pressure-drawdown plot versus superposition time should be used as the first step to identify flow regimes and obtain initial estimates of the product of permeability and fracture half length. The first estimate of $x_f\sqrt{k}$ would be used in the analytical model, Nobakht et al. (2010) and Behmanesh et al. (2014). Select the horizontal multi-fractured horizontal well and set up the model as follows:

1. Select the correct fluid type, i.e. oil, and enter appropriate PVT properties.
    - Specific gravity of oil, γ_o
    - Bubble point pressure of oil, p_{pb}
2. Fluid properties at reservoir temperature, T_R, and initial pressure, p_i
    - Formation volume factor of oil, B_{oi}
    - Compressibility of oil, c_{oi}
    - Viscosity of oil, μ_{oi}
    - Density of oil, ρ_{oi}
    - Solution gas-oil ratio, R_{soi}
3. Define the well and stimulation architecture, Figure 45:

- Horizontal lateral length, L_e
- Fracture half length, x_f
- Number of stimulation stages, n_f
- Width of stimulation stages, 2ye
- Drainage spacing, $2x_e$
- Permeability of stimulated rock, k_{srv}
- Fracture height, h_f

4. Enter dynamic and static parameters
    - Permeability of matrix, k_{mat} - To the best of knowledge, either from core, production data analysis, or analogues
    - Porosity, ϕ_t
    - Saturation of water, S_{wi} and oil, $S_{oil}=1-S_{wi}$
    - Initial reservoir pressure, p_i
    - Reservoir temperature, T_R
    - Formation thickness, h
    - Formation compressibility, c_{fi}
5. Input production data
    - Production rate
    - Bottom-hole pressure

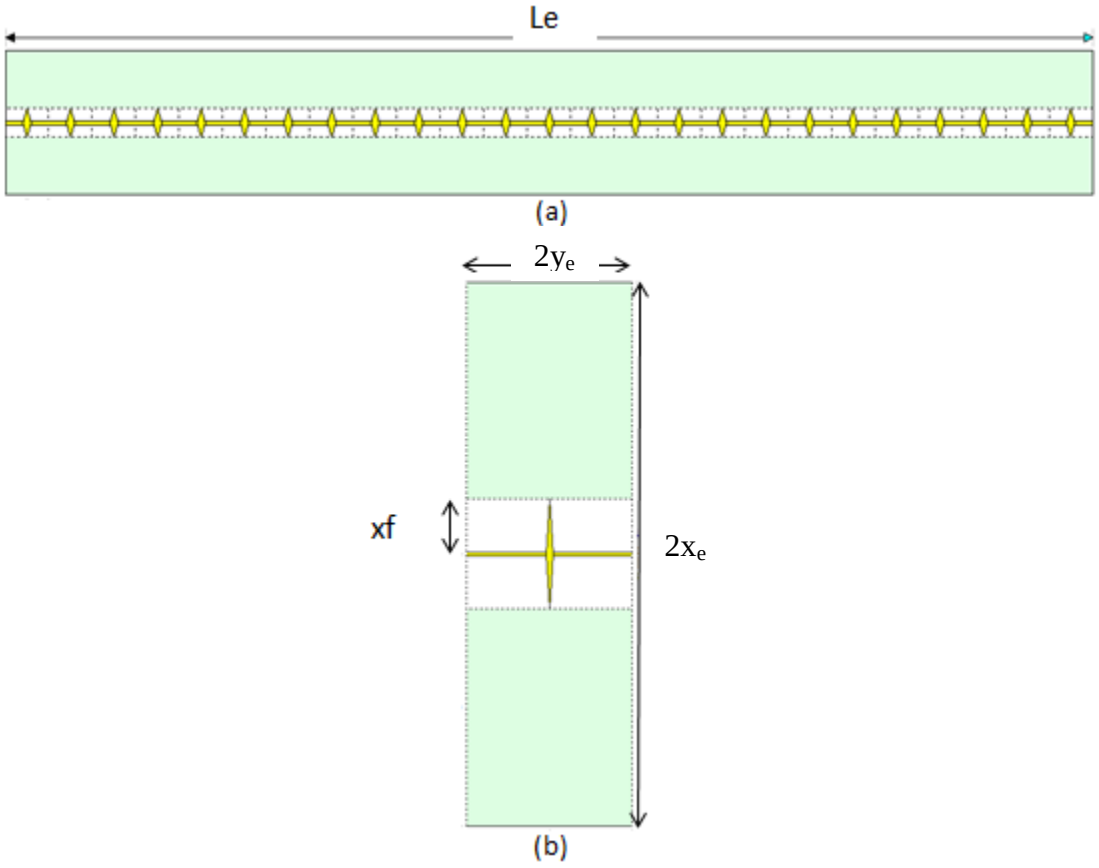

Figure 45—Well and stimulation geometry inputs into a typical analytical model (a) horizontal lateral of a well (b) single hydraulic fracture stimulation stage

History Matching and Forecasting

Match historical pressure and production data (automatic in leading commercial software). For example, given rates, calculate pressures or given pressures, calculate rates, using the least certain input variables as history matching parameters. For example, x_f and permeability are often selected as history match parameters. Usually, because actual rates are more accurately measured, we recommend treating rates as given and calculating flowing bottom-hole pressures. In situations where bottom-hole

pressure is measured, they can be treated as known and rates calculated. Figure 46 shows an example of history matching actual production data using an analytical model.

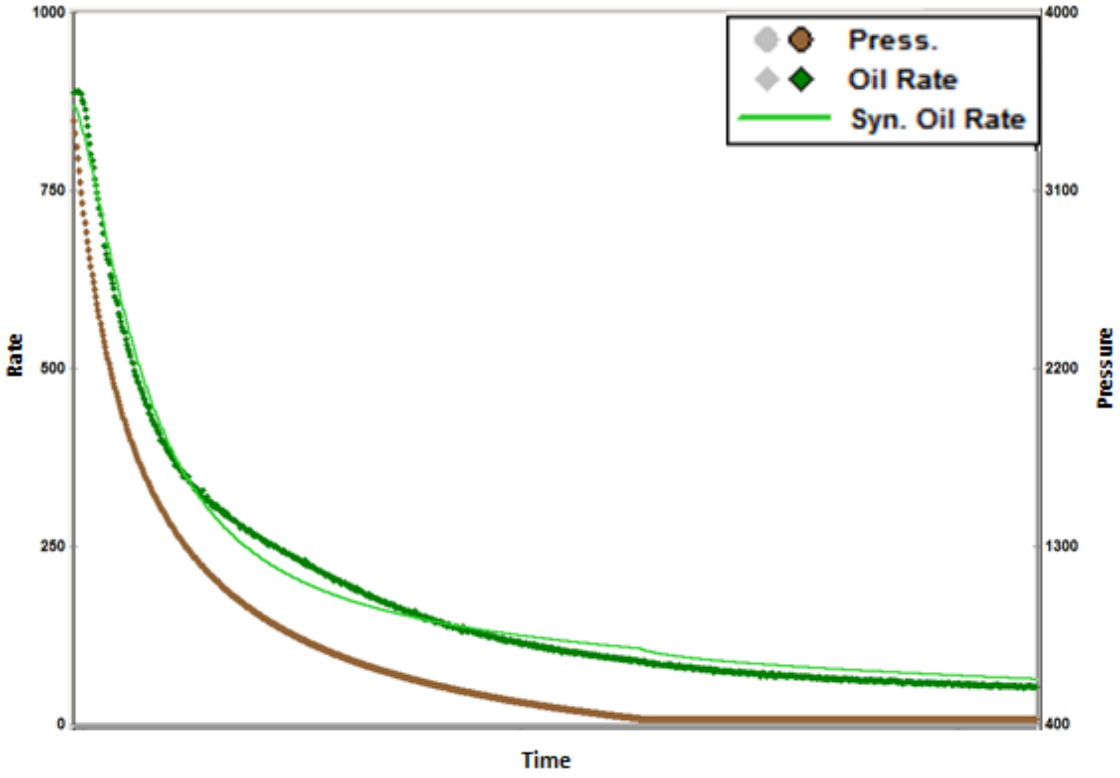

Figure 46—Result of automatic history matching – given actual pressure, model predicts rates (light green line)

Using the calibrated model after history matching, forecast future production by specifying a BHP schedule and a terminal point. The terminal point maybe a certain time in the future or a certain minimum rate. An example of forecasting production using a calibrated model is shown in Figure 47.

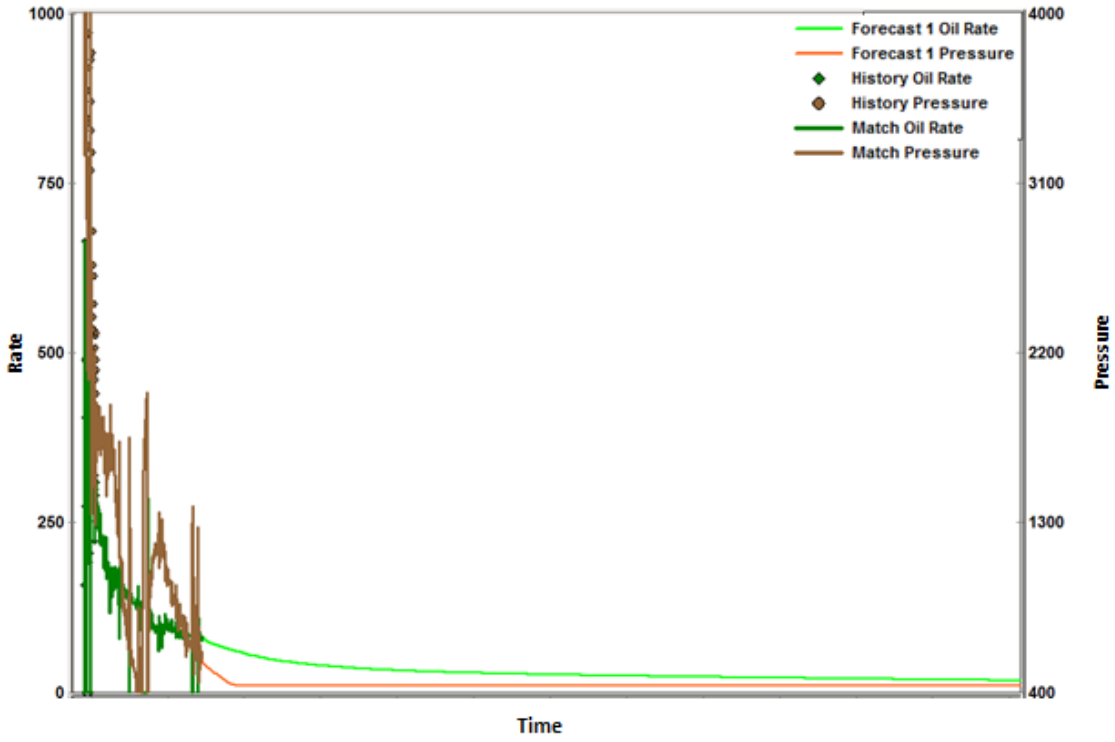

Figure 47—Forecasting production using calibrated analytical model

To validate the use of an analytical model, at least during early production of a liquid-rich shale reservoir before multi-phase flow dominates, a comparison of analytical and numerical model forecasts is presented in the following figures. We compared results for two different fluids, a volatile oil, and a black oil. At earliest times, Figure 48 shows that numerical and analytical models produce similar forecasts.

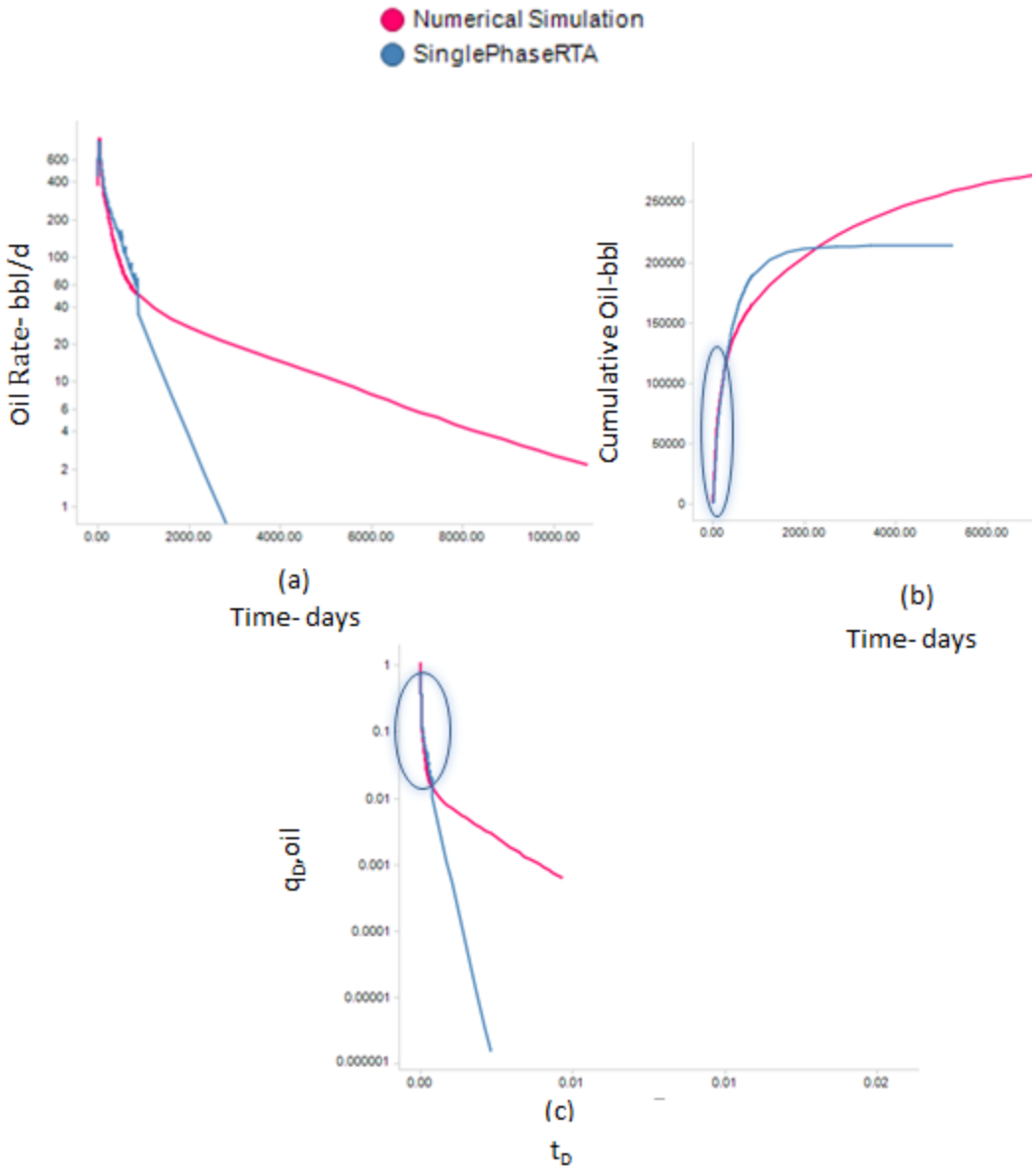

Figure 48—Comparison of analytical and numerical models to show close match during early production

Comparison of analytical and numerical model is also useful in that it can be used to identify the transition point where analytical methodology becomes invalid, Figure 49.

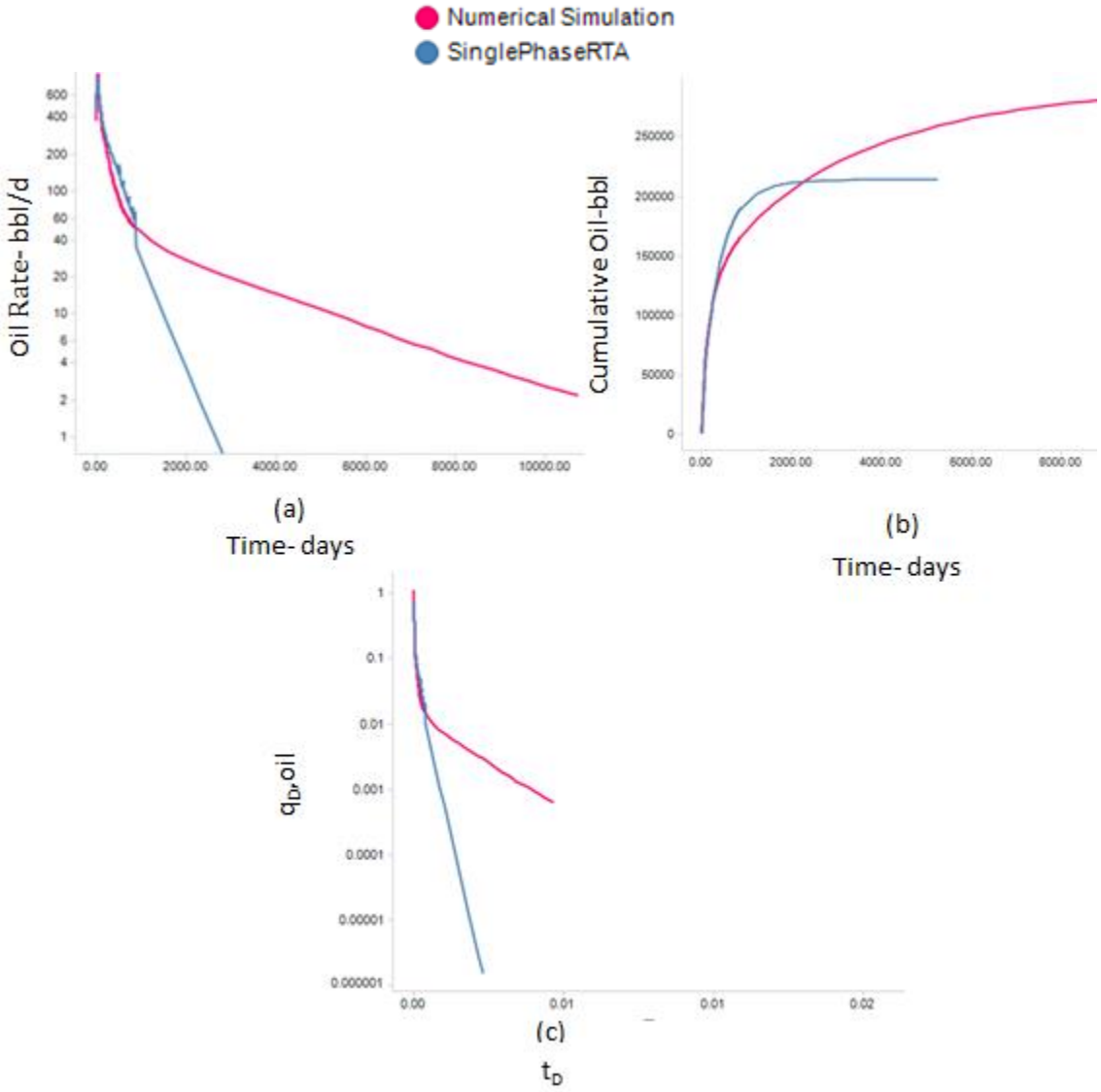

Figure 49—Volatile oil area of interest, comparison of analytical single phase flow versus compositional numerical simulation; transition point is where the two deviate from one another

Similarly, for a black oil fluid, comparison of analytical model to compositional numerical simulator shows similar forecast for the initial production period, see Figure 50.

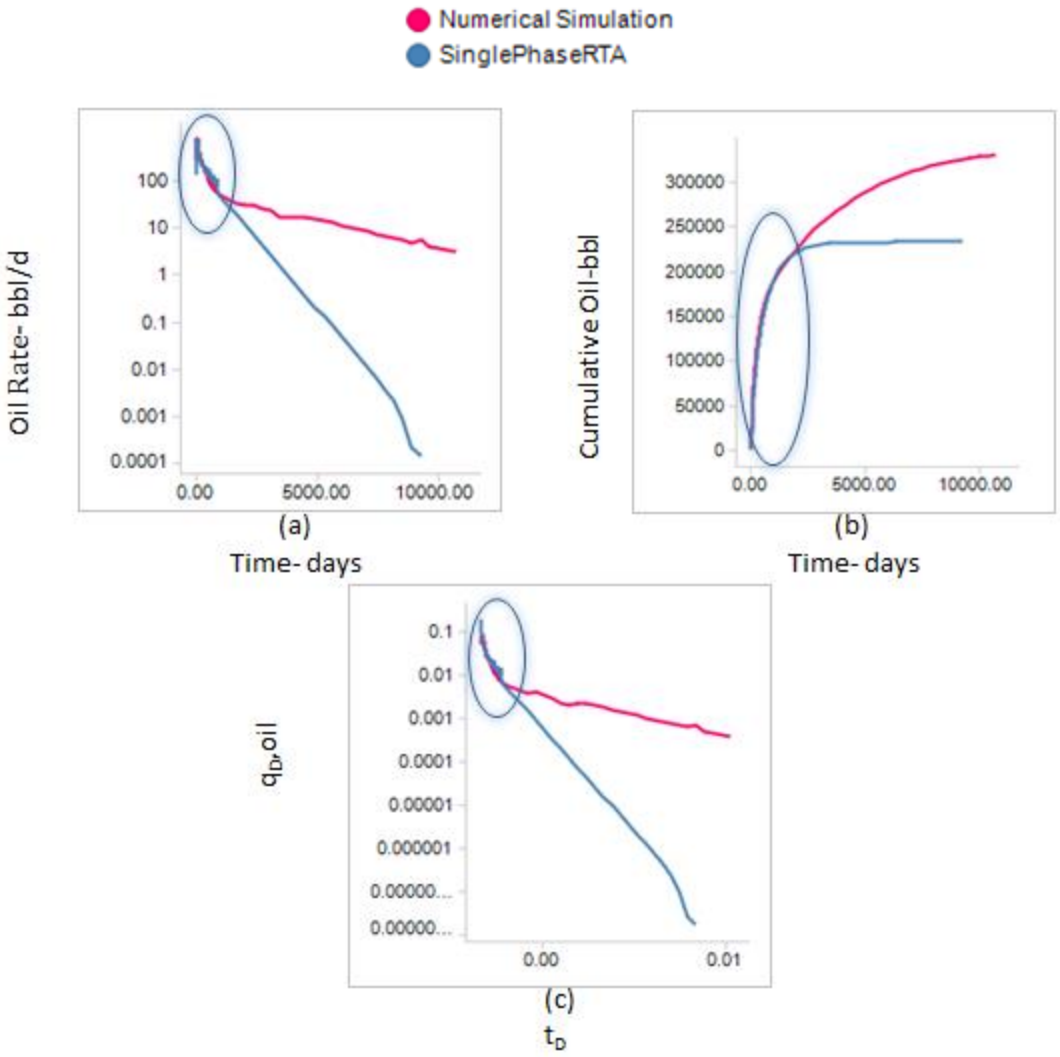

Figure 50—Black oil area of interest, comparison of analytical single phase flow versus numerical simulation show close match during early production

In black oil systems, comparison of the compositional numerical model to the analytical model also shows the point where analytical model deviates from the compositional model, Figure 51. This is referred to as the transition point in following chapters, and it is used to identify the point where the analytical model is no longer valid, and instead the dimensionless rate versus dimensionless time relationship derived from compositional simulation is used to forecast production.

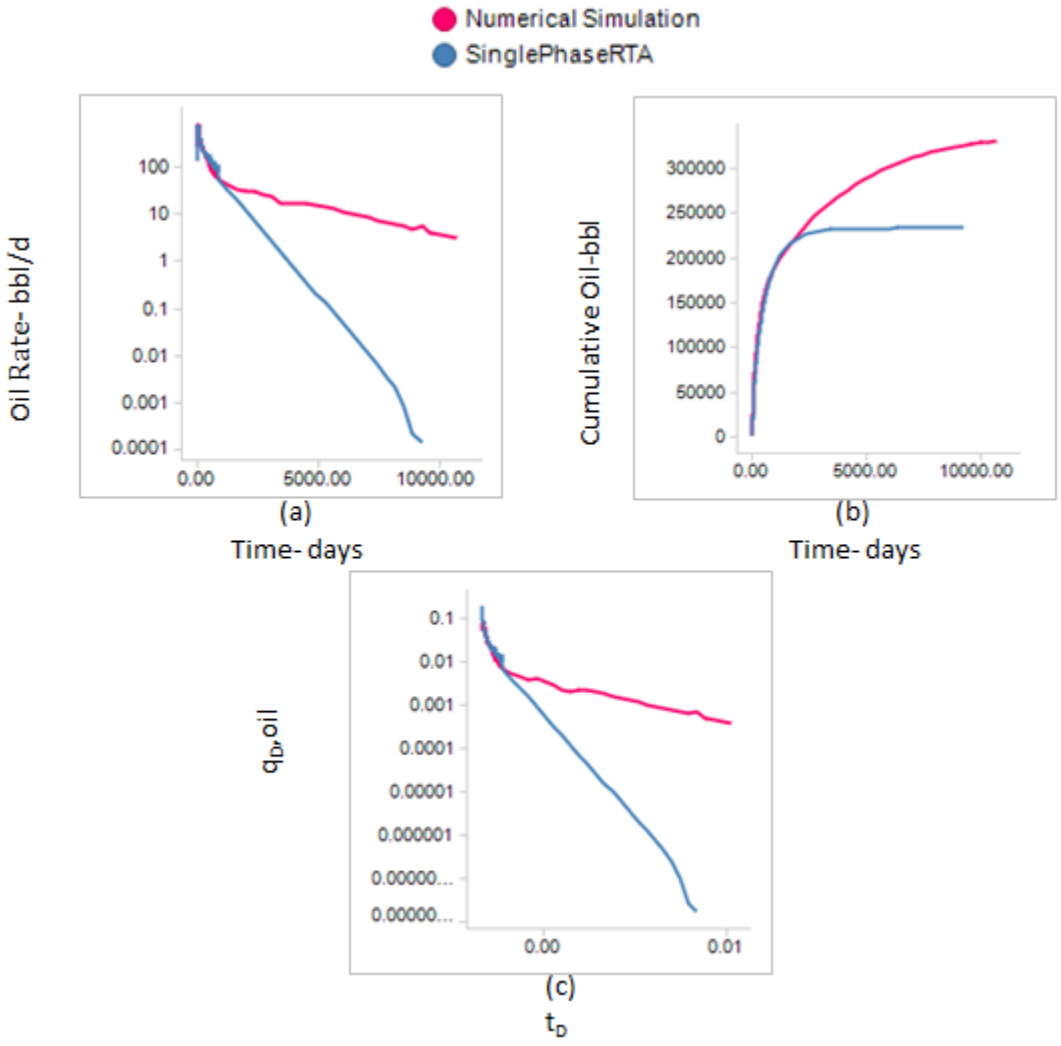

Figure 51—Volatile oil area of interest. Comparison of analytical single phase model and compositional numerical simulation. Transition point is where the two deviate from one another.

Summary and Conclusion

In this chapter, we reviewed analytical simulation based on the trilinear-flow model of Ozkan et al. (2009) and summarized the step-by-step set up of this analytical model for MFHW's, automatic history matching, and forecasting using calibrated models in

commercial software. We then compared analytical and numerical simulation results in the initial flow period, which validated the hypothesis that the analytical model accurately forecasts production in the initial flow period. We also showed that comparison of the compositional numerical model to the analytical model helps determine the transition point beyond which the analytical model is invalid.

In the next chapter, our focus will shift to developing a relationship between dimensionless rate and time. This relationship will be used to forecast production beyond the transition point.

CHAPTER VII

DEVELOPMENT OF DECLINE MODEL FOR AN AREA OF INTEREST

In CHAPTER V it was shown that, for an area of interest with a fluid system of fixed composition and a common completion design, production histories expressed as dimensionless rate vs. dimensionless time converge. In this chapter, two areas of interest are studied and a single relationship of dimensionless time versus dimensionless rate is developed for each. Comparison of analytical model results described in the previous chapter with the equivalent numerical model are used to determine the transition point beyond which the analytical models are no longer valid and for which the workflow calls for the use of the q_D vs. t_D relationship.

In MFHW's, the individual wells behave differently primarily due to the non-unique nature of hydraulic fracture stimulation. This workflow allows the unique signature of each well to be captured in the initial production period with efficient single-phase analytical modelling. Once the well has gone through its initial transient flow and steep decline, the subsequent behavior of the wells in the area of interest can be represented by the respective q_D vs. t_D relationship.

In CHAPTER V, criteria for identifying an area of interest were discussed. It was also shown that modeling of MFHW's can be simplified using an element of symmetry with a single stage fracture. In this chapter, the set up for the simulation model is similar to that discussed in CHAPTER V, with the difference that here a few cases were selected and analyzed to determine the transition point from the initial analytical model to the subsequent q_D vs. t_D relationship. Also, in CHAPTER V, the focus was on displaying the

trends in the subsequent period; in this chapter the trends are used to develop the q_D vs. t_D relationship. The cases for this work were selected to include high, medium, low production scenarios.

To reiterate, the objectives of this part of the workflow are three fold:

1. To determine the transition point from the initial to the subsequent production period, i.e., from the analytical RTA model to the q_D vs. t_D relationship.
2. To determine the q_D vs. t_D relationship for the subsequent period for a fluid system,
3. To determine the gas production using a gas-oil-ratio (GOR) history. Steps 1 and 2 are used to forecast production of the primary oil phase, and the secondary gas phase production is determined using a GOR history for the specific area of interest.

Area of Interest 1- Volatile Oil Case

Compositional numerical simulation for 4 cases representing high, medium, and low production scenarios were carried out. Recall that compositional numerical modeling is used as a bench mark in this study. Therefore, the numerical results are used to establish the expected production history. With the aid of dimensionless parameters discussed in CHAPTER II, the production histories for all cases were shown to converge. Comparisons of numerical production history with the equivalent analytical production histories help determine the transition point where the analytical histories no longer follow the same trend as the numerical histories. The inputs into the simulation model are detailed below.

The numerical model was set up as explained in CHAPTER V for a single fracture stage (Figure 18). A summary of input parameter information follows.

Geometry

The three dimensions of the model are

1. X direction- width of a single fracture stage, 200 ft.
2. Y direction- drainage area height, derived from the well spacing assumption, 656 ft.
3. Z direction- thickness of formation, assumed to be the same as fracture height, 103 ft.

Permeability

Two sets of permeability data were defined, first for the matrix, and second for the stimulated rock. It is assumed that permeability in the X-direction equals that in the Y-direction. Permeability in the Z-direction is $1/10^{th}$ of Permeability in the X-Direction.

1. Matrix permeability- A range of permeabilities covering the expected values in the area of interest with 4 values from 1 e-5 to 8 e-3 mD selected.
2. Stimulated rock permeability- A range of SRV permeabilities covering the expected stimulation intensity in the area of interest with values from 4e-4 to 1.6 mD was selected. SRV permeability was selected such that stimulation varied from 4-40-400 times enhancement over the matrix permeability.

Petrophysical Parameters

Porosity and fluid saturation variations in areas of interest were assumed constant. A porosity of 5% and water saturation of 18.3% were used in our study.

PVT

The representative fluid composition for the specific development area is used for a volatile oil system. The fluid selected was chosen because it was the only volatile oil composition available in the area of interest.

Initial Reservoir Pressure

Four values of initial reservoir pressures, from 6000 to 8100 psia, were used.

Flowing Bottom-Hole Pressure History

Four different pressure histories from the initial reservoir pressure to the abandonment pressure were studied for the workflow to cover the range of possible bottom-hole pressure histories. Note that MFHW's in LRS exhibit steep declines in pressure and production rates. Figure 52 shows the 4 different bottom-hole pressure histories.

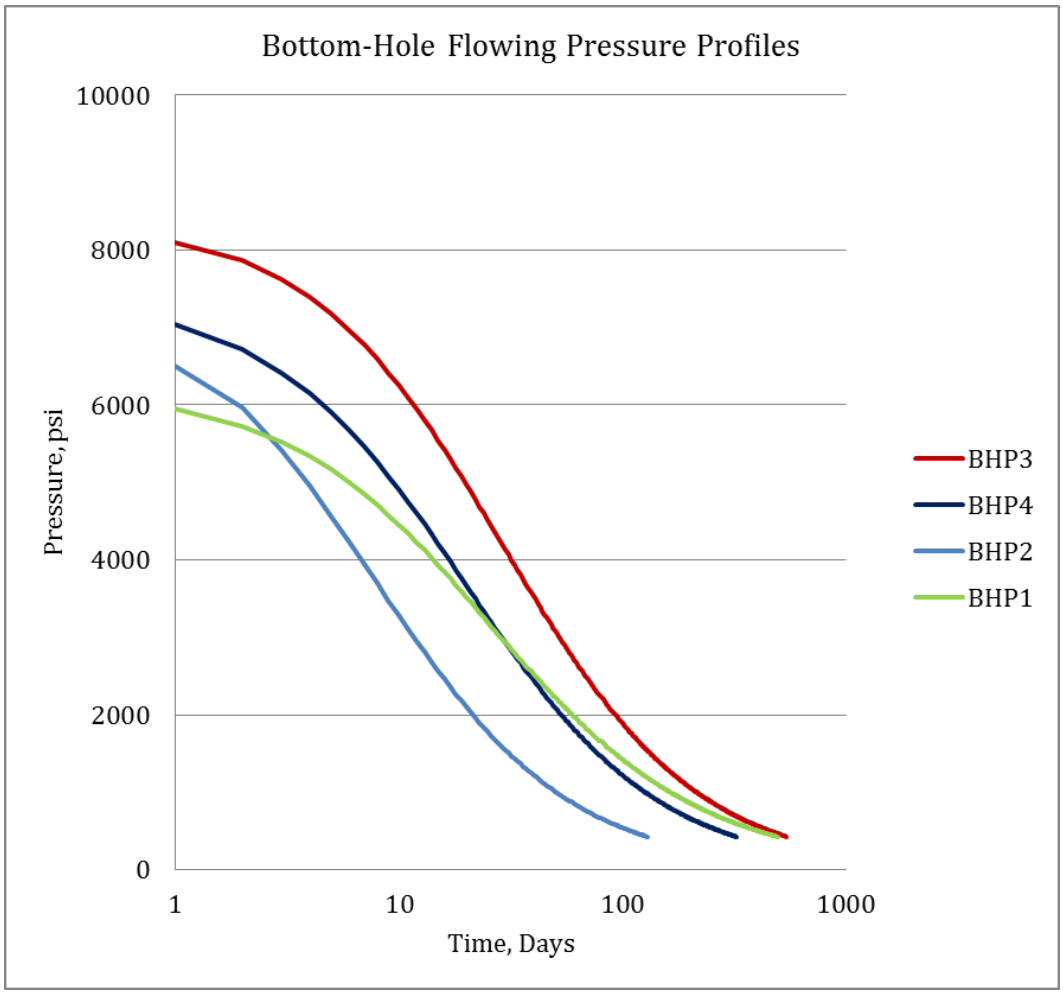

Figure 52—Different bottom-hole pressure histories

Table 9 summarizes properties for the 4 cases in the volatile oil area of interest.

Case No.	BHP Profile	Pi, psi	Matrix Perm, mD	SRV Perm, mD
1	BHP1	6000	2.4E-03	9.6E-03
2	BHP2	6630	1.0E-05	4.0E-04
3	BHP3	8100	4.0E-03	1.6E+00
4	BHP4	7050	8.0E-03	3.2E-01

Table 9—Volatile oil area of interest, 4 different scenarios with different permeabilities and bottom-hole pressure histories.

Oil and gas production histories and gas oil ratio trends for the four scenarios are shown in Figure 53. The oil and gas production histories exhibit large variability.

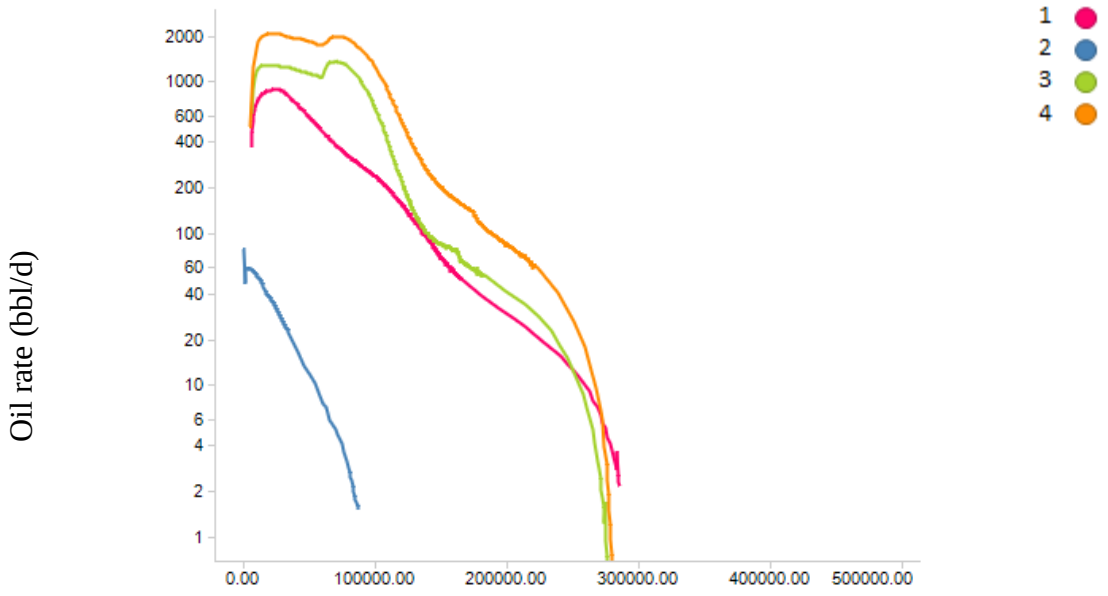

(a)

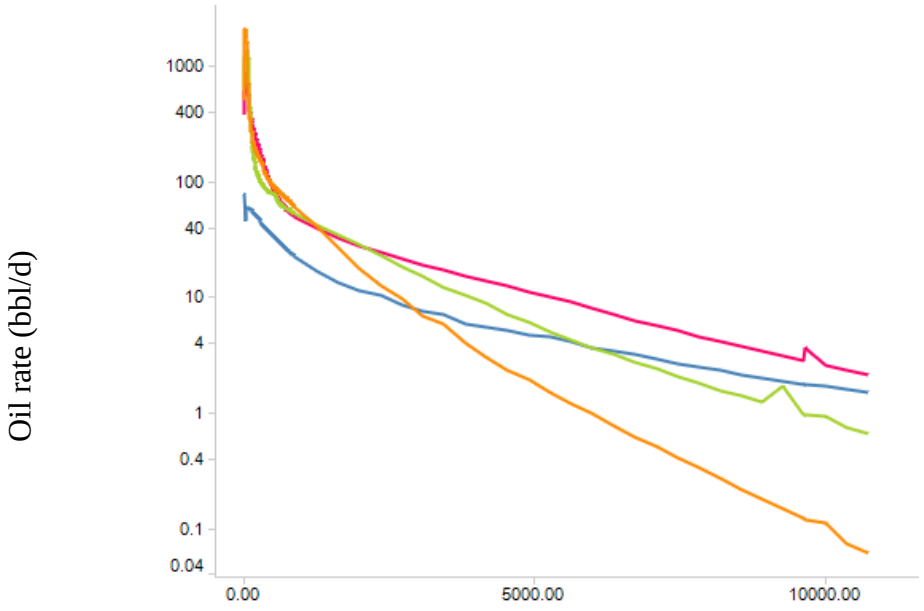

(b)

Figure 53—Volatile oil area of interest- production histories for 4 different scenarios, (a) log oil rate versus cumulative oil production (b) log oil rate versus time, (c) log gas rate versus cumulative oil production, (d) log oil rate versus time

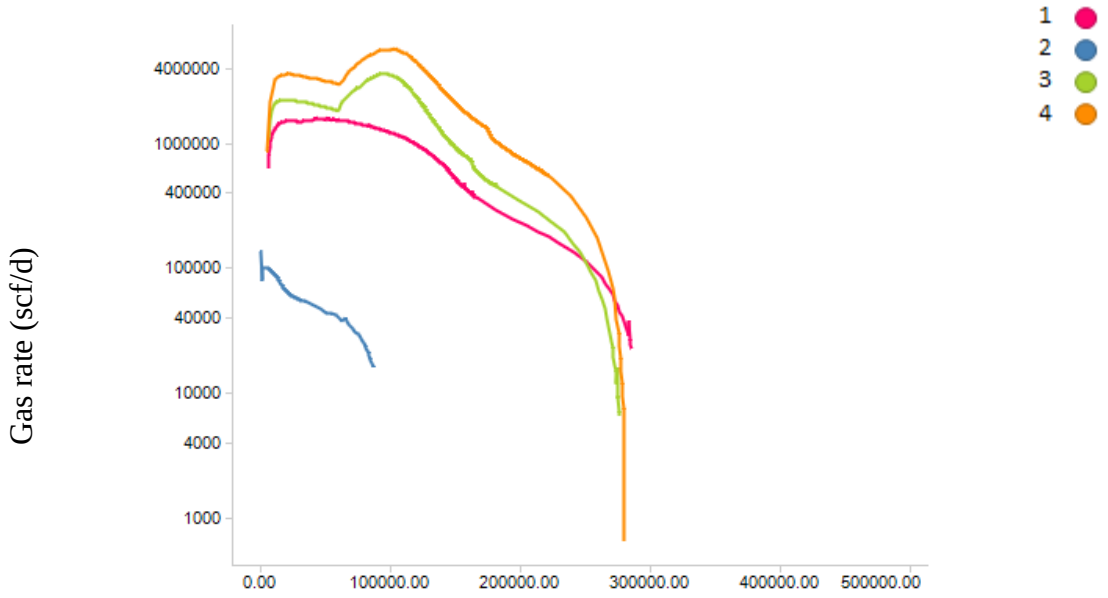

(c)

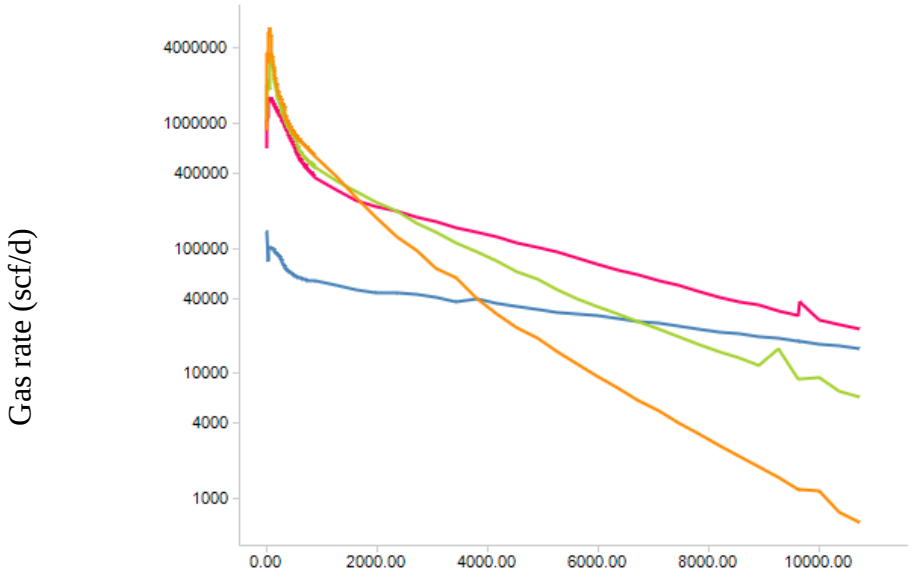

(d)

Figure 53—Continued.

In terms of dimensionless time and dimensionless rate, the production histories converge to those shown in Figure 54.

$$q_{oil\,D}=\frac{q_{oil}(t)\mu_{oil}}{k_{mat}h(p_i-p_{wf})}$$

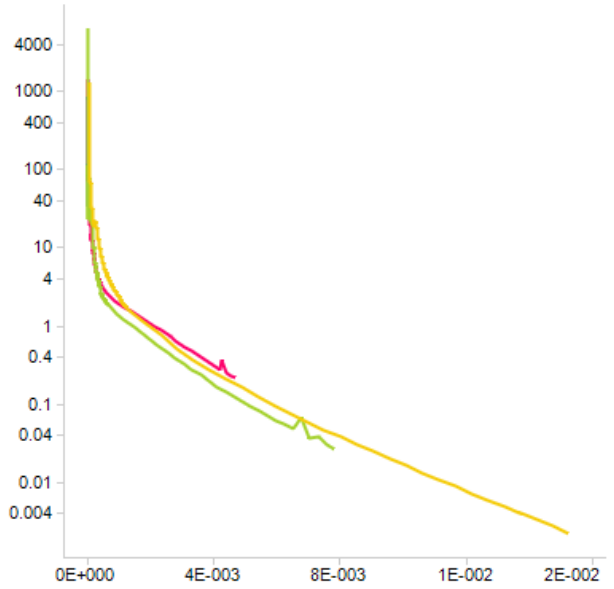

(a)

$$q_{gas\,D}=\frac{q_{gas}(t)\mu_{gas}}{k_{mat}h(p_i-p_{wf})}$$

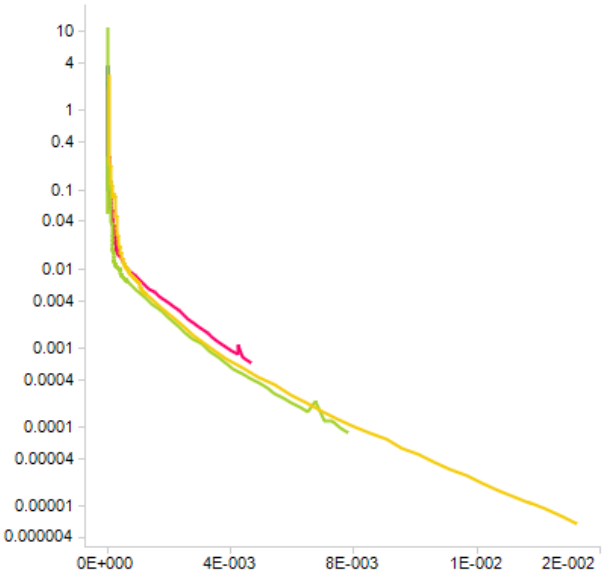

(b)

$$t_D=\frac{k_{mat}t}{\varphi c_t\mu_{oil}(2x_e-2x_f)^2}$$

Figure 54—Volatile oil area of interest – oil and gas production histories in terms of dimensionless parameters variables converge

For each of the 4 cases mentioned above, an equivalent analytical model was developed as explained in CHAPTER VI. Comparisons of the dimensionless histories from the analytical model to those from numerical models indicate the point at which the analytical models diverge from the numerical baseline. The transition point occurs at t_D=3.8e-4 and q_D=0.01 as shown in Figure 55.

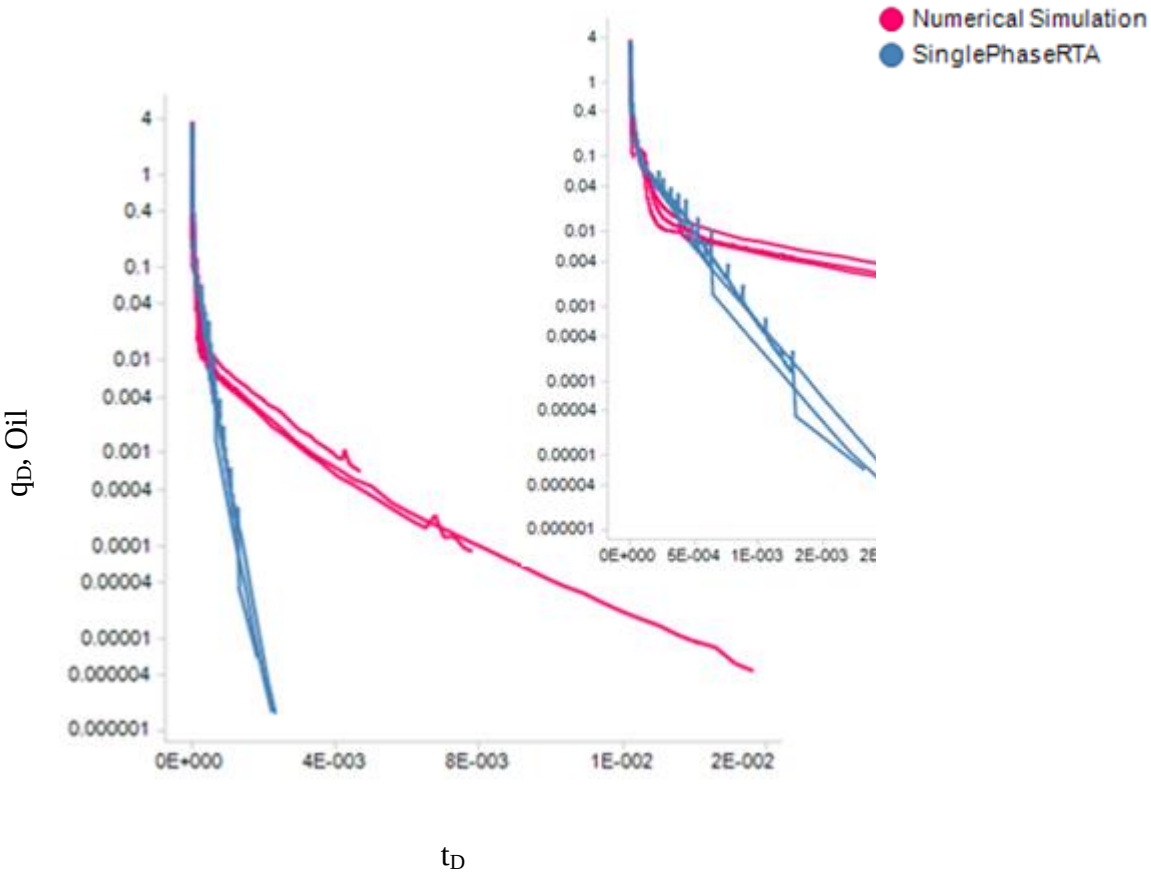

Figure 55—Transition point where workflow requires to switch from analytical model to q_D-t_D relationship

Dimensionless history beyond the transition point was represented by a single q_D-t_D relationship for volatile area of interest. Consistent with common industry practice, the

q_D-t_D relationship was represented with a multi-segment Arps decline model. A standard DCA spreadsheet was used with q_D and t_D values input and curve fitting using linear regression, which resulted in DCA parameters (Figure 56).

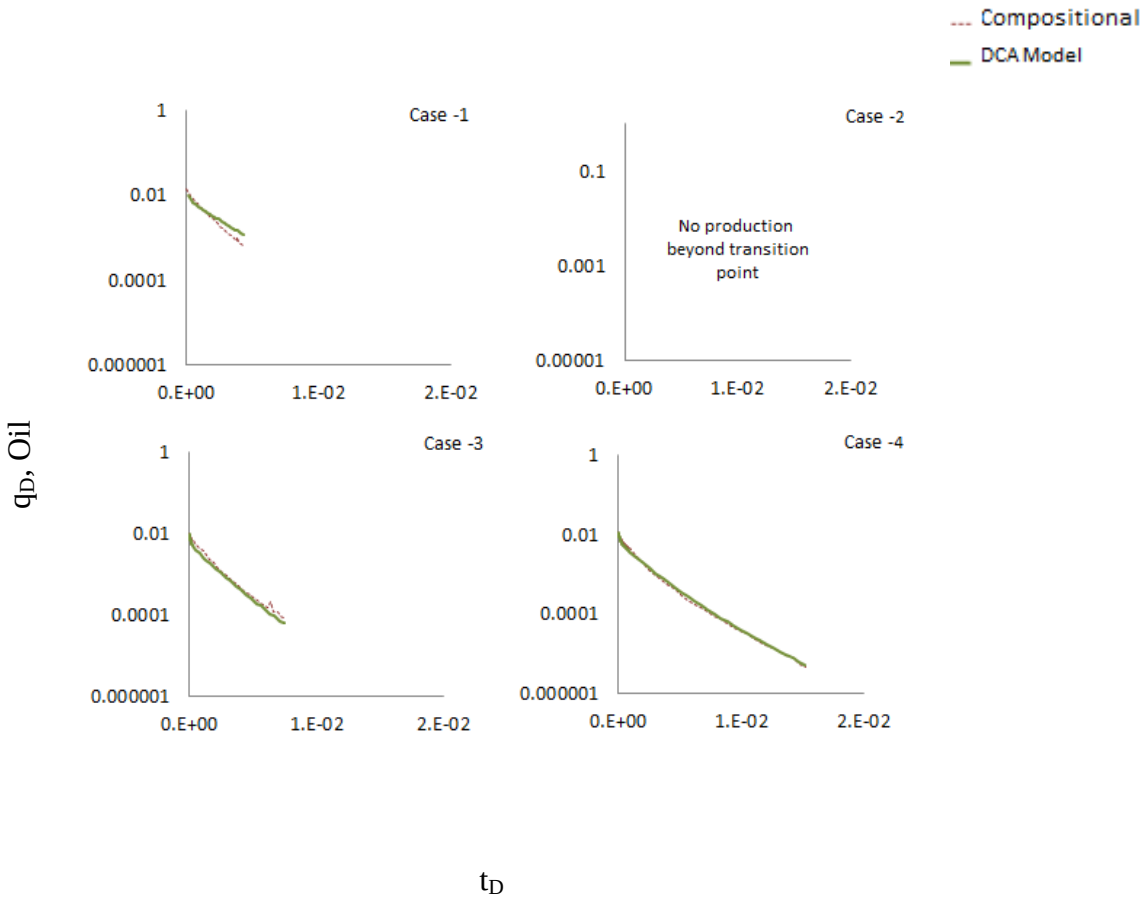

Figure 56—Dimensionless histories beyond transition point represented by volatile oil DCA model

The q_D-t_D relationship in terms of multi-segment Arps hyperbolic decline model parameters for the volatile oil area of interest are presented in Table 10.

Segment	Arps Parameters	Value
Beyond $t_{D,Transition}$ =3.8e-4		
1	q_i	q_D at t_D
	b_i	3.3
	d_i	10.8
Time to switch t_2=0.5		
2	b_2	1.1
Terminal condition		
Final	$q_{D,terminal}$	0.03

Table 10—Decline model parameters used to curve fit the different scenarios in volatile oil area of interest

Gas oil ratios from the four compositional numerical simulators are plotted versus dimensionless time (Figure 57), and an average GOR trend was observed (equations (171) and (172)).

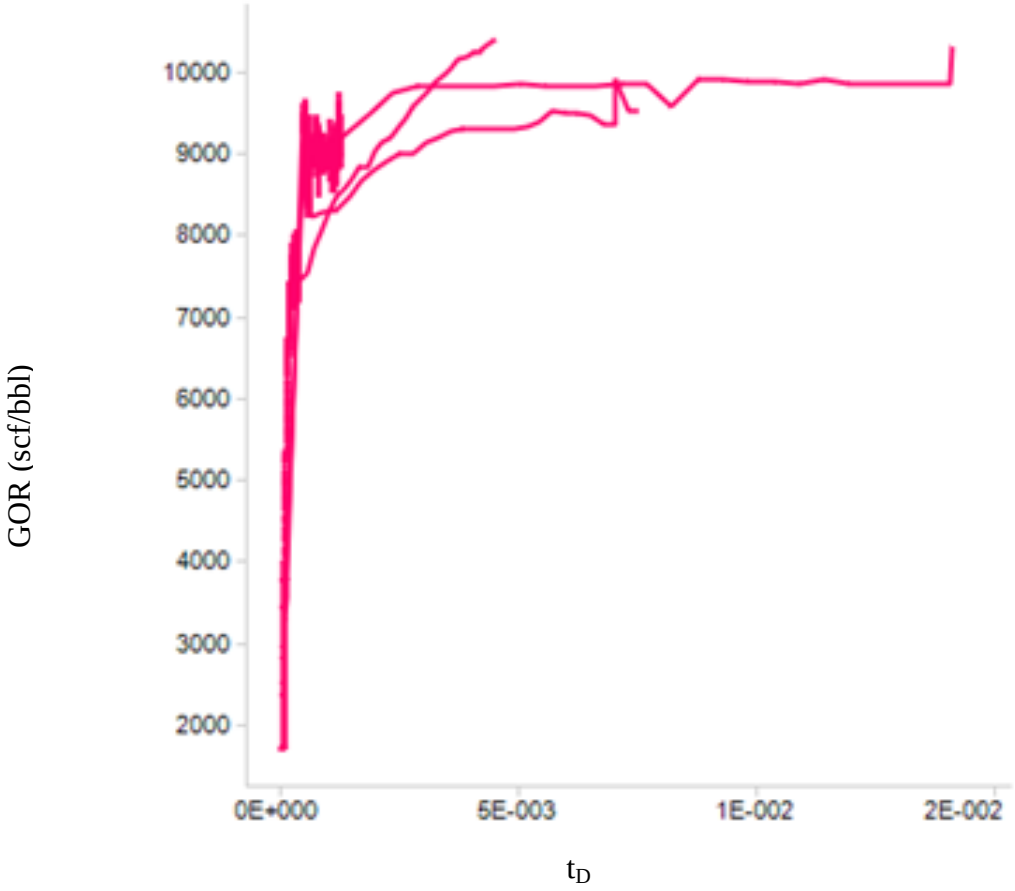

Figure 57—Gas oil ratio trend for volatile oil area of interest, GOR vs. t_D, from compositional numerical model

For $t_D < t_{D\text{-Transition}}$:

$$\text{Gas Oil Ratio } \left(\frac{\text{scf}}{\text{bbl}}\right) = 1.4e^{7} * t_D + 1800 \tag{171}$$

For $t_D > t_{D\text{-Transition}}$:

$$\text{Gas Oil Ratio } \left(\frac{\text{scf}}{\text{bbl}}\right) = 2.1e^{5} * (t_D - 3.8e^{-4}) + 7000 \tag{172}$$

Area of Interest 2- Black Oil Case

Similar to the way in which we studied the volatile oil area of interest, we carried out compositional numerical simulation for 4 cases representing high, medium, low scenarios of production to establish the general trend of production beyond the initial transient period. The simulation model set up was identical to the model of the volatile oil area of interest with the exception of the following properties:

PVT

The representative fluid composition for the specific development area was used for a black oil system. This was the only actual black oil composition from a sample that was available to us.

Initial Reservoir Pressure

Four values of initial reservoir pressures from 6420 to 8100 psi were used.

Flowing Bottom-Hole Pressure History

Four different pressure histories from the initial reservoir pressure to the abandonment pressure were studied similar to the volatile oil area of interest (Figure 58).

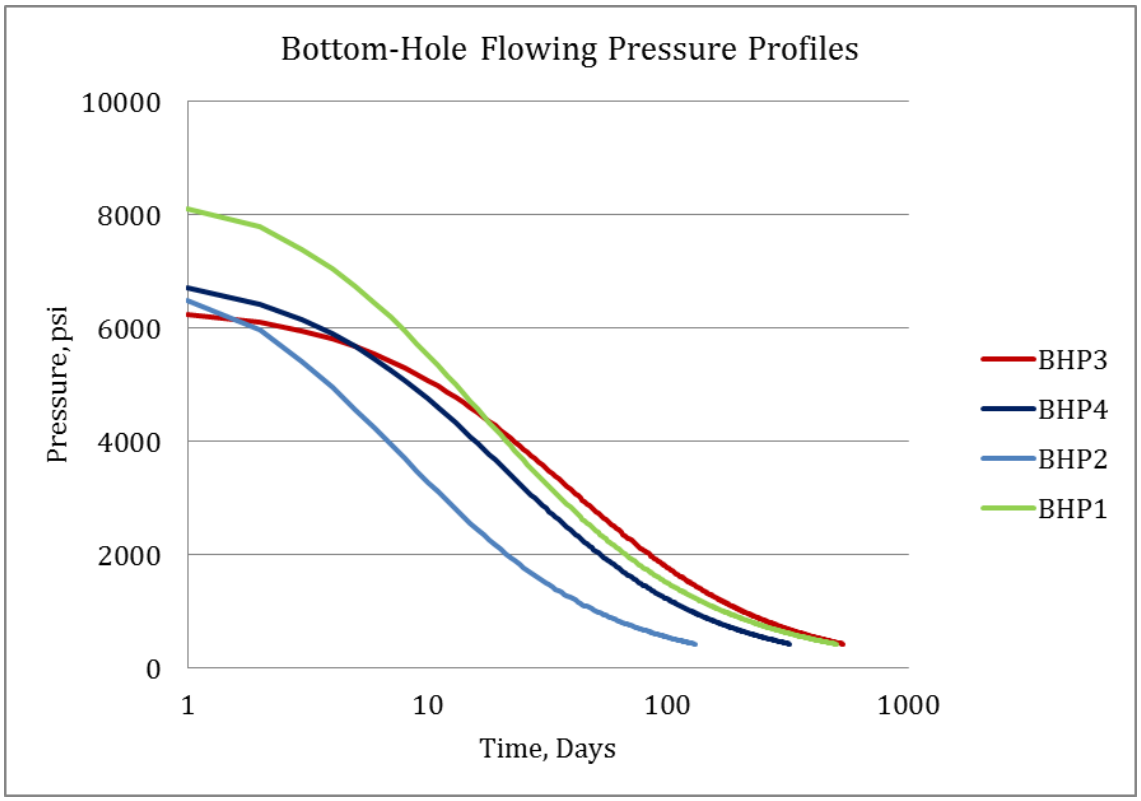

Figure 58—Different bottom-hole pressure histories used in study

Table 11 summarizes the details for the 4 scenarios for the black oil area of interest.

Case No.	BHP Profile	Pi, psi	Matrix Perm, mD	SRV Perm, mD
1	BHP1	8100	4.0E-03	1.6E-02
2	BHP2	6420	8.0E-03	3.2E-01
3	BHP3	6240	4.2E-03	1.7E+00
4	BHP4	6630	8.1E-04	3.2E-02

Table 11—Black oil area of interest - 4 different scenarios with different permeabilities and bottom-hole pressure histories

Oil and gas production histories for the four different scenarios are presented in Figure 59. As shown in this figure the variability in input parameters resulted in different production histories.

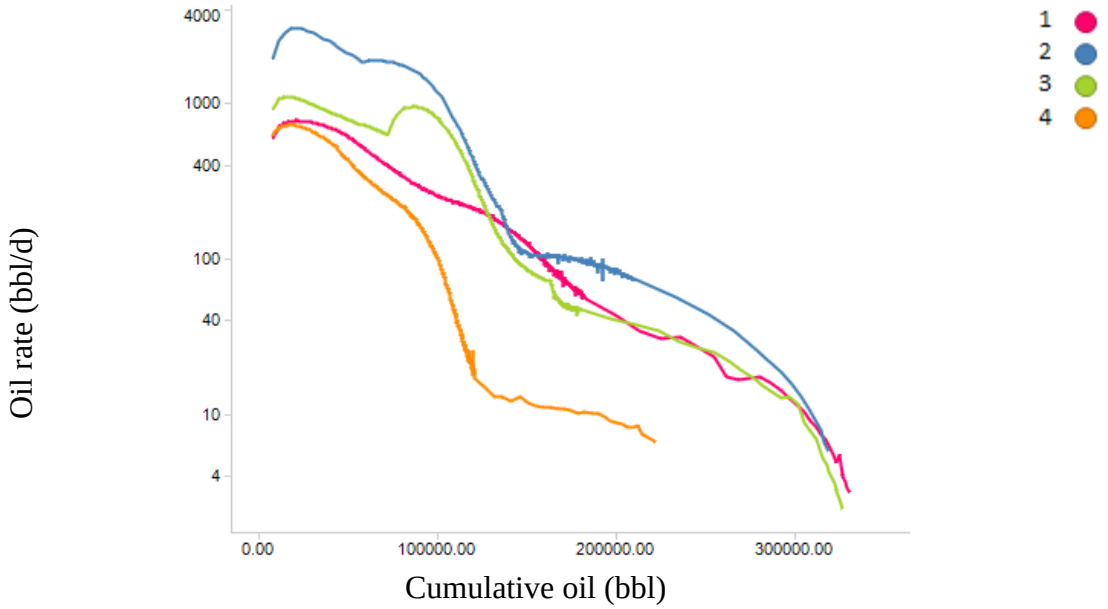

(a)

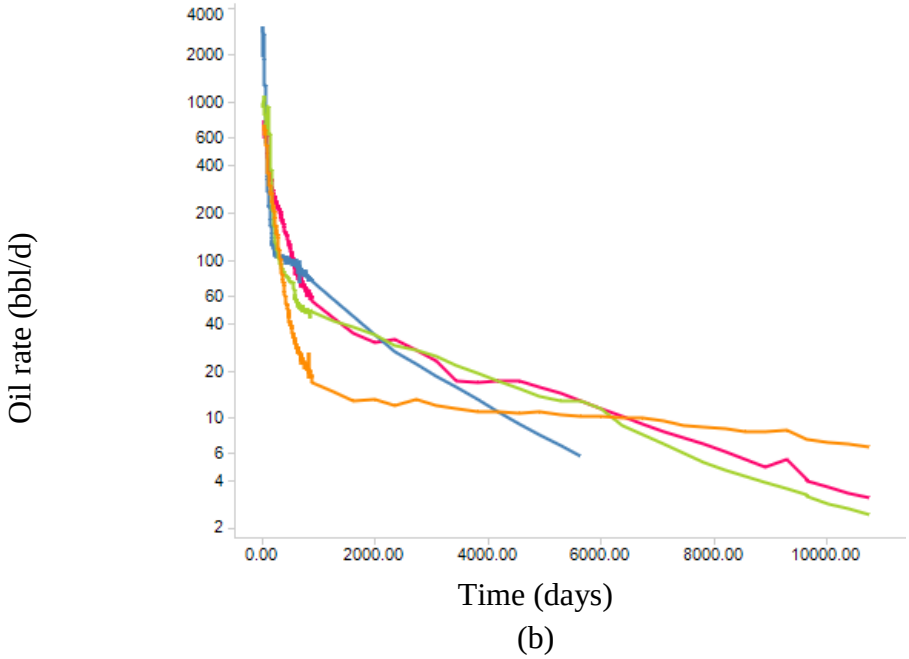

(b)

Figure 59—Black oil area of interest- production histories for 4 different scenarios, (a) log of oil rate versus cumulative oil production, (b) log of oil rate versus time (c) log of gas rate versus cumulative oil production, (d) log of gas rate versus time

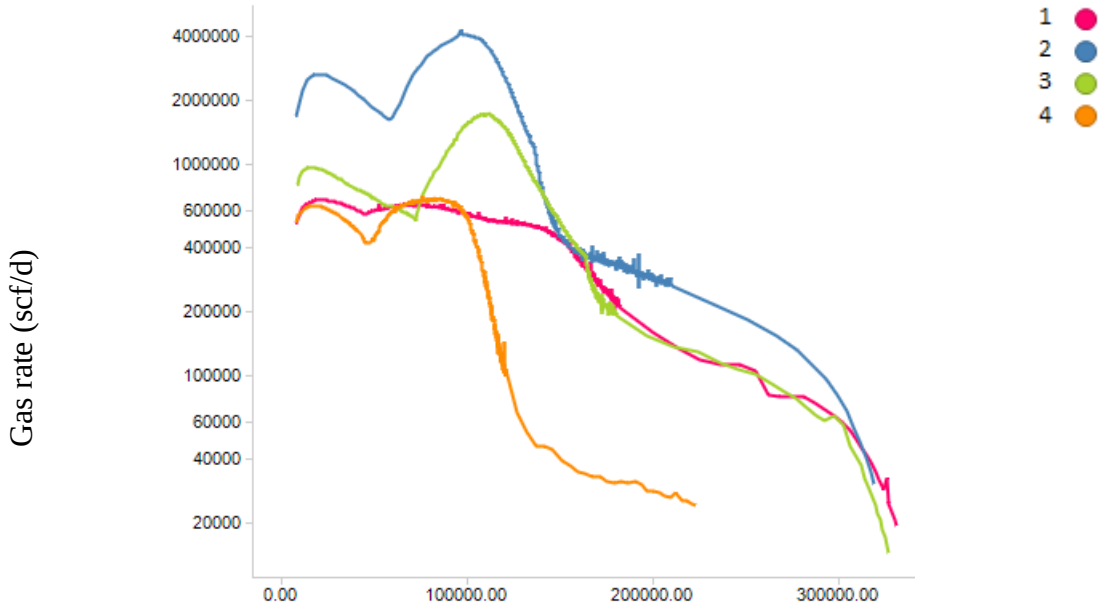

(c)

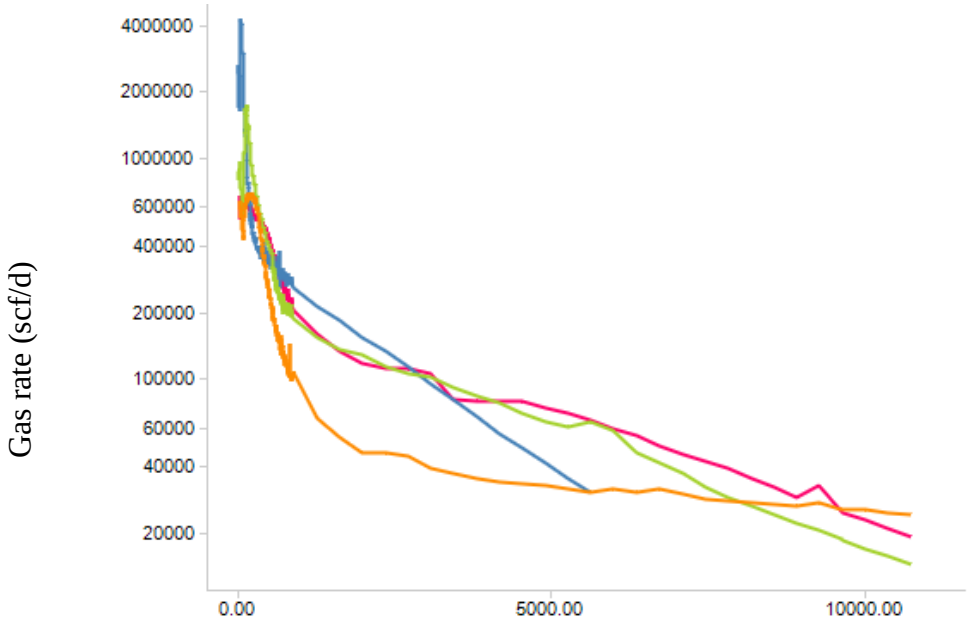

(d)

Figure 59—Continued.

As with the volatile oil area of interest, in plots of q_D vs. t_D, the production histories converge as Figure 60 shows.

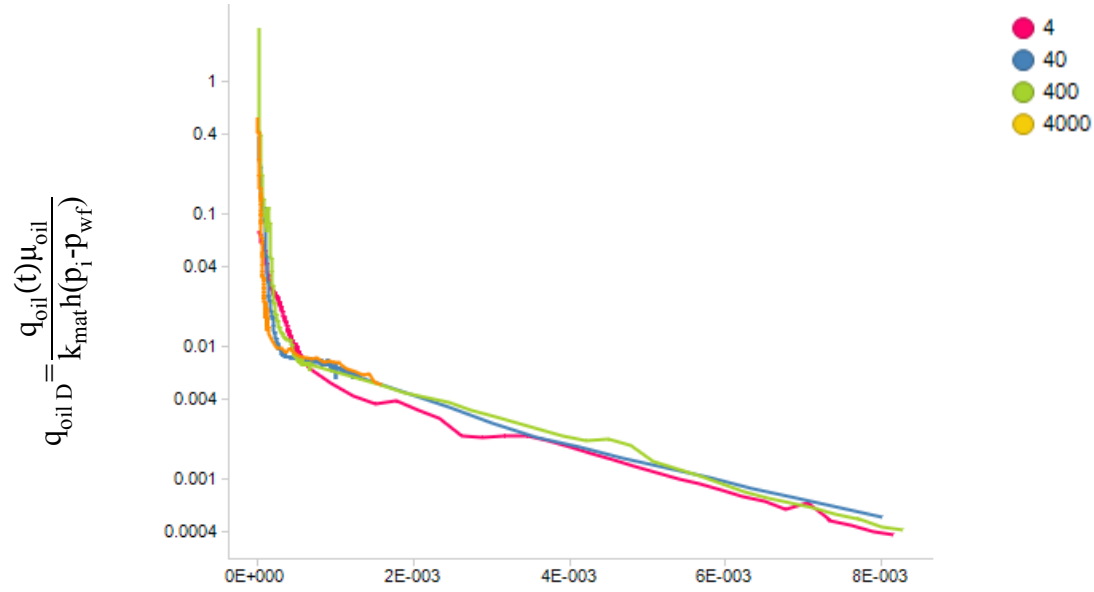

$$q_{oil\,D}=\frac{q_{oil}(t)\mu_{oil}}{k_{mat}h(p_i-p_{wf})}$$

(a)

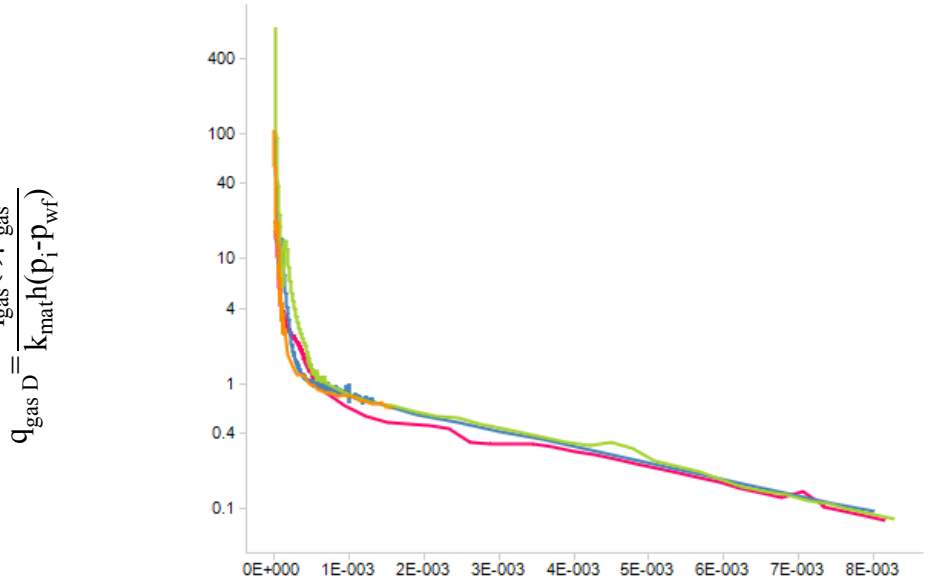

$$q_{gas\,D}=\frac{q_{gas}(t)\mu_{gas}}{k_{mat}h(p_i-p_{wf})}$$

(b)

$$t_D=\frac{k_{mat}t}{\varphi c_t\mu_{oil}(2x_e-2x_f)^2}$$

Figure 60—Black oil area of interest - oil and gas production histories in terms of dimensionless variables converge

As in the volatile oil case, for each of the 4 cases mentioned above, an equivalent analytical model was developed, as discussed in CHAPTER VI. Comparisons of the dimensionless histories from analytical model with those in numerical models provide the point at which the analytical models diverge from the numerical baseline. The transition point occurs at t_D= 6.2e-4 as shown in Figure 61.

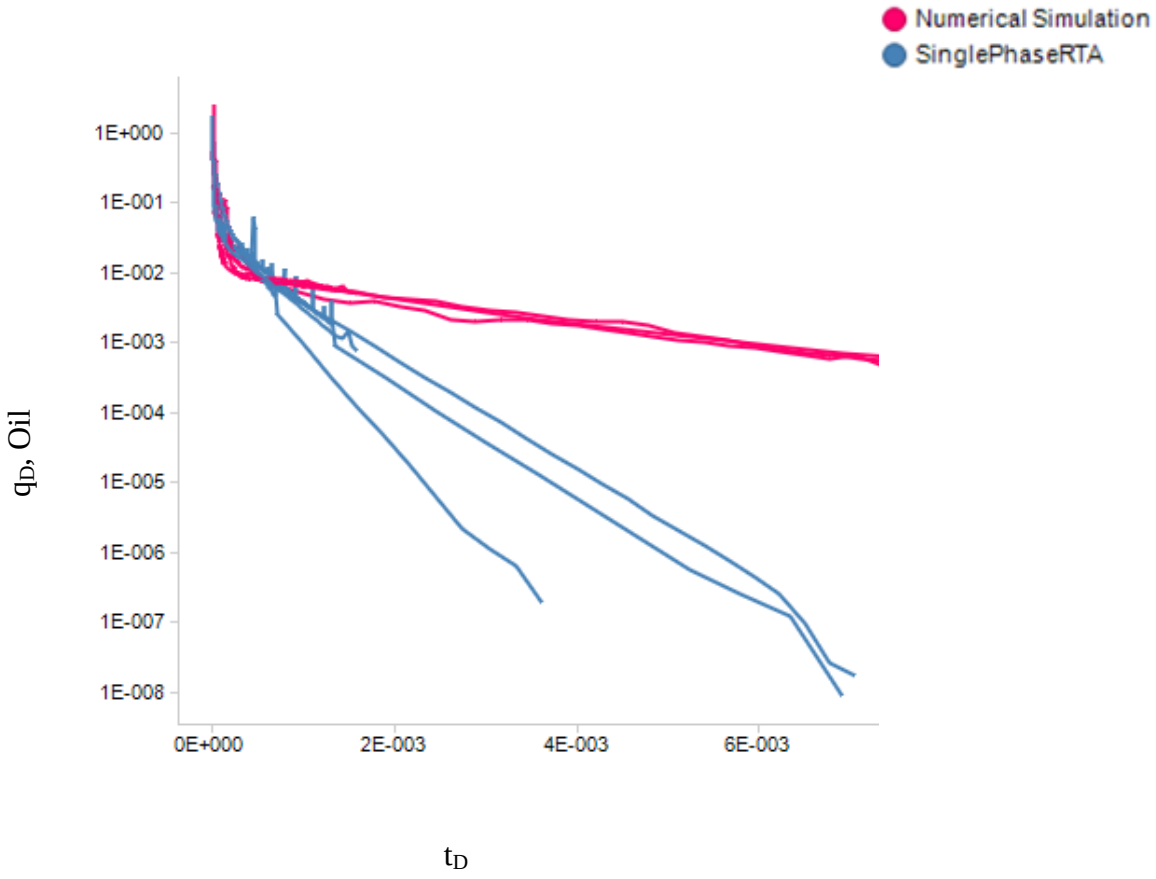

Figure 61—Black oil area of interest transition point where workflow requires to switch from analytical model to q_D-t_D relationship

The history beyond the transition point is represented by a single q_D-t_D relationship for the black oil area of interest. As mentioned before, consistent with industry practices, the q_D-t_D relationship was represented in terms of a multi-segment Arps decline model. A

standard spreadsheet implementing Arps' hyperbolic model was used with q_D and t_D values as input. Curve fitting using linear regression resulted in the Arps model parameters (Figure 62).

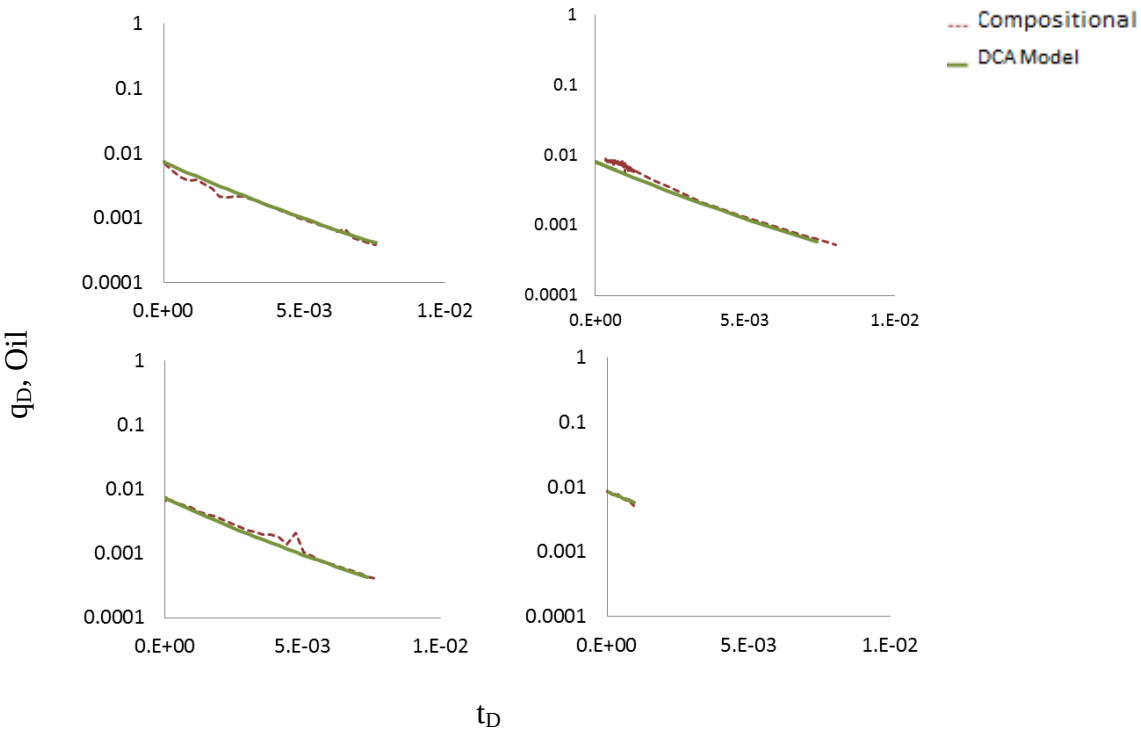

Figure 62—Dimensionless histories beyond transition point represented by black oil Arps hyperbolic decline model

The q_D-t_D relationship in terms of parameters in a multi-segment Arps hyperbolic decline model for the black oil area of interest are presented in Table 12.

Segment	Arps Parameters	Value
Beyond $t_{D,Transition}$		
1	q_i	q_D at t_D
	b_i	1.1
	d_i	0.6
Time to switch (N/A)		
N/A	b_2	-
Terminal condition		
Final	$q_{D,terminal}$	0.03

Table 12— Arps hyperbolic decline model parameters from curve fitting the scenarios in the black oil area of interest

Similar to our methodology for the volatile oil area of interest, we plotted gas-oil ratios from the four compositional numerical simulations vs. dimensionless time (Figure 63), and derived an average GOR trend (equations (173) and (174)).

.

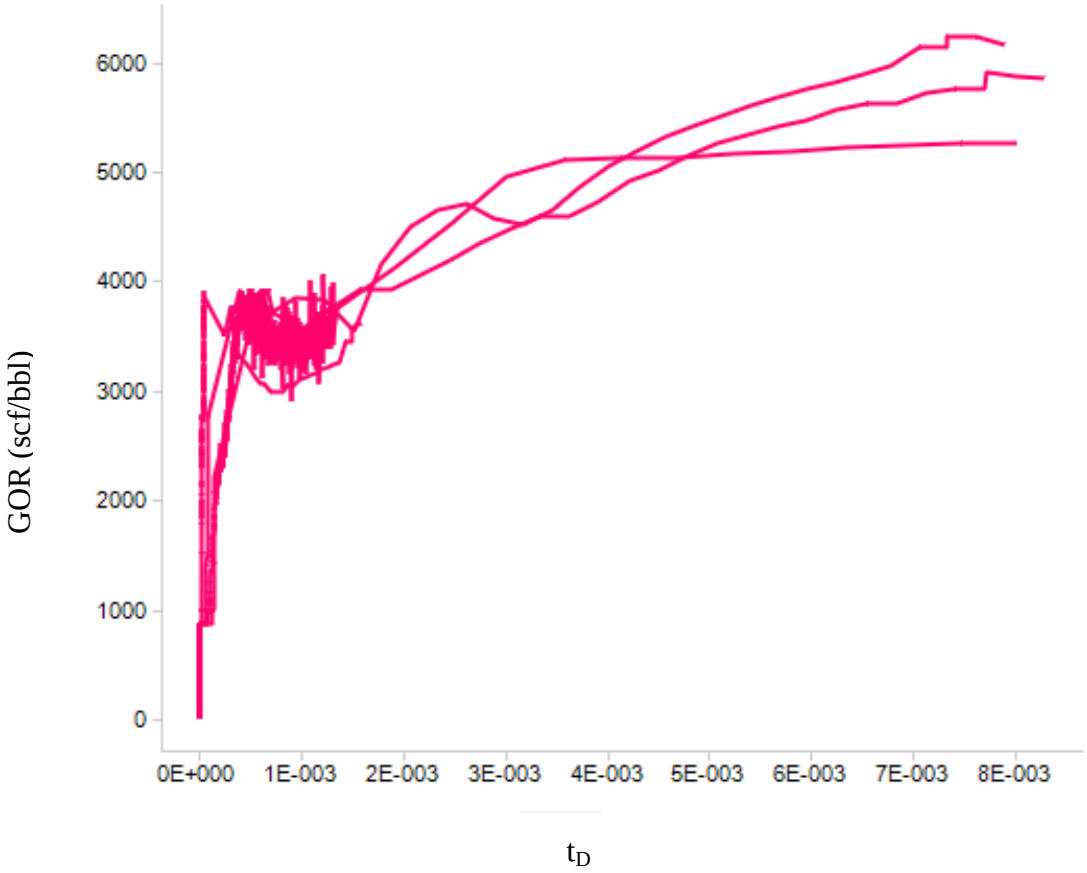

Figure 63—Gas oil ratio trend for black oil area of interest, GOR vs. t_D

For $t_D < t_{D\text{-Transition}}$:

$$\text{Gas Oil Ratio } \left(\frac{\text{scf}}{\text{bbl}}\right) = 4.8e^{7} * t_D + 1000 \tag{173}$$

For $t_D > t_{D\text{-Transition}}$:

$$\text{Gas Oil Ratio } \left(\frac{\text{scf}}{\text{bbl}}\right) = 2.7e^{5} * (t_D - 6.2e^{-4}) + 4000 \tag{174}$$

Summary and Conclusion

In this Chapter, step-by-step instructions of the workflow were discussed using examples of volatile oil and black oil areas of interest. For a specific range of matrix permeability, initial reservoir pressure, and stimulated rock permeability, the high, mid, and low initial production histories were generated using four numerical simulations. Four equivalent histories were also generated using analytical models. Comparison of q_D vs. t_D from numerical to analytical model results identified the transition point between single-phase-dominated flow and multi-phase-dominated flow. We showed that, after the transition point, the four numerical models established a single trend for q_D. Following traditional industry practice, we represented this trend with multi-segment Arps hyperbolic decline model parameters. We also used the four numerical models to generate GOR trends as functions of t_D. The workflow up to this point provides the transition point, q_D-t_D trend beyond the transition point, and the GOR for the life of the well. These results are general for each fluid (volatile oil and black oil).

To forecast production for a specific well, we should use an analytical model prior to the transition point, and the q_D-t_D and GOR vs. t_D correlations beyond the transition point.

In CHAPTER VIII, we use the trends established in CHAPTER VII for the volatile oil area of interest and the black oil area of interest to illustrate forecasts using our workflow. These forecasts are then compared to the results from numerical models.

CHAPTER VIII

RESULTS AND VALIDATION OF WORKFLOW FOR FORECASTING PRODUCTION IN LRS PLAYS

In CHAPTER IV, the hypothesis for forecasting production in MFHW's in LRS plays stipulated that the life cycle production was divided into two flow periods, the initial period and the subsequent period. In the initial period, the flow is dominated by the properties of the stimulated rock volume and assuming single-phase flow does not cause large errors. Due to the complexity of flow in MFHW's, the transition from the initial period is not simply due to a change in flow regimes, for example, as in single-phase flow, from linear flow to boundary-influenced flow where the slope change in a pressure-normalized rate versus time on a log-log plot can be clearly identified. We believe that both the change in flow regimes and multi-phase flow are responsible. Often, these influences are not clearly identifiable on diagnostic plots. Dimensionless functions of rate and time were developed to help normalize production histories. As a result, we used a comparison of results from single-phase analytical models to compositional numerical reservoir simulators to identify the transition point. The numerical model accounts for multi-phase flow and comparing its results to the single-phase analytical model results show where the impact of multi-phase flow becomes significant. In CHAPTER V, using compositional numerical simulation, we showed that MFHW's in LRS, with various matrix permeabilities, stimulated rock permeabilities, fracture length and spacing, and initial reservoir pressure exhibit production trends that converge on plots of dimensionless rate, q_D, vs. dimensionless time, t_D. The trends are specific to each individual fluid, so they have to be developed for each different fluid composition. In CHAPTER VII these trends were developed for a specific volatile oil, and a specific black oil area of interest. The trends were represented with Arps multi-

segment hyperbolic decline model parameters. To forecast the secondary gas phase, we developed an average GOR trend versus dimensionless time from compositional model results. In CHAPTER II we reviewed the trilinear-flow model, and, in CHAPTER VI, we discussed using a single-phase analytical model to forecast production in the initial, single-phase dominated flow period.

In CHAPTER I we stated that compositional numerical simulation is the appropriate benchmark. In this chapter, then, we compare a forecast using our workflow presented in previous chapters to a forecast from a compositional numerical simulator. The results are presented for volatile oil and black oil areas of interest.

The workflow discussed is summarized in Figure 64. The steps shown in this figure are followed to forecast each of the cases discussed below.

Area of Interest 1- Volatile Oil

For each of the cases presented in Table 9, we set up a rate transient analysis model in commercial software and forecasted production using the bottom-hole-pressure history shown in Figure 58. The forecast was used as the initial production period up to the transition point of t_D= 3.8e-4 as shown in Figure 55. The subsequent production was then forecasted using the q_D - t_D relationship shown in Figure 56 which was represented using Arps multi-segment hyperbolic decline model with parameters from Table 10. The GOR-t_D trend in Figure 57 was represented using equations (171) and (172) to forecast the gas phase production. For each of these cases, a numerical simulation was also carried out. The results from the workflow were compared to the corresponding numerical simulation results. These comparisons are presented below by cases corresponding to those in Table 9.

Workflow on a Page

Field-wide

Done only once- Limited to a single composition of fluid

Compositional Numerical Model		Analytical Model
Multi-phase - k_{mat} - k_{SRV} - SRV Geometry	Low, Mid, High	Single Phase - k_{mat} - k_{SRV} - SRV Geometry

Compare q_D vs. t_D

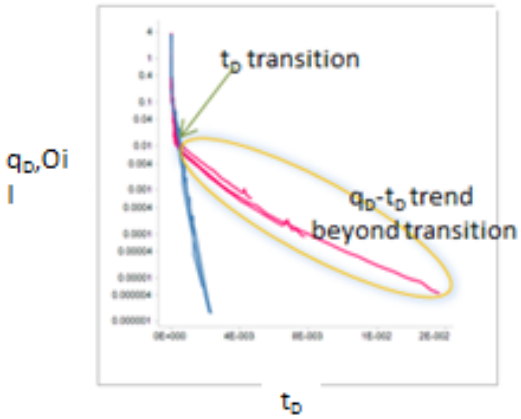

Determine:

1- Transition Point t_D

2- q_D-t_D trend beyond transition (may represent using Arp's multi-segment decline)

3- GOR-t_D trend From Numerical Models

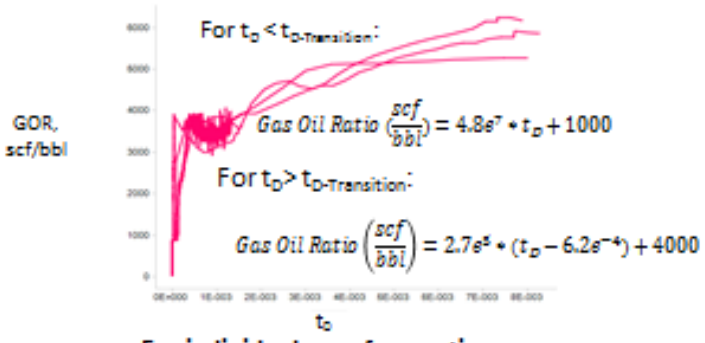

For individual well forecasting

Repeat for each individual well in this PVT window, use 1, 2, 3 above

1- Set up a specific analytical model for the well (use commercial software)

2- If any production available, use automatic history matching

3- Use 1, 2, and 3 above to forecast oil beyond transition point and gas for life of well

Figure 64—Schematic of workflow

Case-1

With matrix permeability of 2.4e-3 mD and SRV permeability of 9.6e-3 mD, with initial pressure of 6000 psi declining with BHP1 drawdown, Figure 65 compares oil and gas production rates and oil and gas cumulative production volumes with time from the workflow to compositional numerical model results. The EUR for oil was 297 kbbl from the workflow versus 286 kbbl from the compositional model, a 4% difference. As the figure below shows, this difference occurs near the end of the life of the well, so its significance is even less in terms of net present value. For gas, the workflow forecasts 1.92 BCF, and the numerical model 1.75 BCF, a difference of 10%, again mostly near the end of the life of the well with lower net present value. We consider the match between the workflow and the numerical model benchmark to be good.

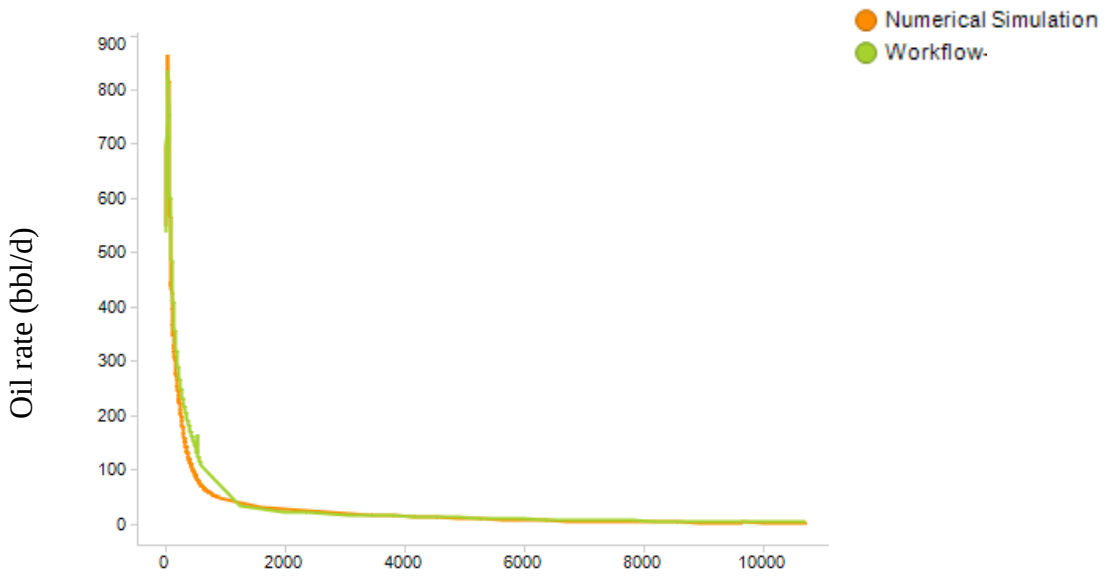

(a)

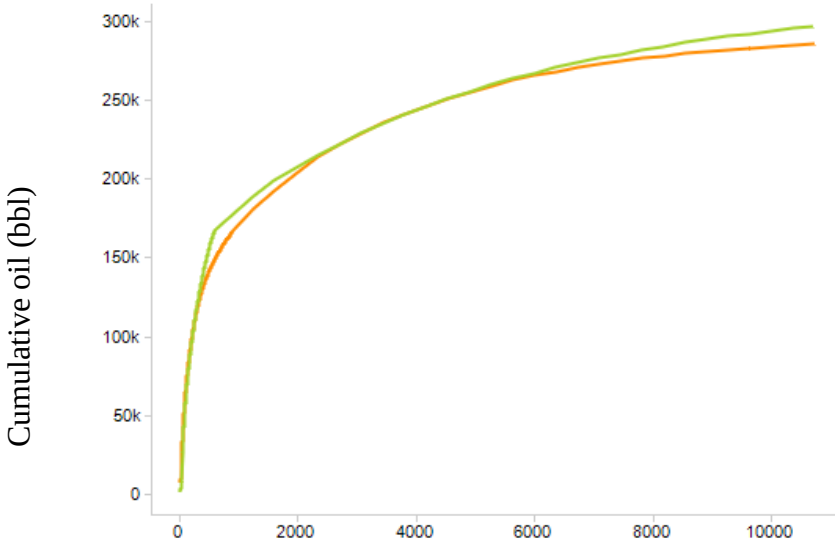

(b)

Time (days)

Figure 65—Volatile oil area of interest- workflow compared to numerical simulation forecast (Case -1)

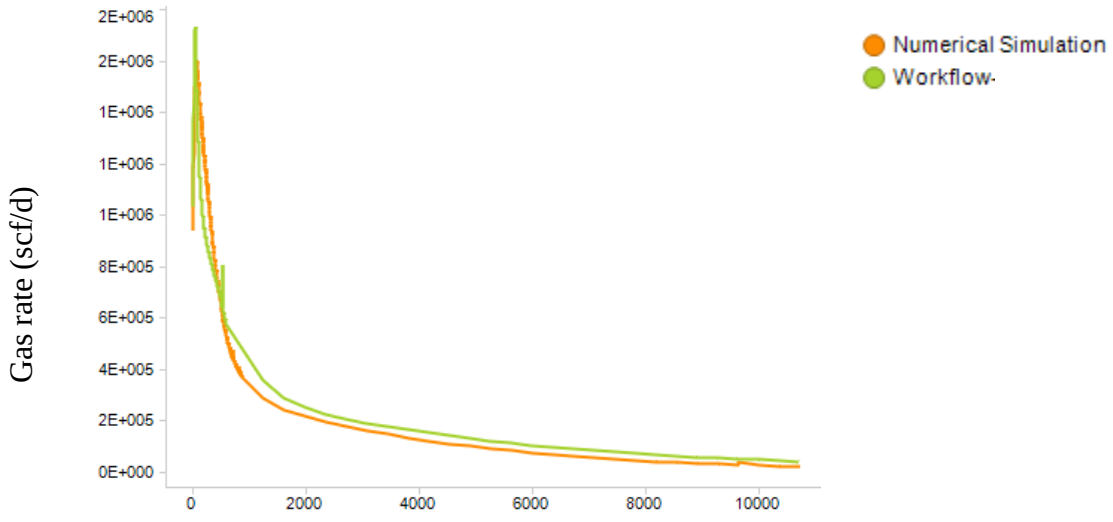

(c)

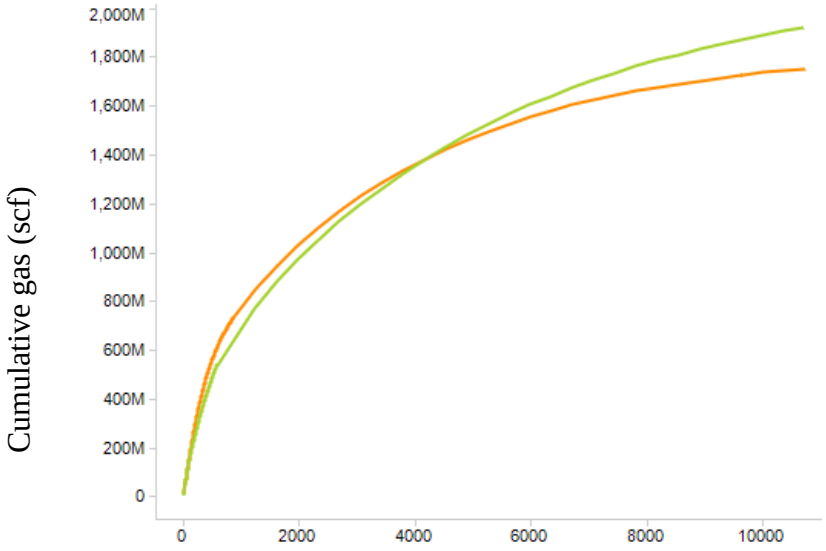

(d)

Time (days)

Figure 65—Continued.

Case-2

With matrix permeability of 1e-5 mD, SRV permeability of 4e-4 mD, initial reservoir pressure of 6630 psi declining at BHP2 drawdown, Figure 66 compares oil and gas production rates and oil and gas cumulative production volumes with time from the workflow to compositional numerical model results. The ultimate recovery for oil is 80

kbbl with workflow versus 84.3 kbbl with the numerical model, a 6% difference. For gas, the workflow forecasts 0.35 BCF, and the numerical model 0.33 BCF, also a 6% difference. This is also a good match.

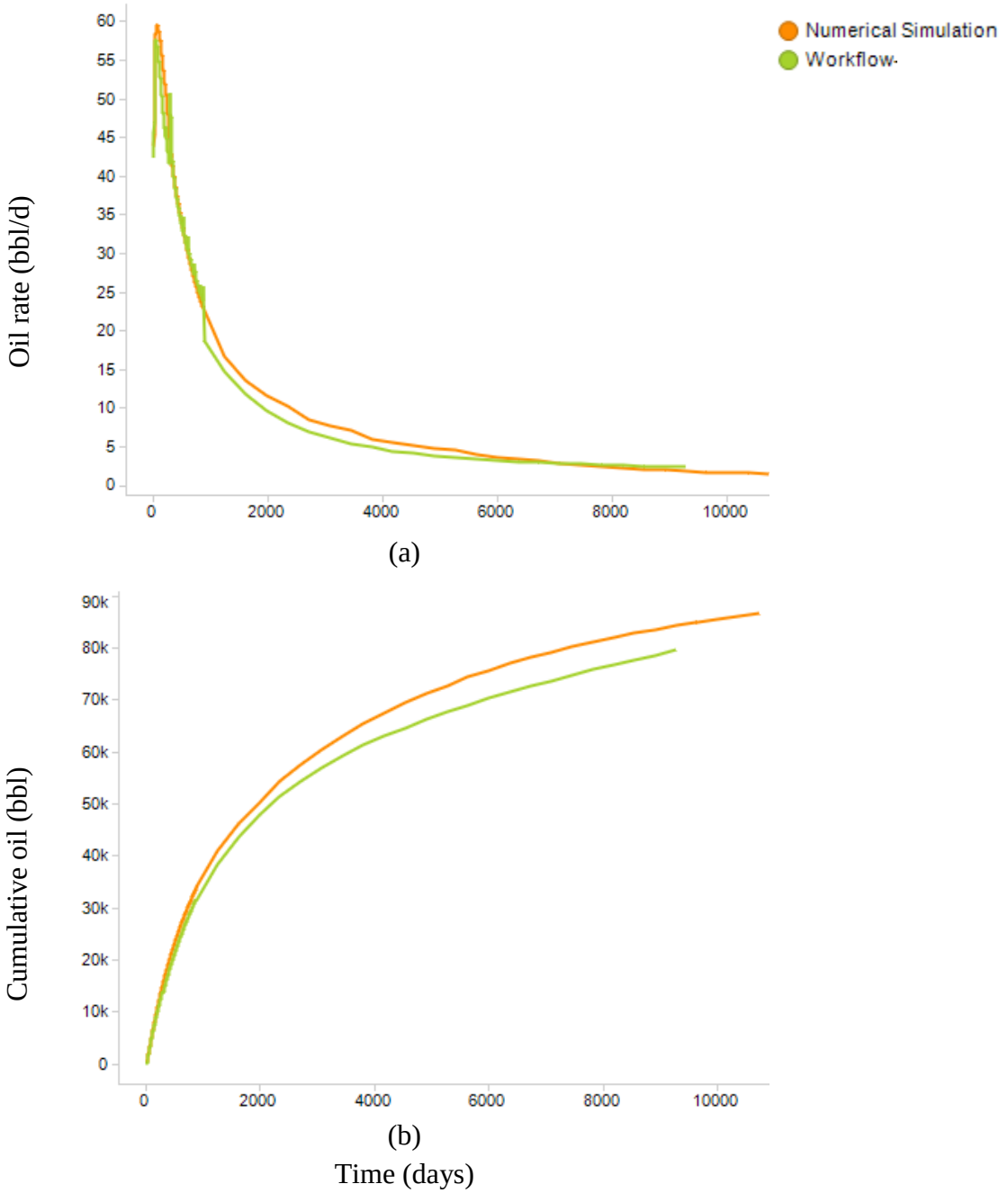

Figure 66—Volatile oil area of interest, workflow compared to numerical simulation forecast (Case -2)

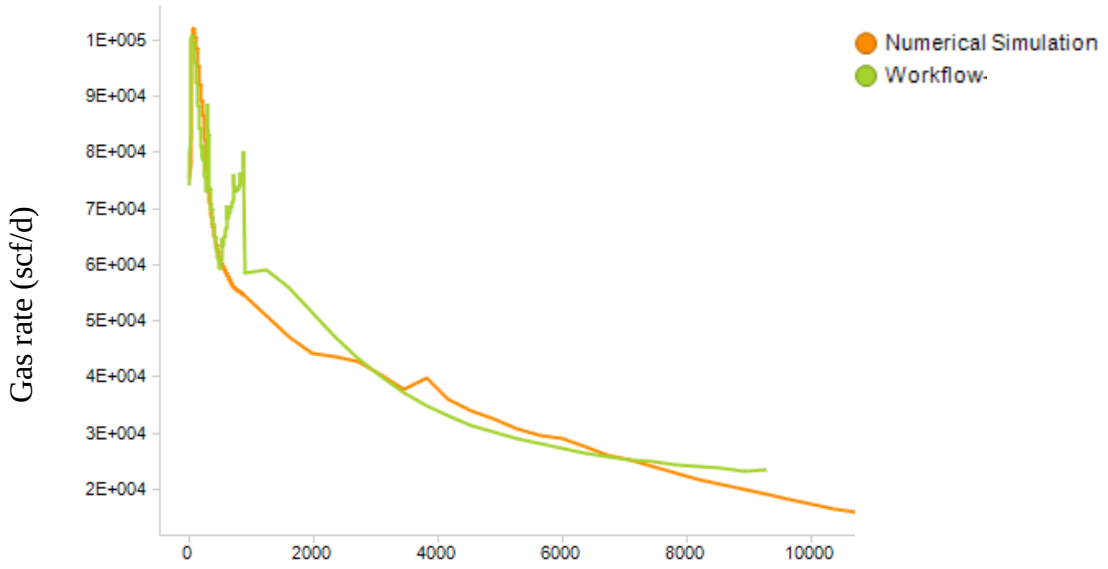

(c)

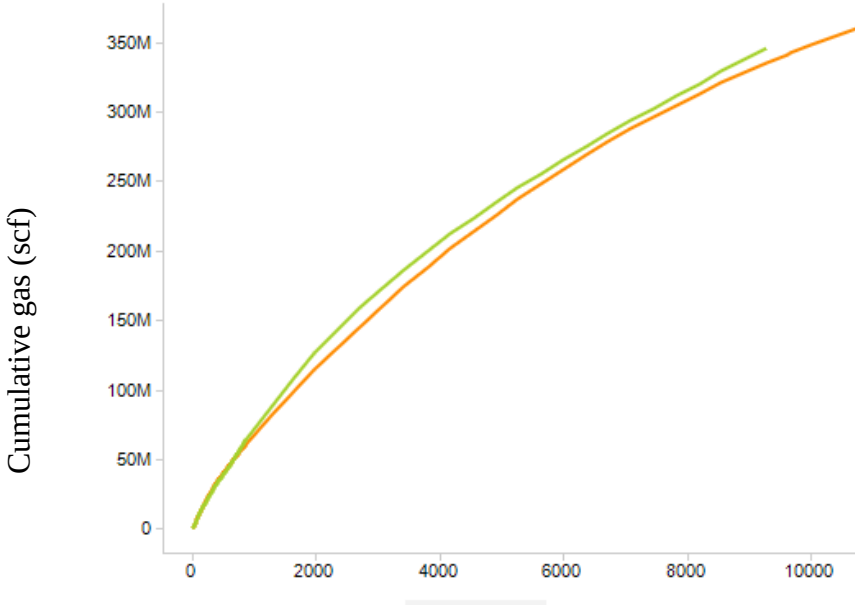

(d)

Time (days)

Figure 66—Continued.

Case-3

With matrix permeability of 4e-3 mD, SRV permeability of 1.6 mD, initial reservoir pressure of 8100 psi, and BHP3 pressure history, Figure 67 compares oil and gas

production rates and oil and gas cumulative production volumes with time from the workflow to compositional numerical model results. The ultimate recovery of oil is 288 kbbl from the workflow versus 276 kbbl from the numerical model, a 4% difference. For gas, the workflow forecasts 1.71 BCF, and the numerical model gives 1.84 BCF, a difference of 7%. This is also a good match.

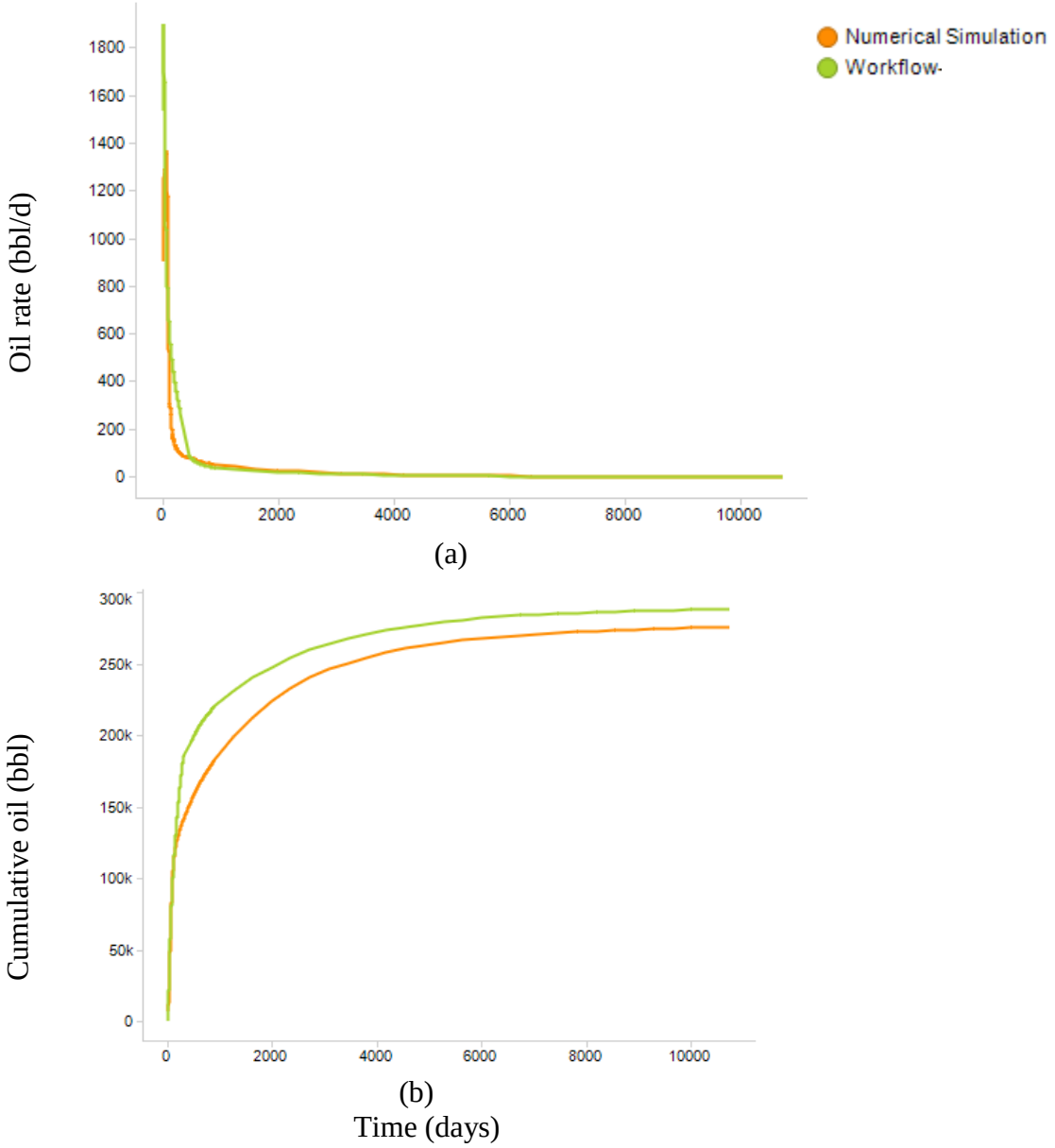

Figure 67—Volatile oil area of interest, workflow compared to numerical simulation forecast (Case -3)

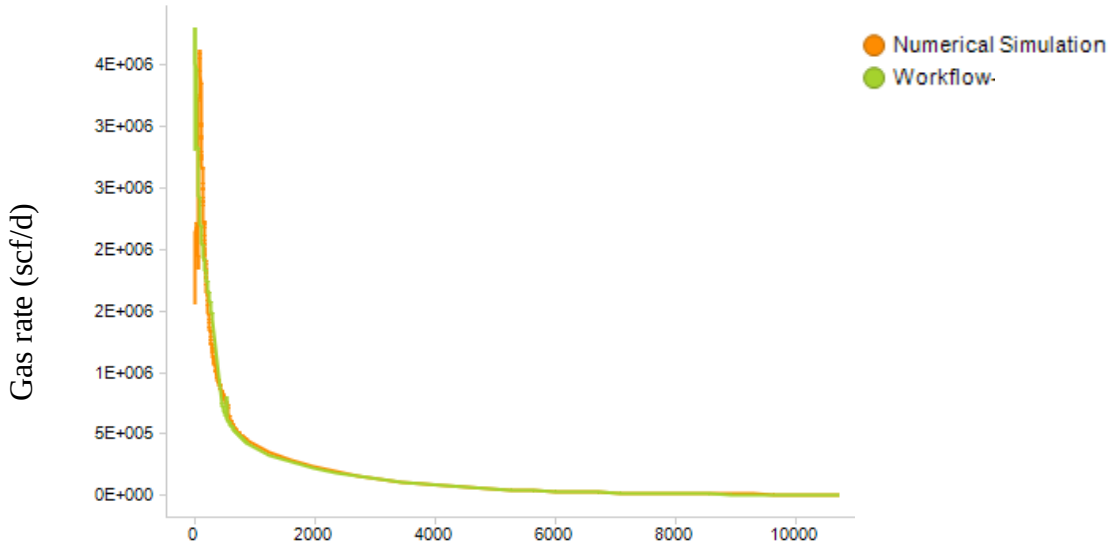

(c)

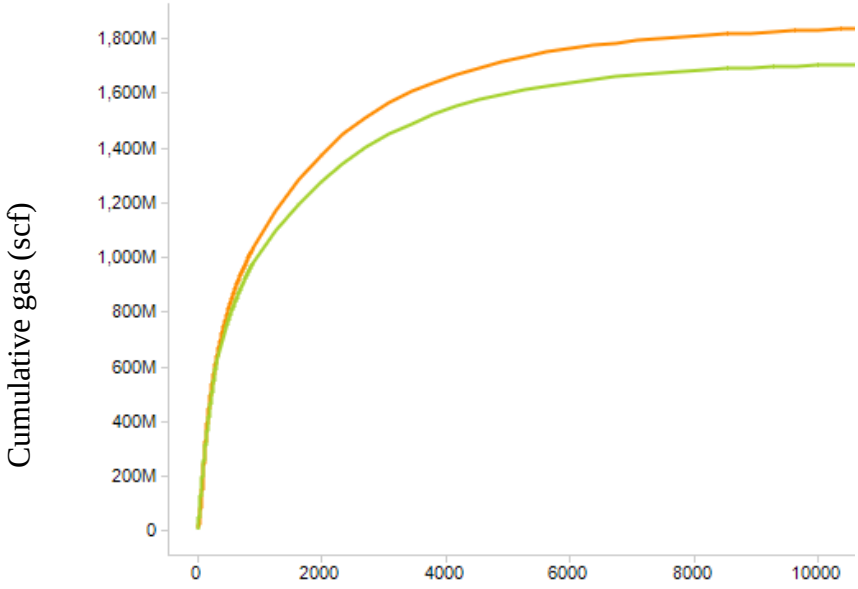

(d)

Time (days)

Figure 67—Continued

Case-4

With matrix permeability of 8e-3 mD, SRV permeability of 3.2e-1 mD, initial reservoir pressure of 7050 psi, and BHP4 pressure history, Figure 68 compares oil and gas production rates and oil and gas cumulative production volumes with time from the

workflow to compositional numerical model results. The ultimate recovery of oil is 301 kbbl with the workflow versus 280 kbbl with the numerical model, an 8% difference. For gas, the workflow forecasts 1.91 BCF, and the numerical model 1.86 BCF, a 3% difference. This is also a good match.

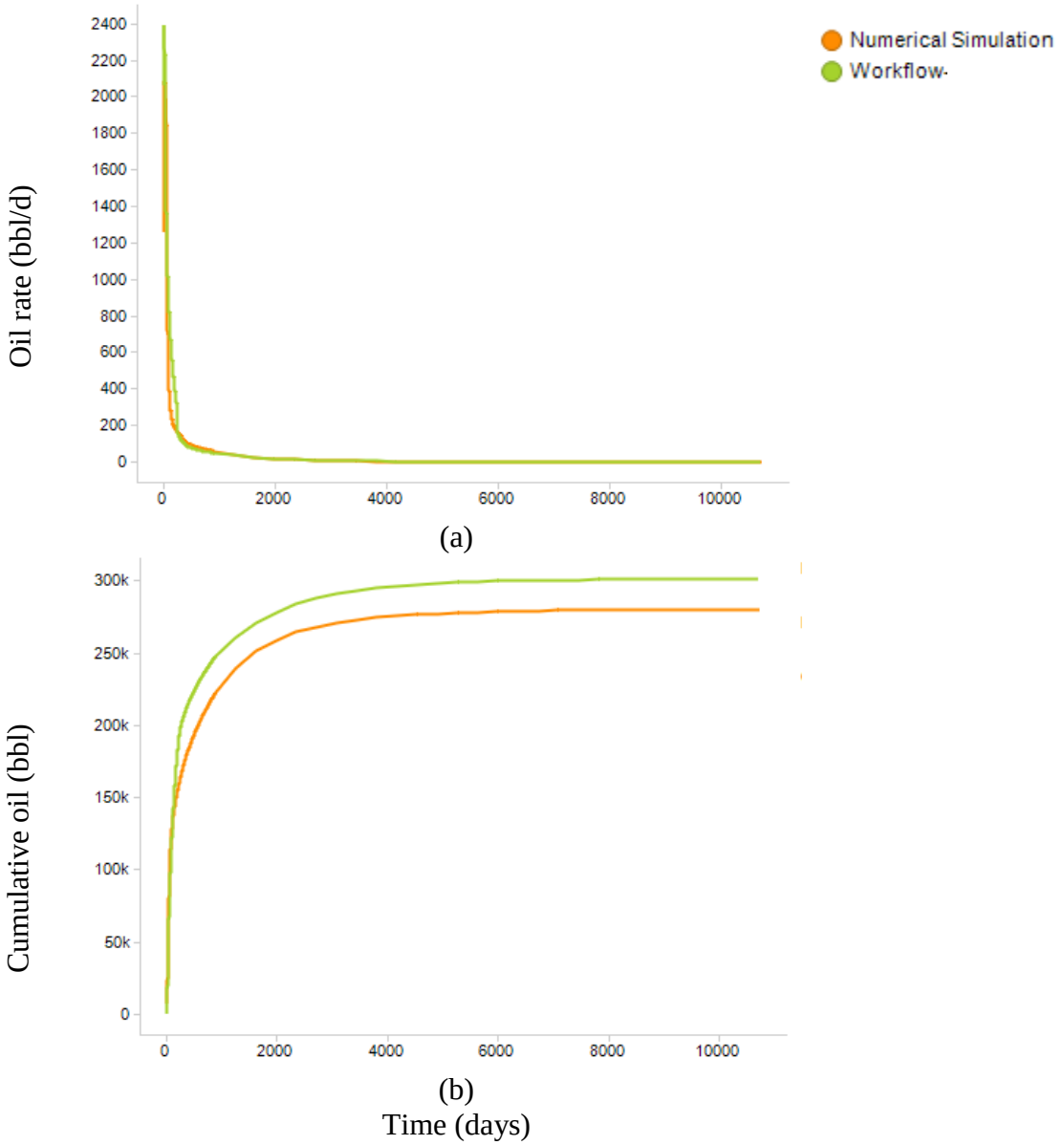

Figure 68—Volatile oil area of interest, workflow compared to numerical simulation forecast (Case -4)

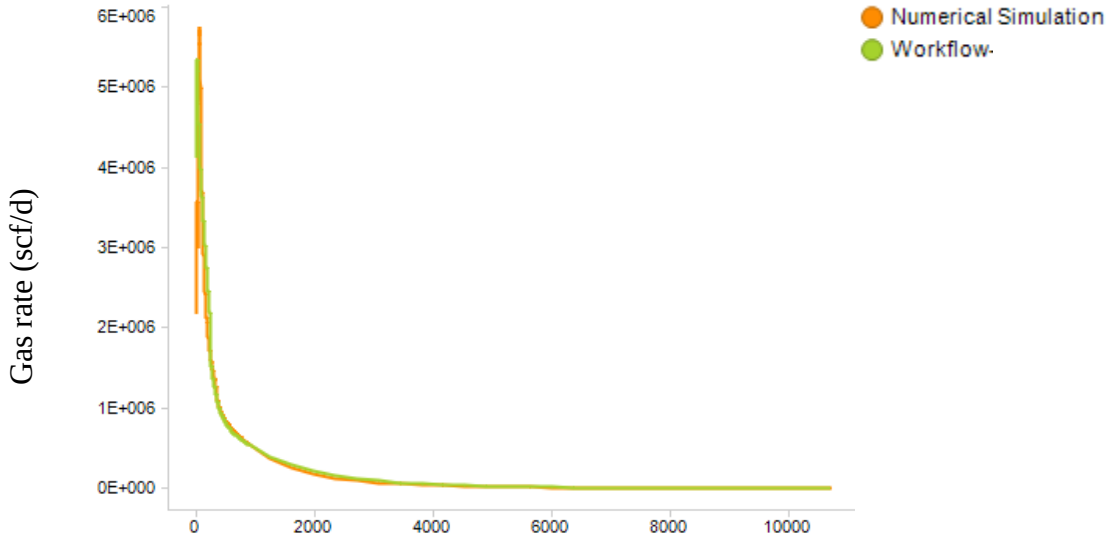

(c)

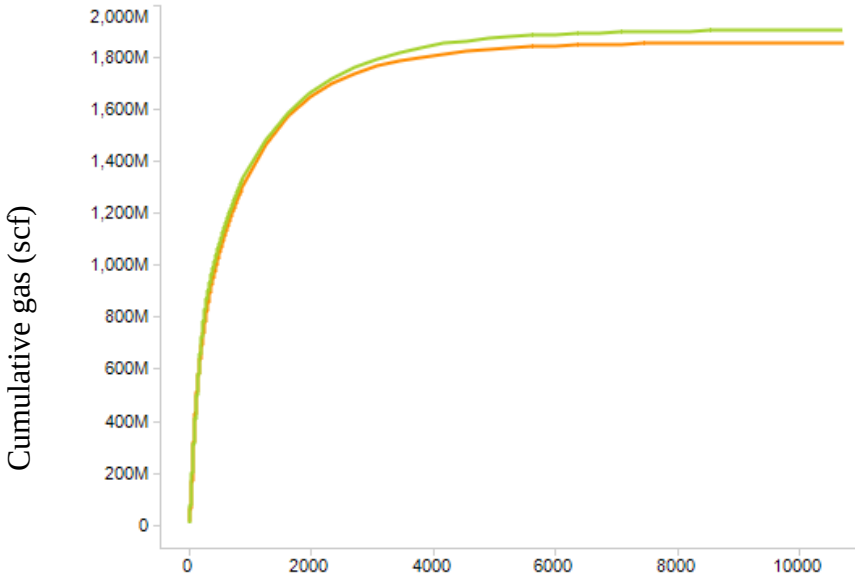

(d)

Time (days)

Figure 68—Continued.

The results of the 4 cases above are summarized in Tables 13 and 14. As explained earlier, these cases include matrix permeabilitities from 1e-5 to 8e-3 mD, and SRV permeabilities of 4e-4 and 1.6 mD.

Table 13 summarizes ultimate recovery of oil and gas using the numerical simulation and our workflow. The results show that for oil, ultimate recovery is within 8%, and for gas, ultimate recovery is within 10% of the numerical models.

	Ultimate Recovery					
	Compositional Numerical		Our Workflow		% Difference	
Case No.	Oil, kbbl	Gas, Bcf	Oil, kbbl	Gas, Bcf	Oil, EUR	Gas, EUR
1	286	1.75	297	1.92	4%	10%
2	84.3	0.33	80	0.35	-6%	6%
3	276	1.84	288	1.71	4%	-7%
4	280	1.86	301	1.91	8%	3%

Table 13—Comparison of ultimate recovery in volatile oil cases

In addition to ultimate recovery, it is also important to evaluate the match during the producing life of the well. Present value of producing volumes at a discount rate of 10% is shown in Table 14. The results for oil are within 10%, and for total gas and oil based on $60/bbl oil and $2.45/Mcf gas are within 7% except for case 2, in which total value of oil and gas is 11% lower. This case is for an extremely low permeability, and the production trends are significantly different. Still, even in this extreme case, the agreement in present value of ultimate recovery is acceptable.

	Present Value of Ultimate Recovery					
	Compositional Numerical		Our Workflow		delta %	
Case No.	Oil, kbbl	Gas, Bcf	Oil, kbbl	Gas, Bcf	Oil	Total Oil and Gas*
1	209	1.10	212	1.08	1%	1%
2	53	0.15	49.7	0.09	-6%	-11%
3	221	1.36	243	1.26	10%	6%
4	246	1.54	267	1.57	9%	7%

** Based on $60/bbl crude and $2.45/Mcf natural gas*

Table 14—Comparison of present value of ultimate recovery in volatile oil cases

Area of Interest 2- Black Oil

Like in the black oil area of interest, for each of the cases presented in Table 11, we set up a rate transient analysis model in commercial software and forecasted production using the bottom-hole-pressure history shown in Figure 58. The forecast was used as the initial production period up to the transition point of t_D = 6.2e-4 as shown in Figure 61. The subsequent production was then forecasted using the q_D - t_D relationship shown in Figure 62 which was represented using Arps multi-segment hyperbolic decline model with parameters from Table 12. The GOR-t_D trend in Figure 63 was represented using equations (173) and (174) to forecast the gas phase production. For each of these cases, a numerical simulation was also carried out. The results from the workflow were compared to the corresponding numerical simulation results. These comparisons are presented below by cases corresponding to those in Table 11.

Case-1

With matrix permeability of 4e-3 mD and SRV permeability of 1.6e-2 mD, with initial pressure of 8100 psi declining with BHP1 drawdown, Figure 69 compares oil and gas production rates and oil and gas cumulative production volumes with time from the

workflow to compositional numerical model results. The EUR for oil was 349 kbbl from the workflow versus 330 kbbl from the compositional model, a 6% difference As the figure below shows, this difference occurs near the end of life of the well, so its significance is less in terms of present value. For gas, the workflow forecasted 1.14 BCF, and the numerical model was 1.05 BCF, a difference of 9%.

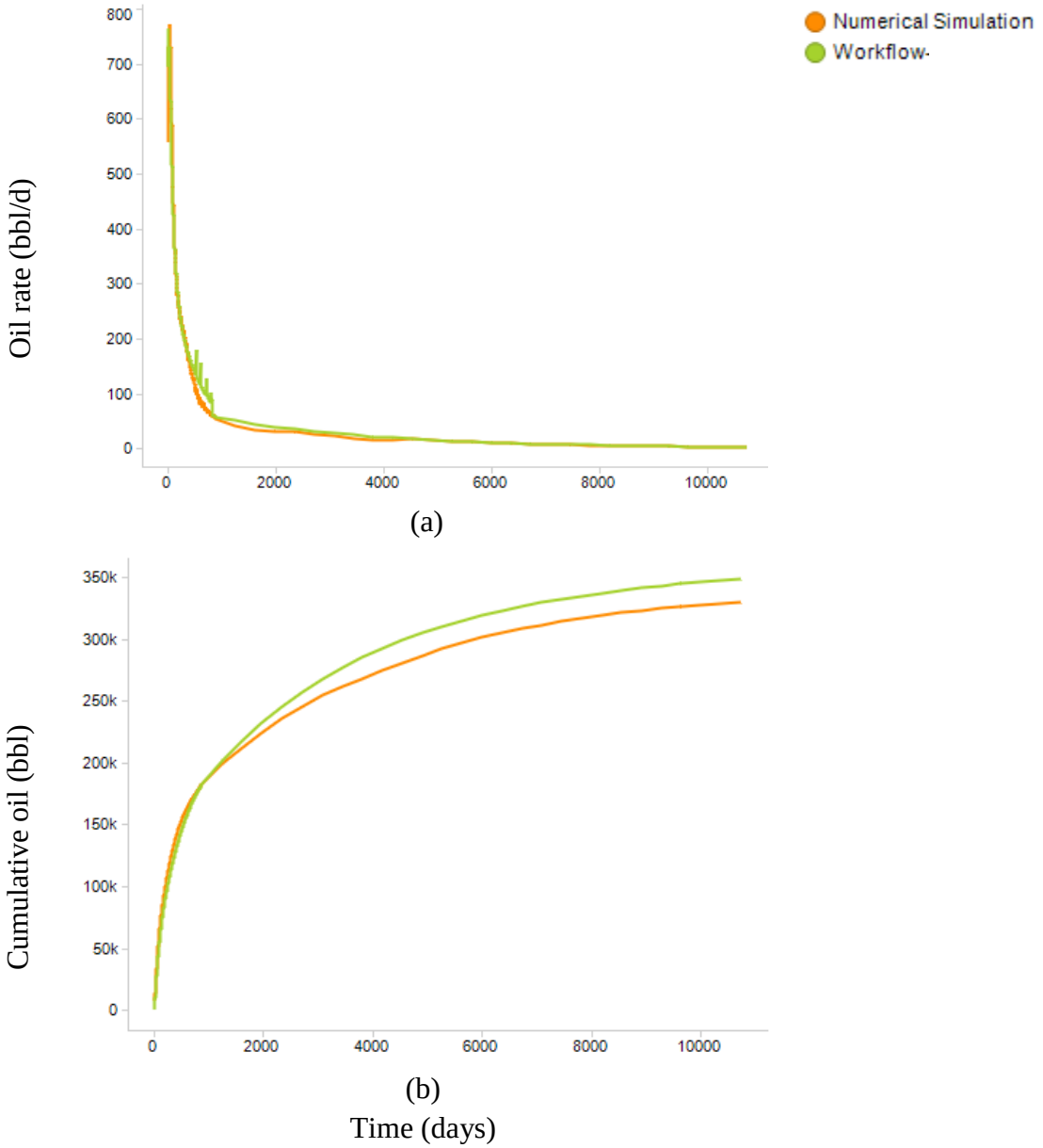

Figure 69—Black oil area of interest, workflow compared to numerical simulation forecast (Case -1)

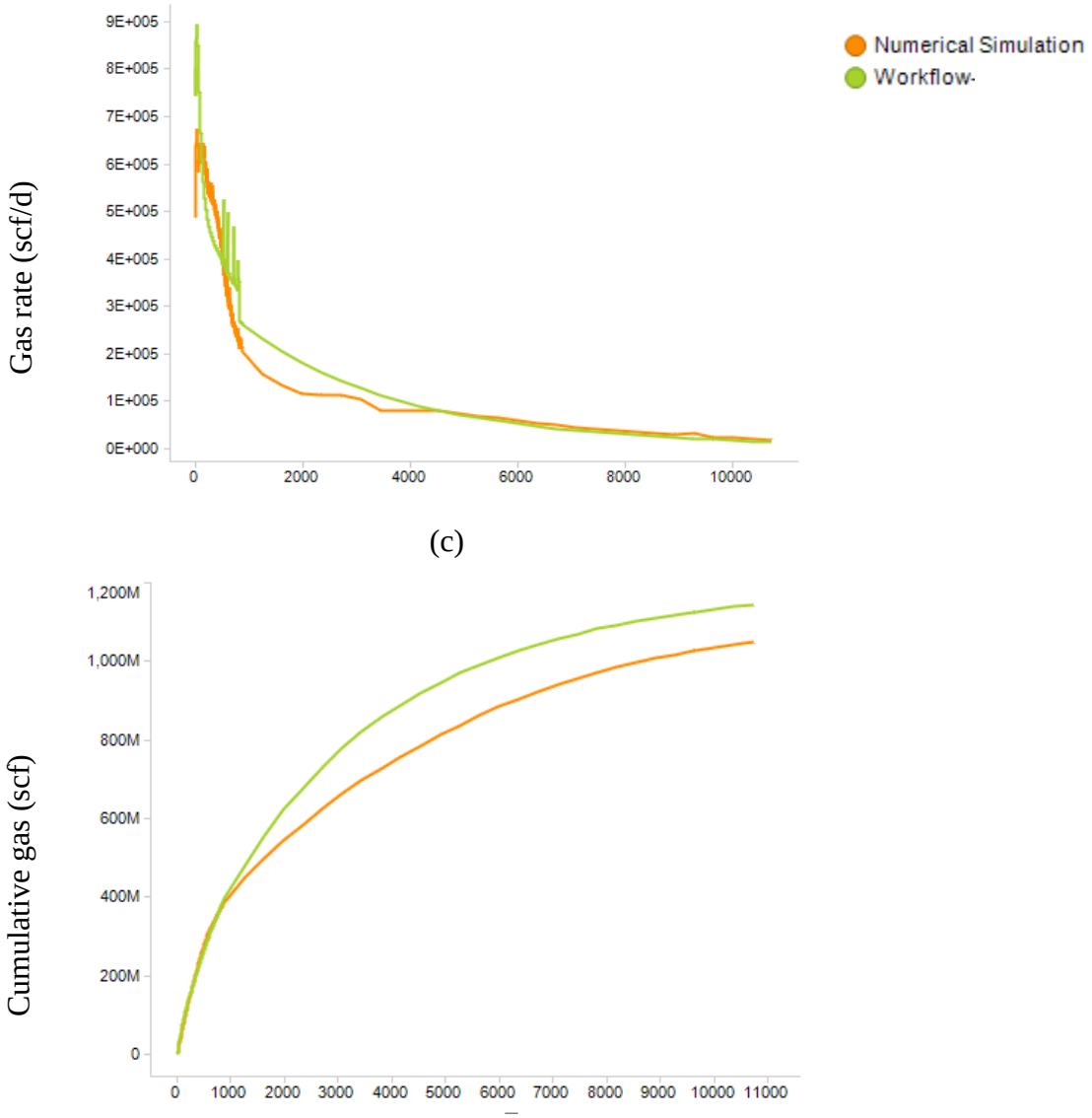

Figure 69—Continued.

Case-2

With matrix permeability of 8e-3 mD, SRV permeability of 3.2e-1 mD, initial reservoir pressure of 6420 psi declining at BHP2 drawdown, Figure 70 compares oil and gas production rates and oil and gas cumulative production volumes with time from the workflow to compositional numerical model results. The ultimate recovery for oil is 319

kbbl with workflow versus 317 kbbl with the numerical model. For gas, the workflow and the numerical forecasts are identical at 1.08 BCF.

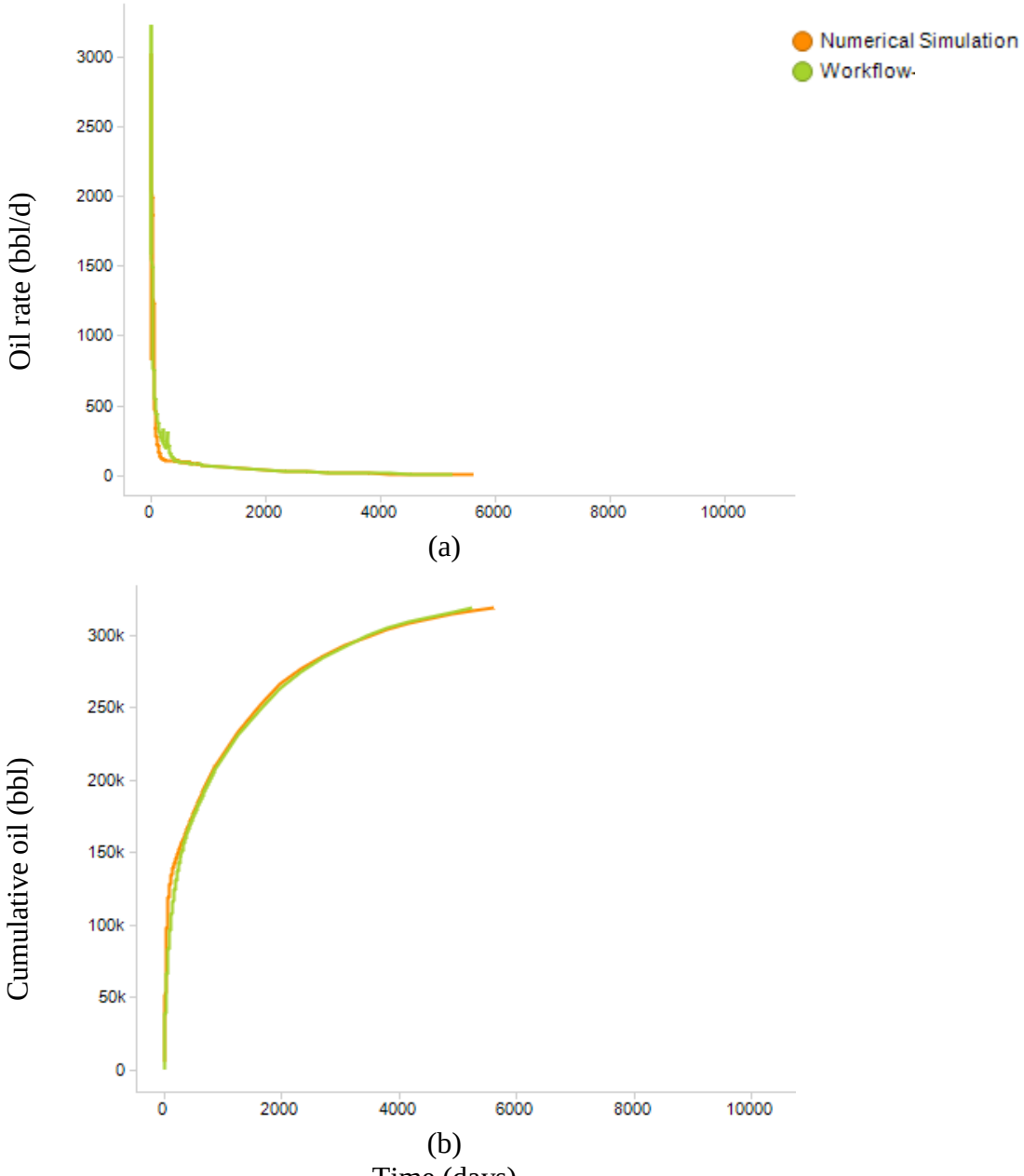

Figure 70—Black oil area of interest, workflow compared to numerical simulation forecast (Case -2)

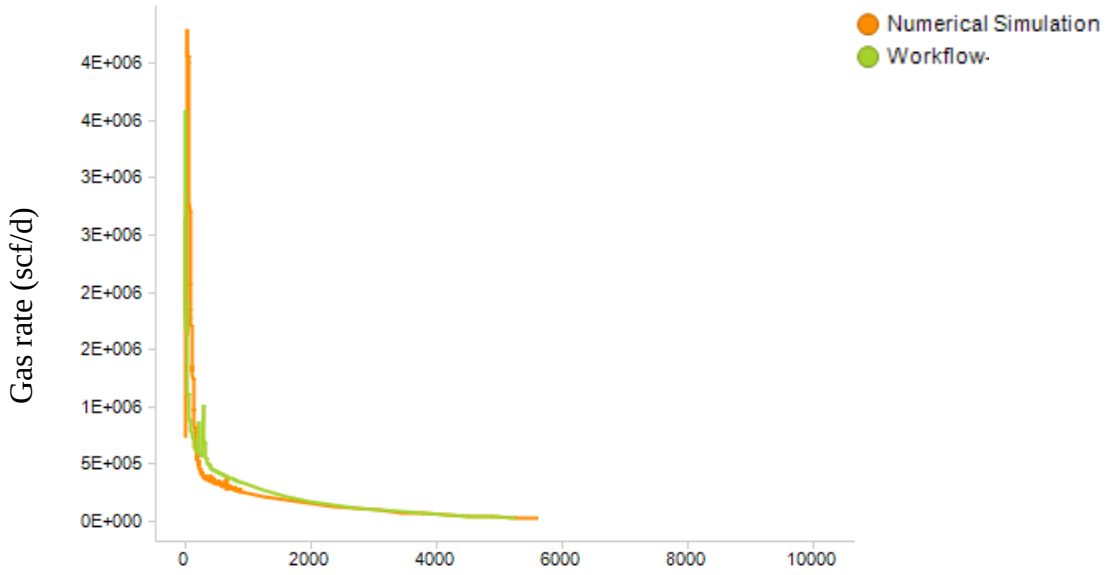

(c)

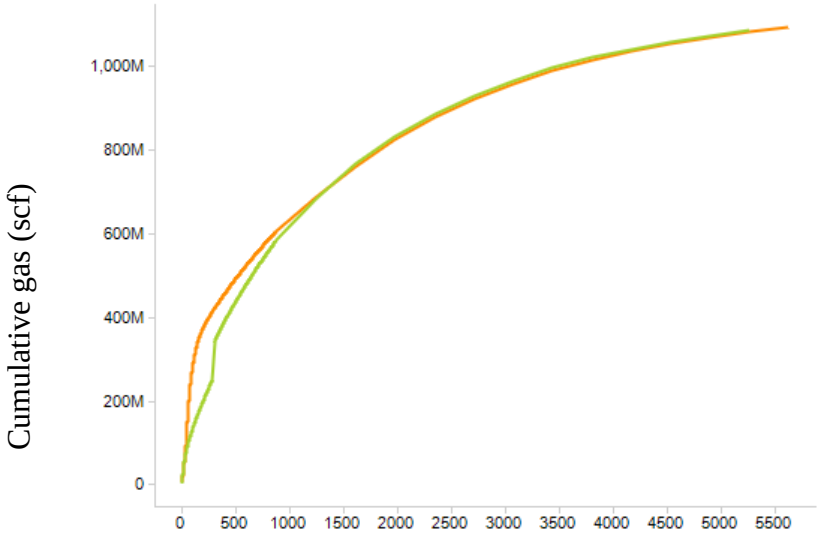

(d)

Time (days)

Figure 70—Continued.

Case-3

With matrix permeability of 4.2e-3 mD, SRV permeability of 1.7 mD, initial reservoir pressure of 6240 psi declining at BHP3 drawdown, Figure 71 compares oil and gas production rates and oil and gas cumulative production volumes with time from the

workflow to compositional numerical model. The ultimate recovery for oil is 307 kbbl with workflow versus 323 kbbl with the numerical model, a 5% difference. For gas, the workflow and the numerical model gives the same forecast of 1.11 BCF.

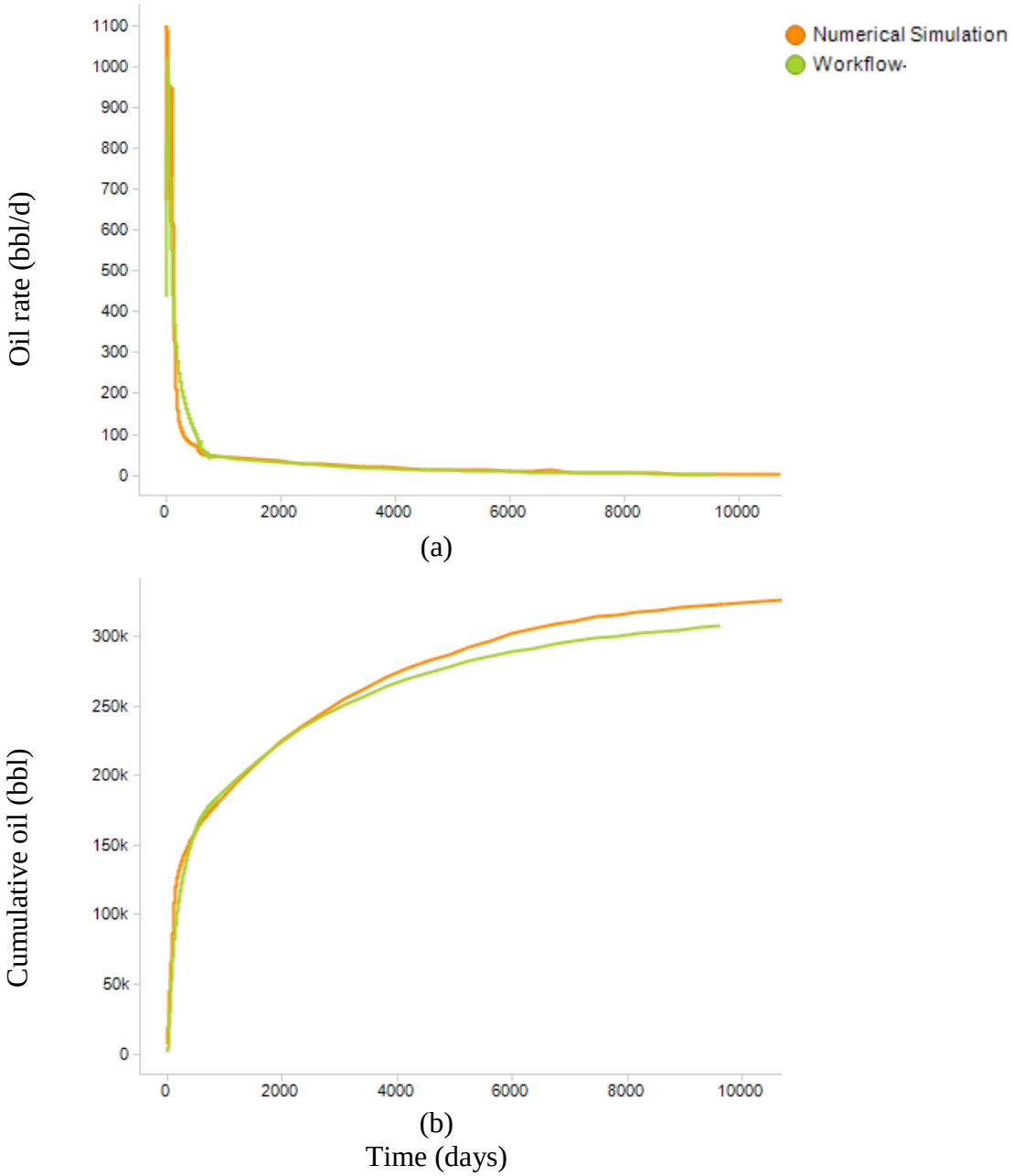

Figure 71—Black oil area of interest, workflow compared to numerical simulation forecast (Case -3)

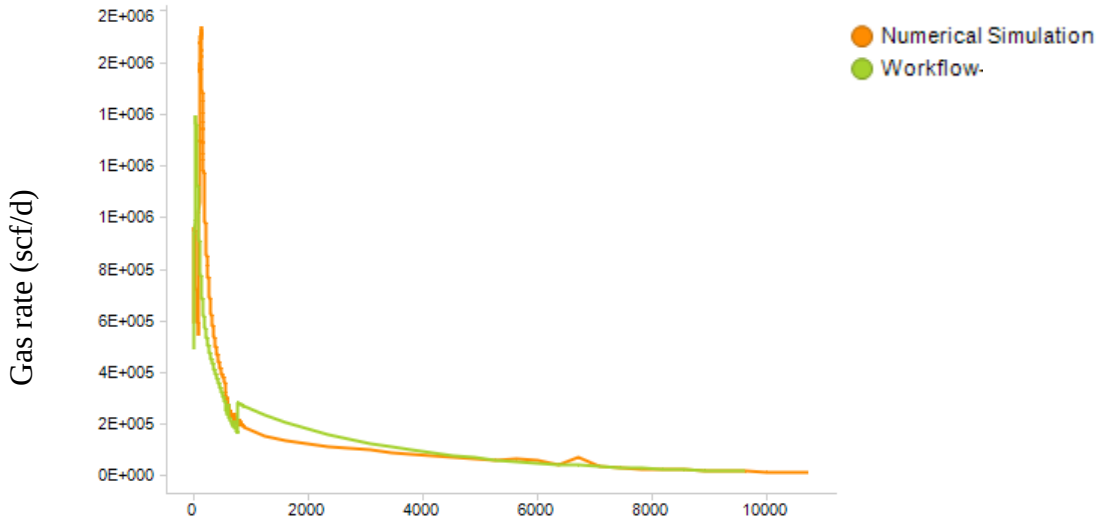

(c)

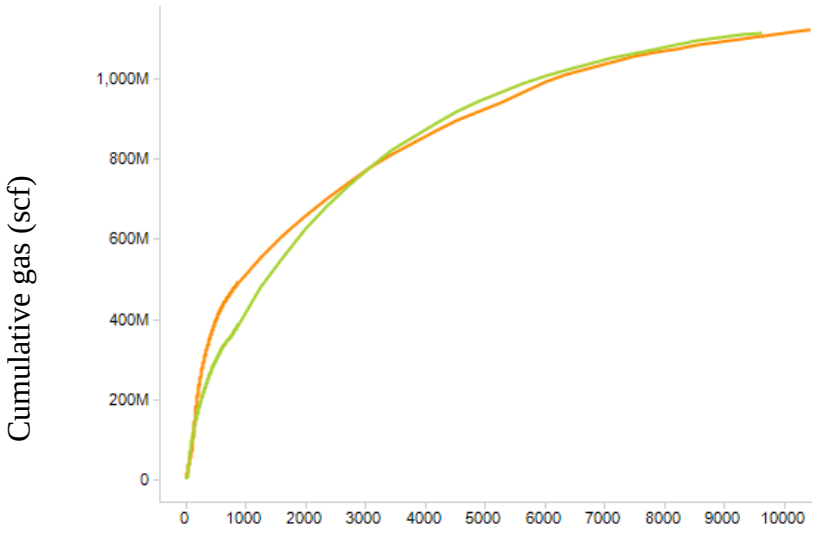

(d)

Time (days)

Figure 71—Continued.

Case-4

With matrix permeability of 8.1e-4 mD, SRV permeability of 3.2e-2 mD, initial reservoir pressure of 6630 psi, and BHP4 pressure history, Figure 72 compares oil and gas production rates and oil and gas cumulative production volumes with time from the workflow to compositional numerical model. The ultimate recovery of oil is 223 kbbl

with the workflow versus 220 kbbl with the numerical model. For gas, the workflow forecasts 0.66 BCF, and the numerical model 0.65 BCF.

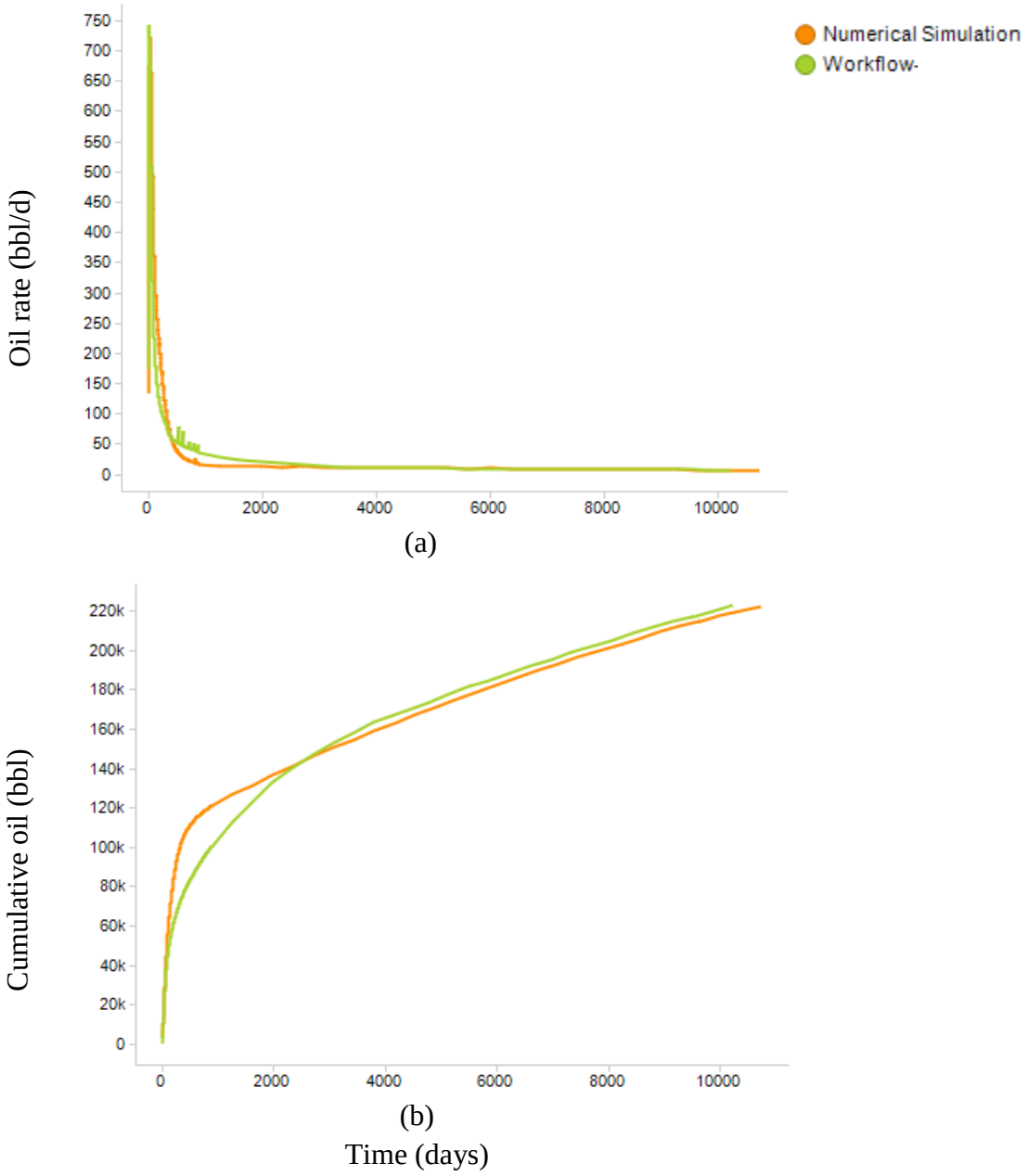

Figure 72—Black oil area of interest, workflow compared to numerical simulation forecast (Case -4)

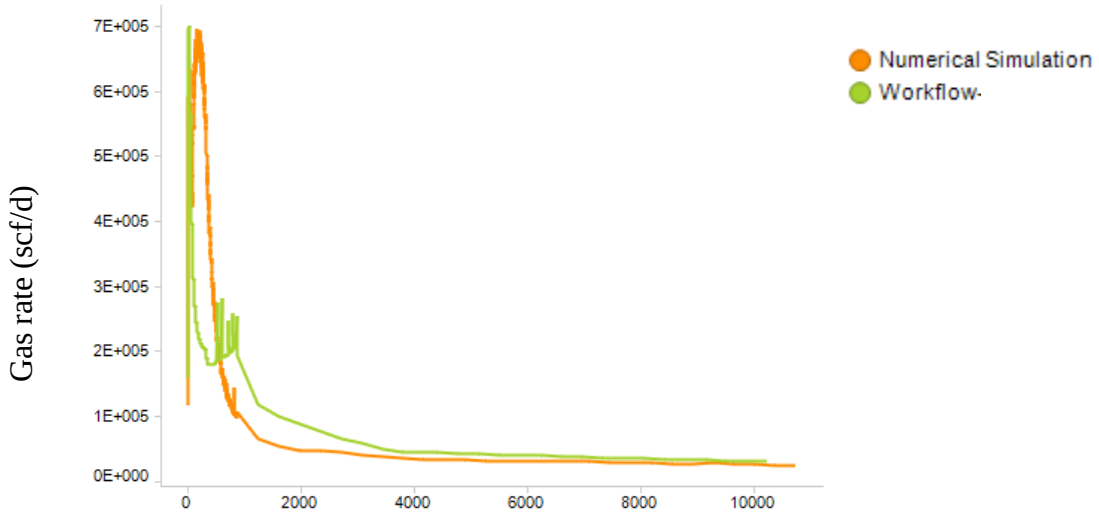

(c)

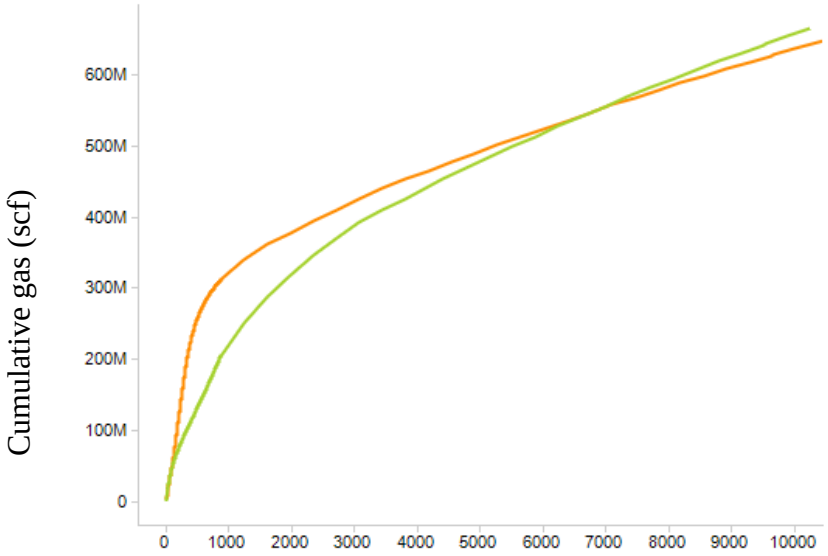

(d)

Time (days)

Figure 72—Continued.

The results of the 4 cases above are summarized in Tables 15 and 16. As explained in the previous chapter, these cases include matrix permeabilities from 8.1e-4 to 4e-3 mD, and SRV permeabilities of 1.6e-2 and 1.7 mD. Table 15 summarizes ultimate recovery of oil and gas using the numerical simulation and our workflow. The results show that

for oil, ultimate recovery is within 6%, and for gas, ultimate recovery is within 9% of the numerical models.

	Ultimate Recovery					
	Compositional Numerical		Our Workflow		%Difference	
Case No.	Oil, kbbl	Gas, Bcf	Oil, kbbl	Gas, Bcf	Oil, EUR	Gas, EUR
1	330	1.05	349	1.14	6%	9%
2	317	1.08	319	1.08	1%	0%
3	323	1.11	307	1.11	-5%	0%
4	220	0.646	223	0.66	1%	1%

Table 15—Comparison of ultimate recovery in black oil cases

In addition to ultimate recovery, it is also important to evaluate the match during the producing life of the well. Present value of producing volumes at a discount rate of 10% are shown in Table 16. The results, for oil are within 4%, and for total value of oil and gas, at the price of $60/bbl for oil and $2.45/Mcf for gas, are within 5% .

	Present Value of Ultimate Recovery					
	Compositional Numerical		Our Workflow		delta %	
Case No.	Oil, kbbl	Gas, Bcf	Oil, kbbl	Gas, Bcf	Oil	Total Oil and Gas*
1	233	0.60	241	0.68	3%	4%
2	259	0.82	257	0.83	-1%	-1%
3	234	0.71	228	0.68	-3%	-3%
4	147	0.40	141	0.35	-4%	-5%

** Based on $60/bbl crude and $2.45/Mcf natural gas*

Table 16—Comparison of present value of ultimate recovery in black oil cases

Sensitivity to the Fluid Model

In this section, the question of impact of fluid variability is addressed. In the cases above, the composition of black oil and volatile oil fluids are quite different. Volatile oil model has 3.6 time higher methane composition than the black oil. Composition of black oil has 2.5 times $C7^{+}$ molecules. Therefore, the question is how the workflow forecast will be impacted by using the trends for a different fluid. For instance, consider volatile oil case-1: what is the impact of using the transition point of 6.2e-4 (black oil), q_D - t_D relationship and GOR-t_D trend from the black oil area instead of from the volatile oil area? Figure 73 shows q_D - t_D for volatile oil case-1 numerical, analytical, and workflow in addition to that for workflow if black oil trends were used.

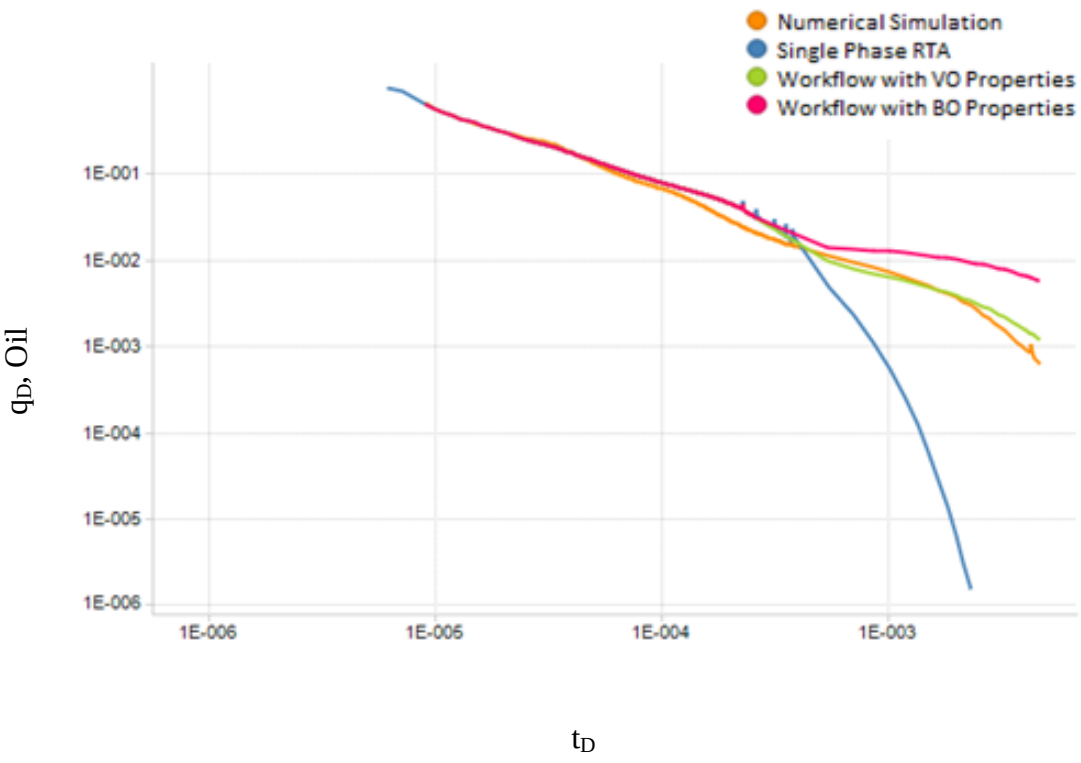

Figure 73—Impact of using black oil trends beyond transition point in a volatile oil case

Figure 74 highlights the deviation that occurs after transition point if black oil trends were used instead of trends for volatile oil.

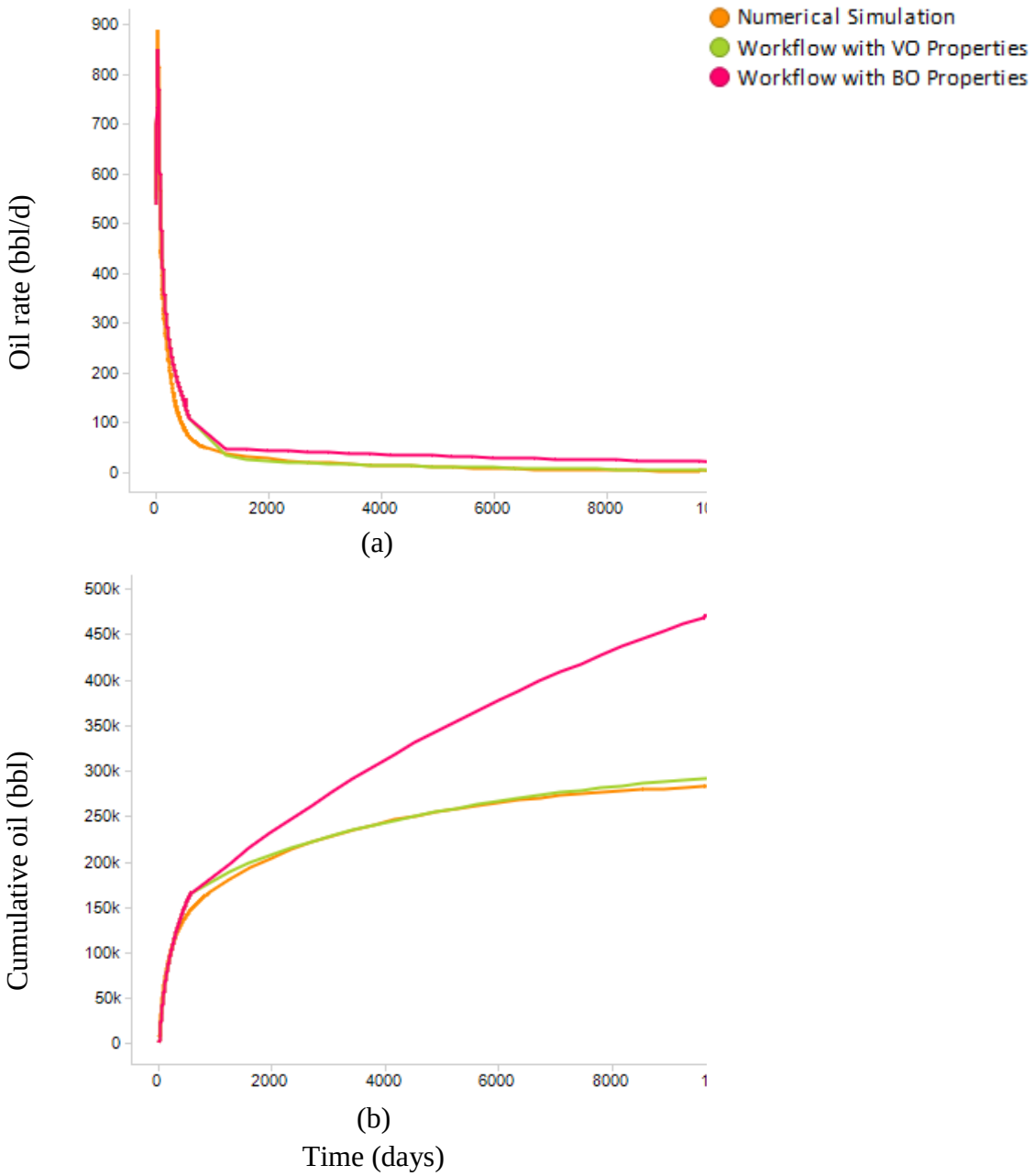

Figure 74—Impact of using black oil trends beyond transition point on (a) oil rate vs. time, (b) cumulative oil vs. time, (c) gas rate vs. time, (d) cumulative gas vs. time.

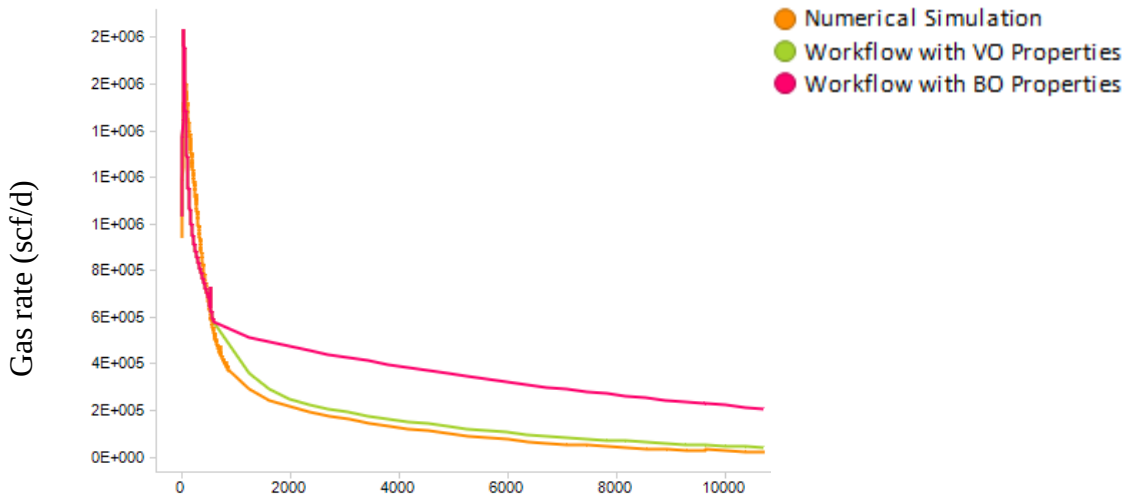

(c)

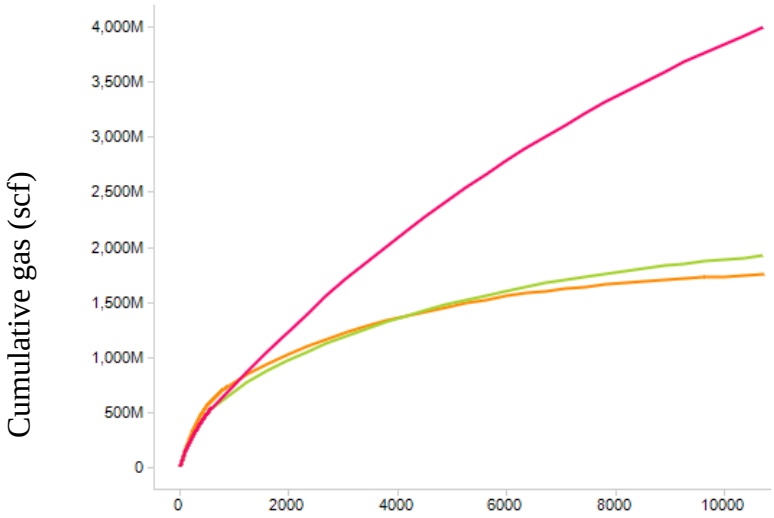

(d)

Time (days)

Figure 74—Continued.

Table 17 shows that using the black oil trends to forecast volatile oil case-1 would result in a 72% overestimation of oil, however in terms of present value at 10% discount rate, in the first 4.5 years, this difference is 11% for both oil and gas.

	Ultimate Recovery					
	Compositional Numerical		Our Workflow		% Difference	
Case No.	Oil, kbbl	Gas, Bcf	Oil, kbbl	Gas, Bcf	Oil, EUR	Gas, EUR
1	286	1.75	297	1.92	4%	10%
1-BO	286	1.75	492	4	72%	129%

Table 17—Ultimate recovery volatile oil case-1 and that with black oil area of interest trends beyond transition point

	Cumulative Volume at 4.5 years					
	Compositional Numerical		Our Workflow		%Difference	
Case No.	Oil, kbbl	Gas, Bcf	Oil, kbbl	Gas, Bcf	Oil, EUR	Gas, EUR
1	194	0.95	199	0.88	3%	-7%
1-BO	194	0.95	215	1.05	11%	11%

Table 18—Cumulative 4.5 year production for volatile oil case-1 and that with black oil area of interest trends beyond transition point

These results indicate that, despite the large difference in fluid properties and compositions of the two fluids, the cumulative production volumes in the first 4.5 years, which dominate present value of production, are still in reasonable agreement.

CHAPTER IX

SUMMARY AND CONCLUSIONS

In this study, we concluded that, to the best of our knowledge, there are no adequate existing workflows for forecasting production from MFHW's in liquid rich shales other than compositional numerical modeling. Numerical modelling is time-consuming and impractical for forecasting production of large numbers of wells. Liquid-rich shale plays are being developed continuously throughout the world, and a gap remains in having a reliable workflow for forecasting multiphase production of large numbers of development wells in short periods of time. In this work, with the help of a correlation of simulated results using dimensionless rate and time (equations (157) and (158)), a practical workflow was developed to forecast multi-phase production in MFHW's in LRS. The workflow was validated using compositional numerical simulation; a summary of this workflow is presented in graphical format in Figure 64.

$$q_{oil\,D}=\frac{q_{oil}(t)\mu_{oil}}{k_{mat}h(p_i-p_{wf})} \tag{157}$$

$$t_D=\frac{k_{mat}t}{\varphi c_t\mu_{oil}(2x_e-2x_f)^2} \tag{158}$$

Workflow on a Page

Field-wide

Done only once- Limited to a single composition of fluid

Compositional Numerical Model		Analytical Model
Multi-phase - k_{mat} - k_{SRV} - SRV Geometry	Low, Mid, High	Single Phase - k_{mat} - k_{SRV} - SRV Geometry

Compare q_D vs. t_D

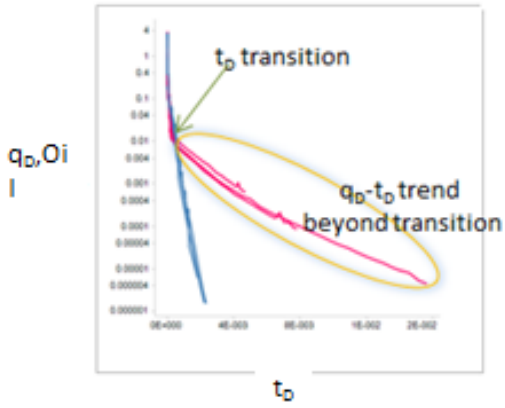

Determine:

1- Transition Point t_D

2- q_D-t_D trend beyond transition (may represent using Arp's multi-segment decline)

3- GOR-t_D trend From Numerical Models

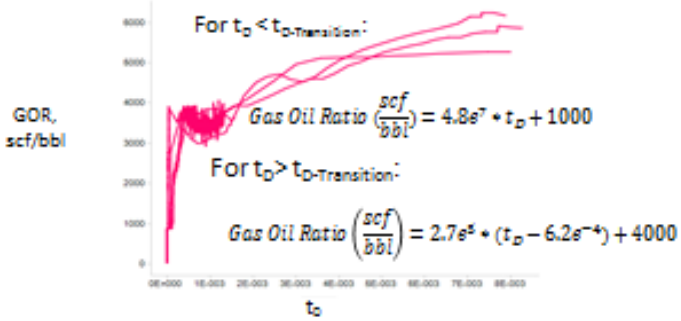

For individual well forecasting

Repeat for each individual well in this PVT window, use 1, 2, 3 above

1- Set up a specific analytical model for the well (use commercial software)

2- If any production available, use automatic history matching

3- Use 1, 2, and 3 above to forecast oil beyond transition point and gas for life of well

Figure 64—Schematic of workflow.

First, the hypothesis that life cycle production in a MFHW in LRS may be divided into two distinct flow periods was validated in Chapter V. The two flow periods are:

1. Initial period- during this period, flowing-bottom-hole pressure varies significantly and fluid flow is predominantly oil. Therefore, we can forecast production using single-phase MFHW rate transient analysis methodology (Ozkan's trilinear flow solution).
2. Subsequent period- during this period, the flowing-bottom-hole pressure is less variable, and multiphase flow is abundant. Therefore, single-phase rate transient analysis is no longer valid. Using our dimensionless rate – dimensionless time correlations, we can define a transition point between single-phase flow domination and multi-phase flow domination. Beyond the transition point, we can use the observed trend of the dimensionless rate vs. dimensionless time to forecast production of the primary phase oil. This trend may be represented in the form of Arps hyperbolic decline model parameters. Similarly, correlation of GOR vs. dimensionless time provides a means to forecast production of the secondary gas phase.

As indicated in Figure 64, the workflow requires defining an area of interest, primarily based on a common reservoir fluid. Secondary requirements for defining an area of interest include common completion practices, formation thickness, and a given range of initial reservoir pressure. For the common area of interest, a one-time evaluation of transition point, a single trend of dimensionless rate versus dimensionless time, and a single trend of GOR versus dimensionless time, is carried out. High, medium, low case scenarios with the range of initial pressure, matrix permeability, stimulated zone permeability, fracture half-length, and minimum bottom-hole flowing pressures are generated using a compositional numerical model. The equivalent scenarios are also generated using single phase analytical models. Comparison of dimensionless rate versus dimensionless time plots from the numerical and analytical models identifies the transition point. This is the point beyond which the two forecasts of numerical and

analytical models deviate, and a single-phase analytical method is no longer valid. Beyond the transition point, the trend of dimensionless rate versus dimensionless time from the compositional numerical model is determined for the area of interest. As mentioned before, this trend may be represented in the form of common decline parameters, if desired. Finally, trend of gas-oil ratio vs. dimensionless time is also determined for the area of interest. This one-time exercise for an area of interest would probably require 2-5 days depending on modeling experience of the user. An area of interest, for example in some well-known liquid rich shale plays such as the Eagle Ford or Duvernay shale in the volatile oil window or the black oil window, could include hundreds or even thousands of wells.

The term "common reservoir fluid" in an area of interest refers to fluids with relatively uniform composition; i.e. the in-situ fluid is volatile oil, or black oil, or retrograde condensate. To investigate the impact of variability in composition, two cases with a wide range of C1 and C7+ compositions from a volatile oil was compared with a black oil. The C1 composition in the volatile oil was 3 times that of the black oil fluid. The transition point and dimensionless rate versus dimensionless time trends from black oil area of interest were used to forecast production in the volatile oil area. The results showed that even with these large variations in fluid composition, the net present value of the first 4.5 years of production at 10% discount rate was within 11% of the numerical compositional benchmark. Therefore, the forecast in the earlier part of the life of the well may still be reliable enough for investment decision making. However, the expected ultimate recovery deviated significantly (70% error), so we conclude that this workflow be applied only to reservoir fluids with reasonably uniform compositions. In other words, this is a limitation of this workflow.

The workflow was validated using a compositional numerical simulator as a benchmark with similar inputs and assumptions in both the workflow and the simulator. Two different areas of interest with two different reservoir fluids of volatile oil and black were studied. In each area of interest, matrix permeability ranged from 100-8000 nano-

Darcies, stimulated rock volume permeability ranged from 4 times to 4000 times that of the matrix permeability, fracture half-length varied from 30-150 ft, initial reservoir pressure ranged from 6500 to 8100 psi, and minimum flowing bottom-hole pressure varied from 450 to 1800 psi.

Eight cases in the two areas of interest including high, medium, and low production forecasts were compared to equivalent compositional numerical models forecasts. In the volatile oil area, expected ultimate recovery from the workflow was within 8% for oil and 10% for gas of the compositional numerical model benchmark. The net present values of production from the workflow were within 10% of the compositional numerical model results. In the black oil area of interest, expected ultimate recovery from the workflow were within 6% for oil and 10% for gas of those forecasted with compositional numerical benchmark. The net present values were within 5% of that from the compositional numerical model.

In closing, a workflow to forecast production and estimate reserves in multi-phase production of multi-fractured horizontal wells in liquid rich shale reservoirs was developed; this workflow honors physical principles of flow, and is rigorous while practical for analyst to apply to numerous wells in a time-efficient manner.

REFERENCES

Anderson, D. M., & Mattar, L. (2003, January 1). Material-Balance-Time During Linear and Radial Flow. *Petroleum Society of Canada.* doi:10.2118/2003-201

Anderson, D., & Mattar, L. (2004, January 1). Practical Diagnostics Using Production Data and Flowing Pressures. *Society of Petroleum Engineers*. doi:10.2118/89939-MS

Arps, J. J. (1945, December 1). Analysis of Decline Curves. *Society of Petroleum Engineers*. doi:10.2118/945228-G

Araya, A., & Ozkan, E. (2002, January 1). An Account of Decline-Type-Curve Analysis of Vertical, Fractured, and Horizontal Well Production Data. *Society of Petroleum Engineers*. doi:10.2118/77690-MS

Behmanesh, H., Hamdi, H., & Clarkson, C. R. (2013, November 5). Production Data Analysis of Liquid Rich Shale Gas Condensate Reservoirs. *Society of Petroleum Engineers*. doi:10.2118/167160-MS

Behmanesh, H., Tabatabaie, S. H., Heidari Sureshjani, M., & Clarkson, C. R. (2014, April 1). Modification of the Transient Linear Flow Distance of Investigation Calculation for Use in Hydraulic Fracture Property Determination. *Society of Petroleum Engineers*. doi:10.2118/168981-MS

Behmanesh, H., Hamdi, H., & Clarkson, C. R. (2015, January 26). Analysis of Transient Linear Flow Associated with Hydraulically-Fractured Tight Oil Wells Exhibiting Multi-Phase Flow. *Society of Petroleum Engineers*. doi:10.2118/172928-MS

Behmanesh, H., Clarkson, C. R., Tabatabaie, S. H., & Heidari Sureshjani, M. (2015, November 1). Impact of Distance-of-Investigation Calculations on Rate-Transient Analysis of Unconventional Gas and Light-Oil Reservoirs: New Formulations for Linear Flow. *Society of Petroleum Engineers*. doi:10.2118/178928-PA

Blasingame, T. A., McCray, T. L., & Lee, W. J. (1991, January 1). Decline Curve Analysis for Variable Pressure Drop/Variable Flowrate Systems. *Society of Petroleum Engineers*. doi:10.2118/21513-MS

Blasingame, T. A., Amini, S., & Rushing, J. (2007, January 1). Evaluation of the Elliptical Flow Period for Hydraulically-Fractured Wells in Tight Gas Sands --

Theoretical Aspects and Practical Considerations. *Society of Petroleum Engineers*. doi:10.2118/106308-MS

Blasingame, T. (1995). *Fluid Flow in Petroleum Reservoirs*. Department of Petroleum Engineering, Texas A&M. Course Notes.

Brown, M. L., Ozkan, E., Raghavan, R. S., & Kazemi, H. (2009, January 1). Practical Solutions for Pressure Transient Responses of Fractured Horizontal Wells in Unconventional Reservoirs. *Society of Petroleum Engineers*. doi:10.2118/125043-MS

Carlson, E. S., & Mercer, J. C. (1991, April 1). Devonian Shale Gas Production: Mechanisms and Simple Models. *Society of Petroleum Engineers*. doi:10.2118/19311-PA

Carslaw, H. S., and Jaeger, J. C., *Conduction of Heat in Solids*. London: Oxford University Press, 1959. Print.

Cheng, Y., Lee, W. J., & McVay, D. A. (2008, October 1). Improving Reserves Estimates From Decline-Curve Analysis of Tight and Multilayer Gas Wells. *Society of Petroleum Engineers*. doi:10.2118/108176-PA

Cinco-Ley, H., & Samaniego-V., F. (1981, September 1). Transient Pressure Analysis for Fractured Wells. *Society of Petroleum Engineers*. doi:10.2118/7490-PA

Clarkson, C. R., Production data analysis of unconventional gas wells: Review of theory and best practices, *International Journal of Coal Geology* (2013), http://dx.doi.org/10.1016/j.cola.2013.01.002

Clarkson, C. R., Production data analysis of unconventional gas wells: Workflow, *International Journal of Coal Geology* (2013), *http://dx.doi.org/10.1016/j.cola.2012.11.016*

Clarkson, C. R., & Qanbari, F. (2015, November 1). An Approximate Semianalytical Multiphase Forecasting Method for Multifractured Tight Light-Oil Wells With Complex Fracture Geometry. *Society of Petroleum Engineers*. doi:10.2118/178665-PA

Duong, A. N. (2010, January 1). An Unconventional Rate Decline Approach for Tight and Fracture-Dominated Gas Wells. *Society of Petroleum Engineers*. doi:10.2118/137748-MS

Eker, I., Kurtoglu, B., & Kazemi, H. (2014, September 30). Multiphase Rate Transient Analysis in Unconventional Reservoirs: Theory and Applications. *Society of Petroleum Engineers*. doi:10.2118/171657-MS

El-Banbi, A. H., & Wattenbarger, R. A. (1998, January 1). Analysis of Linear Flow in Gas Well Production. *Society of Petroleum Engineers*. doi:10.2118/39972-MS

Fekete F.A.S.T RTA Training 2013. *http://fekete.com/training/Pages/FAST-RTA.aspx* (Accessed 15 July 2013)

Fetkovich, M. J. (1980, June 1). Decline Curve Analysis Using Type Curves. *Society of Petroleum Engineers*. doi:10.2118/4629-PA

Fetkovich, M. J., Vienot, M. E., Bradley, M. D., & Kiesow, U. G. (1987, December 1). Decline Curve Analysis Using Type Curves: Case Histories. *Society of Petroleum Engineers*. doi:10.2118/13169-PA

Fuentes-Cruz, G., Camacho-Velazquez, R., & Vasquez-Cruz, M. (2004, January 1). Pressure Transient and Decline Curve Behaviors for Partially Penetrating Wells Completed in Naturally Fractured-Vuggy Reservoirs. *Society of Petroleum Engineers*. doi:10.2118/92116-MS

Gringarten, A. C., Ramey, H. J., & Raghavan, R. (1975, July 1). Applied Pressure Analysis for Fractured Wells. *Society of Petroleum Engineers*. doi:10.2118/5496-PA

Ilk, D., Perego, A. D., Rushing, J. A., & Blasingame, T. A. (2008, January 1). Integrating Multiple Production Analysis Techniques To Assess Tight Gas Sand Reserves: Defining a New Paradigm for Industry Best Practices. *Society of Petroleum Engineers*. doi:10.2118/114947-MS

Ilk, D., Rushing, J. A., Perego, A. D., & Blasingame, T. A. (2008, January 1). Exponential vs. Hyperbolic Decline in Tight Gas Sands: Understanding the Origin and Implications for Reserve Estimates Using Arps' Decline Curves. *Society of Petroleum Engineers.* doi:10.2118/116731-MS

Ilk, D., Anderson, D. M., Stotts, G. W. J., Mattar, L., & Blasingame, T. (2010, June 1). Production Data Analysis--Challenges, Pitfalls, Diagnostics. *Society of Petroleum Engineers*. doi:10.2118/102048-PA

J. Wust, R. A., Cui, A., Nassichuk, B. R., & Bustin, R. M. (2014, December 10). Rock characteristics of oil-, condensate- and dry gas-producing wells of the unconventional Devonian Duvernay Formation, Canada. *International Petroleum Technology Conference*. doi:10.2523/18081-MS

Johnson, N. L., Currie, S. M., Ilk, D., & Blasingame, T. A. (2009, January 1). A Simple Methodology for Direct Estimation of Gas-in-place and Reserves Using Rate-Time Data. *Society of Petroleum Engineers*. doi:10.2118/123298-MS

Kabir, C. S., & Izgec, B. (2006, January 1). Diagnosis of Reservoir Behavior From Measured Pressure/Rate Data. *Society of Petroleum Engineers*. doi:10.2118/100384-MS

Lee, W. J. (2009, October 1). Reserves in Nontraditional Reservoirs: How Can We Account for Them? *Society of Petroleum Engineers*. doi:10.2118/123384-PA

Lee, W. J. Rolins, J.B., Spivey, J. P. *Pressure Transient Testing*. SPE Textbook Series, 1982. Print. ISBN:978-1-55563-099-7

Lewis, A. M., & Hughes, R. G. (2008, January 1). Production Data Analysis of Shale Gas Reservoirs. *Society of Petroleum Engineers*. doi:10.2118/116688-MS

Li, C., Lafollette, R., Sookprasong, A., & Wang, S. (2013, March 26). Characterization of Hydraulic Fracture Geometry in Shale Gas Reservoirs Using Early Production Data. *International Petroleum Technology Conference*. doi:10.2523/16896-MS

McCain, W. D. *The Properties of Petroleum Fluids*. Tulsa: PennWell, 1990. Print.

Medeiros, F., Ozkan, E., & Kazemi, H. (2008, October 1). Productivity and Drainage Area of Fractured Horizontal Wells in Tight Gas Reservoirs. *Society of Petroleum Engineers*. doi:10.2118/108110-PA

Miller, M. A., Jenkins, C. D., & Rai, R. R. (2010, January 1). Applying Innovative Production Modeling Techniques to Quantify Fracture Characteristics, Reservoir Properties, and Well Performance in Shale Gas Reservoirs. *Society of Petroleum Engineers*. doi:10.2118/139097-MS

Mayerhofer, M. (2007, November 1). Overview: Tight Reservoirs (November 2007). *Society of Petroleum Engineers*. doi:10.2118/1107-0098-JPT

Nobakht, M., & Mattar, L. (2009, January 1). Diagnostics of Data Quality for Analysis of Production Data. *Petroleum Society of Canada*. doi:10.2118/2009-137

Nobakht, M., & Mattar, L. (2010, January 1). Analyzing Production Data From Unconventional Gas Reservoirs With Linear Flow and Apparent Skin. *Society of Petroleum Engineers*. doi:10.2118/137454-MS

Nobakht, M., Mattar, L., Moghadam, S., & Anderson, D. M. (2010, January 1). Simplified Yet Rigorous Forecasting of Tight/Shale Gas Production in Linear Flow. *Society of Petroleum Engineers*. doi:10.2118/133615-MS

Nobakht, M., Morgan, M. D., & Mattar, L. (2010, January 1). Case Studies of a Simple Yet Rigorous Forecasting Procedure for Tight Gas Wells. *Society of Petroleum Engineers*. doi:10.2118/137456-MS

Ozcan, O., Sarak, H., Ozkan, E., & Raghavan, R. S. (2014, October 27). A Trilinear Flow Model for a Fractured Horizontal Well in a Fractal Unconventional Reservoir. *Society of Petroleum Engineers*. doi:10.2118/170971-MS

Ozkan, E., Brown, M. L., Raghavan, R. S., & Kazemi, H. (2009, January 1). Comparison of Fractured Horizontal-Well Performance in Conventional and Unconventional Reservoirs. Society of Petroleum Engineers. doi:10.2118/121290-MS

Poe, B. D. (2002, January 1). Effective Well and Reservoir Evaluation Without the Need for Well Pressure History. *Society of Petroleum Engineers*. doi:10.2118/77691-MS

Roberts, G.E., Kaufman, H. *Table of Laplace Transforms*. Philadelphia: W. B. Saunders, 1966. Print.

Raghavan, R. S., Chen, C.-C., & Agarwal, B. (1997, September 1). An Analysis of Horizontal Wells Intercepted by Multiple Fractures. *Society of Petroleum Engineers*. doi:10.2118/27652-PA

Taylor, R., Hards, E., Fyten, G., Hoch, O. F., Storozhenko, K., Stobo, B., & Niebergall, G. (2013, November 5). Optimization of Duvernay Fracture Design Workflow. *Society of Petroleum Engineers*. doi:10.2118/167238-MS

Thomas, F. B., Bennion, D. B., & Andersen, G. (2009, July 1). Gas Condensate Reservoir Performance. *Petroleum Society of Canada*. doi:10.2118/09-07-18

US Energy Information Administration, http://eaglefordshaleblog.com/2010/02/19/

Valko, P. P., & Lee, W. J. (2010, January 1). A Better Way To Forecast Production From Unconventional Gas Wells. *Society of Petroleum Engineers*. doi:10.2118/134231-MS

Whitson, C. H., & Sunjerga, S. (2012, January 1). PVT in Liquid-Rich Shale Reservoirs. *Society of Petroleum Engineers*. doi:10.2118/155499-MS

Xu, B., Haghighi, M., Cooke, D. A., & Li, X. (2012, January 1). Production Data Analysis in Eagle Ford Shale Gas Reservoir. *Society of Petroleum Engineers*. doi:10.2118/153072-MS

Yang, T., Basquet, R., Callejon, A., Van Roosmalen, J. J., & Bartusiak, B. (2014, August 28). Shale PVT Estimation Based on Readily Available Field Data. *Society of Petroleum Engineers*. doi:10.15530/urtec-2014-1884129

Yu, W., Wu, K., & Sepehrnoori, K. (2015, October 1). A Semianalytical Model for Production Simulation From Nonplanar Hydraulic-Fracture Geometry in Tight Oil Reservoirs. *Society of Petroleum Engineers*. doi:10.2118/178440-PA